Equalization in Cyclostationary Interference

by

Brent Robert Petersen, B.Eng. , M.A.Sc.

A thesis submitted to
the Faculty of Graduate Studies and Research
in partial fulfillment of
the requirements for the degree of

Doctor of Philosophy

Ottawa-Carleton Institute for Electrical Engineering
Faculty of Engineering
Department of Systems and Computer Engineering
Carleton University
Ottawa, Ontario, Canada, K1S 5B6

October 31, 1991

The undersigned hereby recommend to
the Faculty of Graduate Studies and Research
acceptance of the thesis,

"Equalization in Cyclostationary Interference"
submitted by
Brent Robert Petersen, B.Eng. , M.A.Sc.

in partial fulfillment of the requirements
for the degree of Doctor of Philosophy

Chair, Department of Systems and Computer Engineering
Professor Samy A. Mahmoud

Thesis Supervisor
Professor David D. Falconer

External Examiner
Professor Desmond P. Taylor
Communications Research Laboratory
McMaster University, Hamilton, Ontario, Canada

Carleton University

January 6, 1992

Abstract

Techniques to reduce the effect of mutually induced cyclostationary crosstalk interference among increasing numbers of digital communication systems will allow for increased system density without a loss of reliability.

For the case where all systems use linear modulation and identical symbol rates, two new analytical results have been derived to evaluate the system performance. The first result is a determination of the conditions where a linear equalizer receiver may have enough degrees of freedom to completely eliminate all intersymbol interference, co-channel interference and adjacent-channel interference. These conditions incorporate transmitter and receiver bandwidths relative to the symbol rate as well as antenna diversity. The second result is an expression for the minimum mean square performance of a continuous-time infinite-length decision-feedback equalizer in the presence of multiple cyclostationary interferers and additive white noise.

These analytical results were evaluated for a high-speed digital subscriber-line system to show the performance improvements which can occur over the situation where the interference is stationary with the same power spectrum. Linear equalizer performance curves were also added to the comparisons. In addition, the results of adaptive equalizer simulations were incorporated to quantify the effect of the interference cyclostationarity on transversal-filter equalizer implementations. The issues considered were finite precision coefficients and convergence rates of the stochastic gradient algorithm. These results show two important techniques which can provide opportunities for improved equalizer performance by enhancing the cyclostationarity of the interference. The first is by decreasing the misalignment of the phases of the transceiver clocks in the central office transmitters. The second is by using transmitter pulse bandwidths which are wide relative to the symbol rate.

The second application considered was adjacent-channel interference in digital radio. Both new analytical results showed similar predictions regarding increased spectral efficiency by using equalizers with wide bandwidths. This increased spectral efficiency is due to the equalizers being able to suppress the cyclostationary adjacent-channel interference, even under conditions of wide transmitter bandwidth where the interference completely overlaps the signal carrying the data of interest.

Acknowledgments

I am fortunate to have been associated with such gifted people.

Professor David D. Falconer, my supervisor, with his vision, insight, and gentle nature, gave me the perfect environment for my ideas to grow. I could not overstate his contribution.

Glenn D. Golden at AT&T Bell Laboratories and Dr. Michael L. Honig at Bell Communications Research provided me with many valuable comments and ideas, as well as advance copies of their related research publications. Also, the anonymous reviewers of my co-authored publications provided valuable advice from different perspectives.

The faculty, alumni, staff, and students of Carleton University and the University of Ottawa provided me with much support throughout the development of my thesis. In alphabetical order I list those people to whom I am especially grateful: Majeed Abdulrahman, Dr. Gary D. Boudreau, Dr. Stewart N. Crozier, Dr. Charles L. B. Despins, Professor Mohammed S. El-Tanany, Dr. Salim Hanna, Professor Peter A. Galko, Vivienne Gilchrist, Shahram Golestaneh, Professor H. M. Hafez, Faramarz Hendessi, Professor Tad A. Kwasniewski, Wilfred P. Leblanc, Danny Lemay, Norman W. K. Lo, Dina McAteer, Darlene Macmillan, Naren Mehta, Dr. Palanisamy Mohanraj, Leonardo G. Neumeyer, Professor Asrar U. H. Sheikh, Dave Sword, Stephen R. Todd, and Yue Yang.

I am grateful for the direct and indirect funding provided to me by the Cable Telecommunications Research Institute (CTRI), the Ontario Graduate Scholarship Program (OGS), the Telecommunications Research Institute of Ontario (TRIO), the Natural Sciences and Engineering Research Council (NSERC), and Carleton University.

Finally, I thank Neal and Katharine, my parents, and Kenneth, my brother, for their love, their support, and for providing me with the opportunity to pursue my education.

All of them made my thesis a very rewarding experience.

Table of Contents

List of Figures

List of Tables

List of Abbreviations and Acronyms

Abbreviation or Acronym	Meaning
2B1Q	Two Binary One Quaternary (A four-level line code)
ACI	Adjacent-channel Interference
AGC	Automatic Gain Control
AT&T	American Telephone & Telegraph
AWG	American Wire Gauge
AWGN	Additive White Gaussian Noise
B.Eng.	Bachelor of Engineering
BER	Bit-Error Rate
CCI	Co-channel Interference
CDMA	Code-Division Multiple Access
CSA	Carrier Serving Area
CTRI	Canadian Telecommunications Research Institute
dB	decibel
dBs	decibels
DFE	Decision-feedback equalizer
Dr.	Doctor
FDDI	Fiber Distributed Data Interface
Fig.	Figure
Figs.	Figures
ft	feet
HDSL	High-Speed Digital Subscriber Lines
Hz	Hertz (one cycle per second)
ISDN	Integrated Services Digital Network
ISI	Intersymbol Interference
k	kilo (thousand)
k bits/s	kilobits per second (one thousand bits per second)
kHz	kilohertz (one thousand cycles per second)
k symbols/s	kilosymbols per second (one thousand symbols per second)
LMS	Least-Mean Square

Abbreviation or Acronym	Meaning
m	milli (a thousandth)
M	mega (million)
M.A.Sc.	Master of Applied Science
M bits/s	megabits per second (one million bits per second)
MDI	Multi-Dimensional Interference
MHz	megahertz (one million cycles per second)
MLSE	Maximum-Likelihood Sequence Estimation
MMSE	Minimum Mean Square Error
MSE	Mean Square Error
mW	milliwatts (a thousandth of a Watt)
NEXT	Near-end Crosstalk
NSERC	Natural Sciences and Engineering Research Council
OGS	Ontario Graduate Scholarship
PAM	Pulse Amplitude Modulation
Ph.D.	Doctor of Philosophy
RLS	Recursive Least-Square
QAM	Quadrature Amplitude Modulation
QPSK	Quadrature Phase-Shift Keying
s	seconds
SE	Square Error
SINR	Signal to Interference-plus-noise Ratio
T1 bit rate	1.544 M bits/s
TRIO	Telecommunications Reseach Institute of Ontario
W	Watts
μ	micro (a millionth)
μW	microwatts (a millionth of a Watt)
Ω	Ohm
(•.♦)	Equation number ♦ in Chapter or Appendix number •
[•]	Reference(s) number(ed) •

Lists of Mathematical Notation

Table I Roman-based notation

Roman symbol	Meaning
A	is a dummy square matrix.
$\{a_i[n] \mid i \in \mathsf{L}_0\}$	are the set of discrete-time impulse responses of the T-spaced equalizers in the forward filter of the MMSE decision-feedback equalizer. See Fig. 3.10.
$\mathrm{A_r}$	is the number of receiver antennas.
$\arg(\bullet)$	is a function which returns the angle of a complex number.
$a(t)$	is the signal which has the data of interest modulated on a T-spaced time sequence of Dirac delta functions. It is the input to the transmitter filter. See Fig. 2.1.
B	is a dummy bandwidth parameter. See Fig. 2.3 and (3.13).
$b_{dco}[n]$	is the discrete-time impulse response of the feedback filter of the time-invariant decision-feedback equalizer, when the DFE is at the MMSE operating point. See (3.50).
$b_{dco}[n, m]$	is the discrete-time impulse response of the feedback filter of the time-variant decision-feedback equalizer, when the DFE is at the MMSE operating point. See (A.6).
$b_d[n]$	is the discrete-time impulse response of the feedback filter of the time-invariant decision-feedback equalizer. See Figs. 2.6 and 3.9.
$\mathbf{b}_d[n]$	is a vector used in the equalizer simulation. It is the discrete-time impulse response of the feedback filter of the decision-feedback equalizer to an impulse which arrives at time n. Note that this impulse response changes in time as the decision-feedback equalizer adapts. See Fig. 4.20.
$b_d[n, m]$	is the discrete-time impulse response of the feedback filter of the periodically time-variant decision-feedback equalizer. An impulse which arrives at time m causes an impulse response which is indexed by parameter n. See (A.1).
$\mathrm{B_e}$	is the LMS adaptation constant. See Fig. 4.20.

Table I (Continued) Roman-based notation

Roman symbol	Meaning
B_n	is the noise bandwidth where the bandwidth is relative to the symbol rate. B_n/T is the absolute bandwidth of the noise. See (2.25) and (5.14).
B_r	is the receiver bandwidth where bandwidth is relative to the symbol rate. B_r/T is the is the absolute bandwidth of the receiver filter. See Fig. 3.3.
B_{ri}	is a dummy bandwidth parameter where the bandwidth is relative to the symbol rate. B_{ri}/T is the is the absolute bandwidth. See (3.22). Note that $2B_{ri} \in \mathbf{Z}^+$.
B_t	is the transmitter bandwidth where bandwidth is relative to the symbol rate. B_t/T is the bandwidth of the transmitter filter. See Fig. 3.3, (4.4), and (5.6).
C	is the carrier spacing between adjacent-channel interferers where the spacing is relative to the symbol rate. C/T is the absolute carrier spacing. See Fig. 3.3.
$\mathbb{C}$	is the set of complex numbers.
$C_0(f)$	is the frequency response of the channel. See Fig. 4.3, (4.6), and (5.10).
$c_0(t)$	is the impulse response of the channel. See Figs. 2.1 and 4.4.
$c_{00}(t)$, $c_{01}(t)$, $c_{10}(t)$, $c_{11}(t)$	are the impulse responses of a cross-coupled channel. See Figs. A.1 and A.3.
$\{C_{b,i}(f) \mid i \in \mathsf{L}_1\}$	are the bases of the frequency responses of the co-channels. They contain the frequency responses of the NEXT coupling paths. See Figs. 4.6 and 4.7.
$\{C_i(f) \mid i \in \mathsf{L}_1\}$	are the frequency responses of the co-channels. These include $\{C_{b,i}(f) \mid i \in \mathsf{L}_1\}$ in addition to associated parameters of the evaluations. See (4.10), (4.11), and (5.10).
diag(•)	is a square diagonal matrix whose elements on the diagonal are obtained from the corresponding elements of the matrix •. The off-diagonal elements of diag(•) are zero.
$\{c_i(t) \mid i \in \mathsf{L}_1\}$	are the impulse responses of the co-channels. See Fig. 2.2.
C_m	is the coefficient maximum value. The units of C_m are volts. The coefficients that can have a maximum value are $\mathbf{b}_d[n]$ and $\mathbf{r}_d[n]$ in Fig. 4.20.

Table I (Continued) Roman-based notation

Roman symbol	Meaning
$C_{N1}(f)$	is magnitude response, for one-sided frequencies, of the commonly used NEXT coupling model. See Fig. 4.6 and (4.9).
$\mathrm{C_p}$	is the coefficient precision in the equalizer. The units of $\mathrm{C_p}$ are bits. The coefficients that may be quantized are $\mathbf{b}_d[n]$ and $\mathbf{r}_d[n]$ in Fig. 4.20.
$\mathrm{D_0}$	is the relative phase shift (delay) of the transmitted signal over the symbol period. $\mathrm{D_0}$ is in the range from 0 to 1 symbol periods. See Fig. 4.13, (4.8), and (5.10).
$d_0[n]$	is the data of interest at time n. See Fig. 2.1 and (2.7).
$\widehat{d}_0[n]$	is the equalizer's estimate of data of interest at time n. See Figs. 2.5, 2.6, 3.1, and 3.9.
$\widetilde{d}_0[n]$	is the quantized estimate data of interest at time n. See Figs. 2.1, 2.5, 2.6, 3.1, and 3.9.
$\{\mathrm{D}_{b,i} \mid i \in \mathsf{L}_1\}$	are the relative phase shifts (delays) of the NEXT co-channels over a symbol period. $\{\mathrm{D}_{b,i} \mid i \in \mathsf{L}_1\}$ are in the range from 0 to 1 symbol periods. They are used to incorporate the effects of divided cable bundles in the central office. See Fig. 4.8, Fig. 4.9, (4.11), and (4.12).
$\mathrm{D_e}$	is the decision delay. It is the difference between the time a data value is transmitted and the time that data value appears at the output of the equalizer. It is also the number of taps in the delay line $\mathbf{m}_{de}[n]$ in Fig. 4.20.
$\{\mathrm{D}_i \mid i \in \mathsf{L}_1\}$	are the relative phase shifts (delays) of the interferer's signals over a symbol period. $\{\mathrm{D}_i \mid i \in \mathsf{L}_1\}$ are in the range from 0 to 1 symbol periods. See (4.4), (4.5), and (5.10).
$\{d_i[n] \mid i \in \mathsf{L}_1\}$	are the transmitted data of the interferers. See Fig. 2.2 and (2.21).
d_{min}	is the minimum distance between a decision boundary and a transmitted data level.
e	is the base of natural logarithms: $\ln(e) = 1$
$E[\bullet]$	is expectation of the argument $\bullet$ over the ensembles of $\{d_i[n] \mid i \in \mathsf{L}_0, n \in \mathbf{Z}\}$ and $\{n(t) \mid t \in \mathbf{R}\}$. See (2.18).
$e_0[n]$	is the normalized equalizer error. It is the same random process as $e[n]$ except that it has undergone a linear transformation so that $e_0[n]$ has a mean value of zero and a standard deviation of one.

Table I (Continued) Roman-based notation

Roman symbol	Meaning
$E_d[\bullet]$	is expectation of the argument $\bullet$ over the ensemble of $\{d_0[n] \mid n \in \mathbf{Z}\}$. See (2.4).
$\varepsilon_{dc}(b_d, r_d)$	is the MSE of a continuous-time infinite-length DFE in cyclostationary interference for particular forward filter, $r_d(t)$, and feedback filter, $b_d[n]$, impulse responses. See (3.41).
ε_{dco}	is the MMSE of a continuous-time infinite-length DFE in cyclostationary interference. See Table 3.1.
$\varepsilon_{dc}(r_d)$	is the MSE of a continuous-time infinite-length linear equalizer in cyclostationary interference for particular forward filter, $r_d(t)$, and optimal feedback filter, $b_{dco}[n]$, impulse responses. See (3.55).
$\varepsilon_{d(c/s)o}$	is the ratio of the MMSE of a continuous-time infinite-length DFE in cyclostationary interference to the MMSE of a continuous-time infinite-length DFE in stationary noise. See (3.114).
ε_{dso}	is the MMSE of a continuous-time infinite-length DFE in stationary noise. See Table 3.1.
ε_{dwo}	is the MMSE of a continuous-time infinite-length DFE in white noise. See Table 3.1.
E_{gzf}	is equal to $E_{gzf}(\mathrm{B_t}, \mathrm{B_r}, \mathrm{C}, \mathrm{A_r}, \mathrm{N_c})$. It is a region where a generalized zero-forcing equalizer exists in the presence of ISI, ACI, and CCI. This region is based on the number of degrees of freedom being less than or equal to the number of constraints. It involves conditions among: the relative transmitter bandwidth, the relative receiver bandwidth, the relative carrier spacing, the number of receiver antennas, and the number of CCI signals. See (3.22).
ε_{lco}	is the MMSE of a continuous-time infinite-length linear equalizer in cyclostationary interference. See Table 3.1.
$\varepsilon_{l(c/s)o}$	is the ratio of the MMSE of a continuous-time infinite-length linear equalizer in cyclostationary interference to the MMSE of a continuous-time infinite-length linear equalizer in stationary noise. See (3.121).
ε_{lso}	is the MMSE of a continuous-time infinite-length linear equalizer in stationary noise. See Table 3.1.
ε_{lwo}	is the MMSE of a continuous-time infinite-length linear equalizer in white noise. See Table 3.1.

Table I (Continued) Roman-based notation

Roman symbol	Meaning
$E_n[\bullet]$	is expectation of the argument $\bullet$ over the ensemble of $\{n(t) \mid t \in \mathbf{R}\}$. See (2.16).
$e[n]$	is the equalizer error. It is defined to be the data decision minus the equalizer's estimate of the data. See Fig. 4.20 and (4.33).
$\mathrm{E_S}$	is the energy per received symbol, measured at the receiver input. See (5.1) and (5.2).
f	is a dummy parameter used as a frequency index. $f \in \mathbf{R}$.
$f_d[n]$	is the signal at the output of the feedback filter of the DFE. See Figs. 2.6 and 3.9.
$\mathcal{F}_{cc}[\bullet], \mathcal{F}_{cc}^{-1}[\bullet]$	are a continuous-time continuous-frequency Fourier transform and its inverse. See (2.22). With a particular Fourier transform pair, the time function will be denoted by a lower-case letter and the frequency function will be denoted by the corresponding upper case letter.
$F_{c-s}^{\mathrm{T}}(f)$	is the relative improvement in SINR of the cyclostationary interference case over the stationary noise case, relative to the SINR of the stationary noise case. See (3.116).
$\mathcal{F}_{dc}[\bullet], \mathcal{F}_{dc}^{-1}[\bullet]$	are a discrete-time continuous-frequency Fourier transform and its inverse. See (C.1). With a particular Fourier transform pair, the time function will be denoted by a lower-case letter and the frequency function will be denoted by the corresponding upper case letter. Additionally, the frequency function will be superscripted by T to denote that it is periodic in frequency with period equal to $1/\mathrm{T}$.
$\widehat{F}_{E_0}(e_0)$	is an estimate of the cumulative distribution function of the random variables in the wide-sense-stationary white random process $e_0[n]$.
g_{agc}	is the automatic gain control coefficient. This coefficient is precomputed before the simulation is begun and it remains fixed during the simulation. The power at the output of the automatic gain control multiplier is one. See Fig. 4.20 and (4.31).
$g(t)$	is the signal at the receiver input. See Figs. 2.1, 2.5, 2.6, 3.1, 3.9..
$H_0(f)$	is the frequency response of the equalized combined channel. See (3.4).
$\{H_i(f) \mid i \in \mathbf{L}_1\}$	are the frequency responses of the equalized overall co-channels. See (3.4).

Table I (Continued) Roman-based notation

Roman symbol	Meaning
$h_0(t)$	is the impulse response of the equalized combined channel. See Fig. 3.2 and (3.2).
$\{h_i(t) \mid i \in \mathsf{L}_1\}$	are the impulse responses of the equalized combined co-channels. See Fig. 3.2 and (3.3).
$H_{00}(f)$, $H_{01}(f)$, $H_{10}(f)$, $H_{11}(f)$	are the frequency responses of the equalized combined cross-coupled channels. See (A.37).
$h_{00}(t)$, $h_{01}(t)$, $h_{10}(t)$, $h_{11}(t)$	are the impulse responses of the equalized combined cross-coupled channels. See (A.34).
$H_{01e}(f)$, $H_{01o}(f)$, $H_{11e}(f)$, $H_{11o}(f)$	are the frequency responses of the equalized combined cross-coupled channels for the time-variant equalizer. See (A.49) and (A.50).
$h_{01e}(t)$, $h_{01o}(t)$, $h_{11e}(t)$, $h_{11o}(t)$	are the impulse responses of the equalized combined cross-coupled channels for the time-variant equalizer. See (A.46).
$h_{dco,0}[n]$	is the impulse response of the sampled equalized combined channel when the continuous-time infinite-length DFE in cyclostationary interference is at the MMSE operating point. See (3.64).
$\{h_{dco,i}[n] \mid i \in \mathsf{L}_1\}$	are the impulse responses of the sampled equalized combined co-channels when the continuous-time infinite-length DFE in cyclostationary interference is at the MMSE operating point. See (3.65).
$H^{\mathrm{T}}_{dco,0}(f)$	is the frequency response of the sampled equalized combined channel when the continuous-time infinite-length decision-feedback equalizer is at the MMSE operating point. See (3.69) and (3.87).
i	is a dummy parameter used as a general index. $i \in \mathbf{Z}$.
$\Im[\bullet]$	is the imaginary part of the complex number $\bullet$.
$\mathrm{I_a}$	is the number of simulations ensembles used to average the square error in order to get the mean square error. The notation for $\mathrm{I_a}$ refers to iteration average.
$\mathbf{I}_{2K_t-1}$	is the identity matrix of order $2K_t - 1$.
$\mathrm{int}(\bullet)$	is the integer part of the real argument $\bullet$.
$\mathrm{I_t}$	is the number of symbol periods over which a simulation was run. The notation for $\mathrm{I_t}$ refers to iteration time.
j	is an imaginary number satisfying $j^2 = -1$.

Table I (Continued) Roman-based notation

Roman symbol	Meaning
k	is a dummy parameter used as a general index. $k \in \mathbf{Z}$.
K	is the constant of proportionality used in a NEXT model. See (4.9).
K_0	is a linear transformation. See (3.48).
K_d	is a linear transformation. See (3.56).
$k_d(t,\tau)$	is the Hermitian kernel of the linear transformation K_d. See (3.56) and (3.57).
K_l	is a linear transformation. See (3.46).
$k_l(t,\tau)$	is the Hermitian kernel of the linear transformation K_l. See (3.42) and (3.46).
K_t	is the bandwidth of the combined channel and combined co-channels. See (3.19), (3.20), (3.29), and (3.71).
l	is a dummy parameter used as a general index. $l \in \mathbf{Z}$.
L	is the number of interferers present in the signal at the receiver input. See Figs. 2.2, 3.1, and 3.9. Also see (2.21) and (5.9).
$\mathbf{L}_0$	is the set of integers $\{0, 1, 2, \ldots, \mathrm{L}\}$.
$\mathbf{L}_1$	is the set of integers $\{1, 2, 3, \ldots, \mathrm{L}\}$.
$\ln(\bullet)$	is the natural logarithm of the argument $\bullet$.
$\log_{10}(\bullet)$	is the logarithm to the base 10 of the argument $\bullet$.
m	is a dummy parameter used as a general index. $m \in \mathbf{Z}$.
M	is the percent misalignment of the phases of interferers. To facilitate understanding, consider three examples. When M is 0 percent, the beginnings of the impulse responses of the interferers occur at the same relative time in a symbol period. When it is 50 percent, the beginnings of the impulse responses of the interferers occur at time points that are uniformly distibuted over 50 percent of a symbol period. When it is 100 percent, the beginnings of the impulse responses of the interferers occur at time points that are uniformly distibuted over the entire symbol period. See (4.5).
$m_0(t)$	is the impulse response of the filter matched to $\phi_0(t)$. See (3.49).

Table I (Continued) Roman-based notation

Roman symbol	Meaning
$m_A[i]$	is a one-to-one integer mapping from the ACI interferer number, i, to the carrier frequency number, $m_A[i]$. See Table 5.1.
$\max_{\bullet}(\blacklozenge)$	is the maximum value of $\blacklozenge$ over all possible conditions in $\bullet$.
$\mathbf{m}_b[n]$	is a vector representing the finite-length approximation of the memory of the feedback filter of the DFE at time n. It has N_{fd} taps. See Fig. 4.20.
$M_{ci}^{T}(f)$	is the ratio of the powers of the sampled combined channel to the cyclostationary interference plus noise. See Table 3.2.
$\mathbf{m}_{de}[n]$	is a vector representing the memory used to delay the equalizer decisions at time n. It has D_e taps. See Fig. 4.20.
$\min(\bullet, \blacklozenge)$	is the minimum of the two arguments $\bullet$ and $\blacklozenge$.
$\min_{\bullet}(\blacklozenge)$	is the minimum value of $\blacklozenge$ over all possible conditions in $\bullet$.
$M_{ci-w}^{T}(f)$	is the improvement in white noise over cyclostationary interference of the ratio of the powers of the sampled combined channel to the cyclostationary interference plus noise. See (3.109).
$\mathbf{M}_{ci-w}(f)$	is a positive semi-definite matrix. See (3.109).
$m_L[i]$	is a one-to-one integer mapping from the CCI interferer number, i, to the twisted-pair number, $m_L[i]$. See Table 4.1.
$\mathbf{m}_r[n]$	is a vector representing the finite-length approximation of the memory of the forward filter of the DFE at time n. It has N_{fo} taps. See Fig. 4.20.
$M_{sn}^{T}(f)$	is the ratio of the powers of the sampled combined channel to the stationary interference plus noise. See Table 3.2.
$M_{w}^{T}(f)$	is the ratio of the powers of the sampled combined channel to the noise. See Table 3.2.
$\mathbf{m}_{\phi 0}[n]$	is a vector representing the finite-length approximation of the memory of the combined channel at time n. It has 4096 taps. See Fig. 4.20.
$\{\mathbf{m}_{\phi i}[n] \mid i \in \mathsf{L}_1\}$	are vectors representing the finite-length approximations of the memory of the combined co-channels at time n. They each have 64 taps. See Fig. 4.20.
n	is a dummy parameter used as a general index. $n \in \mathbf{Z}$.

Table I (Continued) Roman-based notation

Roman symbol	Meaning
N	is the number of independent data streams. See (3.20), (3.28), and (3.29).
N_a	is the number of ACI signals present after receiver filtering. See (3.21) and Fig. 3.3.
$N_{ar}(B_t, B_{ri}, C)$	is the number of relevant ACI signals that are involved in the determination of the existence of the generalized zero-forcing linear equalizer. If the neighbouring ACI signals do not overlap with the signal carrying the data of interest, then the number of relevant ACI signals is zero. If the neighbouring ACI signals overlap with the signal carrying the data of interest, then the number of relevant ACI signals depends upon the three arguments: the relative transmitter bandwidth, the relative receiver bandwidth, and the relative carrier spacing. See (3.24).
N_c	is the number of CCI signals present after receiver filtering. See (3.21) and Fig. 3.3.
$N_E(B_t, B_{ri}, C, N_c)$	is the number of equations (constraints) involved in the determination of the existence of the generalized zero-forcing linear equalizer. The number of equations depends upon the four arguments: the relative transmitter bandwidth, the relative receiver bandwidth, the relative carrier spacing, and the number of CCI signals. See (3.22) and (3.23).
N_{fo}	is the number of taps in the finite-length forward filter of the decision feedback equalizer. It is the length of the vectors $\mathbf{m}_r[n]$ and $\mathbf{r}_d[n]$ in Fig. 4.20.
N_{fd}	is the number of taps in the finite-length feedback filter of the decision feedback equalizer. It is the length of the vectors $\mathbf{m}_b[n]$ and $\mathbf{b}_d[n]$ in Fig. 4.20.
No	is the two-sided power spectral density of the complex white noise measured in W/Hz. See (2.25).
$No/2$	is the two-sided power spectral density of the real part and the imaginary part of the complex white noise, measured in W/Hz.
$n(t)$	is the complex baseband white noise random process. See Figs. 2.2, 2.4, 3.1, and 3.9. Also see (2.16).

Table I (Continued) Roman-based notation

Roman symbol	Meaning
$N_U(B_t, B_{ri}, A_r)$	is the number of unknowns (degrees of freedom) involved in the determination of the existence of the generalized zero-forcing linear equalizer. The number of unknowns depends upon the three arguments: the relative transmitter bandwidth, the relative receiver bandwidth, and the number of receiver antennas. See (3.22) and (3.25).
$\mathbf{p}_0$	is the row vector formed from the first row of the matrix involving $\{\Phi_0(f)\}$ in (3.19).
$\{\mathbf{p}_i \mid i \in \mathbf{L}_1\}$	are the row vectors formed from the respective rows of the matrix involving $\{\Phi_i(f) \mid i \in \mathbf{L}_1\}$ in (3.19).
$P_{bu}(f)$	is the frequency response of a filter based on a Butterworth filter of order 5. See Fig. 4.1 and (4.1).
$p_{bu}(t)$	is the impulse response of a filter based on a Butterworth filter of order 5. See Fig. 4.2 and (4.2).
P_{ci}	is the total interference power with bandlimited noise, measured at the receiver input. See (2.28).
$P_{ci}(\tau)$	is the instantaneous total interference power with bandlimited noise at a particular time τ, measured at the receiver input. Note that it is defined for $0 \leq \tau \leq T$. See (2.29).
P_I	is the total interference power without noise, measured at the receiver input. See (2.27).
P_{Io}	is the total interference power without noise, measured at the receiver input, that overlaps with the spectrum of the signal which carries the data of interest. See (5.16).
$P_{I,m}$	is the power of the m^{th} interfering signal, measured at the receiver input. See (2.26).
P_N	is the bandlimited noise power at the receiver input. See (2.25).
P_{No}	is the bandlimited noise power at the receiver input which overlaps with the signal carrying the data of interest. See (5.17).
$P_r(f)$	is the frequency response of the receiver filter. See Fig. 3.3, (5.11), (5.12), and (5.13).
P_S	is the power of the signal carrying the data of interest, measured at the receiver input. See (2.13).

Table I (Continued) Roman-based notation

Roman symbol	Meaning
P_{So}	is the power of the signal carrying the data of interest, measured at the receiver input. See (5.15).
$P_{sr}(f;\alpha)$	is the frequency response of a square-root raised cosine pulse with an excess bandwidth parameter equal to α. See (5.5).
$P_{srw}(f;\mathrm{B_t})$	is a modified square root raised cosine pulse with a wide bandwidth capability. See (5.6) and Fig. 5.1.
$P_{t,0}(f)$	is the frequency response of the transmitter of the channel. See Fig. 2.1, (4.4), and (5.8).
$p_{t,0}(t)$	is the impulse response of the transmitter of the channel. See Fig. 2.1.
$\{P_{t,i}(f) \mid i \in \mathsf{L}_1\}$	are the frequency responses of the transmitters of the co-channels. See Fig. 2.2, (4.4), and (5.8).
$\{p_{t,i}(t) \mid i \in \mathsf{L}_1\}$	are the impulse responses of the transmitters of the co-channels. See Fig. 2.2.
P_V	is the ratio of the maximum instantaneous interference power over a symbol period to the minimum instantaneous interference power over a symbol period. See (4.22).
$Q(\bullet)$	is the Q function of the argument $\bullet$. See (4.36).
$Q^{-1}(\bullet)$	is the inverse of the Q function. The Q function is defined in (4.36).
$\Re[\bullet]$	is the real part of the complex number $\bullet$.
R	is the set of real numbers.
$r_c[i,k]$	are the correlation coefficients used to examine the numerical similarity among the shapes of the NEXT impulse responses. See (4.19). Note that $i,k \in \mathsf{L}_1$ and $i \neq k$.
$R_{ci}(\tau)$	is the autocorrelation function of $\nu_{ci}(t)$. See the footnote containing (2.30).
$R_{dco}(f)$	is the frequency response of the forward filter of the continuous-time infinite-length DFE, when that DFE is operating at the MMSE point. See (3.67) and (3.88).
$r_{dco}(t)$	is the impulse response of the forward filter of the continuous-time infinite-length DFE, when that DFE is operating at the MMSE point. See Fig. 3.10, (3.58), and (3.62).

Table I (Continued) Roman-based notation

Roman symbol	Meaning
$\mathbf{r}_d[n]$	is a vector used in the equalizer simulation. It is the discrete-time impulse response of the forward filter of the decision-feedback equalizer to an impulse which arrives at time n. Note that this impulse response changes in time as the decision-feedback equalizer adapts. See Fig. 4.20.
$r_{dno}(t)$	is a periodically time-invariant optimal impulse response observed in the proof that the MMSE DFE is time invariant. See (A.11).
$r_{dn}(t)$	is a periodically time-invariant impulse response observed in the proof that the MMSE DFE is time invariant. See (A.9).
$r_d(t)$	is the impulse response of the forward filter of the continuous-time infinite-length DFE. See Fig. 2.6.
$\mathbf{R}_{\mathrm{dco}}(f)$	is a vector containing $(1/\mathrm{T})$- spaced samples of the frequency response of the forward filter of the continuous-time infinite-length DFE, when that DFE is operating at the MMSE point. See (3.75).
$r_d(t,\tau)$	is the time-variant impulse response of the forward filter of the continuous-time infinite-length DFE. The notation means that $r_d(t,\tau)$ is the impulse response in time t due to an impulse arriving at time τ.
$r_l(t)$	is the impulse response of the continuous-time infinite-length linear equalizer. See Figs. 2.5 and 3.1.
$r_{l,0}(t)$, $r_{l,1}(t)$	are the impulse responses of the continuous-time infinite-length time-invariant cross-coupled linear equalizers. See Fig. A.1.
$r_{l,1\mathrm{e}}(t)$, $r_{l,1\mathrm{o}}(t)$	represent the impulse responses of a continuous-time infinite-length periodically time-invariant cross-coupled linear equalizer. See Fig. A.3.
$R_l(f)$	is the frequency response of the continuous-time infinite-length linear equalizer. See (3.5).
$\mathrm{R_{sr}}$	is the receiver sampling rate. It is the number of samples per symbol period. Equalizers will have a tap spacing equal to $\mathrm{T/R_{sr}}$. See Fig. 4.20.
S	is the scaling factor in dB used in the high-speed digital subscriber lines application to provide a safety margin. The amplitudes of the interferers are multiplied by $10^{\mathrm{S}/20}$. See (4.11).
$s(t)$	is the signal, at the recevier input, which carries the data of interest. See Fig. 2.1.

Table I (Continued) Roman-based notation

Roman symbol	Meaning
$S_{ci}(f)$	is the power spectral density of the cyclostationary interference at the receiver input. See (2.32).
$S_n(f)$	is the power spectral density of the white noise at the receiver input. See (2.17).
$S_{sn}(f)$	is the power spectral density of the stationary noise at the receiver input. See (2.37).
t, t_1, t_2	are dummy parameters used as general time indices. $t, t_1, t_2 \in \mathbf{R}$.
T	is the symbol period. See (2.7) and (2.21).
$1/\mathrm{T}$	is the symbol rate. See (2.7) and (2.21).
T_0, T_1	are the symbol periods used in the analysis of the mixed symbol rate system. See (A.17) and (A.18).
$1/\mathrm{T}_0$, $1/\mathrm{T}_1$	are the symbol rates used in the analysis of the mixed symbol rate system. See (A.17) and (A.18).
$u_d(t)$	is the signal at the output of the forward filter of the DFE. See Fig. 2.6, Fig. 3.9, and (2.40).
$u_d[n]$	is the signal at the output of the sampler of the DFE. See Fig. 2.6, Fig. 3.9, and (2.41).
$u_l(t)$	is the signal at the output of the forward filter of the linear equalizer. See Fig. 2.5, Fig. 3.1, and (2.38).
$u_l[n]$	is the signal at the output of the sampler of the linear equalizer and is equal to $\widehat{d}_0[n]$. See Fig. 2.5 and (2.39).
$u[n]$	is the discrete-time unit step function. See (B.10).
$\mathbf{W}_{ci}(f)$	is a square matrix of order $2K_t - 1$ used in determining $M_{ci}^{\mathrm{T}}(f)$. See Table 3.2.
$W_{n,m}(f)$	is a scalar used in the development of the continuous-time inifinite-length DFE in cyclostationary interference. See (3.70).
$\mathbf{W}_{sn}(f)$	is a square matrix of order $2K_t - 1$ used in determining $M_{sn}^{\mathrm{T}}(f)$. See Table 3.2.
$\mathbf{W}_w(f)$	is a square matrix of order $2K_t - 1$ used in determining $M_w^{\mathrm{T}}(f)$. See Table 3.2.

Table I (Continued) Roman-based notation

Roman symbol	Meaning
x	is a dummy variable. $x \in \mathbf{R}$.
X	is the number of clusters in the subscriber-line cable. X is used to model the possibility that a bundle of twisted pairs may be divided into multiple clusters in the central office. Each cluster would go to a different rack of equipment. See (4.12) and Fig. 4.9.
$x(t)$, $X(f)$	are dummy functions.
$\mathbf{x}_1$, $\mathbf{x}_2$	are dummy vectors.
$x_a[n]$, $x_b[n]$, $x_c[n]$	are dummy functions.
$X_a^{\mathrm{T}}(f)$, $X_b^{\mathrm{T}}(f)$, $X_c^{\mathrm{T}}(f)$	are dummy functions.
y	is a dummy variable. $y \in \mathbf{R}$.
$y(t)$	is the signal at the output of the transmitter filter for the channel. See Fig. 2.1 and (2.9).
$\mathbf{Z}$	is the set of integers. See (2.2).
$\mathbf{Z}^+$	is the set of whole numbers. See (2.2).
$\mathbf{Z}^{++}$	is the set of natural numbers. See (2.2).
$z_-[n]$, $z_+[n]$	These functions were involved in the minimum phase spectral factorization of $1 + M_{ci}^{\mathrm{T}}(f)$. See (3.82).
$Z_-^{\mathrm{T}}(f)$, $Z_+^{\mathrm{T}}(f)$, $Z^{\mathrm{T}}(f)$	These functions were involved in the minimum phase spectral factorization of $1 + M_{ci}^{\mathrm{T}}(f)$. See (3.82).

Table II Greek-based notation

Greek symbol	Meaning
α	is the excess bandwidth parameter for square-root raised cosine pulses. See (5.5).
$\gamma_{dco}^{I,N}$	is the ratio of the power of the signal to the sum of the powers of the cyclostationary interference plus filtered noise. This ratio is determined at the input to the detector of the equalizer. See (3.97).
$\delta[n]$	is the notation used for the Knonecker delta function. See (2.6).
$\delta(t)$	is the notation for the Dirac delta function.
ζ	is a dummy variable. $\zeta \in \mathbb{C}$.
μ	is the mean value of a random variable.
$\mu_{ci}(t)$	is the component of the cyclostationary interference with L interferers but without noise. See Fig. 2.2 and (2.21).
$\nu(t)$	is the interference added to the signal carrying the data of interest. This signal appears at the receiver input. See. Fig. 2.1, (2.15), (2.33).
$\nu_{ci}(t)$	is the cyclostationary interference added to the signal carrying the data of interest. This signal appears at the receiver input. See Fig. 2.1, Fig. 2.2, (2.15), and (2.21).
$\nu_{sn}(t)$	is the stationary noise added to the signal carrying the data of interest. This signal appears at the receiver input. See. Fig. 2.1, Fig. 2.4, and (2.33) to (2.37).
ξ	is a dummy scalar. $\xi \in \mathbb{C}$.
$\Xi(t)$	is a dummy function. $\Xi(t) \in \mathbb{C}$.
π	is the ratio of the circumference of a circle to its diameter.
σ	is the standard deviation of a random variable.
σ_{bd}^2	is that component of ε_{dco} contributed to by the bias in the estimate of the received data. See (3.94) and (3.95).
σ_{ci}^2	is that component of ε_{dco} contributed to by the interference in the sampled equalized combined co-channels. See (3.94) and (3.95).
σ_d^2	is variance of the transmitted data. See (2.4), (2.5), and (2.18).

Table II (Continued) Greek-based notation

Greek symbol	Meaning
σ^2_{isi}	is that component of ε_{dco} contributed to by the precursor ISI in the sampled equalized combined channel. See (3.94) and (3.95).
σ^2_n	is that component of ε_{dco} contributed to by the sampled equalized noise. See (3.94) and (3.95).
τ	is a dummy parameter used as a time index. $\tau \in \mathbf{R}$.
$\phi_0(t)$	is the impulse response of the combined channel. See (2.10), Fig. 4.4, and Fig. 4.10.
$\Phi_0(f)$	is the frequency response of the combined channel. See (2.23), (4.8), and (5.12).
$\{\phi_i(t) \mid i \in \mathbf{L}_1\}$	are the impulse responses of the combined co-channels. See (2.20). Also, see Figs. 4.8, 4.9, and 4.10.
$\{\Phi_i(f) \mid i \in \mathbf{L}_1\}$	are the frequency responses of the combined co-channels. See (2.24), (4.13), and (5.13).
$\{\underline{\phi_i}[n] \mid i \in \mathbf{L}_0\}$	are disrete-time impulse responses obtained by sampling $\{\phi_i(t) \mid i \in \mathbf{L}_0\}$ at a rate above the Nyquist rate. See (4.18), (4.27), and (4.28).
$\mathbf{\Phi}_0(f)$	is a vector containing $(1/\mathrm{T})$- spaced samples of the frequency response of the combined channel. See (3.74).
$\{\mathbf{\Phi}_i(f) \mid i \in \mathbf{L}_1\}$	are vectors containing $(1/\mathrm{T})$- spaced samples of the frequency responses of the combined co-channels. See (3.74).
$\phi_{sn}(t)$	is the impulse response of the spectrum shaping filter used to generate the stationary noise. See Fig. 2.4 and (2.34).
$\Phi_{sn}(f)$	is the frequency response of the spectrum shaping filter used to generate the stationary noise. See (2.34) and (2.35).
$\Psi_0(f)$	is the frequency response of the combined channel when the channel only contains ISI and additive white noise. See (D.7).
$\psi_0(t)$	is the impulse response of the combined channel when the channel only contains ISI and additive white noise. See Fig. D.1, Fig. D.2, and (D.1).

Table III Miscellaneous notation

Miscellaneous symbol	Meaning
$\bullet$	dummy parameter
$\blacklozenge$	dummy parameter
$\therefore$	therefore
$\forall$	for all
$<$	is less than
$\leq$	is less than or equal to
$>$	is greater than
$\geq$	is greater than or equal to
$+$	plus
$-$	minus
$\times$	times
$/$	divided by
$\frac{\bullet}{\blacklozenge}$	$\bullet$ divided by $\blacklozenge$
$=$	is equal to
$\approxeq$	is approximately equal to
$\neq$	is not equal to
$\{\bullet\}$	the set of $\bullet$
$\blacklozenge \mid \bullet$	$\blacklozenge$ evaluated under the condition $\bullet$
$\in$	is an element of
$\notin$	is not an element of
$\sqrt{\bullet}$	the square root of $\bullet$
$\lvert\bullet\rvert$	the magnitude of the complex number $\bullet$, or the absolute value of the real number $\bullet$
∞	infinity

Table III (Continued) Miscellaneous notation

Miscellaneous symbol	Meaning
$\ldots, \vdots, \ddots$	pattern continues as shown
$\cap$	as in $\bullet \cap \blacklozenge$ has the meaning: *the set formed by the intersection of* $\bullet$ *with* $\blacklozenge$
$\cup$	as in $\bullet \cup \blacklozenge$ has the meaning: *the set formed by the union of* $\bullet$ *with* $\blacklozenge$
$\star$	as in $\bullet \star \blacklozenge$, denotes the convolution of the function $\bullet$ with the function $\blacklozenge$. The convolution may be over a continuous integration or a discrete summation. An example of a continuous case is shown in (2.20) and an example of a discrete case is shown in (2.44).
$\mid$	as in $\{\bullet \mid \blacklozenge\}$, has the meaning: *the set of* $\bullet$ *such that* $\blacklozenge$
$\blacklozenge(\bullet)$	often has the meaning: $\blacklozenge$ *is indexed by the continuous variable* $\bullet$
$\blacklozenge[\bullet]$	often has the meaning: $\blacklozenge$ *is indexed by the discrete variable* $\bullet$
$\int$	as in $\int_x^y \blacklozenge(\bullet)\ d\bullet$ is the integral of the function $\blacklozenge(\bullet)$ as $\bullet$ varies from x to y.
$\sum$	as in $\sum_{\bullet=i}^{k} \blacklozenge[\bullet]$ is the sum of the values $\blacklozenge[\bullet]$ indexed over $\bullet$ as $\bullet$ is incremented by one from i to k.
$\bigcup$	as in $\bigcup_{\bullet=i}^{k} \blacklozenge[\bullet]$ is union of the sets $\blacklozenge[\bullet]$ indexed over $\bullet$ as $\bullet$ is incremented by one from i to k.
$(\bullet, \blacklozenge)$	is a point in the two-dimensional Euclidean space.
$[\bullet, \blacklozenge]$	is the set of real numbers in the closed interval from $\bullet$ to $\blacklozenge$.
$*$	denotes complex conjugate transpose. It appears as a superscript, as in $\bullet^*$.
$\langle \bullet \rangle$	is a scalar obtained by integration of the function $\bullet$ according to the definition in (3.90).
$< \bullet, \blacklozenge >_c$	is an inner product formed between the continuous-time functions $\bullet$ and $\blacklozenge$. See (3.44).
$< \bullet, \blacklozenge >_d$	is an inner product formed between the discrete-time functions $\bullet$ and $\blacklozenge$. See (3.45).

Table III (Continued) Miscellaneous notation

Miscellaneous symbol	Meaning
$[\bullet]_-$	is the discrete-time continuous-frequency inverse Fourier transform of the anti-causal part of the sequence whose discrete-time continuous-frequency Fourier transform is given by $\bullet$. See (3.65), (C.2), Appendix C, and Table C.1.
$[\bullet]_{--}$	is the discrete-time continuous-frequency inverse Fourier transform of the strictly anti-causal part of the sequence whose discrete-time continuous-frequency Fourier transform is given by $\bullet$. See Appendix C, (C.3), and Table C.1.
$[\bullet]_+$	is the discrete-time continuous-frequency inverse Fourier transform of the causal part of the sequence whose discrete-time continuous-frequency Fourier transform is given by $\bullet$. See Appendix C, (C.3), and Table C.1.
$[\bullet]_{++}$	is the discrete-time continuous-frequency inverse Fourier transform of the strictly causal part of the sequence whose discrete-time continuous-frequency Fourier transform is given by $\bullet$. See Appendix C, (C.3), and Table C.1.
$\blacklozenge^{\bullet}$	is $\blacklozenge$ raised to the power $\bullet$, provided $\bullet$ is not the symbol T. Another exception is $Q^{-1}(\bullet)$, which means the inverse of the $Q(\bullet)$ function.
$i = \begin{cases} k & , m \\ l & , n \end{cases}$	i is equal to k if m is true, or i is equal to l if n is true.

Chapter 1
Introduction

1.1 Motivation for this Thesis

Demands for digital communication services have been steadily increasing and this trend is expected to continue [1–9]. Among the effects of this trend are associated increases in information rates through communication channels. Often it becomes necessary to make more effective use of existing communication channels if alternatives do not exist. Whether or not these increases are difficult to obtain depends heavily on the type of channel.

A channel which has alternatives are metal telephone wires, also called twisted pairs [10–13]. The telephone companies have spent a great deal of money building up the network of telephone wires for analog voice communication. However, the demand for digital services [1, 2, 10, 11, 13, 14] has resulted in these twisted-pair metal telephone wires being used in a manner beyond what was originally intended. They are used to transmit digital data, and at frequencies much higher than those that are used for analog voice communication. Inevitably, many new problems had to be solved, such as dealing with increasing levels of crosstalk between wires. But alternatives to metal twisted pairs exist, notably fiber optic cables which can carry digital data at very high information rates. However, the widespread use of fiber optic cables for the applications suggested in [2, 13] has not occurred, and the reason is that fiber optic cables are not economical for bit rates less than about 1 Mbits/s for new installations [3]. It is estimated that 25 percent of the assets of the regional phone companies are in the loop plant and at present only a small percentage of those are optical fiber [7]. It is less expensive to use the existing network until it evolves into fiber, and optimistic estimates predict complete fiber penetration by the year 2010 at the earliest [15]. Even after fiber usage has settled into its appropriate share of the communication channels, twisted pairs may have an application as short links to a fiber backbone network [7]. Some evidence of this use

of twisted pairs exists presently in the form of standards for local area networks using twisted pairs at 10 M bits/s over short distances [12].

The radio channel frequently does not have alternatives. The demand for services requires more efficient use of the radio spectrum and the application of many techniques such as closer packing of frequency-division multiplexed [16] signals, or smaller distances among frequency re-use systems [17, 18]. These improvements in spectral efficiency can cause more co-channel interference (CCI) and adjacent-channel interference (ACI). CCI is the interference between signals with similar carrier frequencies, whereas ACI is the interference between signals with different carrier frequencies which are close enough to cause overlaps in the spectrum.

In the examples above, increasing amounts of mutually induced interference occur among digital systems. The term mutually induced is used to reflect the fact that a system which causes more interference to other systems should expect to receive an appropriate amount of interference in return. Since the interference comes from digital systems which transmit their random data at periodic intervals, the interference experienced by a receiver can be statistically periodic. Interference statistics such as the instantaneous power or the autocorrelation function can be periodic, hence the term cyclostationary [19, 20].

This thesis is mainly concerned with receivers that make decisions at the same rate as that used to transmit the data. This rate is called the symbol rate. Therefore some of the analytical subtleties that arise in other continuous-time contexts [20, 64] do not arise here. For example, the results turn out to lead to time-invariant equalizer structures. Thus the interference suppression properties of equalizers that are investigated are essentially based on the property that the interference is synchronous with the signal carrying the data of interest, that is the data of the interferers is transmitted at the same rate as the data of interest.

Dealing with this impairment, called cyclostationary interference, requires improved understanding of communication system design and implementation. The aspect of communications system design that is being considered is equalization. Equalization

has been taken to mean many kinds of processing [21], but it has its roots in the concept of synthesizing the inverse of the distortions in a channel frequency response in order that data can be more easily extracted from a less-distorted (equalized) signal.

The increasing number of digital communication systems often results in increased levels of mutually induced cyclostationary interference. To assist in maintaining reliable communication, equalization is shown to be an effective technique to mitigate the effects of cyclostationary interference.

1.2 Background and Literature Survey

1.2.1 Interference

Applications with mutually induced interference occur frequently in various communication systems. Interference occurs in the quest of an integrated-services digital network (ISDN) by transmission of data over twisted pairs [2, 10, 11, 13, 14, 22] as well as in many different radio applications, such as those for the indoor channel [23–28], the land mobile radio channel [18, 29–43], the microwave radio channel [44, 45], and the satellite channel [46–50]. Also, this mutually induced interference occurs in magnetic disk recording [51–53]. Intersymbol interference (ISI), CCI and ACI occur in twisted pairs and radio applications. But in the magnetic recording channel the interference is mainly due to ISI, inter-track interference, and incompletely erased previous data. It has been pointed out that ISI, CCI and ACI have fundamentally the same structure [54, 55], and they have been called multidimensional interference.

In general, when the communication is digital, the interference is cyclostationary [19, 20, 43, 56–83]. There are many applications where the properties of the cyclostationary interference can be exploited for advantage, as recently summarized in [80]. However, the cyclostationary interference considered in this thesis is the specific type which arises from interfering digital data signals. Also, the specific case has been studied where the symbol rates (signalling intervals) are identical among all the communications systems; however, a brief comment is made later for the case where the systems used mixed

symbol rates.

The amount of cyclostationarity present in the interference can vary dramatically. One issue is the kind of criteria that can be used to measure the amount of cyclostationarity in the interference. The approach taken in this thesis is to use more direct criteria which give the performance of a system, instead of indirect criteria such as those which are confined to describe only the interference. Examples of more direct criteria are minimum mean square error (MMSE) and bit-error rate (BER) [84–87]. An example of a criterion which is confined to describe only the interference is the instantaneous power variation of the interference throughout the symbol period. These indirect measures often lead to similar conclusions about the amount of cyclostationarity present in the interference. For example, if there are a number of interfering data signals at the input to a receiver, there is likely to be more interference cyclostationarity if a few of those interferers contribute to most of the total interference power.

There will often be other impairments besides cyclostationary ISI, ACI, and CCI. However, the only one that is considered is stationary additive white channel noise, and this impairment sets a fundamental limit on the highest performance of a communication system [88, 89].

One final assumption about the interference is that it is of a nature where its suppression is easier by avoiding it, instead of estimating it and subtracting it.

The concept of avoiding interference is similar to the idea of generating nulls in the pattern of an antenna array [90], but it will take more subtle forms and will be expanded throughout this thesis. Examples where the interference has been estimated and subtracted are: echo cancelling [68, 91–99], subtracting adjacent-channel interference in digital radio [33, 100, 101], subtracting cross-polarization interference in digital radio [102], subtracting co-channel interference in satellite systems [46], and finally generalized maximum likelihood sequence estimation of all signals and interferers in code-division-multiplexed multiple-access channels [103].

1.2.2 Equalizer Analyses

The optimal receiver for the interference model used in this work is that receiver which estimates the sequences of the data of interest and all of the interferers [103]. A related receiver is one which estimates only the data of interest but exploits the cyclostationary interference power variations to improve performance [113].

The two main types of equalizers of consideration in this thesis are the further suboptimal linear and the decision-feedback equalizer. More detailed descriptions of these equalizers will follow in later Chapters. The following discussions of equalizer analyses are based mainly upon these two types of equalizers. The discussion is divided into two sub-topics to reflect the two main topics in Chapter 3. The first sub-topic deals with the bandwidth of the transmitter pulses relative to the symbol rate when cyclostationary interference is present in the channel. The second sub-topic deals with expressions for the minimum mean square performance of equalizers.

The first sub-topic regarding the bandwidth of the transmitter pulses in cyclostationary interference has been the subject of relatively little previous research compared to the second sub-topic. To facilitate explanation, let the symbol period be T and the symbol rate be $1/T$. The effect of transmitter pulse bandwidth relative to the symbol rate is well known [104] when only ISI is present. One major result of this work was that the folded frequency spectrum in the frequency range from $-1/(2T)$ to $+1/(2T)$ must be flat to achieve zero ISI.

Later, an idea was described for a linear equalizer in only ISI [85, 105]. This idea is that the contribution of the components of the transmitter signal spectrum in the frequency range from $-1/(2T)$ to $+1/(2T)$ are equivalent for purposes of complete ISI suppression to their corresponding components shifted by integer multiples of $1/T$ outside that range. These results for only ISI suppression were partially generalized for suppression of both ISI and CCI [106], however, in [106] the author mainly dealt with transmitter pulse bandwidth less than the 100 percent excess bandwidth of $1/T$. Since in [54, 55] it is suggested that ISI, ACI, and CCI are fundamentally equivalent signals, this leads to the concept that some of the bandwidth ideas applicable to ISI might be

also applied to ACI and CCI.

Other developments in effects of bandwidth and interference suppression occurred through the development of the theory of *spectral correlation* in [60, 62–64, 77, 79, 80, 107], and this theory is applicable in a wide variety of applications. For the case of systems which use identical symbol rates, the theory of spectral correlation shows that in linear modulation schemes the components of the signals exhibit correlation among frequencies that differ by shifts of $1/T$. This property can be exploited by equalizers and discrete-time filters to achieve interference suppression, as evidenced by the work with fractionally spaced linear equalizers and filters in [20, 107]. In [77, 80] appeared the discovery, based on the theory of spectral correlation, of the result regarding the benefit of wide relative transmitter bandwidth on the ability to suppress cyclostationary interference.

The benefits of wide relative transmitter bandwidths were also recently discovered as shown in [68], in the context of equalizer applications for a wide variety of applications where interference was present.

However, the discovery of the benefit of wide relative transmitter bandwidth on the ability to suppress cyclostationary interference, claimed to be a contribution of this thesis, was originally reported in [67, 69, 78]; it was concurrently discovered and then reported in [68, 77, 80].

Calculations which demonstrated this benefit in subscriber-line interference were concurrently performed, as reported in [74].

The second sub-topic deals with expressions for the minimum mean square error of equalizers. It is centered around the expressions for the continuous-time infinite-length linear and decision-feedback equalizers in the presence of ISI, cyclostationary interference and additive white noise.

In [105] is the expression for the minimum mean square error of a continuous-time infinite-length linear equalizer in the presence of ISI and additive white noise. In [108, 109] is the expression for the minimum mean square error of a continuous-time infinite-length decision-feedback equalizer in the presence of ISI and additive white

noise. Expressions for the MMSE of a finite-length discrete-time DFE in cyclostationary interference are given in [51, 65, 66, 110, 111]. The expressions in [51, 110] appear in a more general situation where a receiver has multiple inputs and is required to estimate the data from multiple streams. Many subtle relationships between single- and multiple-input receivers are described in [74]. However, a brief comment will be made here.

Single-input single-data systems are those where a receiver has a single input from the channel and estimates a single data stream. These systems are considered in this thesis where the receiver is required to estimate the data from a single transmitted sequence in the presence of additive cyclostationary interference and white noise. As evidenced by the following long list, related interference suppression work has been published for: single-user detectors in spread-spectrum systems that are not limited by the interference [112], sequence estimation techniques with improved performance when the cyclostationarity of the interference is enhanced [75, 113], MMSE expressions for linear equalizers with a single interferer for linear and non-linear modulation schemes [114, 115], linear filters which remove the effect of interference [107], finite-length adaptive equalizers to combat fading and adjacent-channel interference [37], MMSE expressions for linear equalizers in cyclostationary interference and stationary noise [68], finite-length linear and decision-feedback equalizers in a radio environment [116, 117], and finally narrowband interference in spread spectrum systems [118, 119].

Single-input multiple-data systems are those where multiple data streams are multiplexed into a single channel and a single-input receiver separates the data streams [106, 120].

Multiple-input single-data systems are those that perform diversity combining from multiple receiver inputs, such as antennas, in order to obtain a better estimate of a single transmitted data sequence [26–28, 30, 100, 121]. An MMSE expression appears in [121] for a continuous-time infinite-length DFE in ISI and additive white noise for dual diversity inputs. These systems are closely related to the next classification.

Multiple-input multiple-data systems are those where a receiver with multiple inputs from the channel estimates data from multiple data streams. As evidenced by the

following long list, related work has been published regarding: linear equalizer MMSE expressions as well as linear equalizer and decision-feedback equalizer simulations in the presence of crosstalk [120, 122], capacity estimates for channels with crosstalk [123], minimizing the probability of error of a matrix receiver [54, 55], cross-polarization interference suppression in a satellite [49], dual-diversity MMSE expressions for continuous-time infinite-length linear equalizers [124], cross-polarization interference cancellation for radio channels [102], MMSE expressions for matrix linear receivers [125], generalized sequence estimation of all the signals in a spread spectrum system [103], adapting the transmitters to suppress crosstalk at a dual-input receiver [126], and MMSE expressions for matrix linear receivers in crosstalk as well as conditions for complete interference suppression [74, 127].

The reason for bringing the multiple-input receivers into the discussion is because they encapsulate the MMSE expressions for the single-input receivers. In [127, 128], the authors analyze one multiple-input multiple-output channel with one multiple-input multiple-output co-channel and additive white noise. However, the same MMSE expression for the receiver may be obtained by judiciously placing zeros in the matrix channel in [125] before the receiver optimization. Thus the presence of interferers can be modelled as a specific case of the situation without interferers; it simply requires a sparse [129] cross-coupled channel matrix. Hence the most general analysis for the receiver is in [125]. However, it has been pointed out that this type of analysis does not hold for the transmitter matrix optimization [74].

1.2.3 High-speed Digital Subscriber-line Systems

As emphasized earlier, one reason for the economies of using subscriber lines was the huge investment over the last 80 to 100 years by the telephone companies. Their original use was to provide analog voice communications, but more recently they have been used for basic-rate ISDN (full duplex 144 k bits/s) [2]. This trend has continued with the goal of full-duplex T1 rates (1.544 M bits/s) [130–132] over a reduced set of subscriber lines as evidenced by [133–136]. The goal of putting T1 rates on one or two

twisted pairs has come under the title high-speed digital subscriber-lines (HDSL) [13]. In addition to the potential for primary-rate ISDN (full duplex 1.536 M bits/s) over twisted pairs, presently HDSL has a more important consideration. This consideration is the goal of reducing the costs of T1 services beyond the line conditioning techniques which originated in [137]. In [4] it was mentioned that there would be interest in lowering the costs of installation and maintenance of existing T1 systems by application of HDSL technology.

The survey paper [13] gives an overview of the issues associated with HDSL transmission. Therefore the remainder of the discussion about this topic is centered around a few key issues that are relevant to exploiting the cyclostationarity of the near-end crosstalk (NEXT). The most significant transmission impairment is the amount of NEXT coupling through twisted pairs in the central office. To make systems more reliable, Bell Communications Research recommended that an additional 6 dB of NEXT power, beyond near-worst case NEXT conditions, be added as a safety margin for prototype HDSL transceivers. Also, for analytical models and simulations this safety margin was recommended to be 12 dB [13].

Systems were being developed in an attempt to achieve HDSL transmission. One system that was presented [138] transmitted data at 772 k bits/s and had a 3.7 dB NEXT margin for a bit–error rate of 10^{-7} on 12000 feet of 24 AWG in the presence of NEXT having a specific power spectral density [13]. It used a decision-feedback equalizer without coding and had a fixed symbol-spaced forward filter. The performance of this system did not quite reach the 6 dB margin and fell short by about 3 dB[1].

The motivation for this research was to find a way to get another 3 dB of NEXT margin in additional to the general goal of finding techniques to improve digital subscriber-line transmission.

A factor that can affect the performance of digital subscriber-line transmission is

---

[1] However through later refinements of making the bandwidth of the forward filter narrower, an additional 3 dB was obtained [139]; the narrower filter caused longer error bursts in the DFE, however the BER was still below 10^{-7}.

the relative alignment of the phases of the transmitters in the central office. From the early work in this area [58, 59] it was concluded that for *randomly aligned* phases of the transmitter clocks an additional 3 dB of NEXT margin was required to account for the potential degradations due to the cyclostationarity of the NEXT. Later in [75, 113] it was observed for maximum-likelihood receivers that improved digital subscriber-line transmission could be obtained by exploiting the cyclostationarity of the NEXT. This idea was carried further in [65, 66, 111] where studies of the effects of a finite-length DFE showed the performance improvements which could be achieved when the transmitter phases were *completely aligned* instead of *completely misaligned.* In [140] were published measurements of crosstalk impulse responses, as well as NEXT power variations throughout a symbol period under various conditions of alignment of the transmitter clock phases.

A simulation of a multi-input receiver for processing digital subscriber-line signals was performed in [141] where the effect of the crosstalk was subtracted in much the same way as a DFE. One conclusion of this study was that the achievable error rates would be lower if the crosstalk was treated as a (cyclostationary) data signal, instead of as noise.

Finite-precision implementation effects of the kind reported in [21, 142, 143] contain general results, but have dealt primarily with channels containing only ISI and noise. More recently in [68], results are presented for linear equalizers that suggest numerical problems in implementations.

HDSL systems will use echo cancellers and consideration must be given to how they will interact with equalizers. In [99] two approaches are studied which use jointly adapted and separately adapted structures for echo cancellation and equalization. In the jointly adapted structure the forward filter of the DFE precedes the point where the echo is removed. In the separately adapted structure, the echo is subtracted before the forward filter of the DFE, however, adaptation issues of the structures were not considered. In [91, 92] it was observed for the jointly adapted structure that if the power of the echo is relatively large compared to the signal carrying the data of interest, then the eigenvalue spread of the autocorrelation matrix at the receiver input is large [21,

144, 145]. This means adaptation of the coefficients would have to proceed very slowly. Since digital subscriber-line channels change very slowly with time, the necessary slow adaptation of the coefficients may not be a problem. In cyclostationary interference, although the channels may not change slowly, the characteristics of the signal presented to the equalizer might change abruptly with neighboring transmitters being turned on and off. Hence the faster adaptation of the separately adapted structure may be required, however, the cost associated with the separately adapted structure is that a fractionally spaced forward filter in the DFE requires a fractionally spaced echo canceller, and echo cancellers consume a large part of digital subscriber-line receiver implementations [10, 11]. Another interesting effect is that the residual echo is cyclostationary [68]. Thus, in the separately adapted structure, any residual echo will appear as another cyclostationary signal to the DFE.

Equalizers which exploit the cyclostationarity of the interference may have severe requirements placed on synchronizers. In subscriber-line transmission, there is already a severe requirement on the synchronizer which comes from the echo cancellers' sensitivity to timing jitter [94–96].

1.2.4 Adjacent-channel Interference in Digital Radio

The following is a brief summary of adjacent-channel interference in frequency-division multiplexed systems. Specifically, radio systems are considered because of the widespread use of methods of frequency-division multiplexing to separate radio signals [16]. There are a plethora of radio systems with each one often optimized for its specific channel. Each channel imposes demands on system design, and one of these demands is the problem of adjacent-channel interference. The summary of this topic is centered on using equalizers to suppress adjacent-channel interference in digital radio.

Surveys of BER analysis for systems which are impaired by interference have been given in [57, 146]. Some interference reduction techniques have also been included, but the emphasis has been on analysis techniques to give the performance of systems in the presence of the remaining insuppressible interference. Recent work has shown that this

hitherto insuppressible interference can often be reduced by the use of equalizers and related signal processing techniques.

The first classification of systems is based on whether or not use is made of the decisions of the data of the adjacent-channel interferers. In [100] the postcursor adjacent-channel interference is subtracted from the received signal and the residual precursor adjacent-channel interference is treated as *stationary* noise. In [33] the two adjacent channel's data are detected, followed by construction of an estimate of the adjacent-channel interference, followed by subtraction of this estimate from the received signal. In [101] a finite-complexity multi-dimensional DFE is used where estimates of the interference due to the two ACI signals are subtracted before the detector and the forward filter of the DFE suppresses the precursor ISI and ACI. They assume the spectrum of the signals is such that a guard band is used for every three signals.

The second classification of systems is based on the equalizer *nulling out* the adjacent-channel interference, not making decisions. This so-called nulling out of the interference can be viewed in a number of ways. One can consider that the equalizers: a.) exploit the time-domain correlation in the interference [26, 30], b.) put nulls in the impulse responses of the equalized combined co-channels [78, 106], or *c.*) exploit the spectral correlation of the interference [77, 80, 107].

The ability of these equalizers to suppress the interference depends on the bandwidth of the equalizer. Smaller spacings between the taps of the equalizer with respect to the symbol rate correspond to larger equalizer bandwidths. A property that has been come to be recognized is that, compared to symbol-spaced equalizers, fractionally spaced equalizers are able to provide more adjacent-channel interference suppression [35, 37, 45, 77, 82, 107, 116, 117, 147].

To combat the effects of fading in a radio environment [148], antenna diversity can be used [26–28, 30, 31, 34, 39, 41, 100, 110, 120, 121, 124, 125, 149]. However, the performance gains which have been obtained using diversity have thus far not incorporated the beneficial effects of wide transmitter bandwidths with respect to the symbol rate.

An issue of importance to equalizers operating in a radio environment is their ability to track the potentially rapid variations of the channel [30, 34, 37, 38, 40, 41, 150, 151]. Often techniques can be employed to assist the receivers such as periodically sending known training information.

The choice of transmitter pulses will affect an equalizers ability to perform the simultaneous operations of extracting a desired signal while eliminating undesired signals. This operation is made easier for the equalizer if the desired signal and undesired signals are made different in some sense. One method that has been suggested is to use different transmitter pulses [152], and re-use them in the same manner as carrier frequencies [18]. One example of the existing use of different transmitter pulse shapes is in spread spectrum systems [30, 86, 103, 112, 118, 119, 153–156].

The final issue discussed is that of synchronization [60, 157–160]. The importance to exploiting adjacent-channel interference using equalizers is the following. The presence of signal at a receiver input with enhanced cyclostationary properties may provide more information to a synchronization circuit, however, the demands that an equalizer puts on the synchronization circuit may be greater. It is difficult to be more precise in this general discussion.

Often it is difficult to summarize previous research in few sentences since many omissions can occur; it is believed that this summary is sufficient to justify the thesis contributions that follow.

1.3 Thesis Contributions

The premise of this thesis is that the channel is presently, or will be, a critical resource whose efficient use requires the use of interference analysis and interference suppression techniques. The contributions described below are interference analysis and suppression techniques for linear and decision-feedback equalizers operating in the presence of ISI, additive white noise, and cyclostationary interference arising from neighboring systems which use similar symbol rates.

The two main classifications of the contributions in Chapter 3 are the analysis of

the conditions for the existence of a generalized zero-forcing linear equalizer and the analysis of the minimum mean square performance of a continuous-time infinite-length decision-feedback equalizer.

The first result deals with the conditions for the existence of a generalized zero-forcing linear equalizer in CCI. This result suggests that: *Every increase in transmitter total bandwidth of size equal to the symbol rate may provide the flexibility to completely suppress an additional cyclostationary interferer by means of linear equalization.*

The second result is a method to predict the existence of a generalized zero-forcing linear equalizer in ISI, ACI, and CCI. The prediction incorporates the effect of transmitter bandwidth, receiver bandwidth, carrier spacing, number of receiver antennas, and the number of CCI signals. From this method comes the prediction that: *With one antenna and a linear equalizer, arbitrarily large receiver bandwidths allow for marginal improvements in spectral efficiency through decreased carrier spacing, but the improvements cannot go below the fundamental carrier spacing value equal to the symbol rate.* Another prediction is that: *Large receiver bandwidths assist multiple antennas in improving the spectral efficiency in that carrier spacing values may go below the symbol rate, even in the presence of co-channel interference.*

The third result that was obtained also deals with the conditions for the existence of a generalized zero-forcing linear equalizer in CCI. This result suggests that: *The number of interferers that may be suppressible by a linear equalizer increases with the product of the total bandwidth relative to the symbol rate and the number of antennas.*

The fourth result is that: *Alternative insight is offered, by the analyses of the generalized zero-forcing linear equalizer about the ability of equalizers to suppress cyclostationary interference.*

The fifth result is that: *Enhancing the differences between combined channel and combined co-channels offers the equalizers a greater opportunity for interference suppression.*

The sixth result is an *expression* for the minimum mean square error of a continuous-time infinite-length decision-feedback equalizer in the presence of intersymbol interfer-

ence, additive white noise, and cyclostationary interference from neighboring systems which use identical symbol rates.

The seventh result is a *derivation* that the aforementioned optimal decision-feedback equalizer is time invariant.

The eighth result is a *demonstration* of how the analyses of the generalized zero-forcing linear equalizer may be extended to the situation where the signal carrying the data of interest uses different symbol rates than the cyclostationary interference.

The ninth result is a theoretical *comparison* of the latter expression with other expressions for the linear equalizer and for stationary noise with the same power spectrum as cyclostationary interference. One of the results of these comparisons is that equalizer performance in cyclostationary interference can be better or worse than that in stationary noise. In the applications in this thesis the performance in cyclostationary interference is rarely worse than in stationary noise, and when it is worse it is slightly worse.

In Chapter 4 there are two additional contributions. The tenth result is that for the model of the subscriber-line system used, equalizers are able to achieve *improved interference suppression* under certain joint conditions of wide enough transmitter pulse bandwidth and sufficiently aligned phases of the transceiver clocks in the central office.

The eleventh result is a comparison between the implementation of an equalizer in cyclostationary interference and stationary noise. It suggests the *implementation costs* to exploit the cyclostationarity of the interference in terms of increased adaptive equalizer coefficient precision, similar convergence rates, and longer convergence times.

In Chapter 5 there are two additional contributions. Results of calculations obtained using the previously derived expressions were compared to predictions from the generalized zero-forcing linear equalizer, in the presence of adjacent-channel interference, with no co-channel interference, and one receiver antenna. The twelfth result is the *agreement* among those analysis techniques of Chapter 3 to predict good system operating points.

The final result is a *demonstration* of how the equalizers are able to extract the signal

of interest and to provide interference suppression even under conditions of complete mutual overlaps of all signals.

Inherently a complete analysis of all ramifications is not possible. The aforementioned issues were those that seemed the most relevant, that is, suggestions of potential for gains and for system operating conditions that appear to provide the best opportunities for equalizers to suppress interference. Such an approach seemed warranted because the absence of a potential for gains would mean no further research would be required. To help clarify the contributions, what remains in this section is description of some potentially relevant issues which have not received attention. This is not intended to diminish their importance, but instead it means that they are beyond the scope of this work. Unconsidered issues were: constrained optimization of the shape of the transmitter pulses by the methods in [74, 105, 106, 108, 124, 125, 141, 161, 162], bit synchronization [60, 61, 95, 96, 158–160], tracking channel variations [30, 34, 37, 38, 40, 41, 150, 151], the optimal number of bits per symbol [51, 163], non-linear modulation [164], and coding [26–28, 37, 86, 134, 136, 162, 165–170].

1.4 Thesis Organization

This description of the thesis organization follows the table of contents.

In Chapter 1, the motivation, background, and literature survey put the thesis contributions into perspective. This section describes how this thesis is organized to make those contributions.

Chapter 2 details the model of the transmitter, channel, the interference types, and the receiver types. The two types of interference are called cyclostationary interference and stationary noise. The stationary noise interference type has the same power spectrum as the cyclostationary interference type. The two receivers are a continuous-time infinite-length linear equalizer and a continuous-time infinite-length decision-feedback equalizer. The primary assumptions about the system are that the data of interest is transmitted at identical symbol rates as the interferers and all the data are mutually uncorrelated.

Chapter 3 shows three types of analyses that are performed on linear and decision-

feedback equalizers. The first deals with the conditions for the existence of a generalized zero-forcing linear equalizer in ISI, ACI, and CCI. This is an analysis based on the degrees of freedom that a linear equalizer might have when it has to trade-off the suppression of ISI, ACI, CCI, and noise. The second type of analysis gives an expression for the MMSE of a continuous-time infinite-length decision-feedback equalizer in the presence of ISI, additive white noise, and cyclostationary ACI and CCI. The third type of analysis gives a theoretical *comparison* of that MMSE with the MMSE of a linear equalizer, as well as a comparison to the MMSE expressions in other interference environments.

In Chapter 4 there are three main parts. The first is the discussion of the model used for the subscriber-line system, with particular emphasis on the model used for the near-end crosstalk. The second part contains calculations using the previously derived MMSE expressions with the subscriber-line system model. These calculations are used to evaluate the ability of linear and decision-feedback equalizers to exploit the cyclostationarity of the subscriber-line near-end crosstalk interference. The third part contains the results of simulations of adaptive equalizers in such an environment in order to further quantify the implementation costs of designing an equalizer to exploit the cyclostationarity of the interference.

In Chapter 5 there is a brief development of the model of the frequency-division multiplexed system, however, the rest of this chapter is concerned with evaluating the performance of equalizers in cyclostationary adjacent-channel interference. These evaluations take place under various conditions of transmitter bandwidth, receiver bandwidth, and carrier spacing, in the presence of no co-channel interference and using one receiver antenna.

In Chapter 6 the thesis is concluded, followed by a discussion of potential future work.

In Appendix A, a few observations are made by relaxing the condition that the equalizers have time-invariant impulse responses. It is shown how the MMSE expression derived in Chapter 3 is the same whether or not the decision-feedback equalizer is time

variant or time invariant. Also, the generalized zero-forcing linear equalizer analysis of Chapter 3 is applied to the situation where the symbol rates of the data of interest and the interference differ by a factor of two.

Appendix B gives the details of calculus minimizations to support the derivation of the MMSE a decision-feedback equalizer in cyclostationary interference which is discussed in Chapter 3.

Appendix C gives some of the properties of an anti-causal operator that appears in the latter derivation in Chapter 3.

In Appendix D are the derivations of previously known MMSE expressions for a linear equalizer in cyclostationary interference and stationary noise, as well as a decision-feedback equalizer in stationary noise. They are included to put those known results in a form to facilitate comparison to the latter derivation in Chapter 3.

Chapter 2
System Model

Fig. 2.1 provides a block diagram of the major components of the system: the transmitted data $d_0[n]$, the transmitter impulse response $p_{t,0}(t)$, the channel impulse response $c_0(t)$, the interference $\nu(t)$, the receiver, and the estimates of the transmitted data $\widetilde{d}_0[n]$. The dummy variables t and n denote the indices in time. The subscripts in $p_{t,0}(t)$ refer to transmitter number 0.

Note the inherent assumptions of this model. The communication is digital. The data is transmitted using a linear modulation scheme, such as quadrature amplitude modulation (QAM) or quadrature phase-shift keying (QPSK) [84–87]. Since this model includes the complex baseband representation [84, 86], the interference can include both co-channel interference (CCI) and adjacent-channel interference (ACI). In the frequency domain the co-channel interference would be centered at 0 Hz and the adjacent-channel interference would be centered at some set of non-zero carrier frequencies so that it would exhibit only vestigial components in the baseband frequencies.

The receiver has only one input from the channel and the receiver is required to estimate the data from only a single transmitter. In Section 3.2, a comment will be made on the effect of multiple-input receivers using antenna diversity; but that discussion is intended to put single-input receiver results in perspective with the multiple-input receiver situation.

2.1 Transmitter

For convenience, the following dummy variables are defined:

$$\begin{aligned} i,\ k,\ l,\ m,\ n &\in \mathbf{Z} \\ t,\ t_1,\ t_2,\ \tau &\in \mathbf{R} \end{aligned} \tag{2.1}$$

$$\begin{aligned} \mathbf{Z} &= \{\text{integers}\} \\ \mathbf{Z}^{+} &= \{z \mid z \in \mathbf{Z},\ z \geq 0\} \\ \mathbf{Z}^{++} &= \{z \mid z \in \mathbf{Z},\ z > 0\} \end{aligned} \tag{2.2}$$

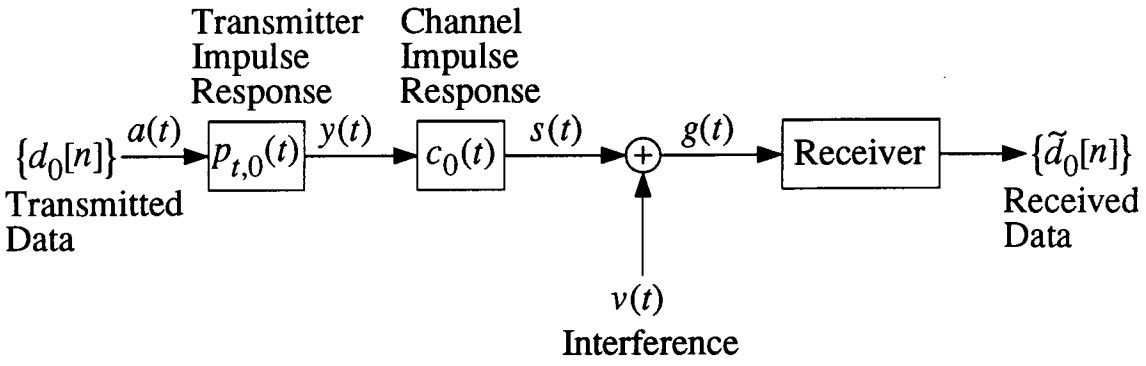

Figure 2.1 System model

$$\begin{aligned} \mathbf{R} &= \{\text{real numbers}\} \\ \mathbf{C} &= \{\text{complex numbers}\}. \end{aligned} \tag{2.3}$$

The transmitted data, $d_0[n]$, shown in Fig. 2.1, have the properties that they are complex, have zero mean, have unit variance, and are mutually uncorrelated in time:

$$\begin{aligned} E_d[\, d_0[n]\,] &= 0 \\ E_d[\, d_0[n]\, d_0^*[m]\,] &= \sigma_d^2\ \delta[n-m] \end{aligned} \tag{2.4}$$

The variance of the data is denoted by:

$$\sigma_d^2 = 1 \tag{2.5}$$

the *Kronecker delta function* is denoted by:

$$\delta[n] = \begin{cases} 1 & , \quad n = 0 \\ 0 & , \quad n \neq 0 \end{cases} \tag{2.6}$$

the symbol $E_d[\bullet]$ denotes expectation of the quantity $\bullet$ over the ensemble of $d_0[n]$ [171], and the symbol $*$ denotes complex conjugate transpose[2]. Note that this model does not limit the number of data levels; only the variance of the data levels is constrained.

The variance of the data, σ_d^2, was set to unity without loss of generality since the appropriate scaling factors can be included in the transmitter impulse response, $p_{t,0}(t)$. Also, it is stressed again that the data is complex unless explicitly specified otherwise. In Fig. 2.1, the notation $\{d_0[n]\}$ applied to the input of the transmitter filter means that conceptually the data is modulated upon a sequence of Dirac delta functions so that the input to the transmitter filter, $a(t)$, is the following signal :

$$a(t) = \sum_{n=-\infty}^{\infty} d_0[n]\ \delta(t - n\mathrm{T}) \tag{2.7}$$

where the *Dirac delta function* is denoted by:

$$\delta(t) \tag{2.8}$$

---

[2] Although the quantities involved are presently scalars, the transpose operation will be more relevant in later chapters when dealing with matrices.

and the *symbol period* is T. The *symbol rate* is $1/\mathrm{T}$. This means that the output of the transmitter is the signal which is linearly modulated with the data:

$$y(t) = \sum_{n=-\infty}^{\infty} d_0[n]\, p_{t,0}(t - n\mathrm{T}). \tag{2.9}$$

2.2 Channel

Define the impulse response of the *combined channel*, $\phi_0(t)$, to be:

$$\begin{aligned} \phi_0(t) &= p_{t,0}(t) \star c_0(t) \\ &= \int_{-\infty}^{\infty} c_0(t-\tau)\, p_{t,0}(\tau)\, d\tau \end{aligned} \tag{2.10}$$

where the symbol $\star$ denotes convolution[3].

The data of interest is carried on the signal $s(t)$, at the input to the receiver, and can be expressed in terms of the impulse response of the combined channel as:

$$s(t) = \sum_{n=-\infty}^{\infty} d_0[n]\, \phi_0(t - n\mathrm{T}). \tag{2.11}$$

The input to the receiver, $g(t)$, is the sum of the signal carrying the data of interest, $s(t)$, and interference, $\nu(t)$, respectively:

$$g(t) = s(t) + \nu(t). \tag{2.12}$$

The different models of interference that have been considered are described in this section.

Define the average power of the signal $s(t)$ to be P_S:

$$P_S = \frac{1}{\mathrm{T}} \int_0^{\mathrm{T}} E\left[|s(n\mathrm{T}+\tau)|^2\right] d\tau. \tag{2.13}$$

---

[3] If the quantities in (2.10) were indexed by a discrete-time variable, then the symbol $\star$ would denote discrete-time convolution and would be computed using a summation instead of an integration [142].

Using (2.11) and (2.4) P_S can be expressed as:

$$P_S = \frac{1}{\mathrm{T}} \int_{-\infty}^{\infty} |\phi_0(t)|^2 \, dt. \tag{2.14}$$

Define the power spectral density [79] of $\nu(t)$ to be $S_\nu(f)$.

2.2.1 Cyclostationary Interference

The cyclostationary interference model is shown in Fig. 2.2 and occurs when the signal $\nu(t)$ in Fig. 2.1 is equal to $\nu_{ci}(t)$ in Fig. 2.2:

$$\nu(t) = \nu_{ci}(t). \tag{2.15}$$

This model is based upon the one described in [54, 55, 58, 106]. Note the following inherent assumptions about this model.

The first component of the interference is the complex baseband white noise which has a two-sided power spectral density No and satisfies:

$$\begin{aligned} E_n[\, n(t) \,] &= 0 \\ E_n[\, n(t_1)\, n^*(t_2) \,] &= \mathrm{No}\, \delta(t_1 - t_2). \end{aligned} \tag{2.16}$$

The symbol $E_n[\bullet]$ denotes expectation of the quantity $\bullet$ over the ensemble of $n(t)$. Unless explicitly stated otherwise No is always positive in order to assure the presence of an impairment which sets a limit on the highest achievable performance of a communication system [89]. The notation for two-sided complex-noise power spectral density, No, implicitly means that the two-sided spectral densities of the real and imaginary components of the noise are each No/2 [84]. Define the two-sided power spectral density of the noise to be:

$$S_n(f) = \mathrm{No}. \tag{2.17}$$

The remaining components of $\nu_{ci}(t)$ are the L additive interfering data signals from neighboring co-channels.

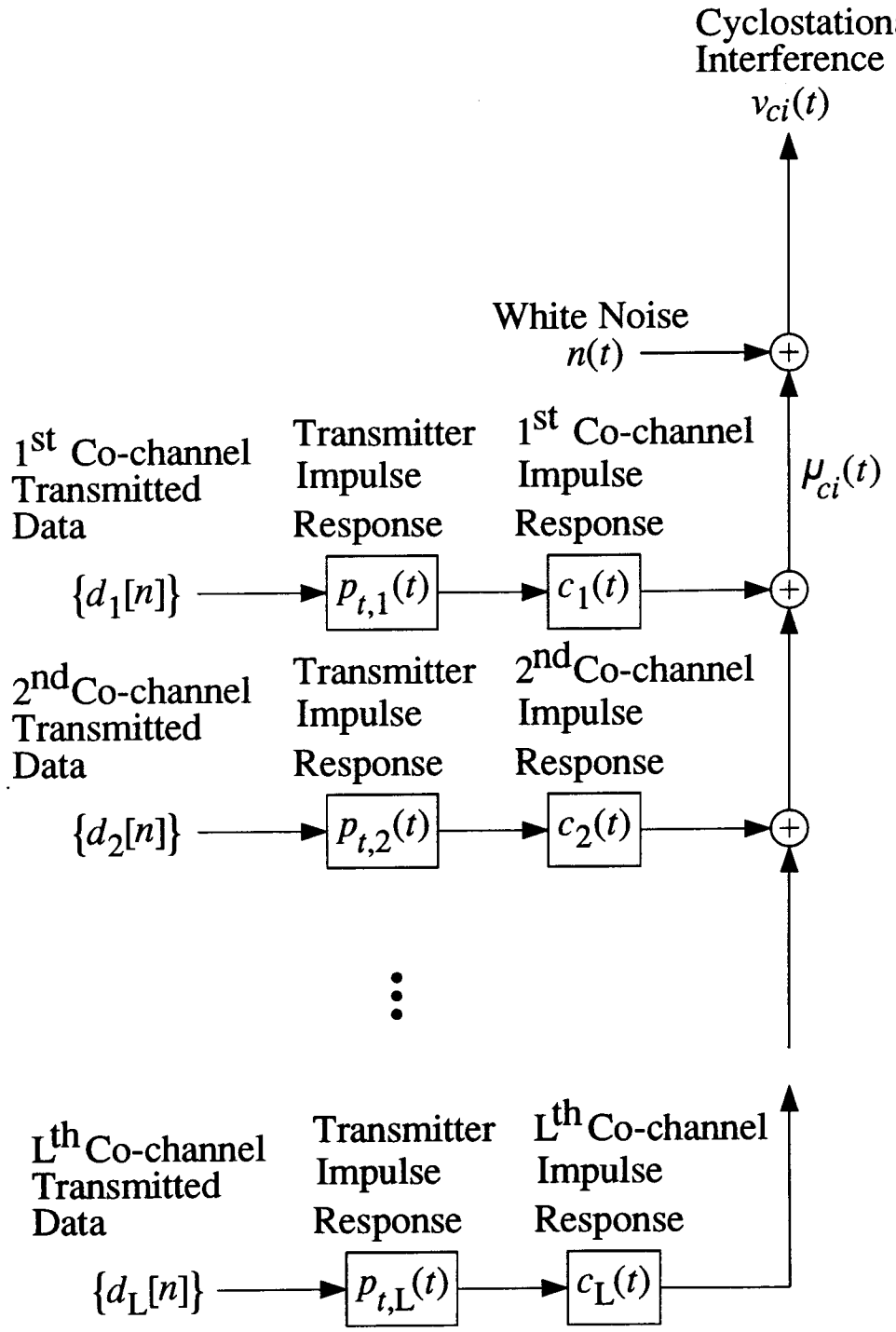

Figure 2.2 Cyclostationary interference model

The data of interest $d_0[n]$, the data of the interferers $\{d_i[n] \mid i \in 1,2,3,\ldots,\mathrm{L}\}$, and the noise $n(t)$ are statistically independent, and the data of the interferers is complex with zero mean and unit variance. Thus:

$$\begin{aligned} E[\, d_i[n] \,] &= 0 \\ E[\, d_i[n]\, d_k^*[m] \,] &= \sigma_d^2\, \delta[i-k]\, \delta[n-m] \\ E[\, d_i[n]\, n^*(t) \,] &= 0 \\ E[\, d_i^*[n]\, n(t) \,] &= 0 \\ E[\, n(t) \,] &= 0 \\ E[\, n(t_1)\, n^*(t_2) \,] &= \mathrm{No}\, \delta(t_1 - t_2) \\ i,k &\in \mathsf{L}_0 \end{aligned} \tag{2.18}$$

where the following definitions are used. The sets L_0 and L_1 are defined as:

$$\begin{aligned} \mathsf{L}_0 &= \{0,1,2,\ldots,\mathrm{L}\} \\ \mathsf{L}_1 &= \{1,2,3,\ldots,\mathrm{L}\} \end{aligned} \tag{2.19}$$

and the symbol $E[\bullet]$ denotes expectation of the quantity $\bullet$ over the ensembles of $\{d_i[n] \mid i \in \mathsf{L}_0\}$ and $n(t)$.

The transmitters of the neighboring co-channels, in Fig. 2.2, use the transmitter impulse responses, $\{p_{t,i}(t) \mid i \in \mathsf{L}_1\}$, and the same symbol rate, 1/T, as that used to transmit the data of interest[4].

Note that the transmitters for both the channel and the co-channels use a linear modulation scheme.

Define the impulse response of *combined co-channel* i as:

$$\begin{aligned} \phi_i(t) &= p_{t,0}(t) \star c_i(t) \\ &= \int_{-\infty}^{\infty} c_i(t-\tau)\, p_{t,i}(\tau)\, d\tau \\ i &\in \mathsf{L}_1. \end{aligned} \tag{2.20}$$

---

[4] A brief comment will be made in Appendix A.2 regarding a situation where the data of interest is transmitted at a different symbol rate than that of the neighboring transmitters; however, Appendix A.2 should not be read until this issue is brought up again in Section 3.2.

Thus the cyclostationary interference, $\nu_{ci}(t)$, at the input to the receiver due to all interferers and noise is given by:

$$\begin{aligned} \nu_{ci}(t) &= n(t) + \mu_{ci}(t) \\ &= n(t) + \sum_{i=1}^{\mathrm{L}} \sum_{n=-\infty}^{\infty} d_i[n]\, \phi_i(t - n\mathrm{T}) \end{aligned} \tag{2.21}$$

where $\mu_{ci}(t)$ is the component of the cyclostationary interference due to the L interferers.

The signal $\nu_{ci}(t)$ is in general *wide-sense cyclostationary* [64]. This means that the autocorrelation function of $\nu_{ci}(t)$ is periodic. Unless stated otherwise, the periodicity is equal to the symbol rate.

The continuous-time continuous-frequency Fourier transform pair is defined to be:

$$\begin{aligned} X(f) &= \mathcal{F}_{cc}[\, x(t)\,] \\ &= \int_{-\infty}^{\infty} x(t)\, e^{-j2\pi ft}\, dt \\ x(t) &= \mathcal{F}_{cc}^{-1}[\, X(f)\,] \\ &= \int_{-\infty}^{\infty} X(f)\, e^{j2\pi ft}\, df \end{aligned} \tag{2.22}$$

where $x(t)$ and $X(f)$ represent time-domain and frequency-domain functions, respectively. Throughout this thesis, a Fourier transform pair will have time-domain and frequency-domain functions denoted by lower-case and corresponding upper-case letters, respectively.

The frequency response of the combined channel is:

$$\Phi_0(f) = \mathcal{F}_{cc}[\, \phi_0(t)\,]. \tag{2.23}$$

The frequency response of the combined co-channels are:

$$\Phi_i(f) = \mathcal{F}_{cc}[\, \phi_i(t)\,] \quad ; \quad i \in \mathsf{L}_1. \tag{2.24}$$

For frequency responses in complex baseband define the term *total bandwidth* to be the difference between the maximum frequency where there is a non-zero component and the minimum frequency[5] where there is a non-zero component. Define the term *bandwidth* to be the half of the total bandwidth. These bandwidth definitions are illustrated in Fig. 2.3. When the bandwidths of any of $\{\Phi_i(f) \mid i \in \mathsf{L}_1\}$ are less than $1/(2\mathrm{T})$, then $\nu_{ci}(t)$ is wide-sense stationary; when the bandwidths of any of $\{\Phi_i(f) \mid i \in \mathsf{L}_1\}$ are greater than or equal to $1/(2\mathrm{T})$, then $\nu_{ci}(t)$ is in general wide-sense cyclostationary [20]. For this reason, the name *cyclostationary interference* is used. It is not intended to imply that this encompasses all types of cyclostationary interference since the model used here is only the case of interfering data signals, and operating at the same symbol rate as the data of interest[6]. More general types and characterizations of cyclostationary interference can be found in [20, 64, 79, 80].

The following notation is used for the powers. The power of the complex noise, called P_N, is given by:

$$P_N = \mathrm{No}\left(2\,\frac{\mathrm{B_n}}{\mathrm{T}}\right) \tag{2.25}$$

where $\mathrm{B_n}$ is the noise bandwidth relative to the symbol rate. The total noise bandwidth is $2\mathrm{B_n}/\mathrm{T}$. The power of the interfering signal at the output of the m^{th} co-channel in Fig. 2.2, called $P_{I,m}$, is given by:

$$P_{I,m} = \frac{1}{\mathrm{T}}\int_0^{\mathrm{T}} |\phi_m(\tau)|^2\, d\tau \quad ; \quad m \in \mathsf{L}_1. \tag{2.26}$$

The power of the signal $\mu_{ci}(t)$, called P_I, is given by:

$$\begin{aligned} P_I &= \frac{1}{\mathrm{T}}\int_0^{\mathrm{T}} E\left[|\mu_{ci}(n\mathrm{T}+\tau)|^2\right] d\tau \\ &= \sum_{m=1}^{\mathrm{L}} P_{I,m}. \end{aligned} \tag{2.27}$$

---

5 This includes negative frequencies.

6 The term synchronous cyclostationary interference has also been used to emphasize the identical symbol rates [68].

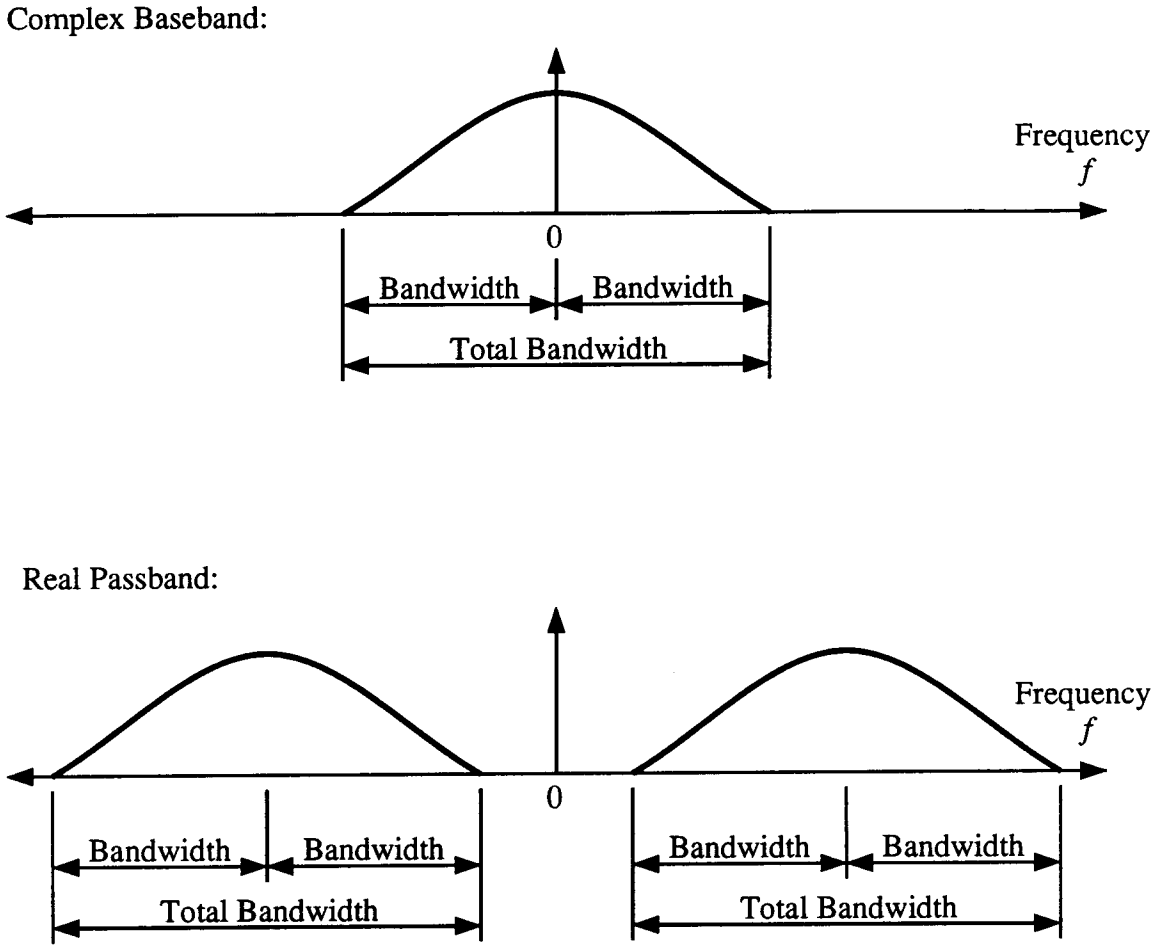

Figure 2.3 Definitions of bandwidth and total bandwidth

The power of the signal $\nu_{ci}(t)$, called P_{ci}, is given by:

$$P_{ci} = \frac{1}{\mathrm{T}} \int_0^{\mathrm{T}} E\left[|\nu_{ci}(n\mathrm{T}+\tau)|^2\right] d\tau. \tag{2.28}$$

The instantaneous power of the signal $\nu_{ci}(t)$, called $P_{ci}(\tau)$, is given by [158]:

$$\begin{aligned} P_{ci}(\tau) &= E\left[|\nu_{ci}(n\mathrm{T}+\tau)|^2\right] \\ &= P_N + \sum_{k=-\infty}^{\infty} \left(\sum_{i=1}^{\mathrm{L}} \frac{1}{\mathrm{T}} \int_{-\infty}^{\infty} \Phi_i\left(f + \frac{k}{\mathrm{T}}\right) \Phi_i^*(f)\, df \right) e^{j(2\pi k/\mathrm{T})\tau}. \end{aligned} \tag{2.29}$$

Note that $P_{ci}(\tau)$ takes the form of a Fourier series where $P_{ci}(\tau)$ is periodic in τ with period T.

Using (2.18), the power spectral density[7] of $\nu_{ci}(t)$, called $S_{ci}(f)$, is given by [79]:

$$S_{ci}(f) = \mathrm{No} + \frac{1}{\mathrm{T}} \sum_{i=1}^{\mathrm{L}} |\Phi_i(f)|^2. \tag{2.32}$$

2.2.2 Stationary Noise

The stationary noise model is shown in Fig. 2.4 and occurs when the signal $\nu(t)$ in Fig. 2.1 is equal to $\nu_{sn}(t)$ in Fig. 2.4:

$$\nu(t) = \nu_{sn}(t). \tag{2.33}$$

---

[7] Since $\nu_{ci}(t)$ is not wide-sense stationary, the power spectral density is the continuous-time continuous-frequency Fourier transform of the mean value of the instantaneous autocorrelation of $\nu_{ci}(t)$, averaged over the time interval $[0, \mathrm{T}]$ [79]. The autocorrelation function is:

$$R_{ci}(\tau) = \frac{1}{\mathrm{T}} \int_0^{\mathrm{T}} E[\nu(x)\, \nu^*(x+\tau)]\, dx. \tag{2.30}$$

The power spectral density is:

$$S_{ci}(f) = \mathcal{F}_{cc}[\, R_{ci}(t)\,]. \tag{2.31}$$

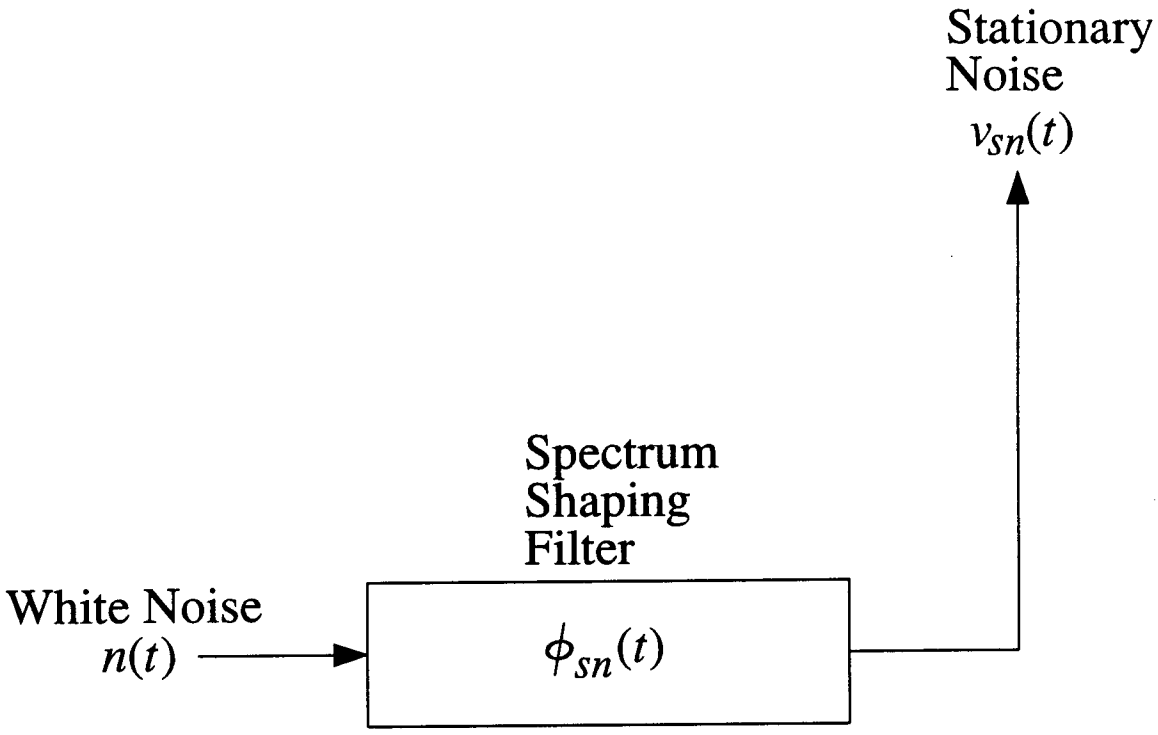

Figure 2.4 Stationary noise model

In Fig. 2.4, the impulse response of the noise-shaping filter is $\phi_{sn}(t)$. The frequency response of the noise-shaping filter is then:

$$\Phi_{sn}(f) \;=\; \mathcal{F}_{cc}[\,\phi_{sn}(t)\,]. \tag{2.34}$$

If $\Phi_{sn}(f)$ is further expressed as:

$$\Phi_{sn}(f) \;=\; \sqrt{\frac{1}{\mathrm{No}}\left(\mathrm{No}+\frac{1}{\mathrm{T}}\sum_{i=1}^{\mathrm{L}}|\Phi_i(f)|^2\right)} \tag{2.35}$$

then by using (2.17) and the relationship:

$$S_{sn}(f) \;=\; |\Phi_{sn}(f)|^2\, S_n(f) \tag{2.36}$$

then:

$$S_{sn}(f) \;=\; \mathrm{No} \;+\; \frac{1}{\mathrm{T}}\sum_{i=1}^{\mathrm{L}}|\Phi_i(f)|^2. \tag{2.37}$$

Note that (2.37) is the same as (2.32); the power spectral density for the stationary noise will be the same as for the cyclostationary interference. Therefore the average power of the signal $\nu_{sn}(t)$, called P_{sn}, will be the same as that for the signal $\nu_{ci}(t)$.

This stationary noise model is included in order to compare the performance of receivers operating in cyclostationary interference versus stationary noise. A comparison using these two interference models would show how the cyclostationarity of the interference influences receiver performance.

2.3 Receiver

The block diagram in Fig. 2.1 does not show details of the receiver. Figs. 2.5 and 2.6 show details of the types of receivers considered, the linear equalizer and decision-feedback equalizer, respectively.

Note that there are no samplers at the input to the equalizers since these models will be used to analyze the best attainable performance of linear and decision-feedback

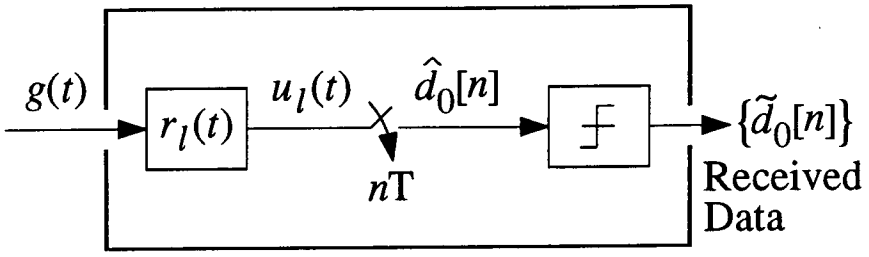

Figure 2.5 Linear equalizer receiver

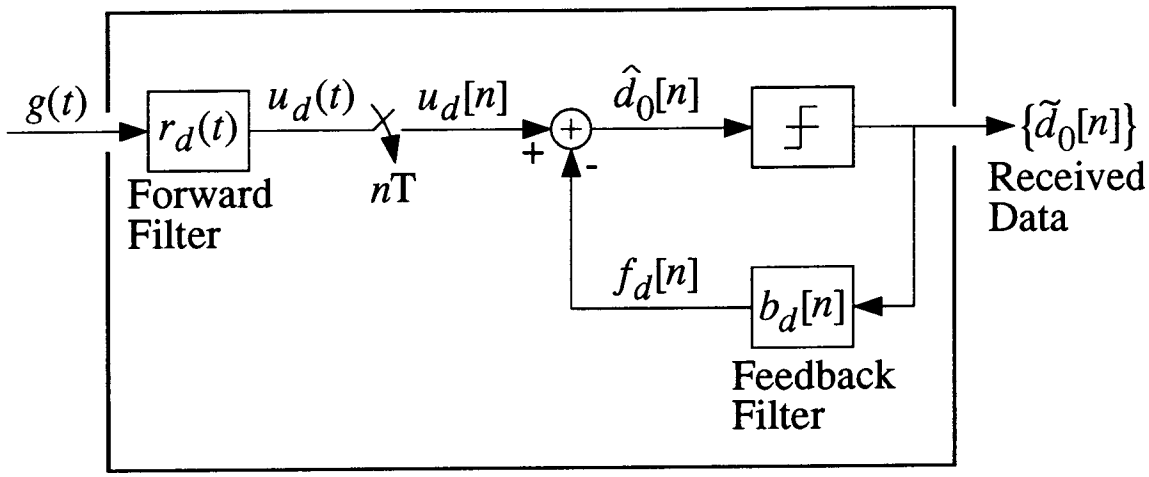

Figure 2.6 Decision-feedback equalizer receiver

equalizers in the interference types considered. The use of samplers at the receiver input as well as other implementation issues will be discussed in Section 4.4.

A second important point is that the equalizers considered have impulse responses which are time invariant[8]. This means that conventional adaptive equalizers can be used for implementation [21, 144, 145].

2.3.1 Linear Equalizer

The input to the receiver is the signal $g(t)$ which enters the linear equalizer's filter. This filter has an impulse response $r_l(t)$, and the output of the filter is the signal $u_l(t)$ which satisfies:

$$u_l(t) = r_l(t) \star g(t). \tag{2.38}$$

The signal $u_l(t)$ is fed to the sampler, which operates at the symbol rate, $1/\mathrm{T}$. The output of sampler is the signal $\widehat{d}_0[n]$ which is defined to be:

$$\begin{aligned} \widehat{d}_0[n] &= u_l(n\mathrm{T}) \\ &= u_l[n]. \end{aligned} \tag{2.39}$$

Note that $\widehat{d}_0[n]$ is an unquantized estimate of the data of interest, $d_0[n]$. The signal $\widehat{d}_0[n]$ is fed to the decision device. The decision device quantizes the input signal to the nearest level from the set of levels of the data of interest. The output of the decision device is the signal $\widetilde{d}_0[n]$ which is an estimate of the data of interest[9].

2.3.2 Decision-feedback Equalizer

The input to the receiver is the signal $g(t)$ which enters the decision-feedback equalizer's forward filter. This filter has an impulse response $r_d(t)$. The output of the filter is the signal $u_d(t)$ which satisfies:

$$u_d(t) = r_d(t) \star g(t). \tag{2.40}$$

---

[8] A brief comment will be made in Appendix A.1 regarding equalizers with time-variant impulse responses; however, Appendix A.1 should not be read until this issue is brought up again in Section 3.2.

[9] In an implementation, $\widetilde{d}_0[n]$ would be a delayed estimate of the data of interest.

The signal $u_d(t)$ is fed to the sampler which operates at the symbol rate, 1/T. The output of sampler is the signal $u_d[n]$ which satisfies:

$$u_d[n] = u_d(n\mathrm{T}). \tag{2.41}$$

The signal $u_d[n]$ and the output of the feedback filter, $f_d[n]$, are fed into the adder. The output of the adder, $\widehat{d}_0[n]$, is obtained from the following operation:

$$\widehat{d}_0[n] = u_d[n] - f_d[n]. \tag{2.42}$$

The signal $\widehat{d}_0[n]$ is fed into the same type of decision device as for the linear equalizer. The output of the decision device, $\widetilde{d}_0[n]$, is fed to the input of the feedback filter which has an impulse response $b_d[n]$. The coefficients of the feedback filter are constrained as follows:

$$b_d[n] = 0 \quad ; \quad n \leq 0. \tag{2.43}$$

The output of the feedback filter is obtained from:

$$\begin{aligned} f_d[n] &= b_d[n] \star \widetilde{d}_0[n] \\ &= \sum_{m=-\infty}^{\infty} b_d[n-m]\, \widetilde{d}_0[m]. \end{aligned} \tag{2.44}$$

As with the linear equalizer, $\widehat{d}_0[n]$ is a unquantized estimate of the data of interest and $\widetilde{d}_0[n]$ is a quantized estimate of the data of interest.

The decision-feedback equalizer has a similar structure to the linear equalizer except for the addition of the feedback filter whose output, $f_d[n]$, is intended to subtract the intersymbol interference that is caused by the data of previous decisions.

Chapter 3
Equalizer Analyses

3.1 Performance Criteria

The following performance criteria were used to analyze the linear and decision-feedback equalizers.

The first performance criterion is the *existence* of a linear equalizer which has the flexibility to suppress all intersymbol interference, all co-channel interference (CCI), and all adjacent-channel interference (ACI). Such an equalizer will be called a *generalized zero-forcing linear equalizer* based upon the work in [106]. A generalized zero-forcing linear equalizer will have the flexibility to suppress all ISI, ACI, and CCI, only under certain conditions of transmitter bandwidth, receiver bandwidth, carrier spacing, antenna diversity, and co-channel interference. This existence criterion is to serve the purpose of suggesting effective system operating points for further evaluations using other more appropriate performance criteria.

The second performance criterion is the *mean square error* (MSE):

$$E\left[\left|\hat{d}_0[n] - \tilde{d}_0[n]\right|^2\right]. \tag{3.1}$$

The MSE was chosen for the following reasons. First, it makes analysis of the equalizer tractable. Secondly, it provides an exponentially tight upper bound on the probability of error [121, 124]. Thirdly, it is minimized in efficient adaptive equalizer implementations [21, 144, 145].

3.2 Generalized Zero-forcing Linear Equalizer

3.2.1 Co-channel Interference and Transmitter Bandwidth

The discussion in this section is intended to develop a new result which states that relatively wider bandwidths, with respect to the symbol rate, in the combined channel and

combined co-channels, $\{\Phi_i(f) \mid i \in \mathsf{L}_0\}$, *may* provide the flexibility to a linear equalizer to suppress larger numbers of cyclostationary interferers. It will be shown that such increases in relative bandwidth enhance the differences among the combined channel and combined co-channels and that these differences allow for potential improvements in a linear or decision-feedback equalizer's interference-suppression capability. Note that the description of this new result emphasized the word *may*; this is because wide relative bandwidths do not guarantee improved cyclostationary interference suppression capability under all conditions. However, under certain conditions wide relative bandwidths allow for substantial equalizer performance improvements over the case where narrow relative bandwidths are used.

Consider Fig. 2.1, used with the cyclostationary interference model in Fig. 2.2, and the linear equalizer in Fig. 2.5. These three figures are combined and shown in Fig. 3.1.

Define the *equalized combined channel* to be:

$$h_0(t) \;=\; \phi_0(t) \star r_l(t). \tag{3.2}$$

Define the *equalized combined co-channels* to be:

$$h_i(t) \;=\; \phi_i(t) \star r_l(t) \quad ; \quad i \in \mathsf{L}_1. \tag{3.3}$$

Finally, define the frequency responses:

$$H_i(f) \;=\; \mathcal{F}_{cc}[h_i(t)] \tag{3.4}$$

$$R_l(f) \;=\; \mathcal{F}_{cc}[r_l(t)]. \tag{3.5}$$

Therefore, (3.2) and (3.3) can be written in the frequency domain as:

$$H_i(f) \;=\; \Phi_i(f)\; R_l(f) \quad ; \quad i \in \mathsf{L}_0. \tag{3.6}$$

From [104] the time-domain condition for zero intersymbol interference can be written as:

$$h_0(n\mathrm{T}) \;=\; \delta[n]. \tag{3.7}$$

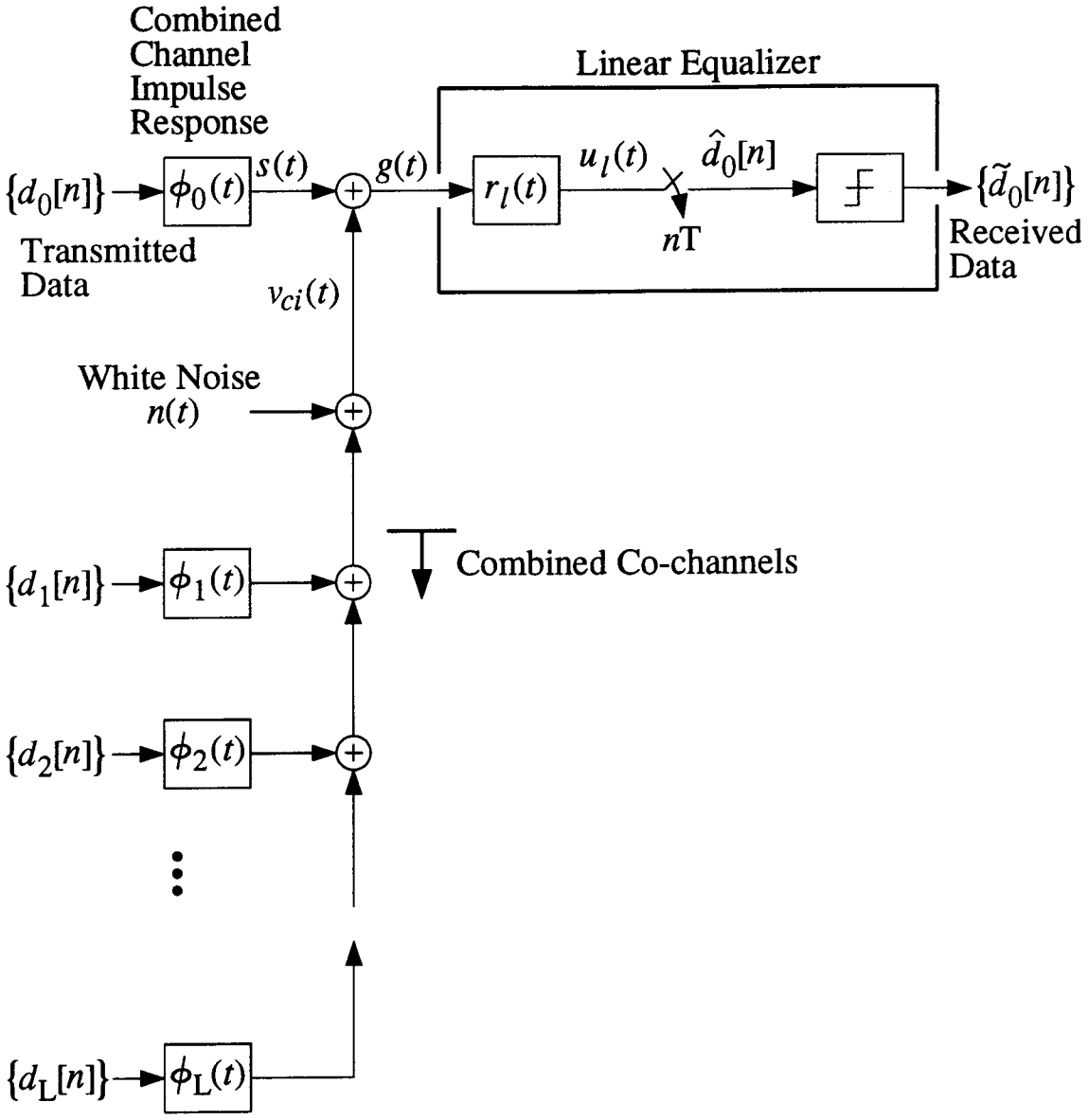

Figure 3.1 Linear equalizer in cyclostationary interference

From [106] the time-domain condition for zero co-channel interference (CCI) can be written as:

$$h_i(n\mathrm{T}) \;=\; 0 \quad ; \quad i \in \mathsf{L}_1. \tag{3.8}$$

The conditions in (3.7) and (3.8) are shown in Fig. 3.2. The concept of avoiding interference by generating nulls in an antenna pattern is similar to the idea in Fig. 3.2 of suppressing interference by putting T-spaced zero crossings in the equalized combined co-channels.

The time-domain condition for zero ISI, (3.7), can be expressed in the frequency domain as:

$$\frac{1}{\mathrm{T}} \sum_{l=-\infty}^{\infty} H_0\left(f + \frac{l}{\mathrm{T}}\right) \;=\; 1 \quad ; \quad \forall f\,. \tag{3.9}$$

The time-domain condition for zero CCI interference, (3.8), can be expressed in the frequency domain as:

$$\frac{1}{\mathrm{T}} \sum_{l=-\infty}^{\infty} H_i\left(f + \frac{l}{\mathrm{T}}\right) \;=\; 0 \quad ; \quad i \in \mathsf{L}_1 \quad ; \quad \forall f\,. \tag{3.10}$$

The two conditions in (3.9) and (3.10) may be combined into the following [106]:

$$\frac{1}{\mathrm{T}} \sum_{l=-\infty}^{\infty} H_i\left(f + \frac{l}{\mathrm{T}}\right) \;=\; \delta[i] \quad ; \quad i \in \mathsf{L}_0 \quad ; \quad \forall f\,. \tag{3.11}$$

Substituting $H_i(f)$ from (3.6) into (3.11) gives:

$$\sum_{k=-\infty}^{\infty} \Phi_i\left(f + \frac{k}{\mathrm{T}}\right) R_l\left(f + \frac{k}{\mathrm{T}}\right) \;=\; \mathrm{T}\;\delta[i] \quad ; \quad i \in \mathsf{L}_0 \quad ; \quad \forall f\,. \tag{3.12}$$

With the absence of further knowledge about the values of the combined channel and combined co-channels, $\{\Phi_i(f) \mid i \in \mathsf{L}_0\}$, it is difficult to proceed. However, if those values are assigned *randomly*, then (3.12) will *likely* have a solution when the number of equations is less than or equal to the number of unknowns. This is the fundamental

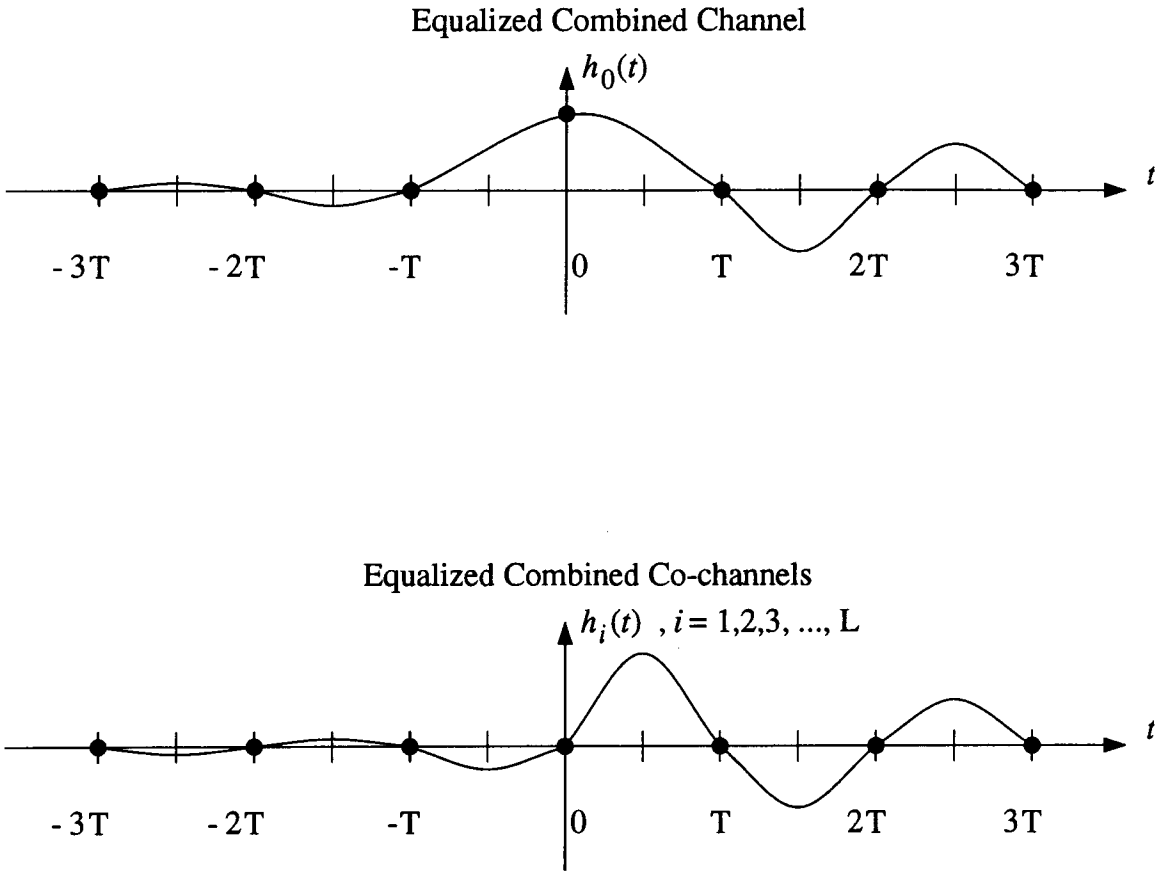

Figure 3.2 Generalized zero-forcing condition

premise of this section, that a generalized zero-forcing linear equalizer will likely *exist* if the number of degrees of freedom is less than or equal to the number of constraints. The effects of relative bandwidth and number of co-channel interferers will be demonstrated by a few small examples before obtaining a more general result.

First, it will be necessary to introduce the term *strictly bandlimited.* If $\{\Phi_i(f) \mid i \in \mathsf{L}_0\}$ are strictly bandlimited to the frequency B, then it means that the following is true:

$$\Phi_i(f) \;=\; 0 \quad ; \quad |f| \geq \mathrm{B} \tag{3.13}$$

where $|\bullet|$ denotes the magnitude of $\bullet$. For the range of frequencies $|f| < \mathrm{B}$ the values of $\{\Phi_i(f) \mid i \in \mathsf{L}_0\}$ may be any number, including the occasional possibility of zero which would correspond to a null in the frequency response.

If the combined channel and combined co-channels, $\{\Phi_i(f) \mid i \in \mathsf{L}_0\}$, are strictly bandlimited to $1/(2\mathrm{T})$, then (3.12) reduces to:

$$\begin{aligned} \Phi_i(f)\, R_l(f) \;&=\; \mathrm{T}\;\delta[i] \quad ; \quad i \in \mathsf{L}_0 \\ 0 < f &< \frac{1}{2\mathrm{T}} \end{aligned} \tag{3.14}$$

for the frequency range shown[10,11]. For the likelihood of a solution to exist, the number of equations must be less than or equal to the number of unknowns. Since there is one unknown:

$$\{R_l(f)\} \tag{3.15}$$

and $\mathrm{L}+1$ equations, it requires that $\mathrm{L}+1 \leq 1$. Therefore L is less than or equal to 0; therefore no interferers can be completely suppressed.

---

[10] Other frequency ranges would produce similar independent equations, except for possibly a finite set of discrete frequencies such as $\{0\}$.

[11] One sufficient constraint is to let *all* the values of $\{\Phi_i(f) \mid i \in \mathsf{L}_0\}$ should be non-zero over the frequency range $|f| < 1/(2\mathrm{T})$. However, this constraint is too severe in that one can allow the occasional discrete null provided that the MSE at the output of the generalized zero-forcing linear equalizer still consists of only one finite component due to channel noise. Stated one final way, the values of $\{\Phi_i(f) \mid i \in \mathsf{L}_0\}$ in the frequency range $|f| < 1/(2\mathrm{T})$ should be non-zero for a sufficiently large subset of frequencies.

If the combined channel and combined co-channels, $\{\Phi_i(f) \mid i \in \mathsf{L}_0\}$, are strictly bandlimited to $2/(2\mathrm{T})$ then (3.12) reduces to:

$$\left[\Phi_i\left(f-\frac{1}{\mathrm{T}}\right)R_l\left(f-\frac{1}{\mathrm{T}}\right) + \Phi_i(f)R_l(f)\right] = \mathrm{T}\,\delta[i] \quad ; \quad i \in \mathsf{L}_0 \qquad 0 < f < \frac{1}{2\mathrm{T}} \tag{3.16}$$

for the frequency range shown[12]. For the likelihood of a solution to exist, the number of equations must be less than or equal to the number of unknowns. A solution of (3.16) will exist if in the following matrix:

$$\begin{bmatrix} \Phi_0(f-\frac{1}{\mathrm{T}}) & \Phi_0(f) \\ \Phi_1(f-\frac{1}{\mathrm{T}}) & \Phi_1(f) \\ \vdots & \vdots \\ \Phi_{\mathrm{L}}(f-\frac{1}{\mathrm{T}}) & \Phi_{\mathrm{L}}(f) \end{bmatrix} \tag{3.17}$$

the first row is linearly independent of all the other rows. Since there are two unknowns:

$$\left\{R_l\left(f-\frac{1}{\mathrm{T}}\right),\ R_l(f)\right\} \tag{3.18}$$

and $\mathrm{L}+1$ equations, it requires that $\mathrm{L}+1 \leq 2$. Therefore L is less than or equal to 1; Therefore up to and including one interferer can be completely suppressed.

Generalizing to any bandwidth, the system of equations in (3.12) represents $\mathrm{L}+1$ equations over $\{i \in \mathsf{L}_0\}$ where the values of $R_l(f)$ are unknown. If the $\{\Phi_i(f) \mid i \in \mathsf{L}_0\}$ are strictly bandlimited to $K_t/(2\mathrm{T})$, then in the frequency range $0 < f < 1/(2\mathrm{T})$ there will be up to K_t unknowns. Other frequency ranges would produce similar independent equations. The system of equations in (3.12) is shown in matrix form for the case where K_t is odd:

$$\begin{bmatrix} \Phi_0(f+\frac{K_t-1}{2\mathrm{T}}) & \Phi_0(f+\frac{K_t-3}{2\mathrm{T}}) & \cdots & \Phi_0(f-\frac{K_t-1}{2\mathrm{T}}) \\ \Phi_1(f+\frac{K_t-1}{2\mathrm{T}}) & \Phi_1(f+\frac{K_t-3}{2\mathrm{T}}) & \cdots & \Phi_1(f-\frac{K_t-1}{2\mathrm{T}}) \\ \vdots & \vdots & \ddots & \vdots \\ \Phi_{\mathrm{L}}(f+\frac{K_t-1}{2\mathrm{T}}) & \Phi_{\mathrm{L}}(f+\frac{K_t-3}{2\mathrm{T}}) & \cdots & \Phi_{\mathrm{L}}(f-\frac{K_t-1}{2\mathrm{T}}) \end{bmatrix} \begin{bmatrix} R_l(f+\frac{K_t-1}{2\mathrm{T}}) \\ R_l(f+\frac{K_t-3}{2\mathrm{T}}) \\ \vdots \\ R_l(f-\frac{K_t-1}{2\mathrm{T}}) \end{bmatrix} = \begin{bmatrix} \mathrm{T} \\ 0 \\ \vdots \\ 0 \end{bmatrix}. \tag{3.19}$$

[12] Again, the values of $\{\Phi_i(f) \mid i \in \mathsf{L}_0\}$ in the frequency range $|f| < 2/(2\mathrm{T})$ should be non-zero for a sufficiently large subset of frequencies.

The case where K_t is even would produce an equivalent derivation.

Again, noting that if the values of the combined channel and combined co-channels, $\{\Phi_i(f) \mid i \in \mathrm{L}_0\}$, are assigned *randomly*, then (3.19) will likely have a solution when the number of equations is less than or equal to the number of unknowns. To state this result another way let $\mathrm{N} = \mathrm{L} + 1$, where N is the number of independent data streams. Then (3.19) will likely have a solution when the number of independent data streams is less than or equal to the number representing the bandwidth:

$$\mathrm{N} \leq K_t. \tag{3.20}$$

Equation (3.20) is the fundamental result.

Even if (3.20) is satisfied, the system of equations in (3.19) will *not* have a solution in pathological cases, such as the case when the combined channel and combined co-channels have identical frequency responses. Define $\mathbf{p}_0$ to be the row vector in (3.19) formed from $\{\Phi_0(f)\}$ and define $\{\mathbf{p}_1, \mathbf{p}_2, \ldots, \mathbf{p}_\mathrm{L}\}$ to be the set of row vectors formed from $\{\Phi_i(f) \mid i \in \mathrm{L}_1\}$, respectively. Since the linear equalizer is required to estimate only the single data stream corresponding to $\mathbf{p}_0$, then (3.19) will have at least one solution if $\mathbf{p}_0$ is linearly independent of $\{\mathbf{p}_1, \mathbf{p}_2, \ldots, \mathbf{p}_\mathrm{L}\}$ [74, 172].

The generalized zero-forcing linear equalizer will exist if (3.19) has solutions for all frequencies, except for possibly some small subset of frequencies provided that the MSE still consists of only one finite component due to channel noise.

In summary, (3.20) states: *Every increase in total bandwidth of size equal to the symbol rate may provide the flexibility to completely suppress an additional interferer by means of linear equalization.* Without further knowledge about the values of the combined channel and combined co-channels, and since the MSE performance of a zero-forcing equalizer must be greater than or equal to that of a minimum-mean-square-error equalizer, the emphasis of this analysis remains on its insight into the *flexibility* that relatively wide bandwidths may provide to *MMSE* linear and decision-feedback equalizers when they trade-off suppression of ISI, CCI, and noise. In the applications

of Chapters 4 and 5, the combined channel and combined co-channels take on specific values; this permits further discussion about the benefits of relatively wide bandwidths.

Note that this analysis also has implications on decision-feedback equalizer interference-suppression capability. Under the assumptions of Chapter 2, the only difference between the linear equalizer (Fig. 2.5) and the decision-feedback equalizer (Fig. 2.6) is that the decision-feedback-equalizer's feedback filter subtracts off the ISI caused by the data of previous decisions. This subtraction alleviates the postcursor ISI problem for the forward filter and hence provides additional flexibility to the forward filter to suppress CCI. In the model of this thesis, the feedback filter of the decision-feedback equalizer does not provide any interference suppression capability.

Appendix A.2 contains a similar analysis to the one of this section, but where the data of interest is transmitted at a different symbol rate than that of the neighboring transmitters. These observations were motivated by [173, 174].

3.2.2 Intersymbol Interference, Adjacent-channel Interference, Co-channel Interference, Transmitter Bandwidth, Receiver Bandwidth, and Antenna Diversity

To this point, the existence of a generalized zero-forcing linear equalizer has been analyzed in terms of the number of co-channel interferers and transmitter bandwidth relative to the symbol rate. This analysis will be generalized to include adjacent-channel interference, receiver bandwidth relative to the symbol rate, and receiver antenna diversity.

Fig. 3.1 shows a linear equalizer which operates in the presence of ISI, white noise, and CCI from L interferers. But in Chapter 2, it was stated that Fig. 2.1 may be generalized to include the effect of ACI. In this generalization, the number of interferers, L, will contain two components:

$$L = N_a + N_c \tag{3.21}$$

where N_a is the number of ACI signals and N_c is the number of CCI signals present at the receiver input. The power spectral densities of the signal which carries the data of interest, the ACI signals, and the CCI signals, at the receiver input, $g(t)$ in Fig. 3.1, are shown in Fig. 3.3. The signal which carries the data of interest and the CCI are centered at 0 Hz and the ACI signals are centered at non-zero carrier frequencies. The CCI is not separately shown in Fig. 3.3 since it is assumed to occupy the same frequency band as the signal which carries the data of interest.[13]

Fig. 3.3 introduces three parameters. The transmitter bandwidth, B_t, receiver bandwidth, B_r, and carrier spacing, C all of which are measured relative to the symbol rate, $1/T$. Therefore the absolute bandwidths and frequencies may be obtained from the relative bandwidths and frequencies by multiplication with $1/T$, as in B_t/T, B_r/T, and C/T. Note that B_t, B_r, and C are real positive values; they are not constrained to be integers. Fig. 3.3 also introduces the concept of the receiver bandwidth. All signals are zero outside the frequencies $[-B_r/T, B_r/T]$.

If the number of receiver antennas is A_r, it will mean that in Fig. 3.1 there are A_r times the number of combined channels and combined co-channels and that receiver inputs are put together using a continuous-time infinite-length optimal combiner [26–28, 30, 31, 100]. In other words, the output of each receiver antenna will be fed to a continuous-time infinite-length linear equalizer with all equalizer outputs added together, and the adder output would be fed to the input of the quantizer.

The analysis that lead to the co-channel interference result was repeated using the model described here and the result is as follows. The five-dimensional region, $E_{gzf}(B_t, B_r, C, A_r, N_c)$, where a generalized zero-forcing linear equalizer has the flex-

[13] Although the CCI will have a different spectrum in many situations of interest.

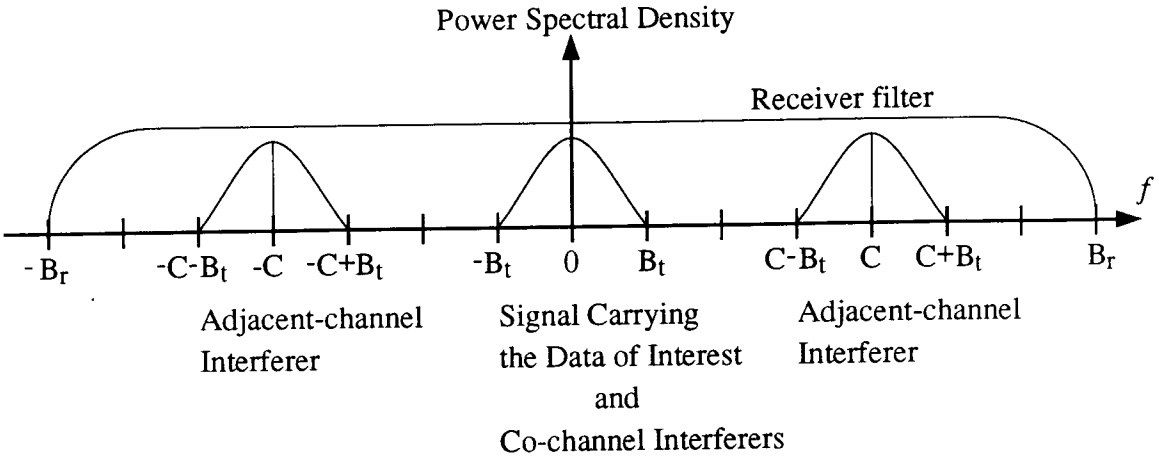

Figure 3.3 Magnitude response of the signals after receiver filtering

ibility to suppress all ISI, ACI, and CCI is:

$$\begin{aligned} E_{gzf} &= E_{gzf}(B_t, B_r, C, A_r, N_c) \\ &= (\, B_t > 0 \,) \\ &\quad \cap (\, B_r > 0 \,) \\ &\quad \cap (\, C > 0 \,) \\ &\quad \cap (\, A_r \in \mathbf{Z}^{++} \,) \\ &\quad \cap (\, N_c \in \mathbf{Z}^{+} \,) \\ &\quad \cap \left(\bigcup_{2B_{ri}=1}^{\mathrm{int}(2B_r)} N_E(B_t, B_{ri}, C, N_c) \leq N_U(B_t, B_{ri}, A_r) \right) \end{aligned} \tag{3.22}$$

where the symbol $\cap$ denotes intersection, the symbol $\cup$ denotes union, the number of equations, $N_E(B_t, B_{ri}, C, N_c)$, is:

$$N_E(B_t, B_{ri}, C, N_c) = 1 + N_{ar}(B_t, B_{ri}, C) + N_c \tag{3.23}$$

the number of relevant ACI signals:

$$N_{ar}(B_t, B_{ri}, C) = \begin{cases} 2\,\mathrm{int}\left(\dfrac{B_t + B_{ri}}{C}\right) & , C \neq 0,\ C < 2B_t \\ 0 & , C \neq 0,\ C \geq 2B_t \end{cases} \tag{3.24}$$

the number of unknowns, $N_U(B_t, B_{ri}, A_r)$, is:

$$N_U(B_t, B_{ri}, A_r) = \begin{cases} 0 & , 2B_t < 1, \\ 2\,A_r\,B_{ri} & , 2B_t \geq 1,\ C < 2B_t \\ 2\,A_r\,\min(B_{ri}, \mathrm{int}(B_t)) & , 2B_t \geq 1,\ C \geq 2B_t \end{cases} \tag{3.25}$$

the function $\mathrm{int}(\bullet)$ denotes the integer part of $\bullet$, and the function $\min(\bullet, \blacklozenge)$ denotes the minimum value among $\bullet$ and $\blacklozenge$. The symbol $\bigcup_{2B_{ri}=1}^{\mathrm{int}(2B_r)}$ denotes the union of the sets where the index of the union, called B_{ri}, takes on the values:

$$\left\{ \frac{1}{2}, \frac{2}{2}, \frac{3}{2}, \cdots, \frac{\mathrm{int}(\,2\,B_r\,)}{2} \right\}. \tag{3.26}$$

The values in (3.26) respectively correspond to the receiver bandwidths:

$$\left\{ \frac{1}{2T}, \frac{2}{2T}, \frac{3}{2T}, \cdots, \frac{\mathrm{int}(\,2\,B_r\,)}{2T} \right\}. \tag{3.27}$$

The meaning of (3.22) is described here. The region of existence of the generalized zero-forcing linear equalizer, (3.22), is defined using the intersection of six subregions. The first five subregions are clear constraints. The sixth subregion is union of repeated applications of the concept in (3.20); the premise being that the generalized zero-forcing linear equalizer exists if in at least one set of receiver bandwidth conditions the zero-forcing condition occurs. The number of equations, (3.23), consists of three terms due to the signal which carries the data of interest, the relevant ACI, and the CCI. The relevant ACI has two cases based on whether or not the signals in adjacent channels overlap with the signal carrying the data of interest. Overlap occurs when $C < 2B_t$. Overlap does not occur when $C \geq 2B_t$; the non-overlap case is shown in Fig. 3.3. If there is no overlap, the number of relevant adjacent channels is zero. If there is an overlap, there is a non-zero number of relevant adjacent-channel interferers. This non-zero number is derived later. The number of unknowns, (3.25), is determined from three cases. If the transmitter bandwidth, B_t is less than $1/2$, then there will be some frequencies where it will not be possible to suppress ISI, therefore the minimum worst-case number of unknowns is zero. If the transmitter bandwidth, B_t is greater than or equal to $1/2$, the number of unknowns is determined by the bandwidth $2B_{ri}$ multiplied by the factor A_r which represents the number of sets of unknowns associated with each receiver diversity branch. The difference when there is no overlap is that the minimum of the truncated transmitter and receiver bandwidth is used. Note that the scaling factor A_r assumes that the channels and co-channels associated with each diversity branch are different in the sense that the number of degrees of freedom scale linearly with diversity. This is an incorporation of the narrowband array processing result in [30, 31] which states that every increase in receiver antenna diversity may allow the ability to suppress an additional interferer:

$$N \leq A_r. \tag{3.28}$$

Interestingly, embodied in (3.22) are the *independent* relationships for CCI without ACI that every increase in receiver antenna diversity may allow the ability to suppress an additional interferer (3.28), and that every increase in transmitter total bandwidth of size 1/T may allow the ability to suppress an additional interferer (3.20). These independent relations can be expressed as:

$$N \leq A_r K_t. \tag{3.29}$$

The statement that the gains associated with increased diversity and increased relative bandwidth are independent assumes the values of the channels and co-channels are assigned randomly, in the absence of any further knowledge that would be available in a specific application. Equation (3.29) suggests the most interesting prospect that the combined use of wide relative transmitter bandwidths with receiver antenna diversity offers interference suppression capability beyond the sum of the interference suppression capability of their separate use.

The structure and sparsity of the system of linear equations that is implied in using (3.22) has not been considered. However, the nature of adjacent-channel interference means that one can arrange the system matrix to have zeroes in the lower left and upper right corners. Hence the system of equations does not initially appear to have a structure that makes this analysis invalid.

The expression for the number of relevant adjacent-channel interferers was derived as follows. In Fig. 3.3, observe that by symmetry that $N_{ar}(B_t, B_{ri}, C)$ is even, and can be zero. If there are $N_{ar}(B_t, B_{ri}, C)$ adjacent-channel interferers present, then the following two inequalities must hold:

$$\begin{aligned} \frac{N_{ar}(B_t, B_{ri}, C)}{2} C - B_t &\leq B_{ri} \\ \frac{N_{ar}(B_t, B_{ri}, C) + 2}{2} C - B_t &> B_{ri}. \end{aligned} \tag{3.30}$$

Referring to Fig. 3.3 the first inequality is a statement that the left edge of the furthest-right ACI component, with carrier frequency $N_{ar}(B_t, B_{ri}, C)C/2$, must lie within the receiver bandwidth. The second inequality is a statement that the left edge of the signal,

with carrier frequency $(N_{ar}(B_t, B_{ri}, C) + 2)C/2$, must lie beyond the right edge of the receiver bandwidth. Rearranging and combining the two inequalities in (3.30) gives:

$$\begin{aligned} \frac{2(B_t + B_{ri})}{C} - 2 &< N_{ar}(B_t, B_{ri}, C) \leq \frac{2(B_t + B_{ri})}{C} \\ \therefore \frac{B_t + B_{ri}}{C} - 1 &< \frac{1}{2} N_{ar}(B_t, B_{ri}, C) \leq \frac{B_t + B_{ri}}{C} \\ \therefore N_{ar}(B_t, B_{ri}, C) &= 2 \operatorname{int}\left(\frac{B_t + B_{ri}}{C}\right). \end{aligned} \tag{3.31}$$

The expressions for the number of relevant adjacent-channel interferers (3.24) and for the region of existence of the generalized zero-forcing equalizer (3.22) were evaluated.

For the case when the receiver bandwidth is equal to the transmitter bandwidth, the number of relevant adjacent-channel interferers, $N_{ar}(B_t, B_{ri}, C)$ from (3.24), is equal to the number of ACI signals present, N_a. Equation (3.24) was evaluated and is plotted in Fig. 3.4. The two-dimensional region is divided into subregions corresponding to particular (C, B_t) operating points where there are the same number of adjacent-channel interferers.

For the case where:

$$\begin{aligned} B_r &= B_t \\ A_r &= 1 \text{ antennas} \\ N_c &= 0 \text{ CCI signals} \end{aligned} \tag{3.32}$$

the region where a generalized zero-forcing linear equalizer exists was determined using (3.22) and plotted in Fig. 3.5; note that for clarity only the lower left boundary of the region is shown in the figure even though the region extends up to and beyond the upper right corner. Interestingly, there are operating points such as when $C = 1.75$ where increases in bandwidth pass in and out of regions where the generalized zero-forcing linear equalizer exists. The explanation is as follows. Under certain conditions, such as a change from a (C, B_t) point of $(1.75, 1.0)$, which is in E_{gzf}, to a point $(1.75, 1.4)$, which is not in E_{gzf}, the increase in bandwidth causes more ACI than the linear equalizer is capable of suppressing. However, with a change from $(1.75, 1.4)$ to

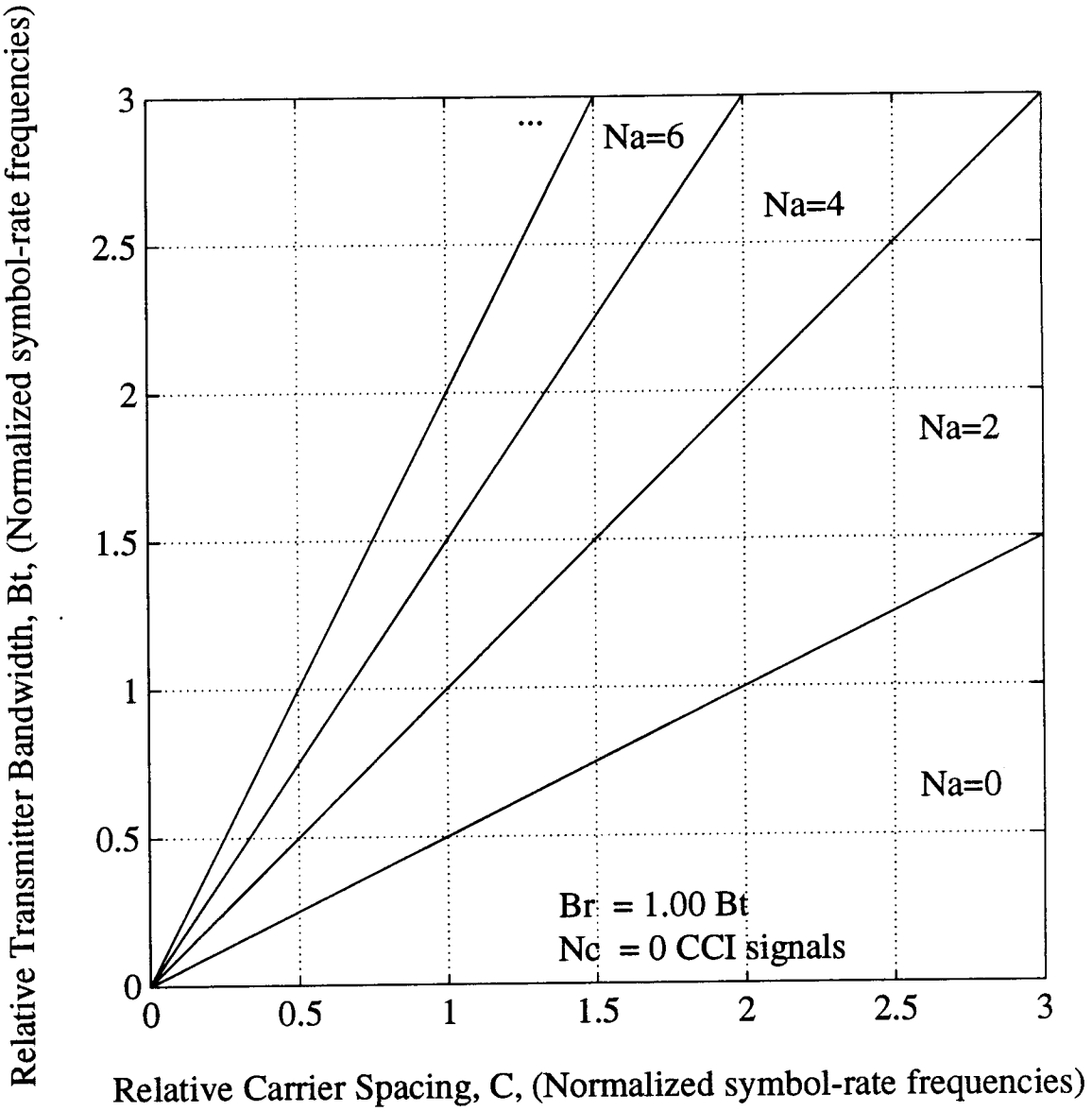

Figure 3.4 Number of ACI signals present after receiver filtering

$(1.75, 1.6)$, which is in E_{gzf}, it is true that there is more ACI, but there is increased interference suppression capability at that particular bandwidth[14]. Curves for other values of receiver bandwidth equal to $2B_t$ and $3B_t$ are also shown in the Fig. 3.5, and as with the $1B_t$ case only the lower left boundary of the region is shown. Figure 3.5 suggests that arbitrarily large receiver bandwidths allow for marginal improvements in spectral efficiency through decreased carrier spacing, but the improvements are not better than the fundamental carrier spacing value of $1/T$ confirmed by (3.20). In an implementation, increases in relative bandwidth would reach diminishing returns, meaning that these results about potentially useful operating points would become increasingly optimistic as the receiver bandwidth increases.

Fig. 3.6 is a plot of (3.22) where the fixed parameters are:

$$\begin{aligned} B_r &= B_t \\ N_c &= 0 \text{ CCI signals} \end{aligned} \tag{3.33}$$

and the number of receiver antennas is varied. Increases in antenna diversity provide improvements in spectral efficiency below the $1/T$ limit associated with only increased receiver bandwidth from Fig. 3.5. Note again that these results are based on the assumption that the channels and co-channels are random. In an implementation, increases in diversity would reach diminishing returns [26-28, 30, 31, 100].

Fig. 3.7 is a plot of (3.22) where the fixed parameters are:

$$\begin{aligned} B_r &= B_t \\ A_r &= 1 \text{ antennas} \end{aligned} \tag{3.34}$$

and the number of additional CCI signals is varied. As expected, increasing amounts of CCI reduce the regions where all ISI, ACI, and CCI can be suppressed.

Fig. 3.8 is a plot of (3.22) where the fixed parameters are:

$$\begin{aligned} B_r &= 3\,B_t \\ N_c &= 1 \text{ CCI signal} \end{aligned} \tag{3.35}$$

---

[14] Specifically, as the transmitter and receiver bandwidths exceed 1.5 an aliased version of the spectrum of the signal carrying the data of interest, as well as the interferers signals, completely covers the frequencies $\{0 < f < 1/(2T)\}$; thus guaranteeing more non-zero coefficients in the matrix in (3.19).

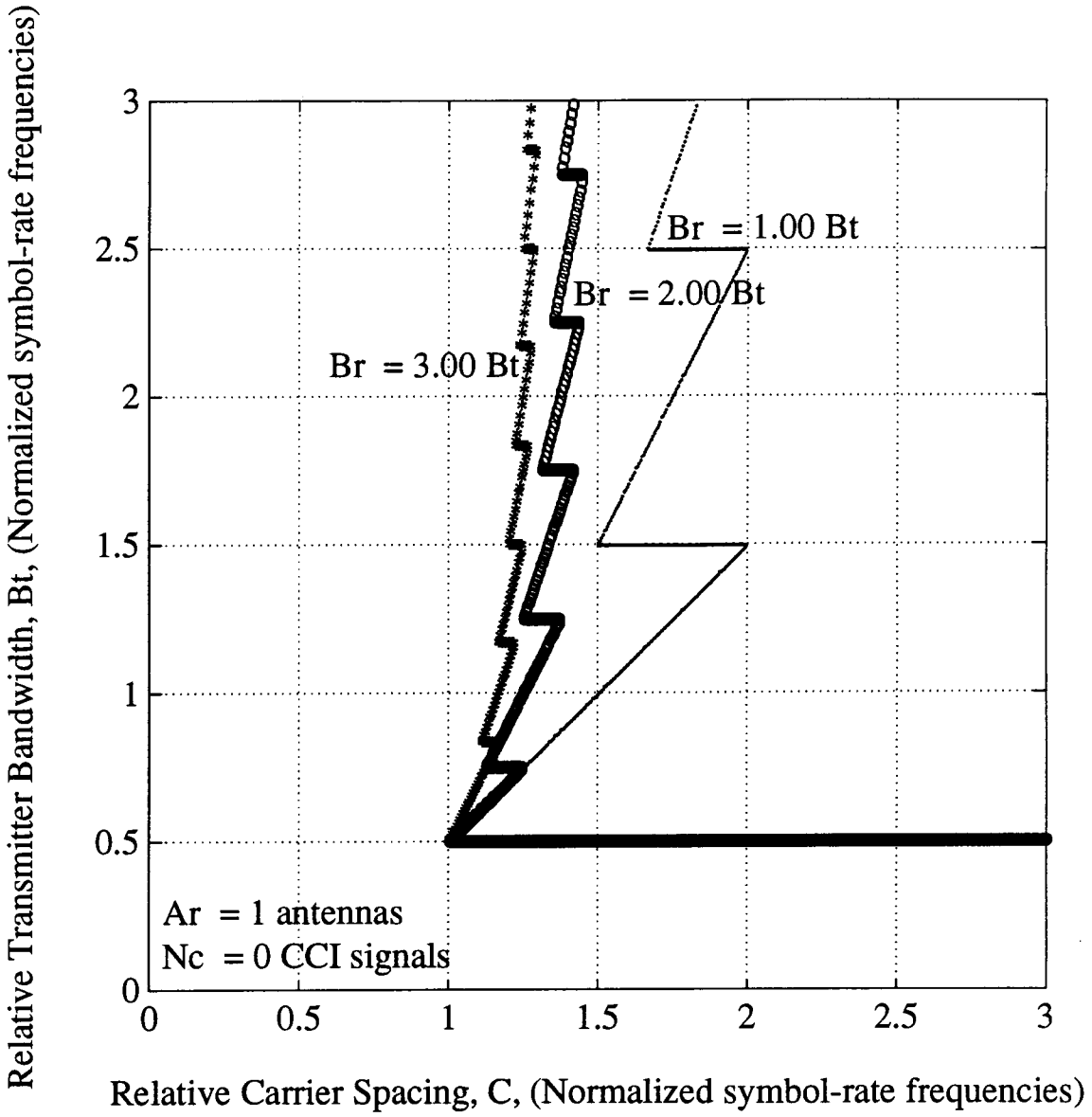

Figure 3.5 Region of suppressible ISI, ACI, and CCI — Receiver bandwidth effects

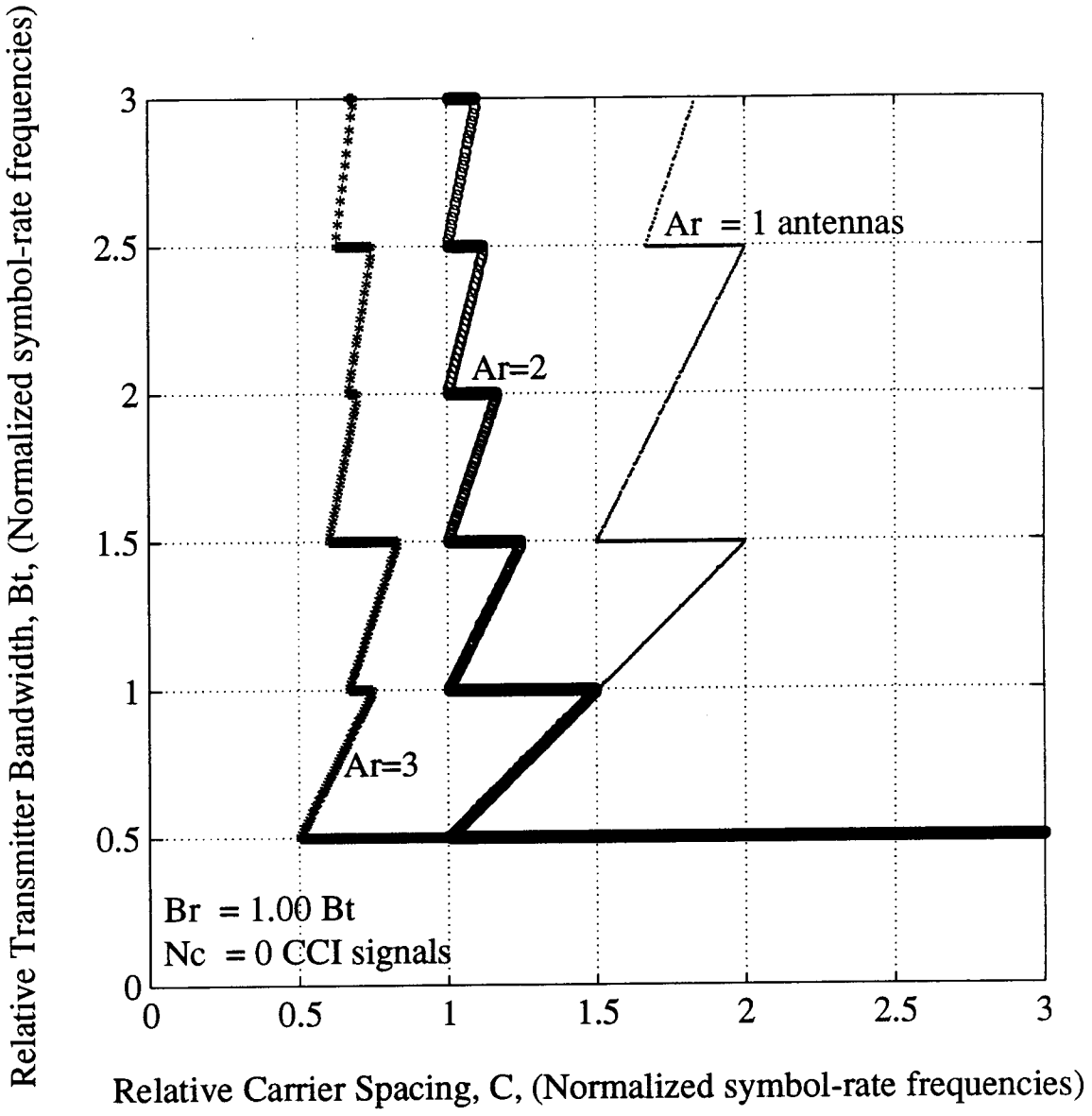

Figure 3.6 Region of suppressible ISI, ACI, and CCI — Receiver antenna effects

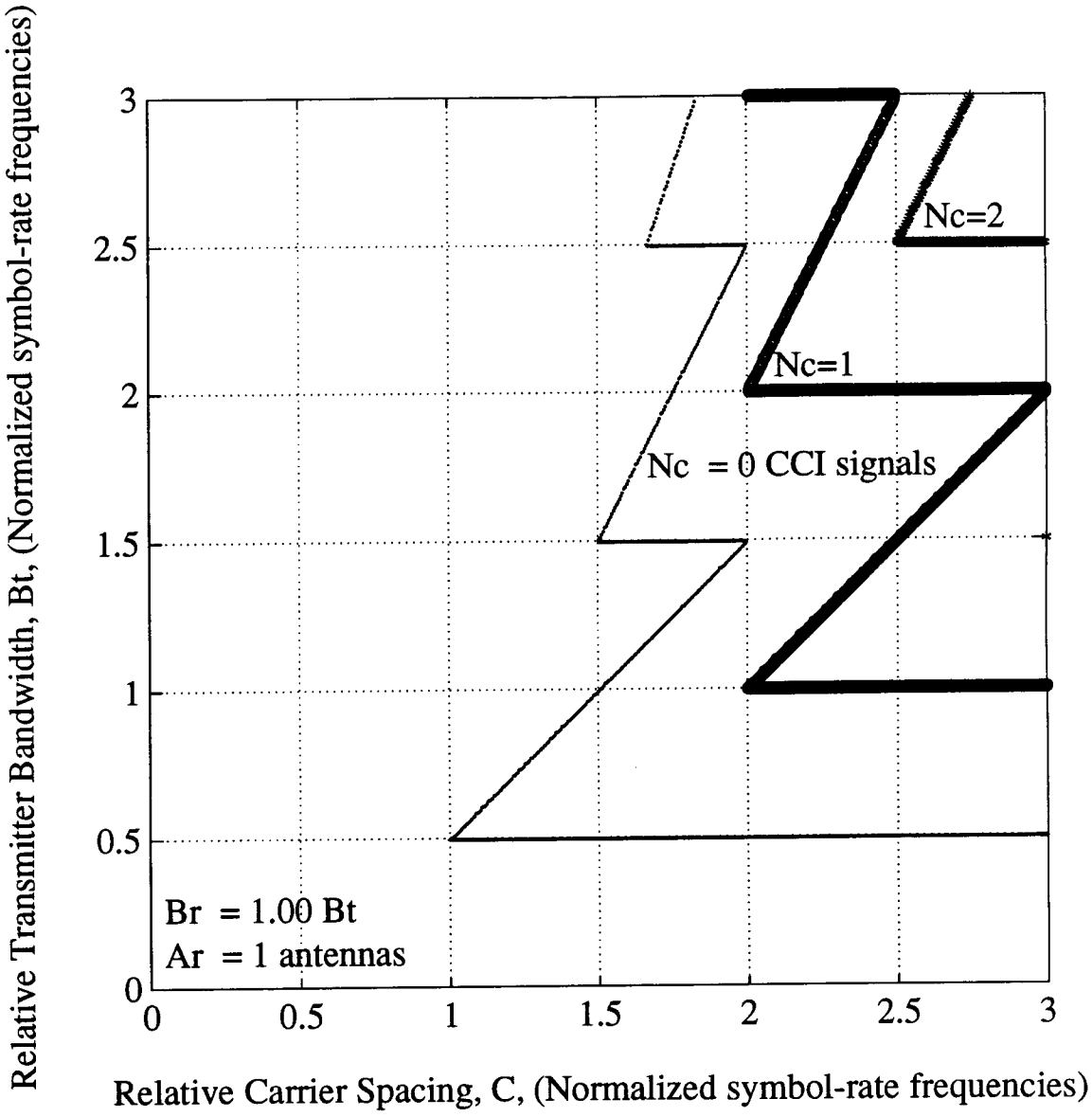

Figure 3.7 Region of suppressible ISI, ACI, and CCI — Additional CCI signal effects

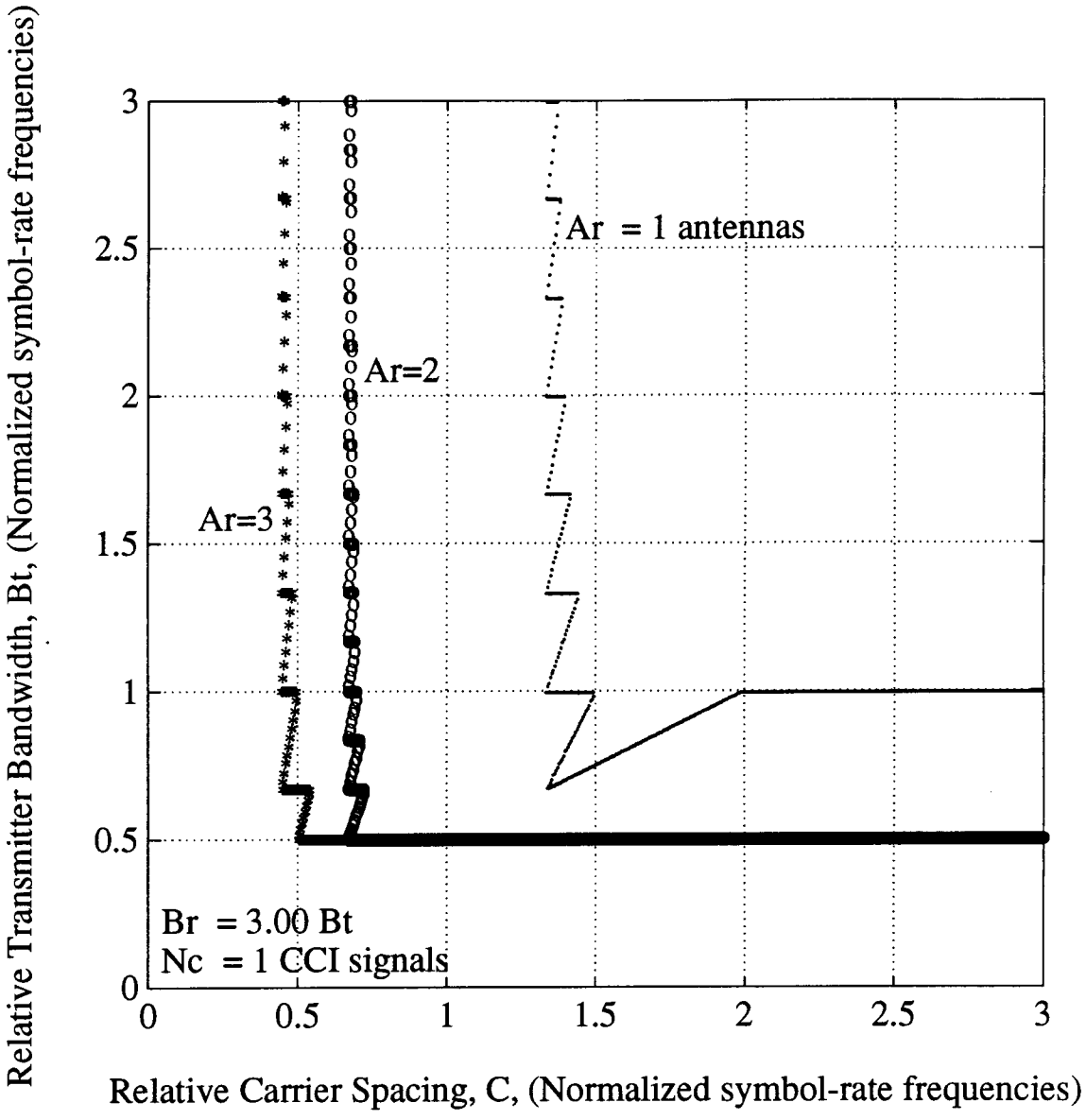

Figure 3.8 Region of suppressible ISI, ACI, and CCI — Receiver antenna effects with one CCI signal and a wide receiver bandwidth

and the number of antennas is varied. Even with the presence of one additional CCI signal, the combined benefits of increased diversity and relative bandwidth suggest operating points with spectral efficiencies comparable to the case with no additional CCI signals present.

3.3 Minimum-mean-square-error Decision-feedback Equalizer

3.3.1 Cyclostationary Interference

This section describes the development of an expression for the minimum mean square error of a continuous-time infinite-length decision-feedback equalizer in the presence of intersymbol interference, additive white noise, and cyclostationary co-channel interference. The system model, interference type, and receiver type shown in Figs. 2.1, 2.2, and 2.6. These three figures are combined and shown in Fig. 3.9.

The following two assumptions are made to facilitate analysis.

First, it is assumed that the decision-feedback equalizer makes correct decisions. Therefore:

$$d_0[n] = \widetilde{d}_0[n]. \tag{3.36}$$

The effect of this assumption is that the derived expression is an asymptotic result. By asymptotic it means that the MSE achievable by an equalizer implementation can approach but never go below the MMSE expression derived in this section[15]. Stated another way, the MMSE expression is a lower bound on the MSE performance of an equalizer implementation.

The second assumption is that the combined channel and combined co-channels, $\{\phi_i(t), \Phi_i(f) \mid i \in \mathsf{L}_0\}$, are known. The effect of this assumption is minimal since adaptive equalizer implementations do not necessarily require such knowledge [21, 144, 145], provided that the channels vary slow enough for equalizers to track the changes.

---

[15] This statement presumes that the system model used in this work accurately and completely models the real system.

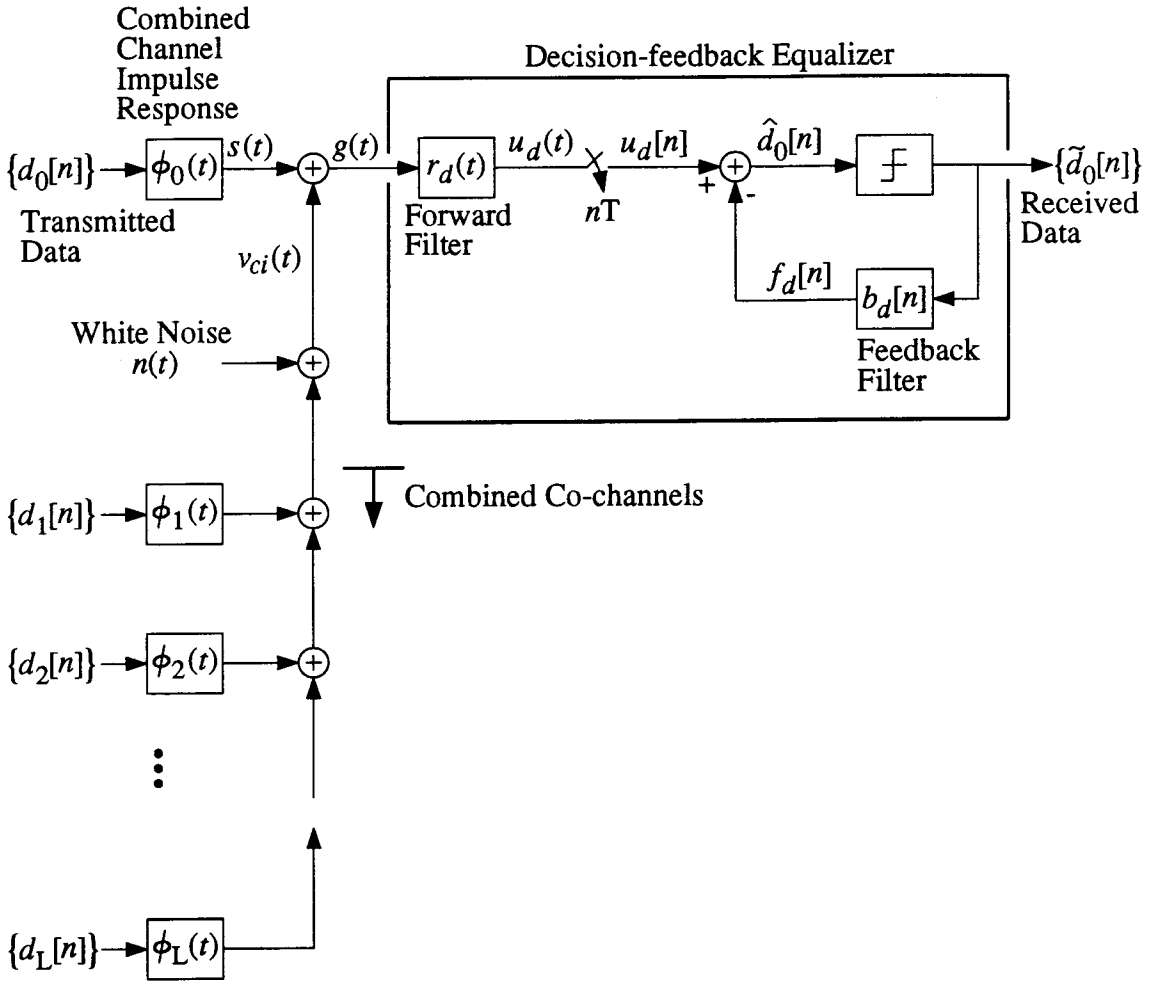

Figure 3.9 Decision-feedback equalizer in cyclostationary interference

Using equations (3.1) and (3.36), the MSE, called $\varepsilon_{dc}(b_d, r_d)$, of the decision-feedback equalizer in Fig. 3.9 is given by:

$$\varepsilon_{dc}(b_d, r_d) = E\left[\left|\widehat{d}_0[n] - d_0[n]\right|^2\right]. \tag{3.37}$$

The problem at this point in the development is to find expressions for the impulse responses of the feedback filter, $b_d[n]$, and the forward filter, $r_d(t)$, to make $\varepsilon_{dc}(b_d, r_d)$ as small as possible. This will make the unquantized estimate of the data of interest, $\widehat{d}_0[n]$, as close as possible to the data of interest, $d_0[n]$, in the mean square sense. Those values of $b_d[n]$ and $r_d(t)$ which make $\varepsilon_{dc}(b_d, r_d)$ the smallest are called the optimal values and are denoted by $r_{dco}(t)$ and $b_{dco}[n]$, respectively. The notation uses subscripts d, c, and o which denote *decision-feedback equalizer*, *cyclostationary interference*, and *optimal*, respectively. Once the values of $r_{dco}(t)$ and $b_{dco}[n]$ are known, they can be used to find the MMSE, defined to be:

$$\varepsilon_{dco} = \varepsilon_{dc}(b_{dco}, r_{dco}). \tag{3.38}$$

At any point in the following development, the impulse responses of the combined co-channels, $\{\phi_i(t) \mid i \in \mathsf{L}_1\}$, can be set to zero to get the familiar situation of a linear channel with additive white noise. The development in this section is a generalization of elements of [108, 109, 175] which are based on a linear channel with additive white noise.

The first step is to obtain an expression for $\varepsilon_{dc}(b_d, r_d)$ in terms of the known and unknown quantities.

The MSE in (3.37) may be expanded to get:

$$\varepsilon_{dc}(b_d, r_d) = E\left[\widehat{d}_0[n]\widehat{d}_0^*[n]\right] - E\left[\widehat{d}_0^*[n]d_0[n]\right] - E\left[\widehat{d}_0[n]d_0^*[n]\right] + E[d_0[n]d_0^*[n]]\,. \tag{3.39}$$

Using (2.42), only the first term in (3.39) will be expanded and $\varepsilon_{dc}(b_d, r_d)$ becomes:

$$\begin{aligned}
\varepsilon_{dc}(b_d, r_d) \;=\;& E[\, u_d[n]\, u_d^*[n]\,] \\
& - E\left[\, \widehat{d_0^*}[n]\, d_0[n]\,\right] \\
& - E\left[\, \widehat{d_0}[n]\, d_0^*[n]\,\right] \\
& + E[\, d_0[n]\, d_0^*[n]\,] \\
& - E[\, u_d^*[n]\, f_d[n]\,] \\
& - E[\, u_d[n]\, f_d^*[n]\,] \\
& + E[\, f_d[n]\, f_d^*[n]\,].
\end{aligned} \tag{3.40}$$

Using $\widehat{d_0}[n]$ from (2.42), $\widetilde{d_0}[n]$ from (3.36), $u_d[n]$ from (2.41), $u_d(t)$ from (2.40), $f_d[n]$ from (2.44), part of $b_d[n]$ from (2.43), $g(t)$ from (2.12), $s(t)$ from (2.11), $\nu(t)$ from (2.15), $\nu_{ci}(t)$ from (2.21), $E[\bullet]$ from (2.18), and σ_d^2 from (2.5), then by some algebraic manipulations and evaluation of expectations the MSE $\varepsilon_{dc}(b_d, r_d)$ from (3.40) can be rewritten as:

$$\begin{aligned}
\varepsilon_{dc}(b_d, r_d) \;=\;& \int_{-\infty}^{\infty} r_d^*(t) \left(\int_{-\infty}^{\infty} k_l(t,\tau)\, r_d(\tau)\, d\tau \right) dt \\
& - \int_{-\infty}^{\infty} r_d^*(t)\, \phi_0^*(-t)\, dt \\
& - \int_{-\infty}^{\infty} r_d(t)\, \phi_0(-t)\, dt \\
& + 1 \\
& - \sum_{n=-\infty}^{\infty} \left(\int_{-\infty}^{\infty} \phi_0^*(n\mathrm{T} - t)\, r_d^*(t)\, dt \right) b_d[n] \\
& - \sum_{n=-\infty}^{\infty} \left(\int_{-\infty}^{\infty} \phi_0(n\mathrm{T} - t)\, r_d(t)\, dt \right) b_d^*[n] \\
& + \sum_{n=-\infty}^{\infty} |b_d[n]|^2
\end{aligned} \tag{3.41}$$

where $k_l(t,\tau)$ is a Hermitian kernel of the integral operator:

$$k_l(t,\tau) \;=\; \mathrm{No}\delta(t-\tau) \;+\sum_{i=0}^{\mathrm{L}}\sum_{n=-\infty}^{\infty} \phi_i^*(n\mathrm{T}-t)\;\phi_i(n\mathrm{T}-\tau). \tag{3.42}$$

Note also that the seven terms in (3.40) correspond respectively to the seven terms in (3.41).

The notation in (3.41) can be expressed in the following more compact manner [175]:

$$\begin{aligned}\varepsilon_{dc}(b_d,r_d) \;=\;& < r_d \;,\; K_l r_d >_c \;-\; < r_d \;,\; m_0 >_c \;-\; < r_d^* \;,\; m_0^* >_c \;+1 \\ & - \;< K_0 r_d \;,\; b_d >_d \\ & - \;< K_0 r_d^* \;,\; b_d^* >_d \\ & + \;< b_d \;,\; b_d >_d\end{aligned} \tag{3.43}$$

where the inner product for continuous-time functions is defined as:

$$< \bullet \;,\; \blacklozenge >_c \;=\; \int_{-\infty}^{\infty} \bullet^*(t)\;\blacklozenge(t)\;dt \tag{3.44}$$

the inner product for discrete-time functions is defined as:

$$< \bullet \;,\; \blacklozenge >_d \;=\; \sum_{n=-\infty}^{\infty} \bullet^*[n]\;\blacklozenge[n] \tag{3.45}$$

the notation for the Fredholm integral operator [176], K_l, of the function $\bullet(t)$ is defined as[16]:

$$\begin{aligned}K_l \bullet (t) \;&=\; (K_l \bullet (t))(t) \\ &=\; \int_{-\infty}^{\infty} k_l(t,\tau)\;\bullet(\tau)\;d\tau\end{aligned} \tag{3.46}$$

the kernel of the integral operator is:

$$k_l(t,\tau) \tag{3.47}$$

---

[16] The Fredholm integral operator is linear transformation.

the linear transformation, K_0, of the function $\bullet(t)$ is defined as:

$$\begin{aligned} K_0 \bullet [n] &= (K_0 \bullet (t))[n] \\ &= \int_{-\infty}^{\infty} \phi_0(n\mathrm{T} - \tau) \bullet (\tau) \; d\tau \end{aligned} \tag{3.48}$$

and finally $m_0(t)$ is defined as:

$$m_0(t) = \phi_0^*(-t). \tag{3.49}$$

The minimization of $\varepsilon_{dc}(b_d, r_d)$ in (3.43) with respect to $b_d[n]$ and $r_d(t)$ will be done one argument at a time, starting with $b_d[n]$. Appendix B.1 describes the use of the differential calculus to find the optimal values of the coefficients of the feedback filter, $b_{dco}[n]$, and they are given by:

$$b_{dco}[n] = u[n-1] \; K_0 r_d[n] \tag{3.50}$$

where the discrete-time unit step function, $u[m]$, is defined in (B.10). Expanding (3.50) using (B.10) and (3.48) gives:

$$b_{dco}[n] = \begin{cases} 0 & , \; n \leq 0 \\ \int_{-\infty}^{\infty} \phi_0(n\mathrm{T} - t) \; r_d(t) \; dt & , \; n > 0. \end{cases} \tag{3.51}$$

This gives $b_{dco}[n]$ in terms of the presently unknown function $r_d(t)$. But it means that to minimize the MSE, $\varepsilon_{dc}(b_d, r_d)$, requires the strictly-causal coefficients of the feedback filter, $b_d[n]$, be set equal to the samples of the equalized combined channel. Note that this result is based upon the assumptions in the system model of Chapter 2, assumptions such as mutually uncorrelated data. This is the same result found in [108, 109] where there is a linear channel, additive white noise, but no cyclostationary interference. Setting the coefficients according to (3.51) means that the feedback filter of the decision-feedback equalizer subtracts off the postcursor intersymbol interference.

The values of $b_{dco}[n]$ could be determined after $r_{dco}(t)$ has been found but it will turn out that they will not be explicitly needed to find the MMSE ε_{dco}. Eliminate $b_d[n]$

from $\varepsilon_{dc}(b_d, r_d)$ by substituting the optimal value of $b_d[n]$, $b_{dco}[n]$ from (3.50), into (3.43) to get the MSE which is only a function of $r_d(t)$, called $\varepsilon_{dc}(r_d)$:

$$\begin{aligned}\varepsilon_{dc}(r_d) = \quad & < r_d \, , \, K_l r_d >_c - < r_d \, , \, m_0 >_c - < r_d^* \, , \, m_0^* >_c + 1 \\ & - < K_0 r_d \, , \, u[n-1] \, K_0 r_d >_d \\ & - < K_0 r_d^* \, , \, u[n-1] \, K_0 r_d^* >_d \\ & + < u[n-1] \, K_0 r_d \, , \, u[n-1] \, K_0 r_d >_d \end{aligned} \tag{3.52}$$

$$\begin{aligned}\therefore \varepsilon_{dc}(r_d) = \quad & < r_d \, , \, K_l r_d >_c - < r_d \, , \, m_0 >_c - < r_d^* \, , \, m_0^* >_c + 1 \\ & - < K_0 r_d \, , \, u[n-1] \, K_0 r_d >_d \\ & - < K_0 r_d^* \, , \, u[n-1] \, K_0 r_d^* >_d \\ & + < K_0 r_d \, , \, u[n-1] \, K_0 r_d >_d \end{aligned} \tag{3.53}$$

$$\begin{aligned}\therefore \varepsilon_{dc}(r_d) = \quad & < r_d \, , \, K_l r_d >_c - < r_d \, , \, m_0 >_c - < r_d^* \, , \, m_0^* >_c + 1 \\ & - < K_0 r_d^* \, , \, u[n-1] \, K_0 r_d^* >_d \end{aligned} \tag{3.54}$$

$$\therefore \varepsilon_{dc}(r_d) = < r_d \, , \, K_d r_d >_c - < r_d \, , \, m_0 >_c - < r_d^* \, , \, m_0^* >_c + 1 \tag{3.55}$$

where the notation for the Fredholm integral operator[17], K_d, of the function $\bullet(t)$ is defined as:

$$\begin{aligned} K_d \bullet (t) &= (K_d \bullet (t))(t) \\ &= \int_{-\infty}^{\infty} k_d(t, \tau) \bullet (\tau) \, d\tau \end{aligned} \tag{3.56}$$

and the Hermitian kernel of the integral operator is:

$$\begin{aligned} k_d(t, \tau) = \; & \mathrm{No}\delta(t-\tau) + \sum_{n=-\infty}^{0} \phi_0^*(n\mathrm{T} - t) \, \phi_0(n\mathrm{T} - \tau) \\ & + \sum_{i=1}^{\mathrm{L}} \sum_{n=-\infty}^{\infty} \phi_i^*(n\mathrm{T} - t) \, \phi_i(n\mathrm{T} - \tau). \end{aligned} \tag{3.57}$$

[17] If this had been a derivation for the *linear* equalizer in cyclostationary interference instead of the *decision-feedback* equalizer in cyclostationary interference, the Fredholm integral operator in (3.55) would have been K_l instead of K_d.

The minimization of $\varepsilon_{dc}(r_d)$ in (3.55) with respect to the forward filter, $r_d(t)$, has been performed using the calculus of variations [177] and is shown in Appendix B.2. The optimal value of $r_d(t)$ satisfies the following equation:

$$K_d r_{dco}(t) \;=\; m_0(t) \tag{3.58}$$

which can be expanded to get the following *Fredholm integral equation of the first kind* [178] for the unknown $r_{dco}(t)$:

$$\int_{-\infty}^{\infty} k_d(t,\tau)\, r_{dco}(\tau)\, d\tau \;=\; \phi_0^*(-t)\,. \tag{3.59}$$

Before proceeding with the solution of (3.59), a few observations can be made.

The first observation is regarding an expression for the MMSE, ε_{dco}. By substituting (3.58) into (3.55) the MMSE becomes:

$$\varepsilon_{dco} \;=\; < r_{dco}\,,\, m_0 >_c \;-\; < r_{dco}\,,\, m_0 >_c \;-\; < r_{dco}^*\,,\, m_0^* >_c \;+ 1 \tag{3.60}$$

$$\begin{aligned} \therefore\ \varepsilon_{dco} \;&=\; -\,< r_{dco}^*\,,\, m_0^* >_c + 1 \\ &=\; 1 - \,< r_{dco}^*\,,\, m_0^* >_c \\ &=\; 1 \;-\; \int_{-\infty}^{\infty} \phi_0(-t)\, r_{dco}(t)\, dt. \end{aligned} \tag{3.61}$$

The second observation is regarding the form of the optimal decision-feedback equalizer. By expanding the integral in (3.59) and grouping all integrals over $d\tau$ into *constants* which are not functions of t, and rearranging gives the form of the decision-feedback equalizer (Note No $\neq$ 0):

$$r_{dco}(t) \;=\; \sum_{n=-\infty}^{0} a_0[n]\, \phi_0^*(n\mathrm{T} - t) \;+\; \sum_{i=1}^{\mathrm{L}} \sum_{n=-\infty}^{\infty} a_i[n]\, \phi_i^*(n\mathrm{T} - t) \tag{3.62}$$

where the coefficients $a_i[n]$ are defined as:

$$a_i[n] = \begin{cases} -\frac{1}{\mathrm{No}} h_{dco,0}[n] & ; \quad i = 0 \quad ; \quad n < 0 \\ \frac{1}{\mathrm{No}}(1 - h_{dco,0}[0]) & ; \quad i = 0 \quad ; \quad n = 0 \\ -\frac{1}{\mathrm{No}} h_{dco,i}[n] & ; \quad i \in \mathsf{L}_1 \quad ; \quad \forall n \end{cases} \tag{3.63}$$

the *sampled equalized combined channel* when the decision-feedback equalizer is operating at the MMSE point is:

$$h_{dco,0}[n] = \int_{-\infty}^{\infty} \phi_0(n\mathrm{T} - \tau)\, r_{dco}(\tau)\, d\tau \tag{3.64}$$

and finally the *sampled equalized combined co-channels* when the decision-feedback equalizer is operating at the MMSE point are:

$$h_{dco,i}[n] = \int_{-\infty}^{\infty} \phi_i(n\mathrm{T} - \tau)\, r_{dco}(\tau)\, d\tau \quad ; \quad i \in \mathsf{L}_1. \tag{3.65}$$

The form of (3.62) indicates that the optimal forward filter can be interpreted as a bank of filters matched to the individual $\{\phi_i(t) \mid i \in \mathsf{L}_0\}$ followed by discrete-time filters (T-spaced tapped delay lines) with impulse responses $a_i[n]$. The form of the optimal decision-feedback equalizer is shown Fig. 3.10. The discrete-time filter following the matched filter $\phi_0^*(-t)$ is anti-causal while the discrete-time filters following the filters matched to the interferers are two-sided. Note that for the case where all the interferers are zero, Fig. 3.10 reverts to the familiar form of a matched filter followed by an anti-causal synchronous equalizer which minimizes the MSE component due to the precursor ISI [108, 109].

An important note about this equalizer is that it is *time invariant.* The time invariance occurs because the MSE is minimized only at symbol-rate samples, and because the output of the channel is wide-sense stationary when sampled at the symbol rate. To properly verify that the equalizer is time invariant, the development should have been started from a time-variant point of view, but the excess notation would make the explanation more complex. For completeness, such a development is outlined briefly in

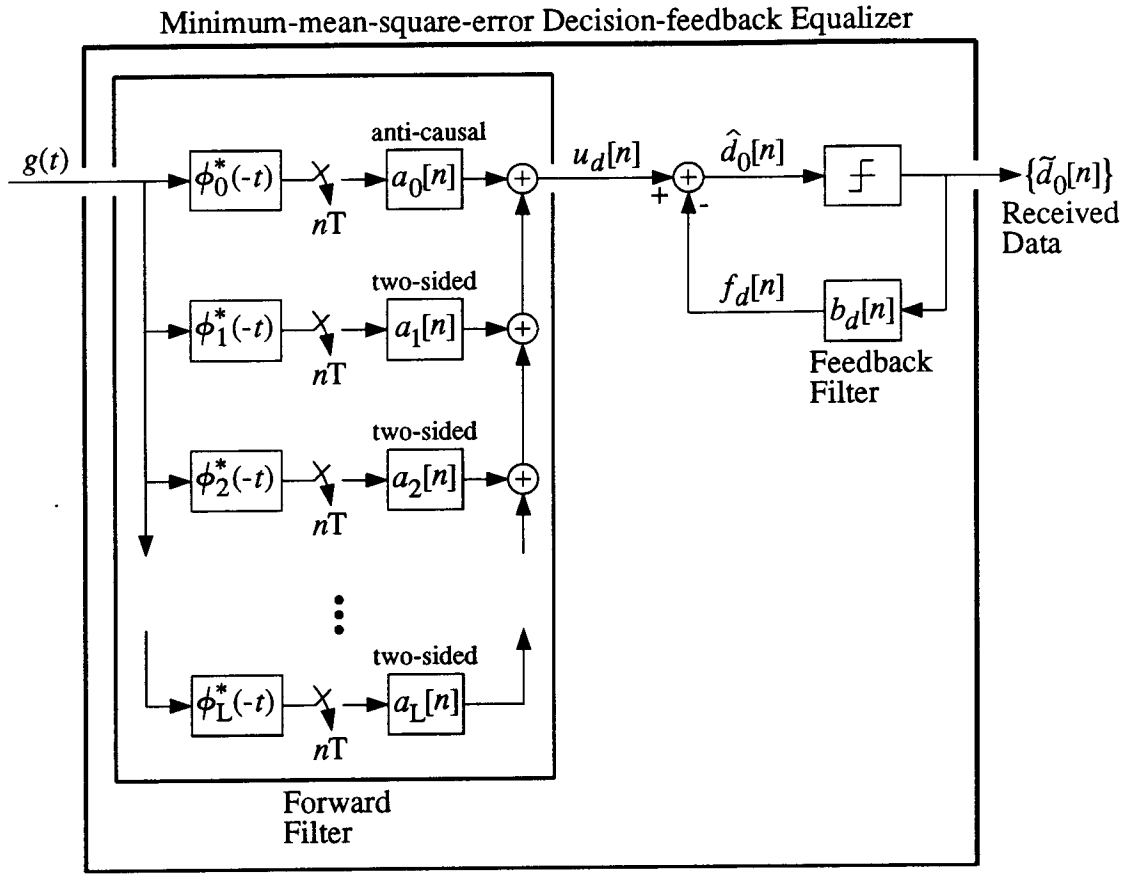

Figure 3.10 Form of the minimum-mean-square-error decision-feedback equalizer

Appendix A.1. Note also that the classical MMSE equalizer for a data signal without crosstalk is also time invariant even though the data signal is cyclostationary [179].

Having made these observations, the next step in the development is to find the impulse response of the optimal forward filter, $r_{dco}(t)$, from the integral equation (3.59). The problem of finding $r_{dco}(t)$ can be interpreted as finding the unknown input, $r_{dco}(t)$, to a linear system with a known periodically time-invariant impulse response, $k_d(t,\tau)$, and a known output, $\phi_0^*(-t)$. In [176], is suggested a solution of the Fredholm integral equation with a conjugate symmetric kernel using a set of eigenvectors of the operator. Since sinusoids are eigenvectors of stable linear systems in steady state [180], the solution of (3.59) will be done by Fourier analysis.

Take continuous-time continuous-frequency Fourier transforms, $\mathcal{F}_{cc}[\bullet]$, of equation (3.59), to get the following:

$$\Phi_0^*(f)\left[\frac{1}{\mathrm{T}}\sum_{l=-\infty}^{\infty}\Phi_0\left(f+\frac{l}{\mathrm{T}}\right)R_{dco}\left(f+\frac{l}{\mathrm{T}}\right)\right]_- + \mathrm{No}\,R_{dco}(f) + \sum_{i=1}^{\infty}\Phi_i^*(f)\left[\frac{1}{\mathrm{T}}\sum_{l=-\infty}^{\infty}\Phi_i\left(f+\frac{l}{\mathrm{T}}\right)R_{dco}\left(f+\frac{l}{\mathrm{T}}\right)\right] = \Phi_0^*(f) \quad \forall f \tag{3.66}$$

where:

$$R_{dco}(f) = \mathcal{F}_{cc}[\, r_{dco}(t)\,]. \tag{3.67}$$

Note that (3.66) is defined for all frequencies, f. The anti-causal operator, $[\bullet]_-$, is defined in Appendix C[18]. The third term on the left side of (3.66) indicates the presence of cyclostationary interferers instead of just white noise in the channel. The presence of the anti-causal operator will influence the solution of (3.66).

---

[18] The presence of the anti-causal operator, $[\bullet]_-$, means that this is the equation for the *decision-feedback* equalizer in cyclostationary interference instead of the *linear* equalizer in cyclostationary interference.

In (3.66), replace f by $f + (k/\mathrm{T})$, where $k \in \mathbf{Z}$, shift an index of summation, and rearrange to get an equivalent equation:

$$\Phi_0^*\left(f+\frac{k}{\mathrm{T}}\right)\left[H_{dco,0}^{\mathrm{T}}(f)\right]_- + \sum_{m=-\infty}^{\infty} W_{k,m}(f)\, R_{dco}\left(f+\frac{m}{\mathrm{T}}\right) = \Phi_0^*\left(f+\frac{k}{\mathrm{T}}\right)$$
$$-\frac{1}{2\mathrm{T}} < f \leq \frac{1}{2\mathrm{T}}$$
$$k \in \mathbf{Z} \tag{3.68}$$

where the sampled equalized combined channel when the decision-feedback equalizer is operating at the MMSE point is:

$$H_{dco,0}^{\mathrm{T}}(f) = \frac{1}{\mathrm{T}} \sum_{l=-\infty}^{\infty} \Phi_0\left(f+\frac{l}{\mathrm{T}}\right) R_{dco}\left(f+\frac{l}{\mathrm{T}}\right) \tag{3.69}$$

and

$$W_{n,m}(f) = \mathrm{No}\,\delta[n-m] + \frac{1}{\mathrm{T}} \sum_{i=1}^{\infty} \Phi_i^*\left(f+\frac{n}{\mathrm{T}}\right) \Phi_i\left(f+\frac{m}{\mathrm{T}}\right). \tag{3.70}$$

The superscript T in a frequency response such as $H_{dco,0}^{\mathrm{T}}(f)$ is used to indicate that it is the discrete-time continuous-frequency Fourier transform, $\mathcal{F}_{dc}[\bullet]$, of $h_{dco,0}[n]$. Note $H_{dco,0}^{\mathrm{T}}(f)$ that is periodic in the frequency domain with period being $1/\mathrm{T}$. The discrete-time continuous-frequency Fourier transform, $\mathcal{F}_{dc}[\bullet]$, is described in Appendix C. At this point, the situation can be interpreted as there being two unknowns, $R_{dco}(f)$ and $H_{dco,0}^{\mathrm{T}}(f)$, and two equations, (3.68) and (3.69).

In fact, equation (3.68) represents an infinite number of equations in k. However, the number of equations will become finite if the combined channel and combined co-channels, $\{\Phi_i(f) \mid i \in \mathsf{L}_0\}$, are strictly bandlimited to $K_t/(2\mathrm{T})$:

$$\Phi_i(f) = 0 \quad ; \quad i \in \mathsf{L}_0 \quad ; \quad |f| \geq K_t/(2\mathrm{T}) \quad ; \quad K_t \in \mathbf{Z}^+. \tag{3.71}$$

Equation (3.68) reduces to a set of $2K_t - 1$ equations for:

$$k \in \{\, -(K_t-1)\,,\, \ldots\,,\, -1\,,\, 0\,,\, 1\,,\, \ldots\,,\, (K_t-1)\,\} \tag{3.72}$$

which can be written in matrix form as:

$$\begin{aligned} \mathbf{\Phi}_0(f)\left[H^{\mathrm{T}}_{dco,0}(f)\right]_- + \mathbf{W}_{ci}(f)\,\mathbf{R}_{\mathbf{dco}}(f) &= \mathbf{\Phi}_0(f) \\ -\frac{1}{2\mathrm{T}} < f &\leq \frac{1}{2\mathrm{T}} \end{aligned} \tag{3.73}$$

where $\mathbf{\Phi}_0(f)$ and $\mathbf{R}_{\mathbf{dco}}(f)$ are column vectors with $(2K_t - 1)$ rows:

$$\mathbf{\Phi}_i(f) = \begin{bmatrix} \Phi_i^*(f - \frac{K_t-1}{\mathrm{T}}) \\ \vdots \\ \Phi_i^*(f - \frac{1}{\mathrm{T}}) \\ \Phi_i^*(f) \\ \Phi_i^*(f + \frac{1}{\mathrm{T}}) \\ \vdots \\ \Phi_i^*(f + \frac{K_t-1}{\mathrm{T}}) \end{bmatrix} \tag{3.74}$$

$$\mathbf{R}_{\mathbf{dco}}(f) = \begin{bmatrix} R_{dco}(f - \frac{K_t-1}{\mathrm{T}}) \\ \vdots \\ R_{dco}(f - \frac{1}{\mathrm{T}}) \\ R_{dco}(f) \\ R_{dco}(f + \frac{1}{\mathrm{T}}) \\ \vdots \\ R_{dco}(f + \frac{K_t-1}{\mathrm{T}}) \end{bmatrix} \tag{3.75}$$

$\mathbf{W}_{ci}(f)$ is a $(2K_t - 1) \times (2K_t - 1)$ matrix:

$$\mathbf{W}_{ci}(f) = \begin{bmatrix} W_{-(K_t-1),-(K_t-1)}(f) & \cdots & W_{-(K_t-1),+(K_t-1)}(f) \\ \vdots & \ddots & \vdots \\ W_{+(K_t-1),-(K_t-1)}(f) & \cdots & W_{+(K_t-1),+(K_t-1)}(f) \end{bmatrix} \tag{3.76}$$

$$\therefore\ \mathbf{W}_{ci}(f) = \mathrm{No}\,\mathbf{I}_{2K_t-1} + \frac{1}{\mathrm{T}}\sum_{i=1}^{\mathrm{L}} \mathbf{\Phi_i}(f)\,\mathbf{\Phi_i^*}(f) \tag{3.77}$$

and $\mathbf{I}_{2K_t-1}$ is an identity matrix of order $2K_t - 1$.

Solve equation (3.73) for $\mathbf{R}_{\mathbf{dco}}(f)$, by inverting the positive definite matrix [181] $\mathbf{W}_{ci}(f)$, then premultiply both sides of the equation by $(1/\mathrm{T})\mathbf{\Phi_0^*}(f)$ to get:

$$M^{\mathrm{T}}_{ci}(f)\left[H^{\mathrm{T}}_{dco,0}(f)\right]_- + H^{\mathrm{T}}_{dco,0}(f) = M^{\mathrm{T}}_{ci}(f) \tag{3.78}$$

$$\therefore\ H^{\mathrm{T}}_{dco,0}(f) \;=\; M^{\mathrm{T}}_{ci}(f)\left(1-\left[H^{\mathrm{T}}_{dco,0}(f)\right]_{-}\right) \tag{3.79}$$

where (3.71) and (3.69) imply that $H^{\mathrm{T}}_{dco,0}(f)$ can also be written as:

$$H^{\mathrm{T}}_{dco,0}(f) \;=\; \frac{1}{\mathrm{T}}\,\mathbf{\Phi_0^*}(f)\,\mathbf{R_{dco}}(f) \tag{3.80}$$

and

$$M^{\mathrm{T}}_{ci}(f) \;=\; \frac{1}{\mathrm{T}}\;\mathbf{\Phi_0^*}(f)\;\mathbf{W}^{-1}_{ci}(f)\;\mathbf{\Phi_0}(f). \tag{3.81}$$

$M^{\mathrm{T}}_{ci}(f)$ is real and non-negative for all frequencies; thus it has the form of a power spectrum. Equation (3.78) contains only $H^{\mathrm{T}}_{dco,0}(f)$; $R_{dco}(f)$ is not present.

Equation (3.79) may be solved for $H^{\mathrm{T}}_{dco,0}(f)$ by minimum phase spectral factorization [171, 182, 183] of $1+M^{\mathrm{T}}_{ci}(f)$ into a causal component, $Z^{\mathrm{T}}_{+}(f)$, and an anti-causal component, $Z^{\mathrm{T}}_{-}(f)$, that satisfy:

$$\begin{aligned}
1+M^{\mathrm{T}}_{ci}(f) \;&=\; Z^{\mathrm{T}}_{+}(f)\,Z^{\mathrm{T}}_{-}(f) \;=\; Z^{\mathrm{T}}(f)\\
\delta[n]+m_{ci}[n] \;&=\; z_{+}[n]\;\star\; z_{-}[n]\\
Z^{\mathrm{T}^*}_{+}(f) \;&=\; Z^{\mathrm{T}}_{-}(f)\\
Z^{\mathrm{T}}_{-}(f) \;&=\mathcal{F}_{dc}[z_{-}[n]]\\
Z^{\mathrm{T}}_{+}(f) \;&=\mathcal{F}_{dc}[z_{+}[n]]
\end{aligned} \tag{3.82}$$

and by breaking $H^{\mathrm{T}}_{dco,0}(f)$ into the following components (See Appendix C, property (C.7)):

$$H^{\mathrm{T}}_{dco,0}(f) \;=\; \left[H^{\mathrm{T}}_{dco,0}(f)\right]_{-} \;+\; \left[H^{\mathrm{T}}_{dco,0}(f)\right]_{++} \tag{3.83}$$

to get:

$$\left[H^{\mathrm{T}}_{dco,0}(f)\right]_{-} \;+\; \left[H^{\mathrm{T}}_{dco,0}(f)\right]_{++} \;=\; \left(Z^{\mathrm{T}}_{-}(f)\,Z^{\mathrm{T}}_{+}(f)\;-\;1\right)\left(1\;-\;\left[H^{\mathrm{T}}_{dco,0}(f)\right]_{-}\right) \tag{3.84}$$

$$\therefore\ Z^{\mathrm{T}}_{-}(f)\left[H^{\mathrm{T}}_{dco,0}(f)\right]_{-} \;=\; Z^{\mathrm{T}}_{-}(f)\;-\;\frac{1}{Z^{\mathrm{T}}_{+}(f)}\;-\;\frac{1}{Z^{\mathrm{T}}_{+}(f)}\left[H^{\mathrm{T}}_{dco,0}(f)\right]_{++}. \tag{3.85}$$

Apply the anti-causal operator, $[\bullet]_-$, to both sides of this equation and using property (C.11) in Appendix C to observe that the last term on the right-hand side is zero gives:

$$Z_-^{\mathrm{T}}(f)\left[H_{dco,0}^{\mathrm{T}}(f)\right]_- = Z_-^{\mathrm{T}}(f) - \left[\frac{1}{Z_+^{\mathrm{T}}(f)}\right]_- \tag{3.86}$$

or:

$$\left[H_{dco,0}^{\mathrm{T}}(f)\right]_- = 1 - \frac{1}{Z_-^{\mathrm{T}}(f)}\left[\frac{1}{Z_+^{\mathrm{T}}(f)}\right]_- . \tag{3.87}$$

Substitute $\left[H_{dco,0}^{\mathrm{T}}(f)\right]_-$ from equation (3.87) into equation (3.73) and solve for $\mathbf{R}_{\mathbf{dco}}(f)$ to get:

$$\begin{aligned}\mathbf{R}_{\mathbf{dco}}(f) &= \mathbf{W}_{ci}^{-1}(f)\ \mathbf{\Phi_0}(f)\ \frac{1}{Z_-^{\mathrm{T}}(f)}\ \left[\frac{1}{Z_+^{\mathrm{T}}(f)}\right]_- \\ -\frac{1}{2\mathrm{T}} &< f \leq \frac{1}{2\mathrm{T}}\end{aligned} \tag{3.88}$$

from which $R_{dco}(f)$ may be taken from the components of $\mathbf{R}_{\mathbf{dco}}(f)$.

The expression for the MMSE, ε_{dco}, can be obtained as follows. From (3.61) and (3.64), ε_{dco} can be written as:

$$\begin{aligned}\varepsilon_{dco} &= 1 - h_{dco,0}[0] \\ &= \left\langle 1 - \left[H_{dco,0}^{\mathrm{T}}(f)\right]_- \right\rangle\end{aligned} \tag{3.89}$$

where

$$\langle \bullet \rangle = \mathrm{T}\int_{-\frac{1}{2\mathrm{T}}}^{+\frac{1}{2\mathrm{T}}} [\bullet]\, df. \tag{3.90}$$

Using (3.87), ε_{dco} from (3.89) can be written as:

$$\varepsilon_{dco} = \left\langle \frac{1}{Z_-^{\mathrm{T}}(f)}\left[\frac{1}{Z_+^{\mathrm{T}}(f)}\right]_- \right\rangle. \tag{3.91}$$

From (3.82) and the analysis in [108, 109], ε_{dco} from (3.91) can be written as:

$$\varepsilon_{dco} = e^{-\left\langle \ln\left(Z^{\mathrm{T}}(f)\right)\right\rangle}. \tag{3.92}$$

Once again from (3.82), ε_{dco} can be written as:

$$\varepsilon_{dco} = e^{-\left\langle \ln\left(1 + M_{ci}^{\mathrm{T}}(f)\right)\right\rangle}. \tag{3.93}$$

Equation (3.93) is the final result, the expression for the MMSE of a continuous-time infinite-length decision-feedback equalizer in the presence of intersymbol interference, multiple cyclostationary interferers, and additive white noise. In summary, the related functions and assumptions necessary to calculate ε_{dco} are defined in (3.81), (3.77), (3.74), (3.71), and (3.36).

Additional insight can be gained about the behavior of the MMSE DFE by using another form of the MMSE. The alternate DFE MMSE form can be obtained from (3.61), by substituting the complex conjugate of $\phi_0^*(-t)$ from (3.59) into (3.61), expanding using (3.57), (3.64), (3.65), and rearranging to get:

$$\varepsilon_{dco} = \sigma_{bd}^2 + \sigma_{isi_-}^2 + \sigma_{ci}^2 + \sigma_n^2 \tag{3.94}$$

where

$$\begin{aligned}
\sigma_{bd}^2 &= \left| 1 - h_{dco,0}[0] \right|^2 \\
\sigma_{isi_-}^2 &= \sum_{n=-\infty}^{-1} \left| h_{dco,0}[n] \right|^2 \\
\sigma_{ci}^2 &= \sum_{i=1}^{\mathrm{L}} \sum_{n=-\infty}^{\infty} \left| h_{dco,i}[n] \right|^2 \\
\sigma_n^2 &= \mathrm{No} \int_{-\infty}^{\infty} \left| r_{dco}(t) \right|^2 dt.
\end{aligned} \tag{3.95}$$

The MMSE consists of four components due to the bias in the estimate of the data σ_{bd}^2 [86], the precursor ISI $\sigma_{isi_-}^2$, the ACI, CCI, or both σ_{ci}^2, and the noise σ_n^2. The terms $\sigma_{isi_-}^2$ and σ_{ci}^2 have also been grouped into a single term called the multi-dimensional interference (MDI) [54, 55]. The forward filter of the DFE acts to cause the sampled equalized combined channel to be at or near zero at the sampling points before the time origin and at or near unity at the time origin [65, 66, 108–111, 161]. The sampled

equalized combined channel to the right of the time origin is not relevant to the forward filter because the feedback part of the DFE subtracts off the postcursor ISI. This is the same as the additive white noise case with no interferers. However, in the presence of interferers, the forward filter also acts to make the sampled equalized combined co-channels at or near zero for all sampling points.

At the detector input, signal $\widehat{d}_0[n]$ in Fig. 3.9, the ratio of the powers of the signal carrying the data of interest to the interference-plus-noise is given by:

$$\gamma_{dco}^{I,N} = \frac{| h_{dco,0}[0] |^2}{\sigma_{isi}^2 + \sigma_{ci}^2 + \sigma_n^2} \tag{3.96}$$

where the terms are defined in (3.64), (3.65), (3.67), (3.88), and (3.95). By using (3.89), (3.94), (3.95) $\gamma_{dco}^{I,N}$ can be rewritten as:

$$\gamma_{dco}^{I,N} = \frac{1 - \varepsilon_{dco}}{\varepsilon_{dco}}. \tag{3.97}$$

3.4 Theoretical Comparisons among Equalizer and Interference Types

In Tables 3.1 and 3.2 is a summary of the MMSE expressions for *six* cases. They are obtained from *two* equalizer types in the presence of *three* interference types. The two equalizer types are linear and decision-feedback. The three interference types are white noise, stationary noise of Chapter 2, and cyclostationary interference of Chapter 2. The sources of the MMSE expressions are described in Appendix D. This section contains a few theoretical comparisons among these six MMSE expressions which are denoted by ε_{lwo}, ε_{lso}, ε_{lco}, ε_{dwo}, ε_{dso}, and ε_{dco}; the subscripts l, d, w, s, c, o, respectively denote *linear*, *decision-feedback*, *white noise*, *stationary noise*, *cyclostationary interference*, and *optimal*.

If the combined co-channels are zero, then by comparison of the expressions in Tables 3.1 and 3.2 the performance in white noise, stationary noise and cyclostationary

Table 3.1 Minimum mean square error expressions

Interference Types	Equalizer Types	
	Linear	**Decision-feedback**
White Noise	$\varepsilon_{lwo} = \left\langle \frac{1}{1+M_w^{\mathrm{T}}(f)} \right\rangle$	$\varepsilon_{dwo} = e^{-\left\langle \ln\left(1+M_w^{\mathrm{T}}(f)\right)\right\rangle}$
Stationary Noise	$\varepsilon_{lso} = \left\langle \frac{1}{1+M_{sn}^{\mathrm{T}}(f)} \right\rangle$	$\varepsilon_{dso} = e^{-\left\langle \ln\left(1+M_{sn}^{\mathrm{T}}(f)\right)\right\rangle}$
Cyclostationary Interference	$\varepsilon_{lco} = \left\langle \frac{1}{1+M_{ci}^{\mathrm{T}}(f)} \right\rangle$	$\varepsilon_{dco} = e^{-\left\langle \ln\left(1+M_{ci}^{\mathrm{T}}(f)\right)\right\rangle}$

Table 3.2 Ratios of powers of sampled equalized combined channel to interference type

Interference Type	**Ratios of Powers of Sampled Equalized Combined Channel to Interference Type** $M_w^{\mathrm{T}}(f),\ M_{sn}^{\mathrm{T}}(f),\ M_{ci}^{\mathrm{T}}(f) \quad ; \quad \lvert f\rvert \leq \frac{1}{2\mathrm{T}}$
White Noise	$M_w^{\mathrm{T}}(f) = \frac{1}{\mathrm{T}}\,\mathbf{\Phi}_0^*(f)\,\mathbf{W}_w^{-1}(f)\,\mathbf{\Phi}_0(f)$ $\mathbf{W}_n(f) = \mathrm{No}\mathbf{I}_{2K_t-1}$
Stationary Noise	$M_{sn}^{\mathrm{T}}(f) = \frac{1}{\mathrm{T}}\,\mathbf{\Phi}_0^*(f)\,\mathbf{W}_{sn}^{-1}(f)\,\mathbf{\Phi}_0(f)$ $\mathbf{W}_{sn}(f) = \mathrm{No}\mathbf{I}_{2K_t-1} + \frac{1}{\mathrm{T}}\sum_{i=1}^{\mathrm{L}}\mathrm{diag}[\mathbf{\Phi_i}(\mathrm{f})\,\mathbf{\Phi_i^*}(\mathrm{f})]$
Cyclostationary Interference	$M_{ci}^{\mathrm{T}}(f) = \frac{1}{\mathrm{T}}\,\mathbf{\Phi}_0^*(f)\,\mathbf{W}_{ci}^{-1}(f)\,\mathbf{\Phi}_0(f)$ $\mathbf{W}_{ci}(f) = \mathrm{No}\mathbf{I}_{2K_t-1} + \frac{1}{\mathrm{T}}\sum_{i=1}^{\mathrm{L}}\mathbf{\Phi_i}(f)\,\mathbf{\Phi_i^*}(f)$

interference is the same for both equalizers:

$$\begin{aligned} \Phi_i(f) &= 0 \quad ; \quad i \in \mathsf{L}_1 \\ \varepsilon_{lwo} &= \varepsilon_{lso} = \varepsilon_{lco} \\ \varepsilon_{dwo} &= \varepsilon_{dso} = \varepsilon_{dco}. \end{aligned} \tag{3.108}$$

In [184–186] is a proof that $\varepsilon_{lwo} \leq \varepsilon_{lco}$. Such a proof is achieved by expressing $M_{ci}^{\mathrm{T}}(f)$ and $\mathbf{W}_{ci}^{-1}(f)$ as follows:

$$\begin{aligned} M_{ci}^{\mathrm{T}}(f) &= M_{w}^{\mathrm{T}}(f) - M_{ci-w}^{\mathrm{T}}(f) \\ \mathbf{W}_{ci}^{-1}(f) &= \mathbf{W}_{w}^{-1}(f) - \mathbf{M}_{ci-w}(f) \end{aligned} \tag{3.109}$$

where $M_{ci-w}^{\mathrm{T}}(f)$ is a term which satisfies:

$$0 \leq M_{ci-w}^{\mathrm{T}}(f) \leq M_{ci}^{\mathrm{T}}(f) \tag{3.110}$$

and where $\mathbf{M}_{ci-w}(f)$ is a positive semi-definite matrix [181]. Therefore, $M_{ci-w}^{\mathrm{T}}(f)$ provides an MSE degradation in addition to $M_{w}^{\mathrm{T}}(f)$. The proof in [184–186] was achieved by expanding $\mathbf{W}_{ci}^{-1}(f)$, see (3.109), using repetitive applications of the Sherman-Morrison inversion formula [187]. The Sherman-Morrison inversion formula is:

$$[\mathrm{A} + \mathbf{x}_1\mathbf{x}_2^*]^{-1} = \mathrm{A}^{-1} - \frac{\mathrm{A}^{-1}\mathbf{x}_1\mathbf{x}_2^*\mathrm{A}^{-1}}{1 + \mathbf{x}_2^*\mathrm{A}^{-1}\mathbf{x}_1} \tag{3.111}$$

where A is an $n \times n$ matrix, $\mathbf{x}_1$ is an $n \times 1$ vector, $\mathbf{x}_2$ is an $n \times 1$ vector, and $\mathbf{x}_2^*\mathrm{A}^{-1}\mathbf{x}_1 \neq -1$. A similar proof can be used to show that $\varepsilon_{lwo} \leq \varepsilon_{lso}$. Finally, since the MMSE expressions for the decision-feedback equalizer are also based on the expression:

$$\frac{1}{1 + M_{\bullet}^{\mathrm{T}}(f)} \tag{3.112}$$

then the same comparisons apply and one can state:

$$\begin{aligned} \varepsilon_{lwo} &\leq \varepsilon_{lso} \\ \varepsilon_{lwo} &\leq \varepsilon_{lco} \\ \varepsilon_{dwo} &\leq \varepsilon_{dso} \\ \varepsilon_{dwo} &\leq \varepsilon_{dco}. \end{aligned} \tag{3.113}$$

It is of interest to compare the MMSE expressions for the stationary noise and cyclostationary interference cases. Write ε_{dco} as:

$$\varepsilon_{dco} \;=\; \varepsilon_{dso}\;\varepsilon_{d(c/s)o} \tag{3.114}$$

where

$$\begin{aligned} \varepsilon_{d(c/s)o} &= e^{-\left\langle \ln\left(\left(1+M_{ci}^{\mathrm{T}}(f)\right) / \left(1+M_{sn}^{\mathrm{T}}(f)\right) \right)\right\rangle} \\ &= e^{-\left\langle \ln\left(1+F_{c-s}^{\mathrm{T}}(f) \right)\right\rangle} \end{aligned} \tag{3.115}$$

and

$$F_{c-s}^{\mathrm{T}}(f) \;=\; \frac{1}{1+M_{sn}^{\mathrm{T}}(f)}\left[\, M_{ci}^{\mathrm{T}}(f) \;-\; M_{sn}^{\mathrm{T}}(f) \,\right]. \tag{3.116}$$

If $F_{c-s}^{\mathrm{T}}(f)$ was sufficiently positive over ranges of frequencies wide enough such that the averaging in (3.115) made $\varepsilon_{d(c/s)o}$ less than one, then ε_{dco} would be less than ε_{dso}. Conversely, if $F_{c-s}^{\mathrm{T}}(f)$ was sufficiently negative over ranges of frequencies wide enough such that the averaging in (3.115) made $\varepsilon_{d(c/s)o}$ greater than one, then ε_{dco} would be greater than ε_{dso}. To show that one cannot in general state a simple relative relationship among ε_{dco} and ε_{dso} two simple constructed examples will be used. For the first example, let the following apply:

$$\begin{aligned} \mathrm{L} &= 1 \\ \mathrm{No} &= 1 \\ \mathrm{T} &= 1 \\ \Phi_0(f) \;=\; \Phi_1(f) \;&=\; \begin{cases} 1 & ,|f| \le \frac{1}{2\mathrm{T}} \\ -1 & ,\left|f-\frac{3}{4\mathrm{T}}\right| < \frac{1}{4\mathrm{T}} \\ 0 & ,|f| \ge \frac{1}{\mathrm{T}}. \end{cases} \end{aligned} \tag{3.117}$$

This implies:

$$\begin{aligned} M_{ci}^{\mathrm{T}}(f) \;-\; M_{sn}^{\mathrm{T}}(f) &= 3 \;-\; 2 \\ &= 1 \end{aligned} \tag{3.118}$$

for all f except for possibly two removable singularities at 0 and $1/(2\mathrm{T})$ [188]. Therefore $\varepsilon_{d(c/s)o}$ is less than one, and ε_{dco} is less than ε_{dso}. For the second example,

let the following apply:

$$\begin{aligned} \mathrm{L} &= 1 \\ \mathrm{No} &= 1 \\ \mathrm{T} &= 1 \\ \Phi_0(f) &= \Phi_1(f) = \begin{cases} 1 & ,|f| < \frac{1}{\mathrm{T}} \\ 0 & ,|f| \geq \frac{1}{\mathrm{T}}. \end{cases} \end{aligned} \tag{3.119}$$

This implies:

$$\begin{aligned} M_{ci}^{\mathrm{T}}(f) - M_{sn}^{\mathrm{T}}(f) &= \frac{3}{4} - \frac{6}{4} \\ &= -\frac{3}{4} \end{aligned} \tag{3.120}$$

for all f except for possibly two removable singularities at 0 and $1/(2\mathrm{T})$. Therefore $\varepsilon_{d(c/s)o}$ is greater than one, and ε_{dco} is greater than ε_{dso}. By similar analogy with the linear equalizer using:

$$\varepsilon_{l(c/s)o} = -\left\langle \ln\left(\frac{1 + M_{ci}^{\mathrm{T}}(f)}{1 + M_{sn}^{\mathrm{T}}(f)}\right)\right\rangle \tag{3.121}$$

the general relationship between performance in stationary noise and cyclostationary interference will be stated as:

$$\begin{aligned} \varepsilon_{lco} &\begin{cases} < \varepsilon_{lso} & ,\varepsilon_{l(c/s)o} < 1 \\ = \varepsilon_{lso} & ,\varepsilon_{l(c/s)o} = 1 \\ > \varepsilon_{lso} & ,\varepsilon_{l(c/s)o} > 1 \end{cases} \\ \varepsilon_{dco} &\begin{cases} < \varepsilon_{dso} & ,\varepsilon_{d(c/s)o} < 1 \\ = \varepsilon_{dso} & ,\varepsilon_{d(c/s)o} = 1 \\ > \varepsilon_{dso} & ,\varepsilon_{d(c/s)o} > 1. \end{cases} \end{aligned} \tag{3.122}$$

Note that if the combined channel and combined co-channels are strictly bandlimited to $1/(2\mathrm{T})$, then $M_{sn}^{\mathrm{T}}(f)$ and $M_{ci}^{\mathrm{T}}(f)$ are the same, $\varepsilon_{l(c/s)o}$ and $\varepsilon_{d(c/s)o}$ are one, and the performance in stationary noise and cyclostationary interference is the same for both equalizers:

$$\begin{aligned} \varepsilon_{lso} &= \varepsilon_{lco} \\ \varepsilon_{dso} &= \varepsilon_{dco}. \end{aligned} \tag{3.123}$$

This is a result of the cyclostationary interference becoming wide-sense stationary as the bandwidth of the interferers is reduced below $1/(2\mathrm{T})$ [20].

In [108, 109] is a statement that $\varepsilon_{dwo} \leq \varepsilon_{lwo}$. Since the MMSE expressions in Table 3.1 take similar forms, this comparison also applies to the stationary noise and cyclostationary interference cases. For example, in the cyclostationary interference case:

$$\begin{aligned} \varepsilon_{dco} &= e^{-\left\langle \ln\left(1+M_{ci}^{\mathrm{T}}(f)\right)\right\rangle} \\ &= e^{\left\langle \ln\left(\,1\,/\,\left(1+M_{ci}^{\mathrm{T}}(f)\right)\,\right)\right\rangle} \\ &= e^{\left\langle \sum_{k=1}^{\infty}(1/k)\left(\,1\,/\,\left(1+M_{ci}^{\mathrm{T}}(f)\right)\,\right)^{k}\right\rangle} \end{aligned} \tag{3.124}$$

which uses a Taylor series expansion of $\ln(\bullet)$ in the range of convergence [188]. Repeated application of the Cauchy-Schwartz inequality [189] gives:

$$\begin{aligned} \therefore\ \varepsilon_{dco} &\leq e^{\left(\sum_{k=1}^{\infty}(1/k)\left\langle\,1\,/\,\left(1+M_{ci}^{\mathrm{T}}(f)\right)\,\right\rangle^{k}\right)} \\ &\leq e^{\ln\left(\left\langle\,1\,/\,\left(1+M_{ci}^{\mathrm{T}}(f)\right)\,\right\rangle\right)} \\ &\leq \varepsilon_{lco}. \end{aligned} \tag{3.125}$$

Thus, for all three types of interference the following is true:

$$\begin{aligned} \varepsilon_{lwo} &\leq \varepsilon_{dwo} \\ \varepsilon_{lso} &\leq \varepsilon_{dso} \\ \varepsilon_{lco} &\leq \varepsilon_{dco}. \end{aligned} \tag{3.126}$$

Chapter 4
Application to High-speed Digital Subscriber Lines

4.1 Background

The philosophy and economics behind the use of subscriber lines have been briefly discussed in Section 1.2. The goal of this chapter is to show how the general analyses and systems design considerations in Chapter 3 can be used to analyze and improve the performance in the specific application referred to as high-speed digital subscriber-lines [13].

A major goal of HDSL systems is to achieve full-duplex communication at T1 bit rates (1.544 M bits/s) using two twisted pairs which belong to a subset of twisted-pair subscriber lines from the loop plant known as the carrier serving area (CSA) [13]. Two twisted pairs that are at the extreme range of the CSA are 9000 feet of 26 AWG copper and 12000 feet of 24 AWG copper. These are some of the twisted-pair lines in the CSA which provide the greatest challenges to reliable communication.

The HDSL system has been analyzed by considering one twisted pair carrying 800 k bits/s using a 4-level linear modulation scheme called 2B1Q [2, 14]. The number of levels chosen were those obtained from evaluations based on assuming stationary near-end crosstalk [163]. Thus the symbol rate is 400 kHz (400 k symbols/s).

The model for the HDSL system will be expanded with particular emphasis on NEXT, the dominant impairment for HDSL transmission. The system will be analyzed using MMSE expressions derived in Chapter 3. Through calculations, these expressions have allowed predictions of system performance under the joint conditions of relative transmitter bandwidth and central-office clock-phase misalignment. It is shown that under certain conditions linear and decision-feedback equalizers are able to achieve improved performance by exploiting the cyclostationarity of the NEXT interference. Following these calculations are the results of simulations which attempt to quantify

some of the necessary increases in implementation complexity which are required for equalizers to exploit the cyclostationarity of the NEXT interference.

4.2 Models

4.2.1 Transmitter

The transmitter filter is included in Fig. 2.1, with its impulse response $p_{t,0}(t)$. A model for this impulse response will be developed here.

The basis for this model is a pulse that was obtained from a bilinear transform [142] of a 5^{th}-order Butterworth filter. Such a filter would be a discrete-time form and it was converted to a continuous-time form by ideal low-pass interpolation. The reason for these steps was to obtain a compromise between the demands that the filter have a maximum bandwidth and that the filter have realistic time-domain properties. The frequency response of the continuous-time filter, called $P_{bu}(f)$ is shown in Fig. 4.1. The magnitude, $|P_{bu}(f)|$, and phase components, $\arg(P_{bu}(f))$, are related by:

$$P_{bu}(f) = |P_{bu}(f)|\, e^{j \arg(P_{bu}(f))}. \tag{4.1}$$

Fig. 4.1a gives the magnitude response in dB; Fig. 4.1b gives the phase response in radians, modulo 2π.

The corresponding impulse response, called $p_{bu}(t)$, is defined from:

$$p_{bu}(t) = \mathcal{F}_{cc}^{-1}[P_{bu}(f)] \tag{4.2}$$

and is shown in Fig. 4.2.

Note the following properties of the filter. Its bandwidth is 1/T where as stated earlier, and in Fig. 4.1, the symbol rate 1/T is 400 kHz. It has a 3 dB cutoff at the frequencies $\pm 1/(2\mathrm{T})$. If this pulse, $P_{bu}(f)$, were used for $P_{t,0}(f)$ in Fig. 2.1 and the voltage at the output of the transmitter filter were applied to a 1 Ω resistor, then the transmitter output power would be 0.5 mW:

$$\frac{1}{\mathrm{T}} \int_{-\frac{1}{\mathrm{T}}}^{\frac{1}{\mathrm{T}}} |P_{bu}(f)|^2 \, df = 0.5 \text{ mW}. \tag{4.3}$$

[a]

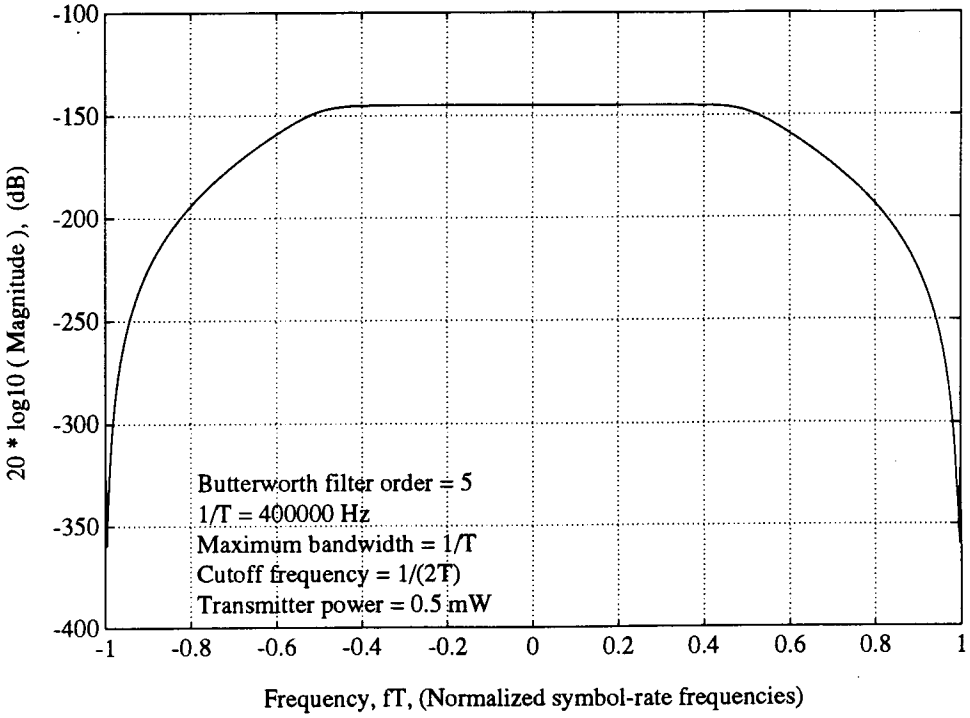

[b]

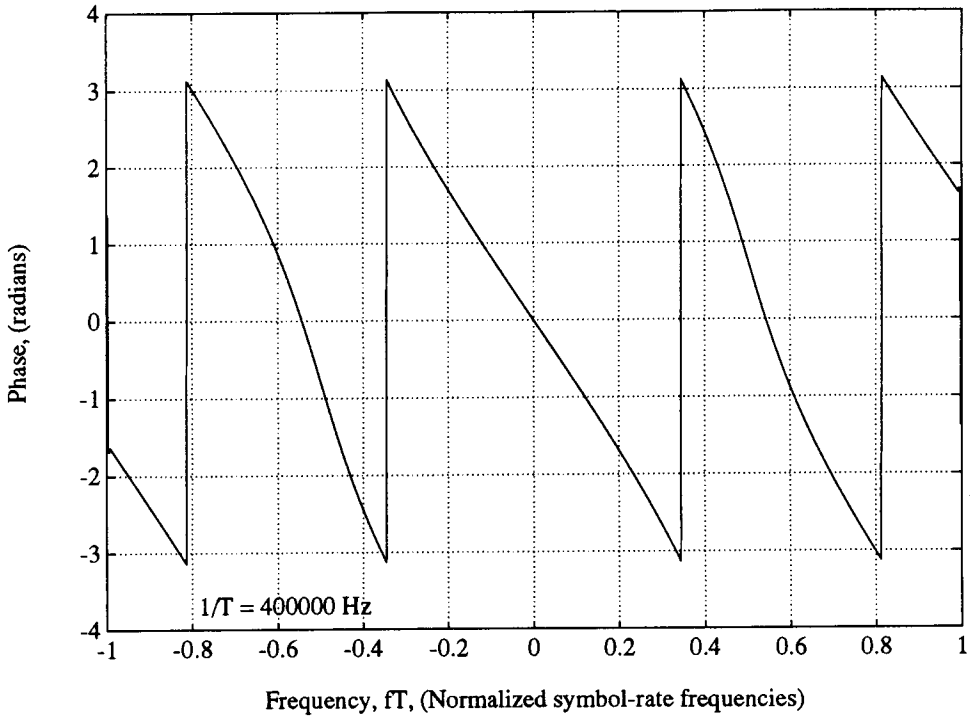

Figure 4.1 Magnitude and phase response of the Butterworth filter, $20\ \log_{10}(|P_{bu}(f)|)$ **and** $\arg(P_{bu}(f))$**, respectively.**

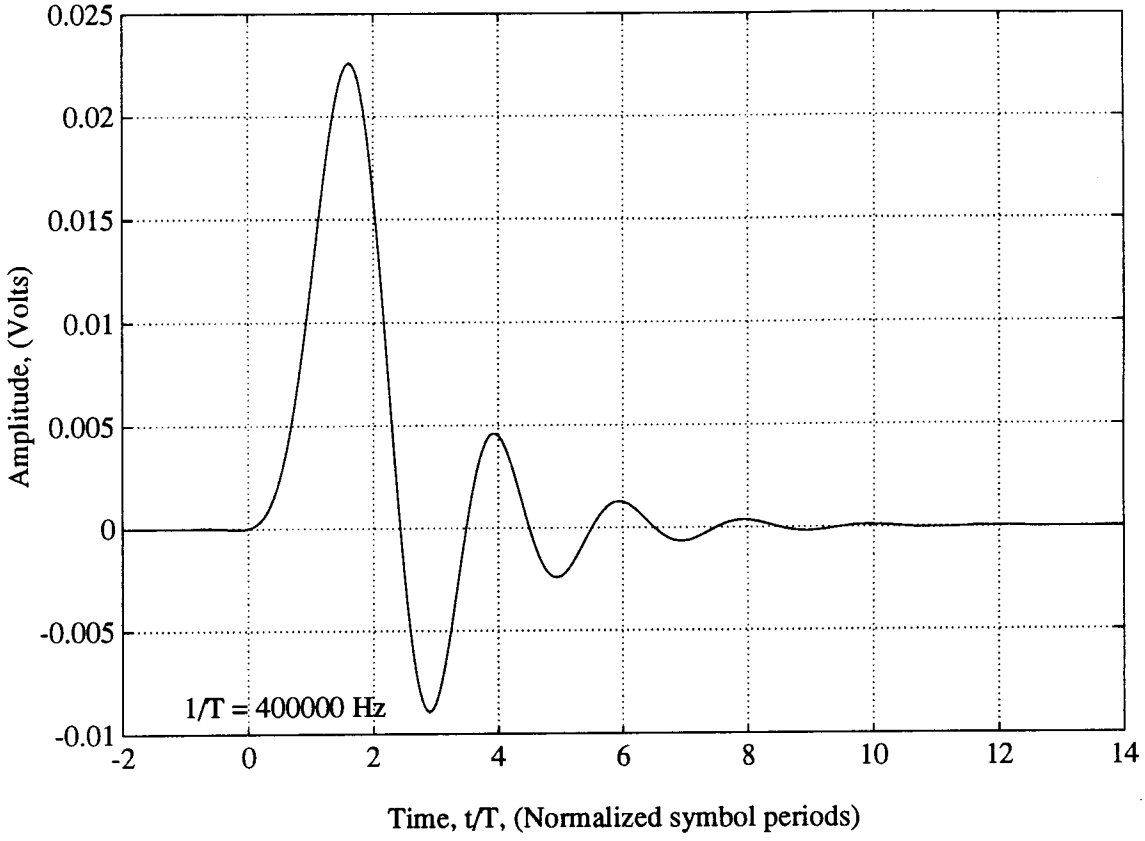

Figure 4.2 Impulse response of the Butterworth filter, $p_{bu}(t)$

Also, the effective bandwidth of this pulse will be less than maximum bandwidth. The extent to which the effective bandwidth is reduced from the maximum depends upon the interference and receiver [172].

The transmitter pulse based solely on $P_{bu}(f)$ does not have all the desirable properties of bandwidth and transmitter phase for the evaluations in this chapter. Therefore for the transmitters shown or implied in Figs. 2.1, 2.2, and 2.4 define:

$$\begin{aligned} P_{t,i}(f) &= \mathcal{F}_{cc}[\, p_{t,i}(t)\,] \\ &= \frac{1}{\sqrt{\mathrm{B_t}}}\, P_{bu}\!\left(\frac{f}{\mathrm{B_t}}\right) e^{-j2\pi f(\mathrm{D}_i/\mathrm{T})} \quad ; \quad i \in \mathsf{L}_0 \end{aligned} \tag{4.4}$$

where the transmitter bandwidth relative to the symbol rate is $\mathrm{B_t}$ ($\mathrm{B_t} \in \mathbf{R},\ \mathrm{B_t} > 0$), the phase shift (delay) of the transmitted signal relative to the symbol period is denoted by D_0 ($\mathrm{D}_0 \in [0,1]$), and the phase shifts (delays) of the interfering signals relative to the symbol period are denoted by $\{\mathrm{D}_i \mid i \in \mathsf{L}_1\}$ ($\{\mathrm{D}_i \in [0,1] \mid i \in \mathsf{L}_1\}$). The units of $\mathrm{B_t}$ will be called *symbol frequencies*. The units of $\{\mathrm{D}_i \mid i \in \mathsf{L}_0\}$ will be called *symbol periods*.

The transmitter pulses defined in (4.4) for $\{P_{t,i}(f) \mid i \in \mathsf{L}_0\}$ have the following properties. As the relative bandwidth $\mathrm{B_t}$ varies, the power at the output of the transmitter filters remains constant at 0.5 mW. When $\mathrm{B_t} = 0.5$ symbol frequencies this pulse has the same maximum bandwidth as a raised cosine pulse [86] with zero-percent excess bandwidth; similarly $\mathrm{B_t} = 1$ symbol frequency corresponds to 100-percent excess bandwidth. However when $\mathrm{B_t}$ is greater than 1 symbol frequency, the bandwidth of the pulse is greater than that which can be modelled using a conventional raised cosine pulse. The large relative bandwidth variability of $\{P_{t,i}(f) \mid i \in \mathsf{L}_0\}$ is important to help quantify the potential for gains suggested in the analysis in Section 3.2.

In this high-speed digital subscriber-line application, NEXT is the dominant impairment [13]. To model this impairment the interference $\nu(t)$ in Fig. 2.1 is chosen to arise from neighboring transmitters the same side of the subscriber-line channel as that of the receiver; also, this side is chosen to be in the central office since the NEXT problem is more severe in the central office than at the customer end. Hence the issue of aligning

the relative phases of the clocks of the transmitters in the central office is modelled by making $\{D_i \mid i \in L_1\}$ as similar as possible in value. It is inherently assumed that the values $\{D_i \mid i \in L_1\}$ are design parameters. However, the relative phase of the clock of the transmitter at the far end (the customer end), D_0, is not considered to be a design parameter. The performance evaluations of the subscriber-line system to follow must assume that the value of D_0 is set to give the worst performance.

The relative phase shifts of the transmitter clocks of the interferers in the central office, $\{D_i \mid i \in L_1\}$, are defined in terms of the single parameter M, the percent misalignment of the transmitter clock phases of the NEXT interferers:

$$D_i = \frac{M}{100} \frac{i-1}{L} \quad ; \quad i \in L_1. \tag{4.5}$$

The parameter M is used to study the effects of aligning the phases of the clocks of the transmitters in a rack of equipment at the central office, not the clocks at the customer end where the NEXT is less severe. M is the percent misalignment over one symbol period. Stated another way, the beginnings of the impulse responses of the clocks of the interferers are uniformly distributed over M percent of a symbol period. When M is 0 percent the interferers are perfectly aligned in phase and the interference has the near-largest amount of cyclostationarity. When M is 100 percent, the interference has the near-smallest amount of cyclostationarity. Note that M was not obtained from measurements but introduced as a parameter in the calculations.

Finally, note the pulse bandwidth was varied but the pulse *shape* was not varied since its effect on performance, in this application, is expected to be less significant than that of the relative pulse bandwidth; a similar effect was observed for stationary interference in [162]. However, in other applications it may be economical to design the shapes of the relatively wide bandwidth transmitter pulses to achieve improved interference suppression capability [190].

4.2.2 Channel

The channel filter is shown in Fig. 2.1, with its impulse response $c_0(t)$. A model for this impulse response will be developed here.

The channel is 9000 feet of 26 gauge wire with hybrid transformers at each end [75, 113]. This is one of the worst-case lines considered for high-speed digital subscriber-line transmission [13].

The frequency response of the channel, called $C_0(f)$, and defined from:

$$C_0(f) \;=\; \mathcal{F}_{cc}[c_0(t)] \tag{4.6}$$

is shown in Fig. 4.3. The magnitude, $|C_0(f)|$, and phase components, $\arg(C_0(f))$, are related by:

$$C_0(f) \;=\; |C_0(f)|\, e^{j \arg(C_0(f))}. \tag{4.7}$$

Fig. 4.3a gives the magnitude response in dB; Fig. 4.3b gives the phase response in radians, modulo 2π.

The impulse response of the channel, $c_0(t)$, is shown in Fig. 4.4.

There are a few items that require further explanation. The magnitude response in Fig. 4.3a has a null at frequency zero because of the hybrid transformer. At the higher frequencies of the magnitude response there is a *ringing*. This is a minor signal processing effect and will not be significant since it occurs about 80 dB below the peak, it will be attenuated by the pulse in Fig. 4.1a, and it will be below the noise floor introduced by $n(t)$ in Fig. 2.1. The phase response in Fig. 4.3b shows a large group delay; again this is due to signal processing and it will have no effect on the performance gains described in Section 4.3. The impulse response in Fig. 4.4 exhibits an extremely long tail, characteristic of subscriber lines with hybrid transformers. Furthermore, not all of the tail of the impulse response is shown and it should be clear that at 400 symbol periods the impulse response has still not decayed to zero.

In summary, the frequency response of the combined channel is:

$$\begin{aligned} \Phi_0(f) \;&=\; P_{t,0}(f)\, C_0(f) \\ &=\; \frac{1}{\sqrt{\mathrm{B_t}}}\, P_{bu}\!\left(\frac{f}{\mathrm{B_t}}\right) e^{-j2\pi f(\mathrm{D_0/T})}\, C_0(f). \end{aligned} \tag{4.8}$$

[a]

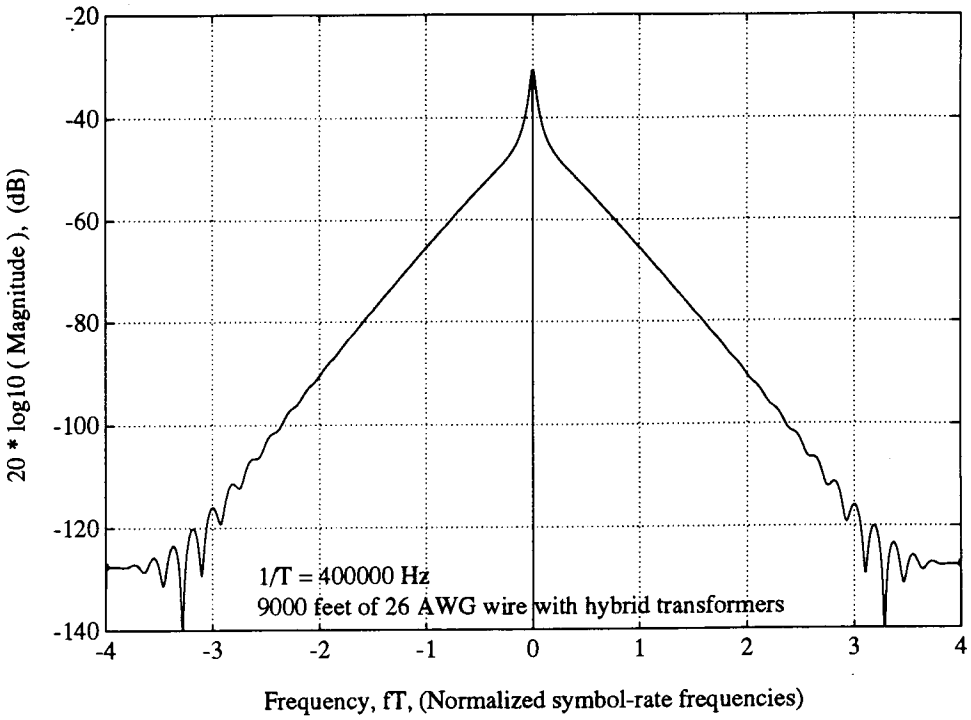

[b]

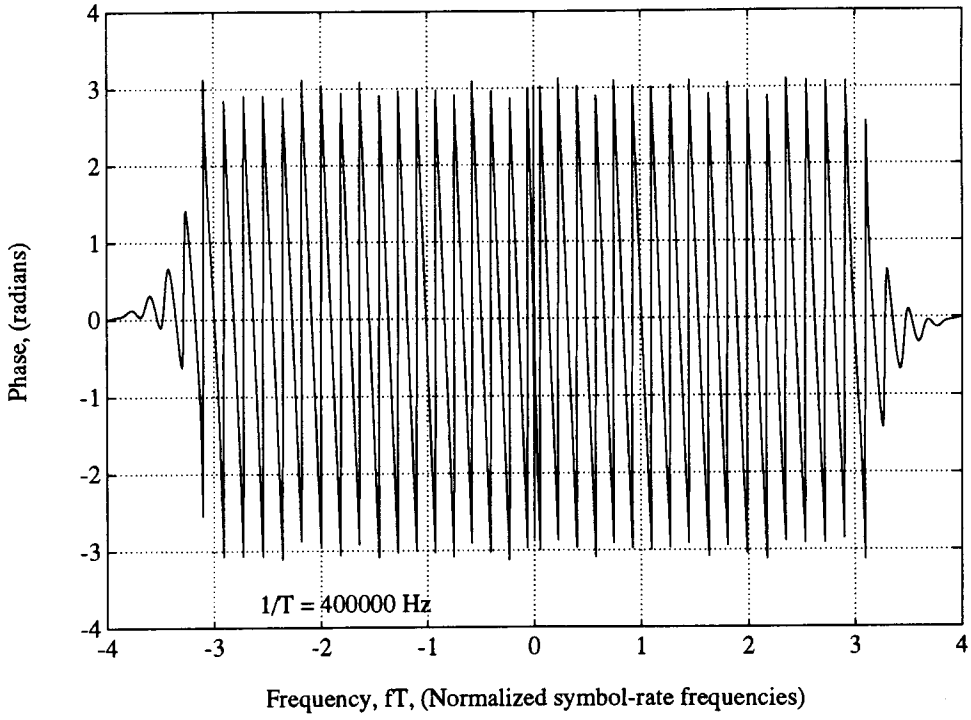

Figure 4.3 Magnitude and phase response of the channel, $10\ \log_{10}(|C_0(f)|)$ **and** $\arg(C_0(f))$**, respectively.**

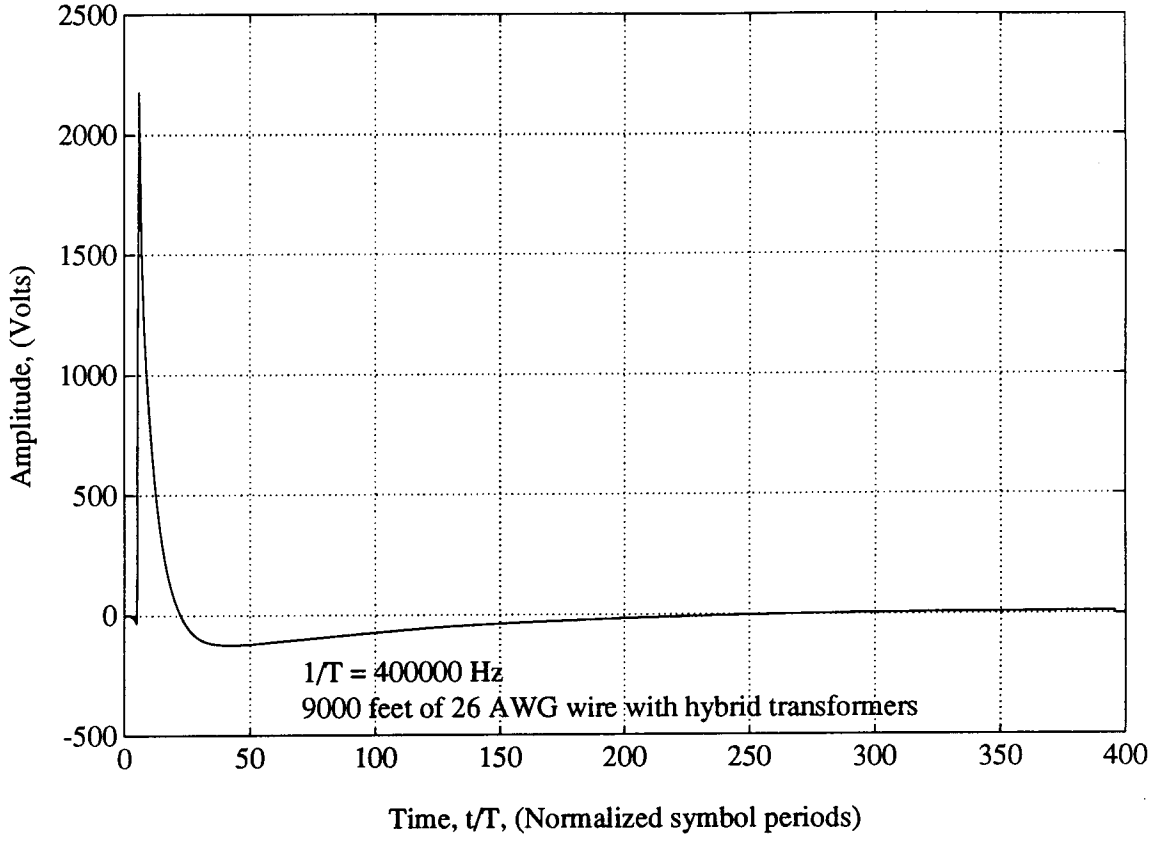

Figure 4.4 Impulse response of the channel, $c_0(t)$

Only one worst case channel for high-speed digital subscriber-line transmission has been considered in the work. The reason for not considering more lines is that the evaluations in this chapter are limited by the component of the entire model which introduces the most uncertainty. The most uncertain component of this system model appears not to be the channel, but the co-channels. The discussion about this uncertainty follows under the topic of interference.

4.2.3 Interference

A model will be described for the impulse responses of the co-channels, $\{c_i(t) \mid i \in \mathsf{L}_1\}$, which are shown in Fig. 2.2 and implied in Fig. 2.4. Also the amount of white noise will be described.

A commonly used [10, 11, 13, 14, 130] worst-case NEXT model has the magnitude-squared response of the coupling between subscriber lines for one-sided frequencies defined to be:

$$|C_{N1}(f)|^2 \;=\; K\, f^{3/2} \quad ; \quad K = 10^{-13} \quad ; \quad f \text{ is in Hz.} \tag{4.9}$$

It assumes that the NEXT at a receiver input is stationary noise, similar to the stationary noise model of Chapter 2. This model is intended to represent the NEXT from 49 subscriber lines. However, one very important item about this model is that is incorporates only magnitude information; it does not incorporate any phase information. But the phase information is essential to an equalizer which exploits the cyclostationary of the interference for improved performance.

For this reason a NEXT model was developed from the measurements described in [140] which incorporated phase information. The apparatus for the measurements was described in [140]. However, note the following important points about the cable:

1. Manufacturer: Northern Electric, Canada
2. Manufactured Date: November 1979
3. Length: 2000 feet
4. Number of twisted pairs: 50

5. Wire gauge: 26 AWG

All the crosstalk coupling paths had similar geometries since all the subscriber lines were in one 50-pair cable bundle. Also, the cables were terminated with hybrid transformers. The measurements were carried out by putting a pulse into one subscriber line and by capturing the wideband pulses at the output of the other 49 subscriber lines. Fig. 4.5 shows one set of the 49 sets of pulses; the input is shown in Fig. 4.5a and the output is shown in Fig. 4.5b. The information of interest are the frequency responses of all the NEXT coupling paths between the input and the outputs. These frequency responses were obtained by deconvolutions and Fourier transforms and they will be called $\{C_{b,i}(f) \mid i \in \mathsf{L}_1, \mathrm{L} = 49\}$; the subscript b refers to these frequency responses being the *basis* of the NEXT model. The frequency responses are two-sided in the frequency domain.

To interpret the validity of the measurements, one comparison that can be performed is between the magnitude-squared responses of measured NEXT, $\{C_{b,i}(f) \mid i \in \mathsf{L}_1, \mathrm{L} = 49\}$, and the commonly used NEXT model, in (4.9). This comparison is shown in Fig. 4.6 for a one-sided frequency interpretation; only frequencies in the range of interest, up to 3 MHz, are shown. Three sets of curves are presented in Fig. 4.6. The first set contains the 49 curves from the individual measured NEXT paths, plotted for one-sided frequencies $\left\{10 \log_{10}\left(2|C_{b,i}(f)|^2\right) \mid i \in \mathsf{L}_1\right\}$. The second set contains the single curve obtained from of the sum of the measured NEXT paths, plotted for one-sided frequencies $10 \log_{10}\left(2\sum_{i=1}^{\mathrm{L}} |C_{b,i}(f)|^2\right)$. The third set is the single curve, a line, for the commonly used NEXT model, $10 \log_{10}\left(|C_{N1}(f)|^2\right)$. The sum of the measured NEXT paths predicts a lower NEXT power below 100 kHz and generally a higher NEXT power above 100 kHz compared to the commonly used NEXT model. The performance evaluations which follow in Section 4.3 will make use of transmitter pulses whose 3-dB bandwidths vary from 100 kHz to 800 kHz. Hence at the middle to highest bandwidths, there will be some balancing of the differences in total NEXT power compared to the commonly used NEXT model. In fact, the sum of magnitudes

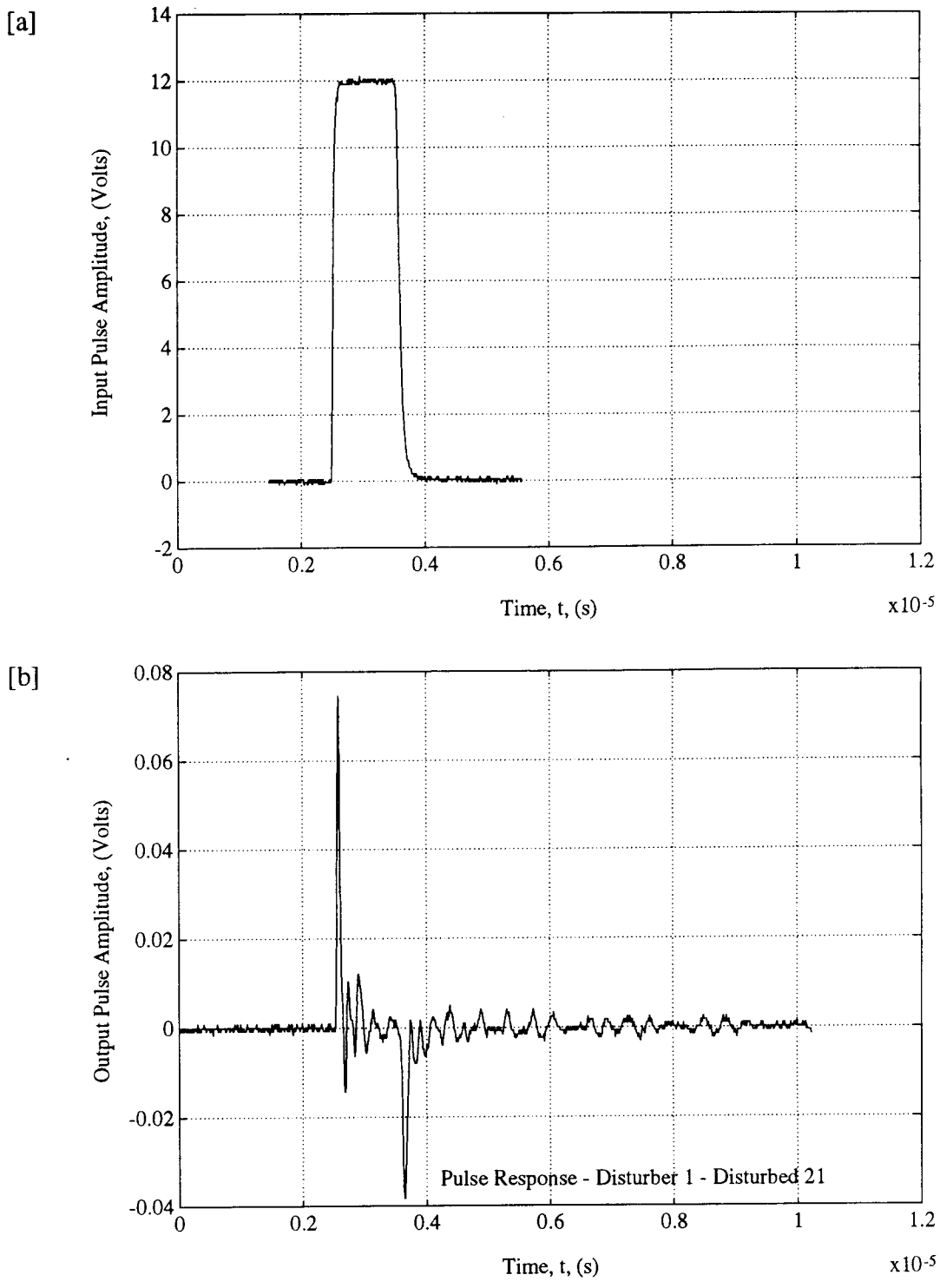

Figure 4.5 NEXT measurements — input pulse and output pulse [140]

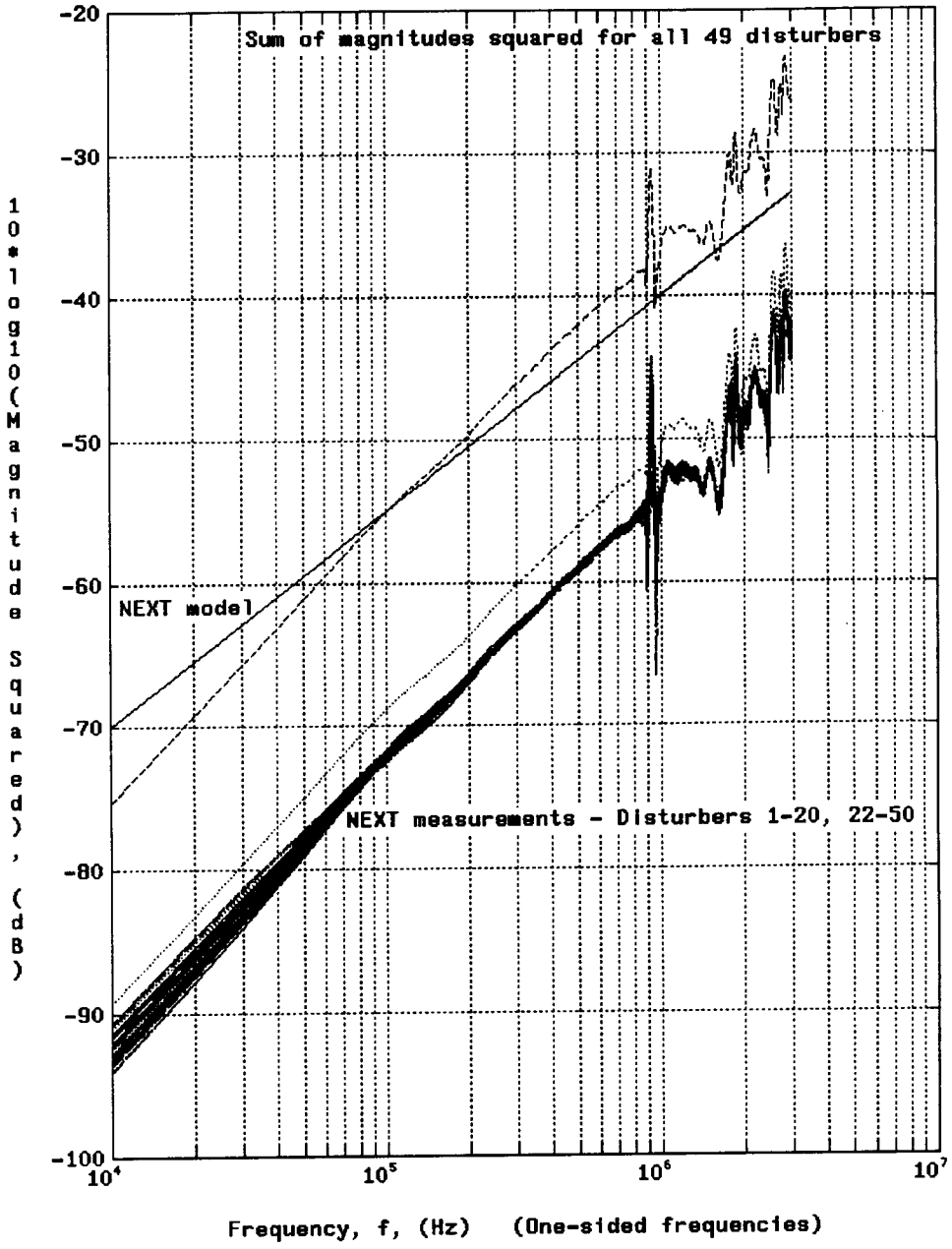

Figure 4.6 Magnitude squared versus one-sided frequencies of: measured crosstalk coupling paths, $\left\{10\ \log_{10}\left(2|C_{b,i}(f)|^2\right)\ |\ i \in \mathrm{L}_1\right\}$**; sum of measured crosstalk coupling paths,** $10\ \log_{10}\left(2\sum_{i=1}^{\mathrm{L}}|C_{b,i}(f)|^2\right)$**; and NEXT model,** $10\ \log_{10}\left(|C_{N1}(f)|^2\right)$**;** $\mathrm{L} = 49$ **disturbers (interferers).**

squared appears to increase with frequency by a power of 2 compared to the NEXT model which increases by a power of 1.5. Two other evident properties of the 49 individual measured NEXT paths are their similar shapes and amplitudes. The amplitude variation among the paths is only 3 dB across the frequency band. These variations are not as great as those exhibited in typical subscriber lines [191–193]. Hence the similar shapes and amplitudes will impact the interpretation of the results of the performance evaluations in Section 4.3; further comments will be made in that section.

For one particular co-channel, $C_{b,19}(f)$, the entire frequency response is shown in Fig. 4.7; the magnitudes are in linear scale and the phase is in radians, modulo 2π. Also shown is the commonly used NEXT model in a two-sided frequency form. There is a negative slope in the phase plot which was caused, at least partly, by delays introduced by signal processing. These delays will not affect the gains obtained in the performance evaluations which are described in Section 4.3. Since the twisted pairs in the measured cable all had similar geometries, the responses obtained from each pair were very similar and subsequently the phase responses, for all the twisted pairs, are very similar. Also evident from Fig. 4.7 are peaks in the magnitude response of the measured NEXT just below 1 and 2 MHz. One might consider these peaks to be the result of unwanted reflections from the far end of the cable during measurements. But it does not seem likely since the time for a reflection to return from a 2000 ft cable would be about 4 μs at the speed of light, and the reduction of the speed of propagation, below the speed of light, in the twisted-pair transmission lines would make that 4 μs delay even greater. However, the effect of the magnitude response being well behaved below about 1 MHz and being not-so-well behaved above about 1 MHz is common in subscriber lines [194].

Relate the frequency responses of the co-channels, called $\{C_i(f) \mid i \in \mathbf{L}_1\}$, to the impulse responses of the co-channels, $\{c_i(t) \mid i \in \mathbf{L}_1\}$ of Figs. 2.2 and 2.4, by the following Fourier transforms:

$$C_i(f) \;=\; \mathcal{F}_{cc}[\, c_i(t)\,] \quad ; \quad i \in \mathbf{L}_1. \tag{4.10}$$

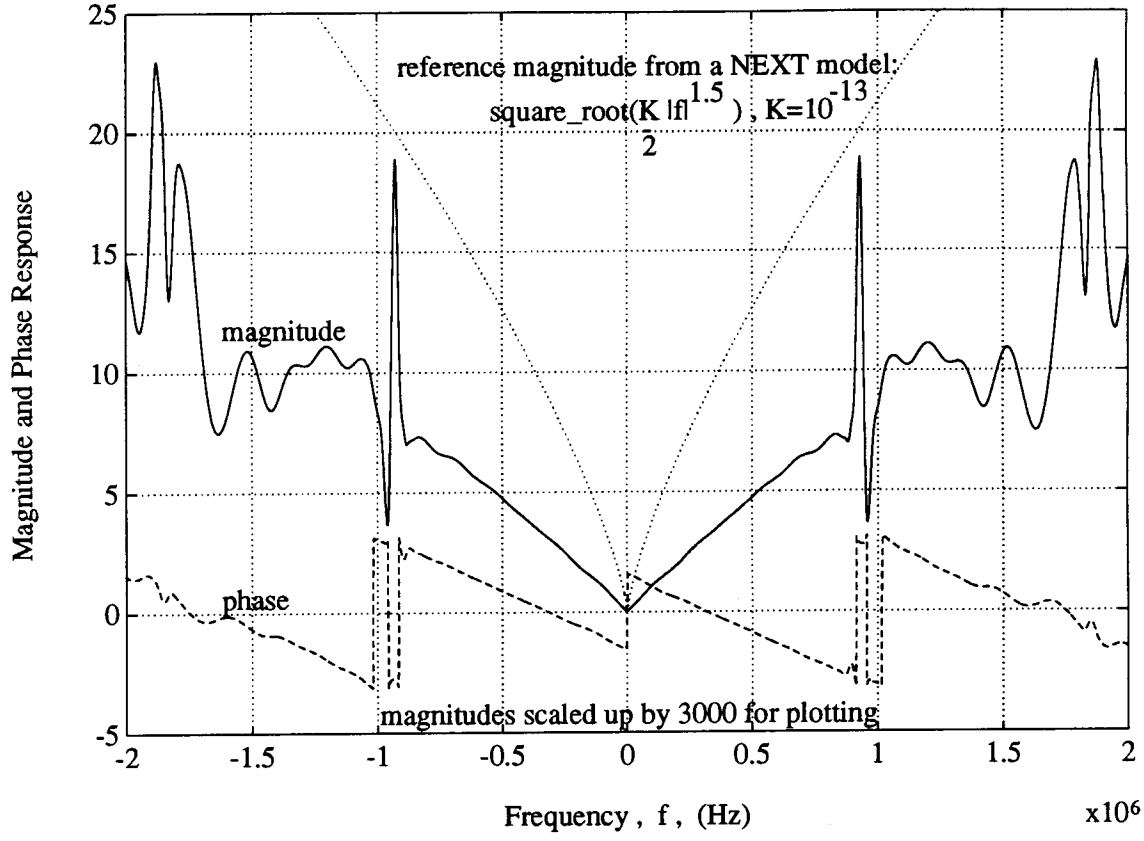

Figure 4.7 Measured frequency response of one near-end crosstalk coupling path, $C_{b,19}(f)$, compared to the commonly used model

Define the frequency responses of the co-channels to be:

$$C_i(f) \quad = \quad 10^{\mathrm{S}/20}\ C_{b,m_{\mathrm{L}}[i]}(f)\ e^{-j2\pi f(\mathrm{D}_{b,i}/\mathrm{T})} \tag{4.11}$$

where S is a scaling factor in dB which used to increase the amount of interference, $m_{\mathrm{L}}[i]$ is a mapping from the co-channel number used here to the twisted-pair number used in [140] and is further defined in Table 4.1, and finally $\{\mathrm{D}_{b,i} \mid i \in \mathsf{L}_1\}$ are relative phase shifts of the co-channels with respect to the symbol period and are further defined in terms of a quantity called X, the number of clusters of twisted pairs in the cable bundle:

$$\mathrm{D}_{b,i} \quad = \quad \begin{cases} 0 & , \mathrm{X} = 1 \text{ cable cluster} \\ 0 & , \mathrm{X} = 2 \text{ cable clusters}\ ,\ i \text{ is odd} \\ \frac{\mathrm{T}}{2} & , \mathrm{X} = 2 \text{ cable clusters}\ ,\ i \text{ is even.} \end{cases} \tag{4.12}$$

The meanings of the components in (4.11) need further explanation. The parameter S is used to provide a system design safety margin [13] by designing the system against increased levels of interference. The mapping $m_{\mathrm{L}}[i]$ is used to introduce the interferers in descending order of power. As i varies from 1 to 49, $m_{\mathrm{L}}[i]$ selects the numbers of the twisted pairs in [140] from highest to lowest powers. This mapping also assures that as the number of interferers, L, varies, the dominant interferers are being used. The relative phase shifts of the co-channels with respect to the symbol period, $\{\mathrm{D}_{b,i} \mid i \in \mathsf{L}_1\}$ are only intermediate variables used to set X, the number of clusters in a cable. The number of clusters considered is 1 or 2 and corresponds to the physical situations in the central office where a particular central office receiver is subjected to NEXT arising from one cluster or two separate clusters of twisted pairs of which the sources of each cluster are separate racks of equipment. If there is $\mathrm{X} = 1$ cluster, then according to (4.12), all the relative phase shifts of the co-channels will be zero. However, if there are $\mathrm{X} = 2$ clusters, then in (4.12) half of the interferers will be given a relative co-channel phase of $\mathrm{T}/2$. Thus the case of $\mathrm{X} = 2$ clusters corresponds to the situation of near-worst-case *inter*-rack phase alignment and will make it most difficult for an equalizer to exploit the cyclostationarity of the NEXT. Note that the parameters $\{\mathrm{D}_i \mid i \in \mathsf{L}_1\}$ in (4.4) are used to explore *intra*-rack phase alignment.

Table 4.1 Mapping from the co-channel number to the twisted-pair number in [140]

Co-channel Number	Twisted-pair Number in [140]	Co-channel Number	Twisted-pair Number in [140]	Co-channel Number	Twisted-pair Number in [140]
i	$m_{\mathrm{L}}[i]$	i	$m_{\mathrm{L}}[i]$	i	$m_{\mathrm{L}}[i]$
1	19	18	20	35	2
2	30	19	46	36	37
3	26	20	34	37	47
4	41	21	16	38	18
5	22	22	33	39	14
6	42	23	31	40	43
7	27	24	36	41	4
8	24	25	8	42	39
9	23	26	3	43	7
10	29	27	32	44	11
11	48	28	49	45	6
12	38	29	40	46	1
13	25	30	12	47	17
14	44	31	10	48	15
15	28	32	50	49	9
16	35	33	13		
17	45	34	5		

In summary, the frequency responses of the combined co-channels are:

$$\begin{aligned} \Phi_i(f) &= P_{t,i}(f)\, C_i(f) \\ &= \left(\frac{1}{\sqrt{\mathrm{B_t}}}\, P_{bu}\left(\frac{f}{\mathrm{B_t}}\right) e^{-j2\pi f(\mathrm{D}_i/\mathrm{T})}\right)\left(10^{\mathrm{S}/20}\, C_{b,m_{\mathrm{L}}(i)}(f)\, e^{-j2\pi f(\mathrm{D}_{b,i}/\mathrm{T})}\right) \\ i &\in \mathsf{L}_1 \end{aligned} \tag{4.13}$$

where $\{\mathrm{D}_i \mid i \in \mathsf{L}_1\}$ are defined in terms of M using (4.5), and $\{\mathrm{D}_{b,i} \mid i \in \mathsf{L}_1\}$ are defined in terms of X using (4.12).

To further elucidate the concepts embodied in (4.13), the impulse responses of the combined co-channels, $\{\phi_i(t) \mid i \in \mathsf{L}_0\}$, will be sketched for two situations. This serves the additional purpose of showing the shapes of the impulse responses of the combined co–channels. These two situations are depicted in Figs. 4.8 and 4.9. In Fig. 4.8, the number of cable clusters is 1 and the interference misalignment is 100 percent. The beginnings of the impulse responses of the $\mathrm{L} = 6$ interferers are uniformly distributed over 100 percent of the symbol period. The interferers are spread out in time for better visibility. After low-pass filtering they have the same shape. Again in typical subscriber lines there will be larger variations in NEXT impulse response shape, even after low-pass filtering [195]. The variations in amplitude are only about 3 dB. In Fig. 4.9, the number of cable clusters is 2 and the interference misalignment is 10 percent. Notice that over one symbol period there are 2 distinct clusters of impulse responses and the beginnings of the impulse responses of each cluster are uniformly distributed over 10 percent of the symbol period.

The details of the NEXT model have been described in order that its strengths and weaknesses can be put into perspective in the context of the performance evaluations in Section 4.3. In any case, this NEXT model based on the measurements in [140] seemed to be the most realistic model in the absence of any other accessible NEXT measurements incorporating phase information of real subscriber lines.

The level of the white noise power spectral density, No in (2.17), was set to be

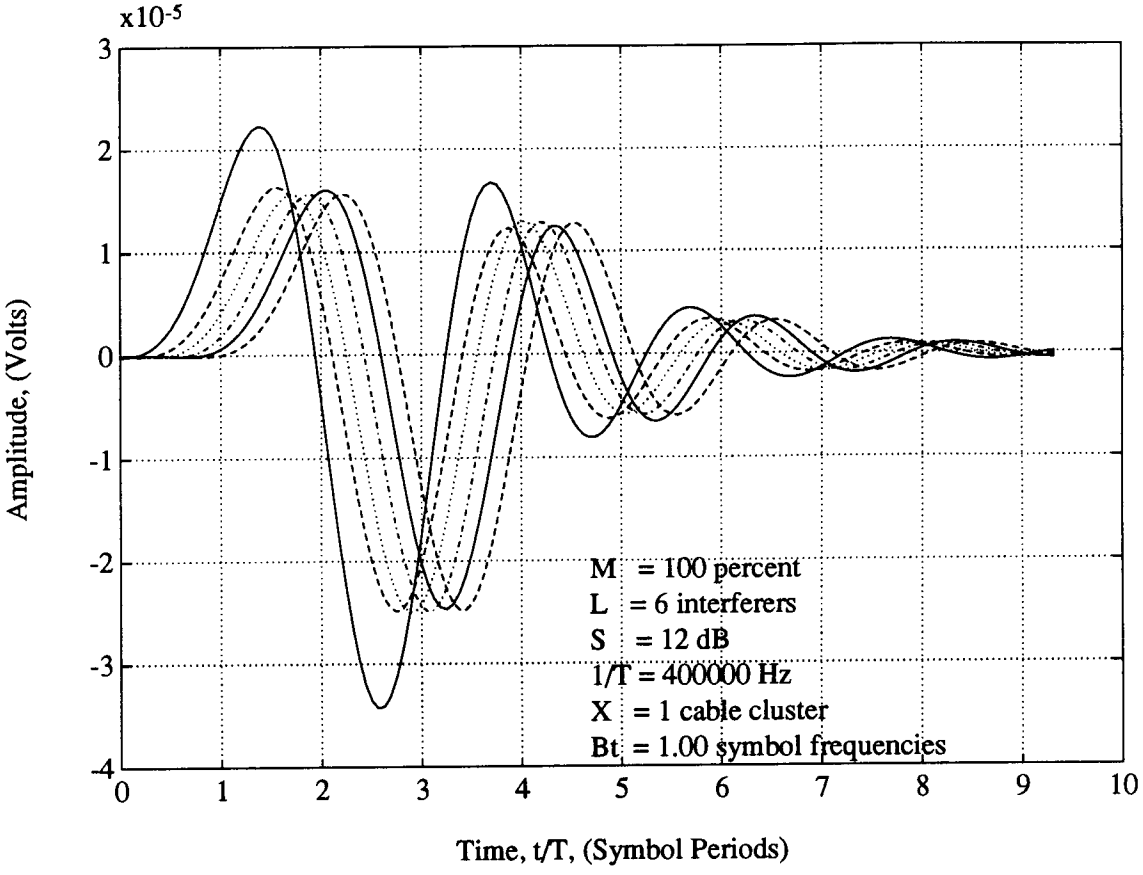

Figure 4.8 Impulse responses of the combined co-channels, $\{\phi_i(t) \mid i \in \mathsf{L}_1\}$

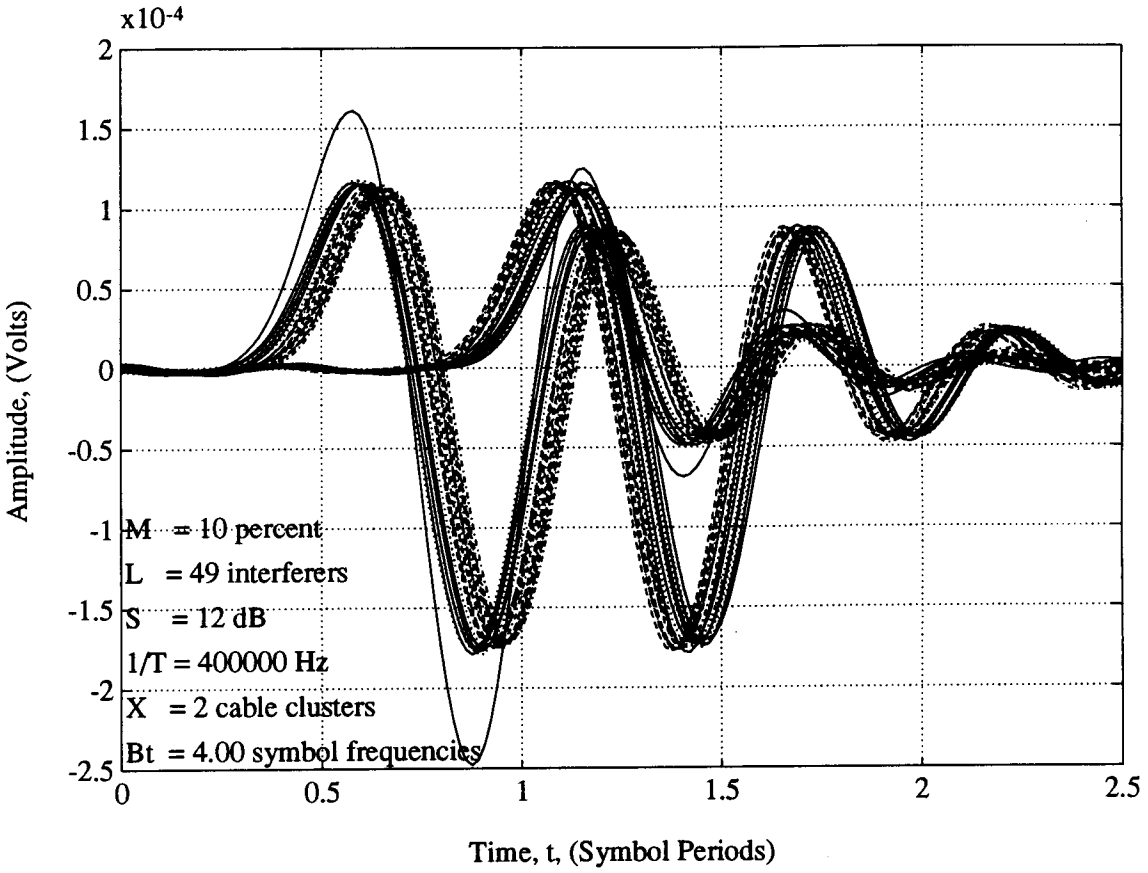

Figure 4.9 Impulse responses of the combined co-channels, $\{\phi_i(t) \mid i \in L_1\}$, with 2 cable clusters

15 dB below the power of the dominant interferer [195]. For the situation where:

$$\begin{aligned} \mathrm{B_t} &= 1 \text{ symbol frequency} \\ \frac{1}{\mathrm{T}} &= 400 \text{ kHz} \\ \mathrm{S} &= 0 \text{ dB} \end{aligned} \tag{4.14}$$

the value of No was chosen to satisfy:

$$10 \log_{10} \left(\frac{\max\limits_{m \in \mathsf{L}_1} \left(P_{I,m} \right)}{P_N} \right) = 15 \text{ dB} \tag{4.15}$$

where $\max(\bullet)$ denotes the maximum value of all of the possible values of the argument $\bullet$ and recall the definitions of $P_{I,m}$ from (2.26) and P_N from (2.25). If the noise bandwidth, $\mathrm{B_n}$, and transmitter bandwidth, $\mathrm{B_t}$, are equal, the following satisfies (4.15):

$$\mathrm{No} = 3.20 \times 10^{-18} \frac{\mathrm{W}}{\mathrm{Hz}}. \tag{4.16}$$

The model of the system is now described. Some of its combined properties will now be considered.

4.2.4 Properties

The similarity in shape of the combined co-channels can be determined qualitatively by examining Fig. 4.8. To quantify the similarity the correlation coefficients [171] were calculated among the vectors obtained by sampling $\{\phi_i(t) \mid i \in \mathsf{L}_1\}$. A slight variation of the situation in Fig. 4.8 is:

$$\begin{aligned} \mathrm{M} &= 0 \text{ percent} \\ \mathrm{B_t} &= 1 \text{ symbol frequency} \\ \mathrm{L} &= 49 \text{ interferers} \\ \frac{1}{\mathrm{T}} &= 400 \text{ kHz} \\ \mathrm{S} &= 12 \text{ dB}. \end{aligned} \tag{4.17}$$

For this varied situation the impulse responses $\{\phi_i(t) \mid i \in \mathsf{L}_1\}$ were sampled at a rate 16/T and 256 samples were taken from over the times from 0 to 16 symbol periods and these sets of samples were used to form the corresponding vectors defined as:

$$\underline{\phi_i}[n] = \begin{cases} 0 & , n \notin \{0,1,2, \ldots ,255\} \\ \phi_i(n\frac{\mathrm{T}}{16}) & , n \in \{0,1,2, \ldots ,255\} \end{cases} \quad ; \quad i \in \mathsf{L}_1. \tag{4.18}$$

The correlation coefficients are:

$$r_c[i,k] = \frac{< \underline{\phi_i}, \underline{\phi_k} >_d}{\sqrt{< \underline{\phi_i}, \underline{\phi_i} >_d < \underline{\phi_k}, \underline{\phi_k} >_d}} \quad ; \quad i,j \in \mathsf{L}_1 \quad ; \quad i \neq k \tag{4.19}$$

where the discrete-time inner product $< \bullet, \blacklozenge >_d$ was defined in (3.45). Using (4.19) and (4.18) the following were determined:

$$\max_{i \neq k}(r_c[i,k]) = 1.000 \quad ; \quad i,k \in \mathsf{L}_1 \tag{4.20}$$

and

$$\min_{i \neq k}(r_c[i,k]) = 0.992 \quad ; \quad i,k \in \mathsf{L}_1 \tag{4.21}$$

where $\min(\bullet)$ denotes the minimum value of all of the possible values the argument $\bullet$. Therefore, from (4.20) and (4.21), the low-pass-filtered NEXT impulse responses are quantitatively very similar under the conditions of (4.17). Similar results would be expected under other conditions of transmitter bandwidth and symbol rate.

Fig. 4.10 compares the impulse response of the combined channel $\phi_0(t)$ and the impulse response of the combined co-channels $\{\phi_i(t) \mid i \in \mathsf{L}_1\}$ for the parameters indicated in the figure. The impulse responses of the combined co-channels extend over a few symbol periods whereas the impulse response of the combined channel extends over thousands of symbol periods, even though a time span of only 25 symbol periods is indicated in the figure.

In, or implied in, Figs. 2.1, 2.2, and 2.4, are the signal which carries the data of interest $s(t)$, the interference without noise $\mu_{ci}(t)$, and the noise $n(t)$. The powers of these three signals are denoted by P_S from (2.13), P_I from (2.27), and P_N from (2.25),

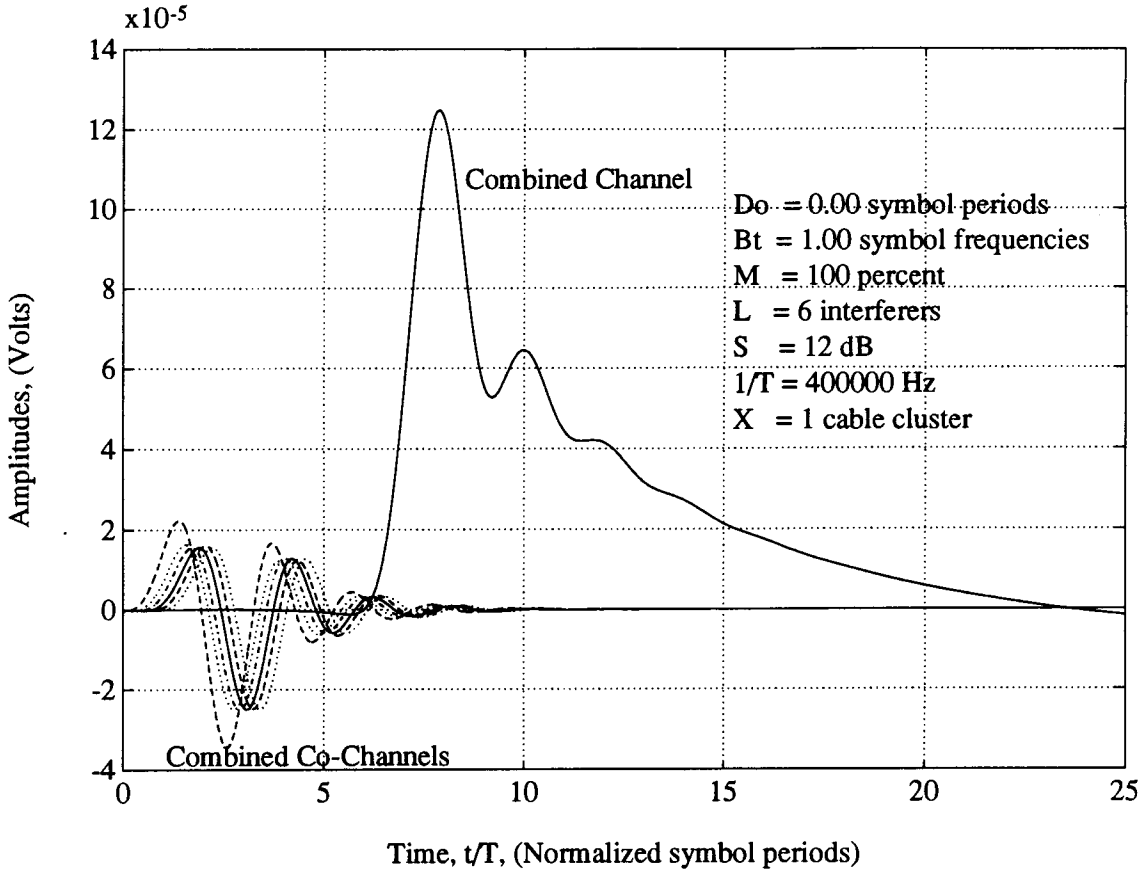

Figure 4.10 Impulse responses of the combined channel and combined co-channels, $\{\phi_i(t) \mid i \in L_0\}$

respectively. These three powers were calculated for increasing numbers of interferers present and the results are shown in Fig. 4.11. At the receiver input, the ratio of the powers in the signal carrying the data of interest to the bandlimited noise is 41.3 dB. With S = 12 dB, the ratio of the powers in the signal carrying the data of interest to the interference without noise varies from about 14 dB to 1 dB as the number of interferers is increased from 1 to 49.

Equation (2.29) gives the instantaneous power of the interference throughout the symbol period. Define the interference power variation to be:

$$P_V = \frac{\max\limits_{0 \le \tau \le T} P_{ci}(\tau)}{\min\limits_{0 \le \tau \le T} P_{ci}(\tau)}. \tag{4.22}$$

Fig. 4.12 contains a plot of interference power variation versus interference misalignment when the noise bandwidth is the same as the transmitter bandwidth $B_n = B_t$. As expected, the power variation decreases as the interference misalignment is increased, indicating that the interference becomes more stationary. The interference power variation is only one way to characterize the amount of cyclostationarity present in the interference. Other more general characterizations can be found in [20, 56, 64, 77, 79, 80, 107, 196]. For these particular combined co-channels, $\{\phi_i(t) \mid i \in L_1\}$, the interference power variation does not go completely to zero as M approaches 100 percent mainly because the interferers have different amplitudes. The power variation does not appear to be closely related to the MSE gains achievable by fractionally spaced equalizers in exploiting the cyclostationary of the interference. Instead the interference power variation is more closely related to the MMSE variations that could be experienced by a symbol-spaced equalizer in cyclostationary interference [66, 111]. Criteria that convey information about just the interference, such as the interference power variation, are indirect measures of the effect of the interference on system performance. By contrast, the following section shows the use of criteria that more directly convey information about performance of the receiver.

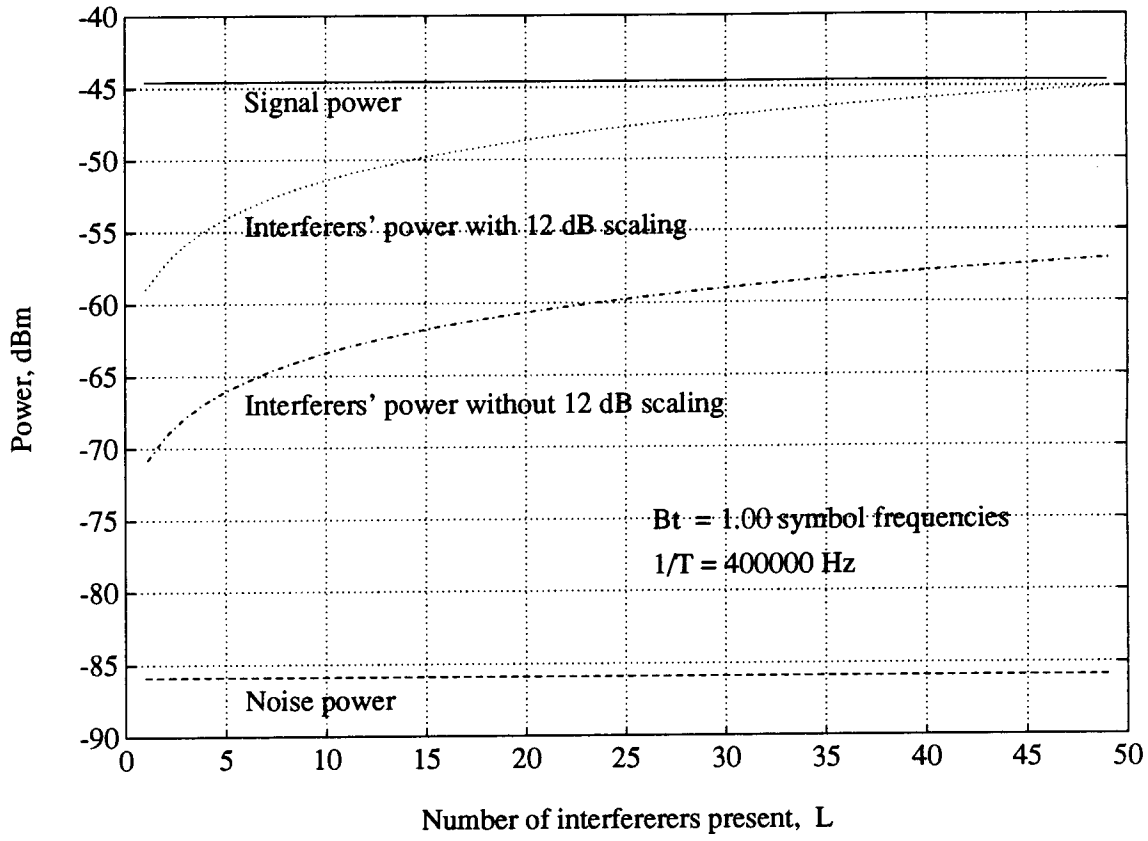

Figure 4.11 Powers of: the signal $s(t)$, P_S, the interference without noise $\mu_{ci}(t)$, P_I, and the noise $n(t)$ bandlimited to B_t, P_N

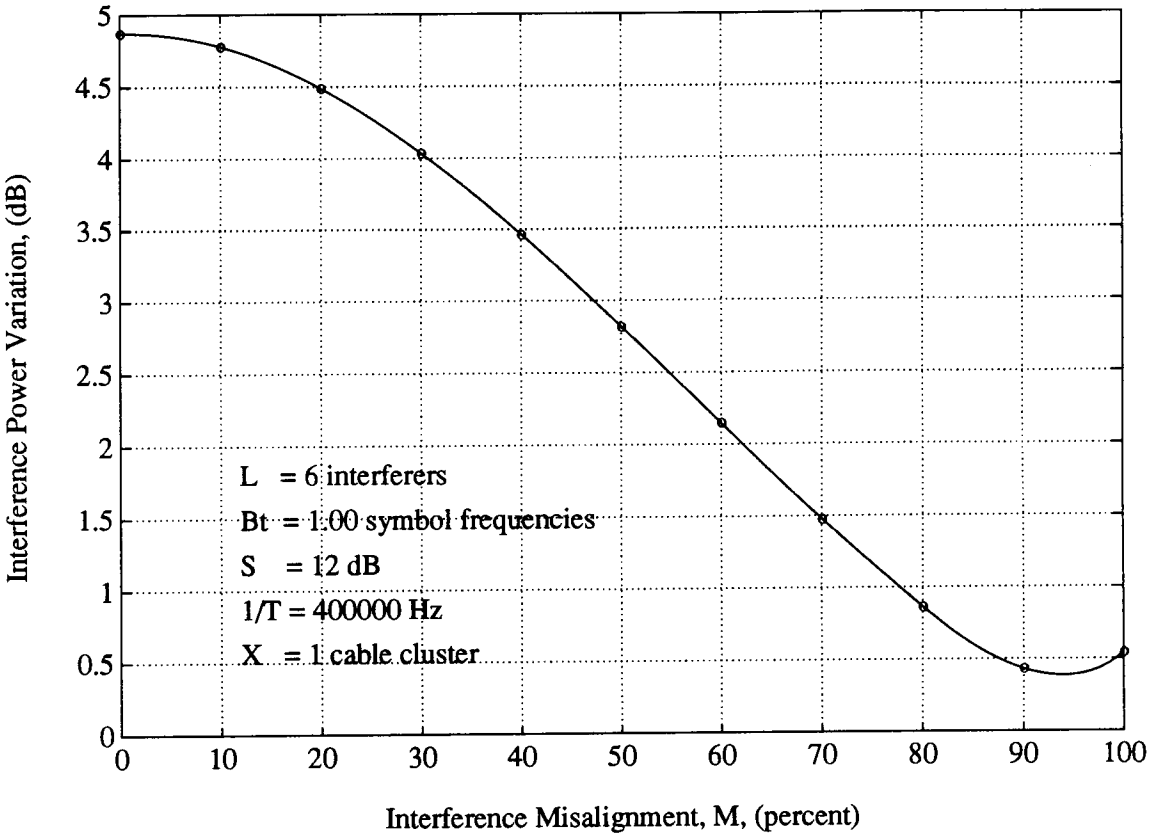

Figure 4.12 Interference power variation P_V, in a symbol period versus interference misalignment, M.

4.3 Performance Evaluation

The goal of the performance evaluations of this section are to demonstrate the performance gains that are possible by having equalizers exploit the cyclostationarity of the subscriber-line NEXT. The performance gains that are of greater interest are the MMSE of linear and decision-feedback equalizers *relative* to the situation where the cyclostationary interference is treated as stationary noise. In other words there is less emphasis in this section on absolute system performance. The two conditions that have the largest effect on the gains are the bandwidth of the transmitter pulses relative to the symbol rate and the misalignment of the phases of the transmitter clocks in the central office. It is shown in this section how combinations of sufficiently wide bandwidths and sufficiently small misalignments provide opportunities for equalizers to exploit the cyclostationarity of the NEXT. The four MMSE expressions that are calculated in this section are shown in Table 3.1. Both linear and decision-feedback equalizers are considered in the presence of cyclostationary interference and stationary noise. The frequency responses of the combined channel and combined co-channels are given in (4.8) and (4.13), respectively. The relevant MMSE expressions in Table 3.1 have been evaluated by numerical integration to within a relative error of 10^{-3} [197]. That which remains in this section are the results and interpretation of MMSE calculations under various conditions of the following parameters: the bandwidth of the transmitter pulses relative to the symbol rate B_t, the misalignment of the phases of the near-end transmitter clocks in the central office M, the number of cable clusters X, the number of interferers L, the relative phase shift of the far-end signal D_0, the interference safety margin S, the white noise power spectral density No, and the symbol rate $1/T$. Instead of showing the values of MMSE directly, the following expression is shown:

$$10 \log_{10} (\text{MMSE}) \tag{4.23}$$

where $\log_{10}(\bullet)$ is the logarithm in base 10 of the argument $\bullet$. There are two reasons for showing the MMSE in the latter form. The first is because it permits displaying a greater dynamic range. The second is because at decreasing values of MMSE the quantity

$-10\log_{10}(\text{MMSE})$ approaches the signal to interference-plus-noise ratio (SINR) at the detector input in dB; see (3.97) for the relationship between the MMSE, ε_{dco}, and SINR, $\gamma_{dco}^{I,N}$, of the continuous-time infinite-length decision-feedback equalizer in ISI, additive white noise and cyclostationary interference. Hence the units of $10\log_{10}(\text{MMSE})$ are crudely considered to be dB s.

Figs. 4.13a and 4.13b show $10\log_{10}(\text{MMSE})$ for the four cases of two equalizers and two interference types versus the relative phase shift of the far-end signal D_0 for the conditions shown in the respective figures. The respective differences in the conditions for Figs. 4.13a and 4.13b are that the misalignment of the clocks phases is 10 and 0 percent, as well as the bandwidths being 1.0 and 1.5 symbol frequencies. As expected, the performance in stationary noise is unchanged with D_0. However, the performance in cyclostationary interference varies with D_0 and the value which causes the performance improvement in cyclostationary interference over stationary noise to be the smallest is 0.72 symbol periods. Even at the worst case alignment of the interference with respect to the signal, the performance in cyclostationary interference is better than in stationary noise. Considering the time-domain power variations of the interference, one might wonder how it is possible that there are still MMSE gains over the stationary noise case. However, note that a bandwidth of $B_t = 1.0$ symbol frequency implicitly means that T/2-spaced equalizers are needed to approach these MMSE results. Therefore an equalizer implementation which samples the received signal two times per symbol period will have, in a simple sense, two chances per symbol period of getting a good signal to interference-plus-noise ratio [65, 66, 111]. If one of the samples is poor, the equalizer would emphasize the value from the other sample. In contrast a T-spaced equalizer which is restricted to sampling the received signal once per symbol interval would have a performance in cyclostationary interference that is worse than in stationary noise, for this channel. Similar results for *finite* numbers of tap coefficients were reported in [65, 66, 111]. Finally note again that D_0 is not a design parameter since it comes from the far end. Therefore the worst value of the relative signal shift, $D_0 = 0.72$ symbol periods, will be used in all further calculations. The performance is sensitive to D_0

[a]

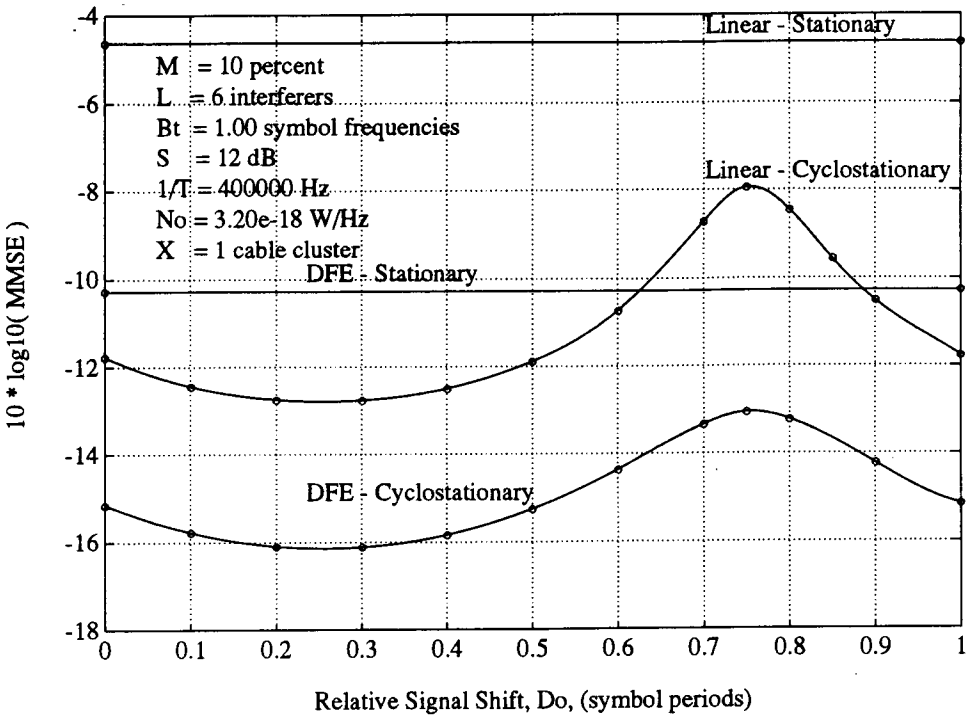

[b]

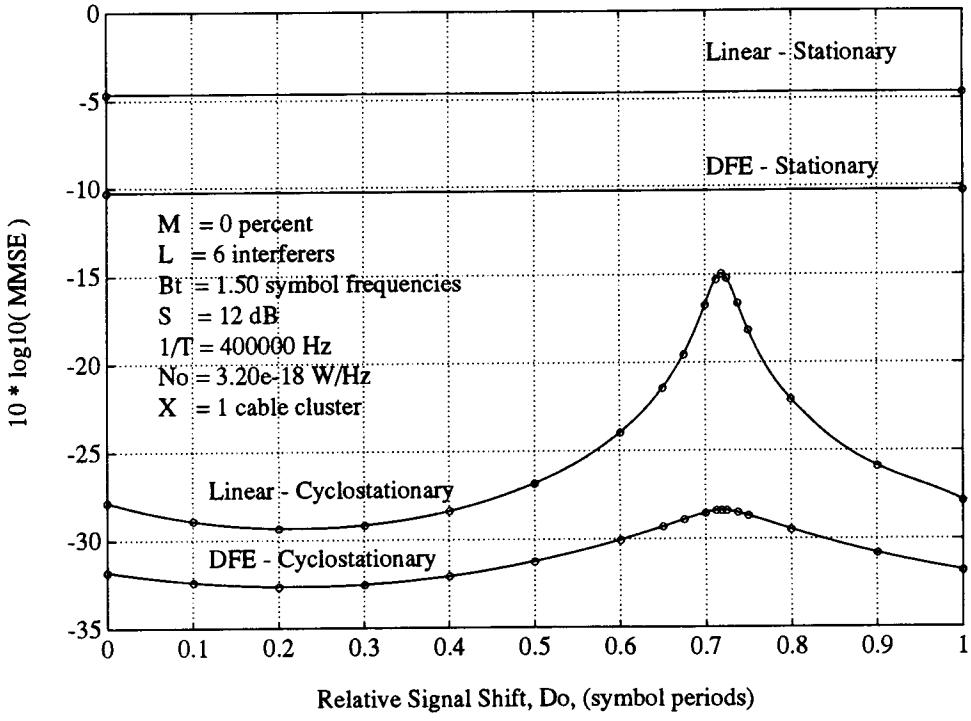

Figure 4.13 Linear and decision-feedback equalizer MMSE versus relative signal shift

when the misalignment is 0 percent. However, at more practical misalignments greater than 0 percent the sensitivity with respect to D_0 diminishes.

Figs. 4.14a and 4.14b show $10\log_{10}(\text{MMSE})$ plotted versus the bandwidth of the transmitter pulses relative to the symbol rate B_t for the conditions shown in the respective figures. As the bandwidth increases, it demonstrates that the gains due to exploiting the cyclostationarity increase significantly. In Fig. 4.14b, at the largest bandwidth of B_t equal to 4.0 symbol frequencies the improvement for the DFE in cyclostationary interference over stationary noise is 21 dB. The MMSE improvements increase with increasing bandwidth, but they reach diminishing returns. This is due to enhancement of the white noise. Thanks is given to the third anonymous reviewer of [83] for pointing out that the curve in Fig. 4.14a may have flattened out but has not reached the noise floor, as evidenced by the further gains shown in Fig. 4.14b.

Consider Fig. 4.14a. The discussion of section 3.2 suggested that bandwidths where $B_t = 1.0$ symbol frequency may provide the flexibility to suppress all ISI and one co-channel interferer, or many synchronized co-channel interferers with nearly the same interfering pulse shape. When the bandwidth is increased to $B_t = 1.5$ symbol frequencies, there may be enough flexibility to suppress all ISI and two co-channel interferers. However, note that the increased relative bandwidth does not mean that the *MMSE* equalizers eliminate one more particular interferer, but instead the increased bandwidths mean that the equalizers have increased flexibility to find a better MMSE solution. The same increased flexibility to suppress additional interferers occurs in Fig. 4.14b as the bandwidth is increased in the steps:

$$\{0.5,\ 1.0,\ 1.5,\ 2.0,\ 2.5,\ 3.0,\ 3.5,\ 4.0\}. \tag{4.24}$$

However the MMSE cases approach the noise floor down at around -40 dB, a number suggested from the differences between signal and noise powers in Fig. 4.11. In [144] is a comparison between two equalizer adaptation algorithms, least-mean square (LMS) and recursive least-square (RLS). The comparison suggests that the LMS algorithm uses *stochastic* properties and the RLS algorithm uses *algebraic* (deterministic) properties

[a]

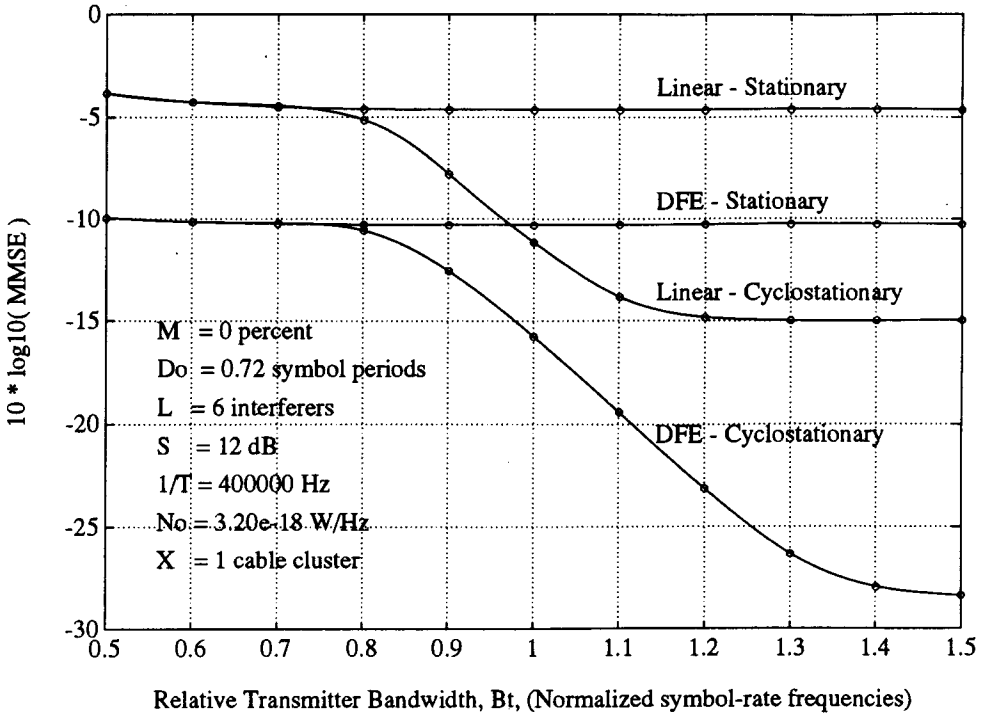

[b]

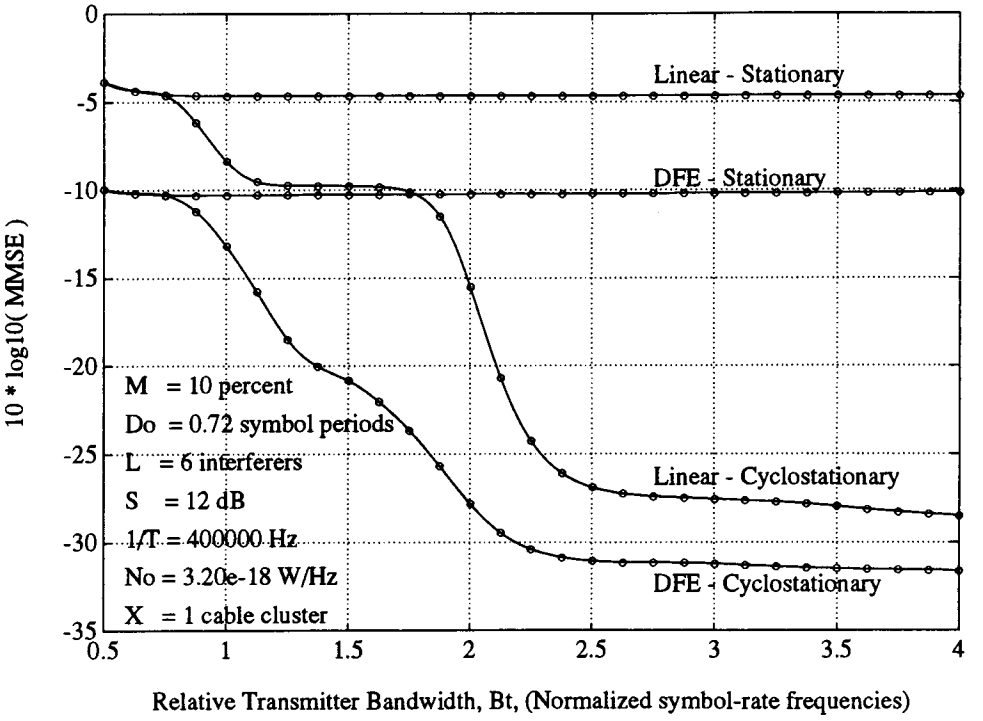

Figure 4.14 Linear and decision-feedback equalizer MMSE versus relative transmitter bandwidth

of the signals to approach convergence. By the use of similar terms, at small relative bandwidths, the performance in cyclostationary interference over stationary noise comes from the equalizers using *stochastic* properties of the interference, such as power variations [61]. At large relative bandwidths, the performance in cyclostationary interference over stationary noise comes from the equalizers using *deterministic* properties of the interference [106]. These two statements are only intended to offer small additional insight into the differences between the cyclostationary interference and stationary noise cases with respect to increasing relative bandwidths.

Naturally, exploiting the gains in cyclostationary interference does not occur without some cost. With increasingly large relative bandwidths as in:

$$\{0.5,\ 1.0,\ 1.5,\ 2.0,\ 2.5,\ 3.0,\ 3.5,\ 4.0\} \tag{4.25}$$

it would be necessary to use fractionally spaced equalizers with respective tap spacings equal to:

$$\left\{\frac{T}{1}, \frac{T}{2}, \frac{T}{3}, \frac{T}{4}, \frac{T}{5}, \frac{T}{6}, \frac{T}{7}, \frac{T}{8}\right\}. \tag{4.26}$$

Using the worst value of the relative signal shift, $D_0 = 0.72$ symbol periods, the four MMSE cases are plotted versus the interference misalignment to explore the effects of aligning the clock phases of the interference at the central office; see Figs. 4.15a and 4.15b. In Fig. 4.15a the DFE MMSE in cyclostationary interference reduces to only 3 dB better than the stationary case when the interference misalignment is increased to 10 percent. For the linear equalizer, the corresponding value of M is 13 percent. These results are based on a transmitter pulse with $B_t = 1.0$ symbol frequency. The discussion of section 3.2 suggested that larger relative bandwidths provide a greater opportunity to suppress interference. Using a wider bandwidth pulse with $B_t = 1.5$ symbol frequencies, and again the worst possible relative signal shift of 0.72 symbol periods, the MMSE expressions versus the interference misalignment, M, were recalculated and are shown in Fig 4.15b. The performance improvements using the relatively wide bandwidth pulse

[a]

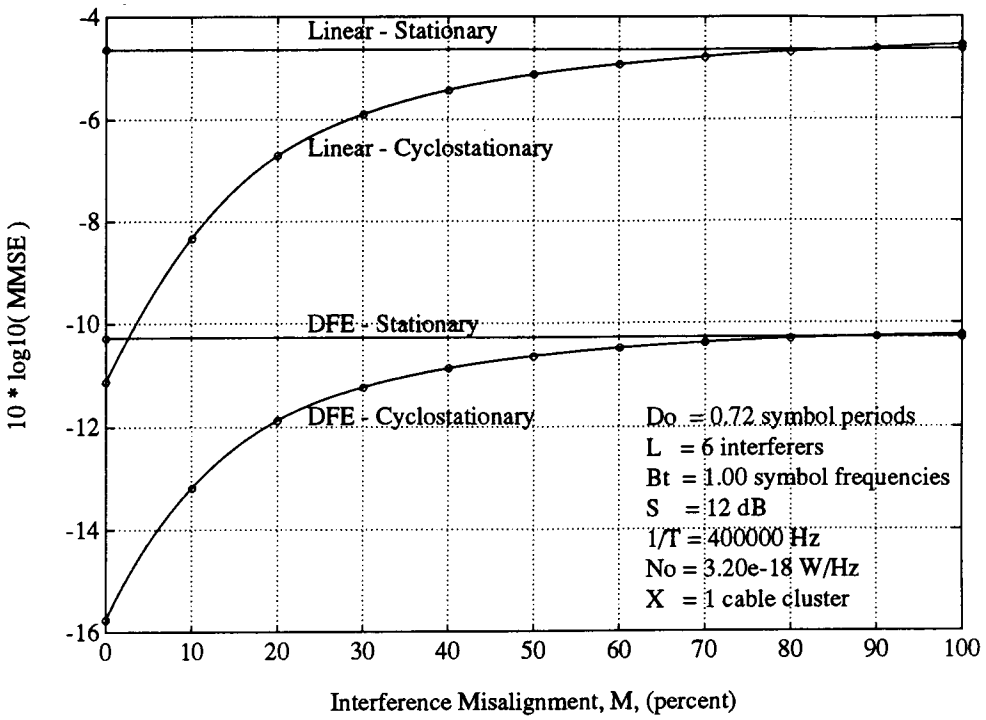

[b]

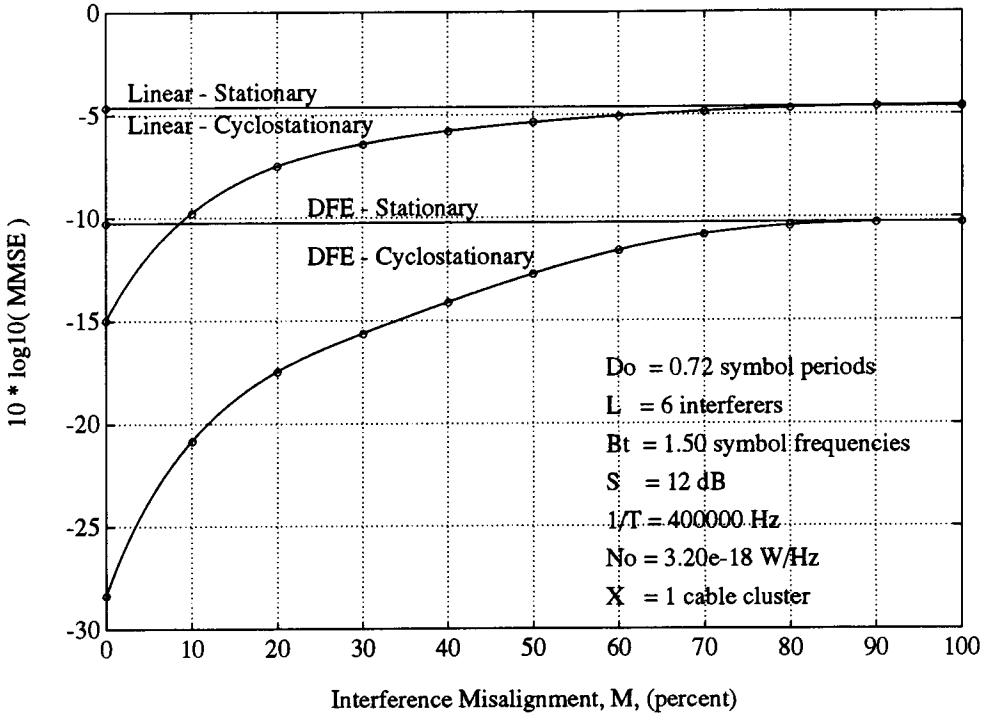

Figure 4.15 Linear and decision-feedback equalizer MMSE versus interference misalignment

are significant. The DFE MMSE in cyclostationary interference maintains at least a 3 dB improvement over the stationary case while the interference misalignment is increased up to 46 percent. For the linear equalizer, the corresponding 3 dB point occurs when the misalignment is 19 percent. The relatively wide bandwidth pulse gives larger gains, and permits a higher interference misalignment for the same performance improvement. Note again that with a bandwidth of $B_t = 1.5$ symbol frequencies T/3- spaced equalizers would be needed for implementation.

Another interpretation will be made regarding the sources of the gains in cyclostationary interference versus stationary noise. This has to do with the similarity among $\{\phi_i(t) \mid i \in L_1\}$ as evidenced numerically by the cross-correlation coefficients in (4.20) and (4.21), and also evidenced qualitatively in Figs. 4.8 and 4.9. As the misalignment is decreased to 0 percent, the co-channel interferers behave more and more as a single interferer for purposes of suppressing them. Whatever impulse response is created by the linear equalizer, or the forward filter of the decision-feedback equalizer, it will be convolved with all the co-channels. Hence, identical interference suppression operations will be performed on all the co-channels. If one is nearly nulled out [106], then all will be nearly nulled out.

There is one more very interesting effect in Fig. 4.15a. Carefully comparing the curves for the linear equalizer at a misalignment of 100 percent, shows that the performance in cyclostationary interference is worse than that of stationary noise by 0.1 dB. This possibility was demonstrated in Section 3.4. Concurrent and independent confirmation of this effect has been reported in [127]. This effect will be occasionally appear in later figures.

Fig. 4.16 is used to demonstrate the effects of the safety margin parameter S. To facilitate comparison Fig. 4.15b is repeated in Fig. 4.16a. The only parameter change from Fig. 4.16a to Fig. 4.16b is that S has been reduced from 12 dB to 0 dB. The effect of this change is to decrease the cyclostationary component of the interference. As stated above, the 3 dB points for the linear and DFE in Fig. 4.16a are at 19 and 46 percent, respectively. For Fig. 4.16b, the 3 dB points for the linear equalizer and decision-

[a]

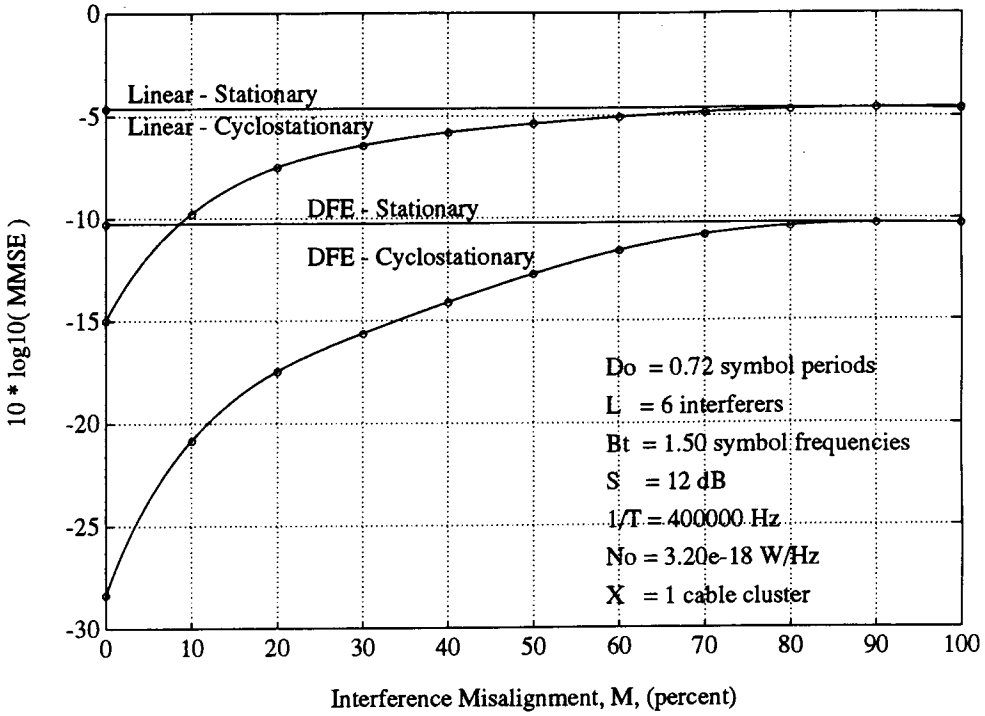

[b]

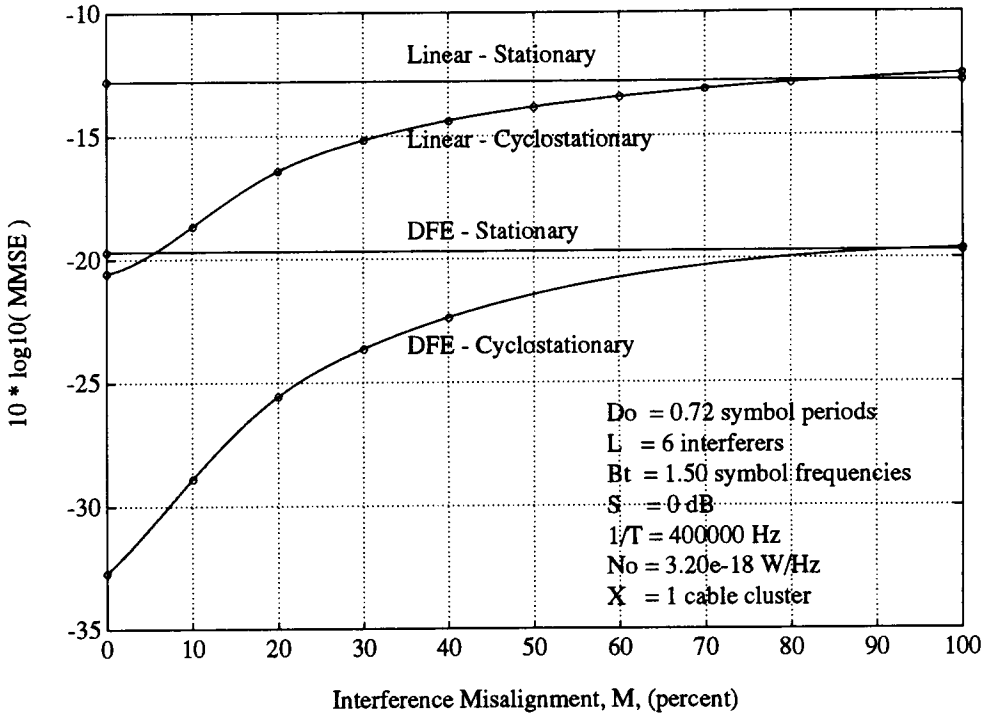

Figure 4.16 Linear and decision-feedback equalizer MMSE versus interference misalignment — without interference safety margin

feedback equalizer are at 24 and 37 percent, respectively. For the linear equalizer, the maximum 3 dB misalignment is more relaxed at 24 percent. However, it is tighter for the decision-feedback equalizer, at 37 percent. One might have always expected the maximum 3 dB misalignment point to move to a lower percentage as S is reduced since the cyclostationary component of the cyclostationary interference is reduced. However, when S is increased to 12 dB it *pushes* and *compresses* all the curves up towards the 0 dB limit[19]. This *compression* would tend to reduce the performance differences between the cyclostationary interference and stationary noise cases. However the rest of the calculations will proceed with the 12 dB safety margin.

Fig. 4.17 contains the same parameters as in Fig. 4.15 except for one change. Instead of $L = 6$ interferers, Fig. 4.17 has been plotted using $L = 49$ interferers. For Fig. 4.17a, the 3 dB points for the linear equalizer and decision-feedback equalizer are at 7 and 5 percent, respectively. For Fig. 4.17b, the 3 dB points for the linear equalizer and decision-feedback equalizer are at 13 and 46 percent, respectively. Comparing Fig. 4.15 to Fig. 4.17, the increase in the number of interferers has a greater harmful effect on the systems which use the lower bandwidth of $B_t = 1.0$ symbol frequency, compared to $B_t = 1.5$ symbol frequencies.

Fig. 4.18 shows a relatively large departure from the previous calculations. The relative bandwidth was changed to $B_t = 4.0$ symbol frequencies. The 3 dB points for the linear equalizer and decision-feedback equalizer are at 70 and 75 percent, respectively. It might at first seem unintuitive how such a large improvement is possible using relatively wide bandwidths in a subscriber-line system because the channel is a low-pass frequency response and the NEXT coupling is a high-pass frequency response. This means that increasing the bandwidths results in reduced powers for the signal carrying the data of interest and increased powers for the NEXT. While it may seem from the point of view of the power ratios that the system should perform worse, it turns out that the relatively wide bandwidths give even more flexibility to extract the signal carrying the data of

[19] The 0 dB limit arises since the variance of the data is one and correct decisions have been assumed.

[a]

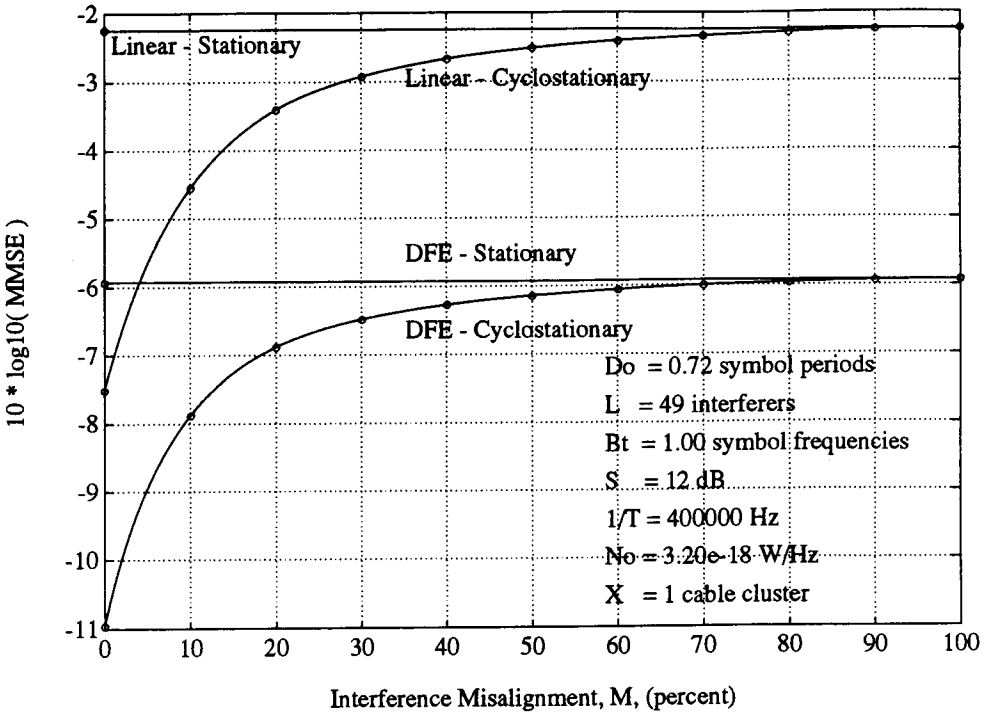

[b]

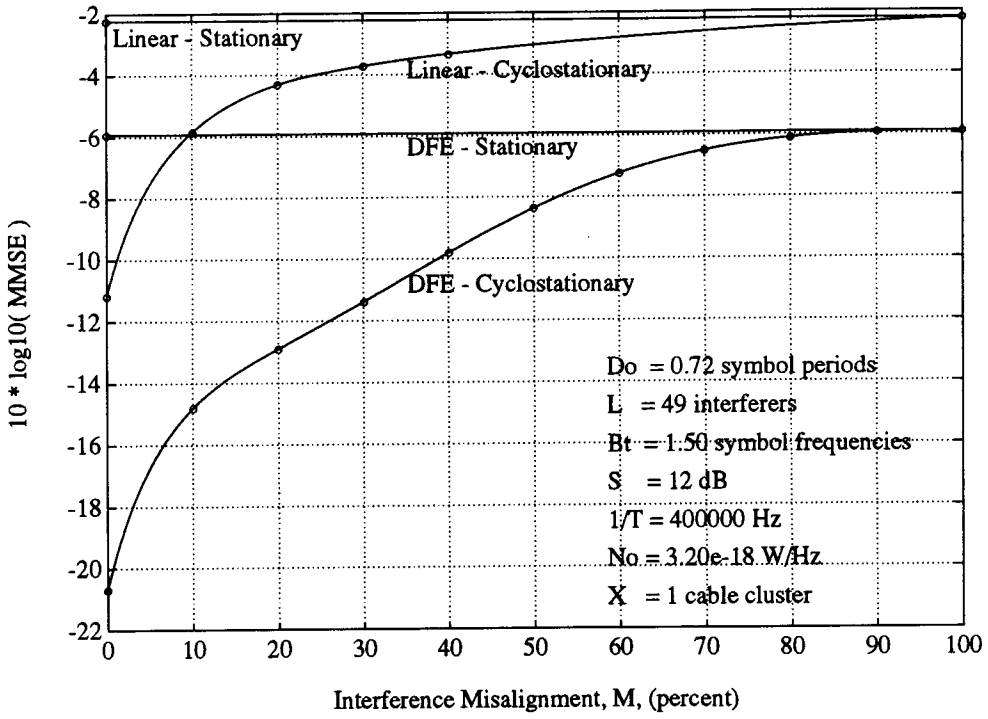

Figure 4.17 Linear and decision-feedback equalizer MMSE versus interference misalignment — with 49 interferers

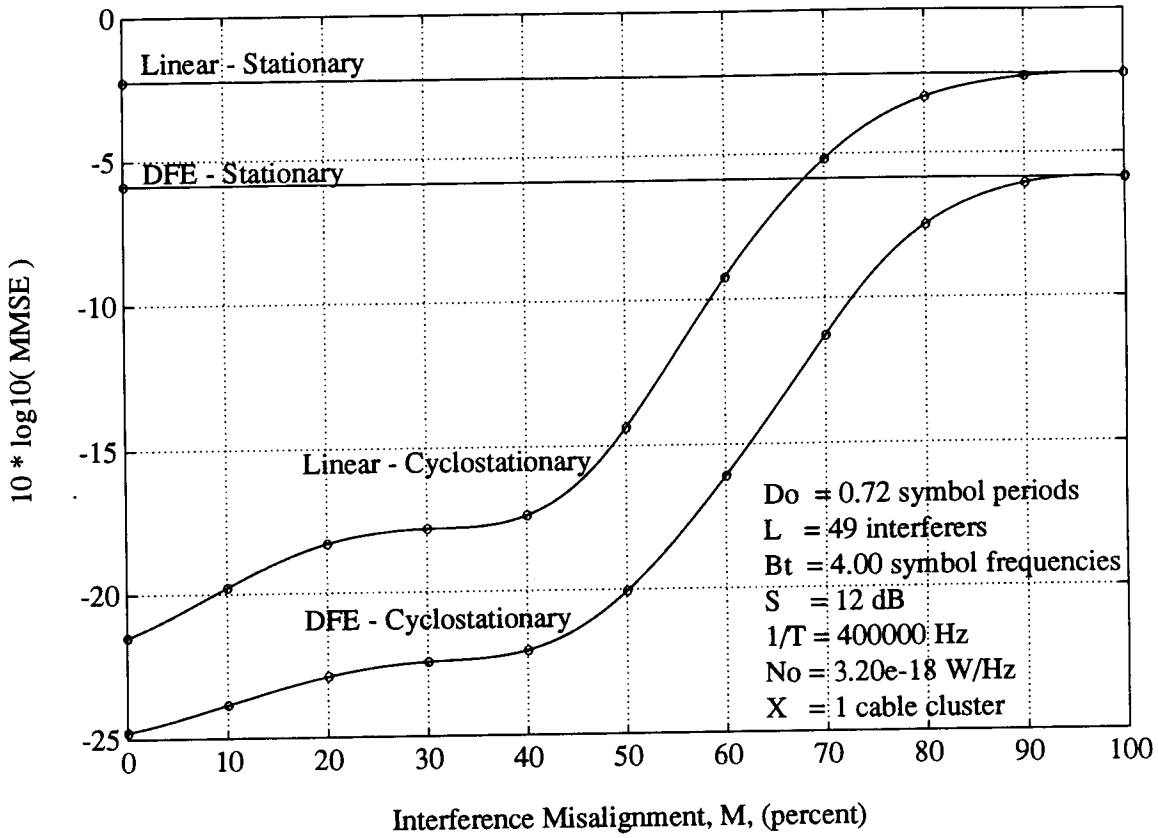

Figure 4.18 Linear and decision-feedback equalizer MMSE versus interference misalignment — very-wide relative transmitter bandwidth

interest while reducing the effect of the cyclostationary interference.

Fig. 4.19 contains the results of evaluations using very-wide relative bandwidths and one or two cable clusters. Only results for a decision-feedback equalizer in cyclostationary interference are shown. Although not shown, for the case of X = 2 clusters with $B_t = 1.5$ symbol frequencies there were no significant differences between the performances for a decision-feedback equalizer in cyclostationary interference and stationary noise. Hence the 3 dB points will be compared relative to case for X = 2 clusters with $B_t = 1.5$ symbol frequencies. The 3 dB points occur at: 15 percent for X = 2 with $B_t = 2.5$, 25 percent for X = 2 with $B_t = 4.0$, 46 percent for X = 1 with $B_t = 1.5$, 62 percent for X = 1 with $B_t = 2.5$, and 75 percent for X = 1 with $B_t = 4.0$. The observation from this figure is that having 2 clusters in the cable can potentially be a difficult impairment to an equalizer's ability to exploit the cyclostationary of the NEXT. To exploit the cyclostationarity under conditions of 2 clusters requires the use of very-wide relative bandwidths with associated increases in equalizer complexity.

4.4 Implementation Issues

Equalizers which exploit the cyclostationarity of the interference may require changes in implementation, compared to the case where the interference in the channel is stationary. Also there may be ramifications throughout the entire receiver design. However, in this section the emphasized issues are coefficient precision and convergence rates. This choice has been influenced by the work in [68] which suggests potential numerical difficulties in equalizer implementations which attempt to exploit the cyclostationarity of the interference. The primary performance criteria considered is the MSE. Some discussion is focused on the BER but this is necessarily limited since it is very difficult to simulate completely a system which has a BER specification of 10^{-7}. Using available computers it would take about 100 weeks to get 100 errors at a BER of 10^{-7}. Instead of simulations, better predictions of low BER values may be obtained through other techniques such as calculations or importance sampling.

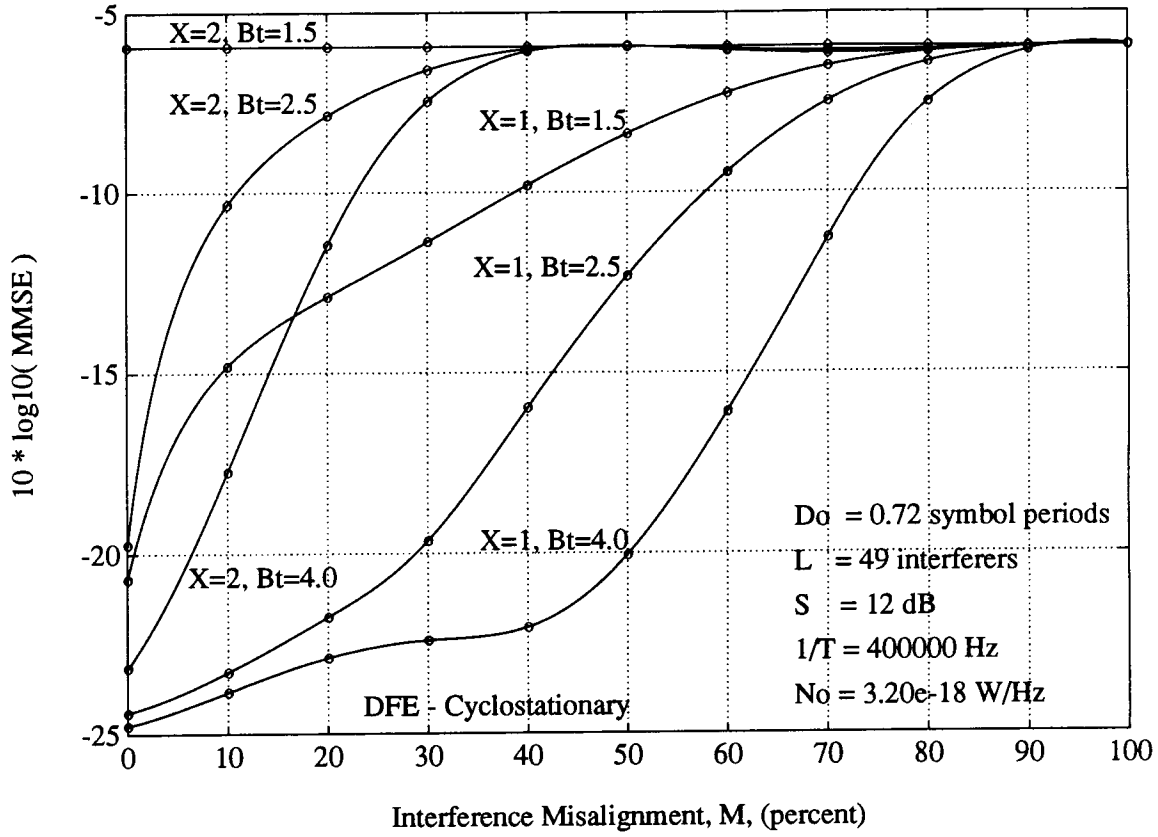

Figure 4.19 Decision-feedback equalizer MMSE in cyclostationary interference versus interference misalignment — very-wide relative transmitter bandwidths — one or two cable clusters

4.4.1 Simulation Description

Fig. 4.20 is a block diagram of the equalizer simulation. Fig. 4.20 shows a discrete-time version of the continuous-time equivalent in Fig. 3.9.

The important structural components in Fig. 4.20 are described as follows. The vectors $\mathbf{m}_{\phi 0}[n]$, $\{\mathbf{m}_{\phi i}[n] \mid i \in \mathsf{L}_1\}$, $\mathbf{m}_r[n]$, and $\mathbf{m}_b[n]$ are finite-length approximations to the memory of the filters for the combined channel, the combined co-channel, the forward filter of the DFE, and the feedback filter of the DFE, respectively. The vector $\mathbf{m}_{de}[n]$ represents the memory used to delay the equalizer decisions. The vector $\underline{\phi_0}$ contains samples of the impulse response of the combined channel and is defined using:

$$\underline{\phi_0}[n] = \begin{cases} 0 & , n \notin \{0,1,2, \ldots ,4095\} \\ \phi_0\left(n\frac{\mathrm{T}}{\mathrm{R_{sr}}}\right) & , n \in \{0,1,2, \ldots ,4095\} \end{cases} \tag{4.27}$$

where $\mathrm{R_{sr}}$ is the receiver sampling rate measured in samples per symbol period. To avoid aliasing, obtain $\mathrm{R_{sr}}$ by rounding the quantity $2\mathrm{B_t}$ up to the next integer, unless it is already an integer. The vectors $\{\underline{\phi_i} \mid i \in \mathsf{L}_1\}$ contain samples of the impulse responses of the combined co-channels. The combined co-channels are defined using:

$$\underline{\phi_i}[n] = \begin{cases} 0 & , n \notin \{0,1,2, \ldots ,63\} \\ \phi_i\left(n\frac{\mathrm{T}}{\mathrm{R_{sr}}}\right) & , n \in \{0,1,2, \ldots ,63\} \end{cases} \quad ; \quad i \in \mathsf{L}_1. \tag{4.28}$$

The vector $\mathbf{r}_d[n]$ represents the finite-length discrete-time impulse response of the forward filter. It is $(\mathrm{T}/\mathrm{R_{sr}})$-spaced and the number of taps in $\mathbf{r}_d[n]$ is $\mathrm{N_{fo}}$. The vector $\mathbf{b}_d[n]$ represents the finite-length discrete-time impulse response of the feedback filter. It is T spaced and the number of taps in $\mathbf{b}_d[n]$ is $\mathrm{N_{fd}}$. The number of taps in the memory delay $\mathbf{m}_{de}[n]$ is $\mathrm{D_e}$. The vectors $\mathbf{m}_{\phi 0}[n]$, $\{\mathbf{m}_{\phi i}[n] \mid i \in \mathsf{L}_1\}$, $\mathbf{m}_r[n]$, and $\mathbf{m}_d[n]$ have as many taps as their respective inner-product counter parts shown in Fig. 4.20. All the signals drawn with light lines are $\mathrm{T}/\mathrm{R_{sr}}$ spaced; these signals occur before the samplers and are roughly located in the upper left half of Fig. 4.20. All the signals drawn with heavy lines are T spaced; these signals occur after the samplers and are roughly located in the lower right half of Fig. 4.20. The square enclosing the letter T is a one symbol delay before the feedback filter. There is a switch labelled

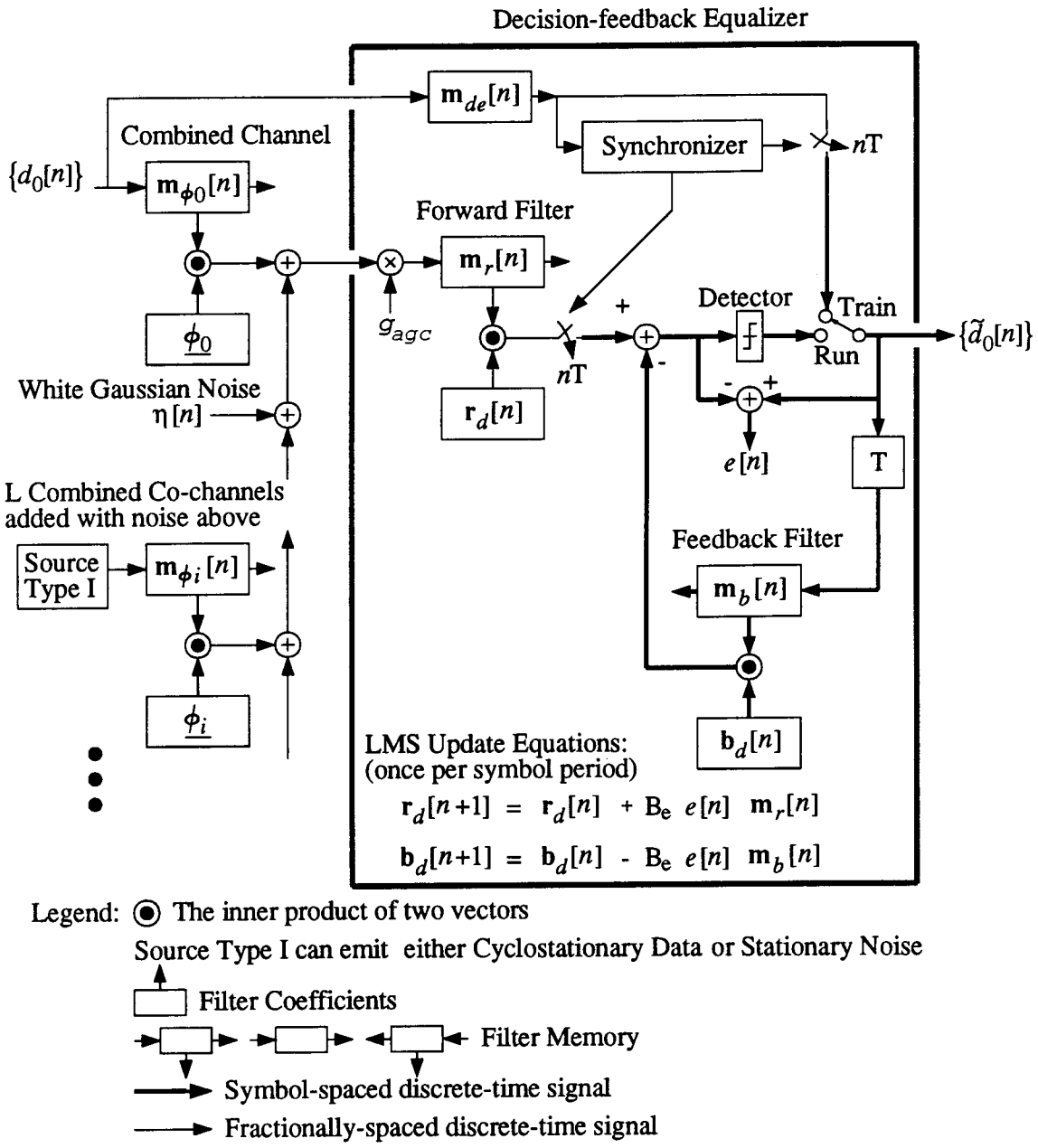

Figure 4.20 Block diagram of the equalizer simulation

train/run. During the simulation the equalizer is trained on known data. In a receiver, this mode would be followed by running with unknown data; however the run mode was not examined here. The input to the combined channel is the real valued data, with variance one, interspersed with $R_{sr} - 1$ zeros. The synchronizer block simply causes the samplers to operate at the correct sampling phase in a symbol period in order to operate on the data. The real white noise followed a Gaussian distribution with mean zero and a variance:

$$\frac{No}{2}\frac{R_{sr}}{T}. \tag{4.29}$$

The data sources for the interferers had two modes of operation. The first was the cyclostationary interference mode where they behaved like the source for $\{d_0[n]\}$. The second was the stationary noise mode where all samples in the symbol period contained real Gaussian-distributed white noise with mean zero and variance chosen to give the same power as in the stationary case; the noise variance was:

$$\frac{1}{R_{sr}}. \tag{4.30}$$

Finally in front of the forward filter is a multiplier. This serves the purpose of automatic gain control (AGC) in order that the signal at the output of the AGC has power one. This is done to improve the adaptation properties of the decision-feedback equalizer. It also helps to normalize the results for comparisons with other equalizer simulations. The value of the AGC coefficient is precomputed and fixed before the simulation is started. Its value is:

$$g_{agc} = \frac{1}{\sqrt{\frac{No}{2}\frac{R_{sr}}{T} + \frac{1}{R_{sr}}\sum_{i=0}^{L}\sum_{n=-\infty}^{\infty}\left|\underline{\phi_i}[n]\right|^2}}. \tag{4.31}$$

The equalizer is adapted using the LMS algorithm. This well known algorithm was used as a basis for comparison between the cyclostationary interference and stationary noise cases. The equations used to update the equalizer coefficients are computed once

per symbol period. The LMS equations are:

$$\begin{aligned} \mathbf{r}_d[n+1] &= \mathbf{r}_d[n] + \mathrm{B_e}\, e[n]\, \mathbf{m}_r[n] \\ \mathbf{b}_d[n+1] &= \mathbf{b}_d[n] - \mathrm{B_e}\, e[n]\, \mathbf{m}_b[n] \end{aligned} \tag{4.32}$$

where $e[n]$ is the equalizer error defined in Fig. 4.20:

$$e[n] = \widetilde{d_0}[n] - \widehat{d_0}[n] \tag{4.33}$$

and $\mathrm{B_e}$ is the adaptation constant.

Fixed-point coefficients are implemented by specifying a maximum coefficient value $\mathrm{C_m}$, the number of bits used to represent the tap value $\mathrm{C_p}$, and quantizing the coefficients to those discrete levels after each LMS update.

4.4.2 Simulation Results

The first set of simulations was performed for a relatively narrow bandwidth situation, $\mathrm{B_t}$ equal to 1.0 symbol frequencies. For these simulations, the number of taps in the forward filter ($\mathrm{N_{fo}}$), feedback filter ($\mathrm{N_{fd}}$) were chosen to be just large enough to reach the desired level of convergence. The memory delay ($\mathrm{D_e}$) was optimized and the adaptation constant $\mathrm{B_e}$ was chosen to be a factor of two smaller than that adaptation constant which caused divergence. The number of symbol periods over which the equalizer was trained was $\mathrm{I_t}$. The number of ensembles used to obtain averages was $\mathrm{I_a}$. When $\mathrm{I_a}$ is one, the equalizer error output, $e[n]$, is displayed as the square error (SE) $|e[n]|^2$. When $\mathrm{I_a}$ is greater than one, the mean of the square error (MSE) is displayed. Figs. 4.21 and 4.22 show the SE and MSE for a pair of stationary noise and cyclostationary interference cases, respectively. For the plots of MSE, at the smallest value of the ordinates is a thick horizontal line representing the MMSE bound that was calculated in the previous section on performance evaluation. Note that the MMSE bound assumes there are an infinite number of equalizer taps. Another reference line is drawn horizontally, 3 dB above the MMSE bound line. These two lines show how closely the equalizer approaches the bounds of the previous section.

It was of interest to determine if the residual equalizer error, $e[n]$, is Gaussian and if the statistics of the equalizer error could be used to estimate the BER. These

[a]

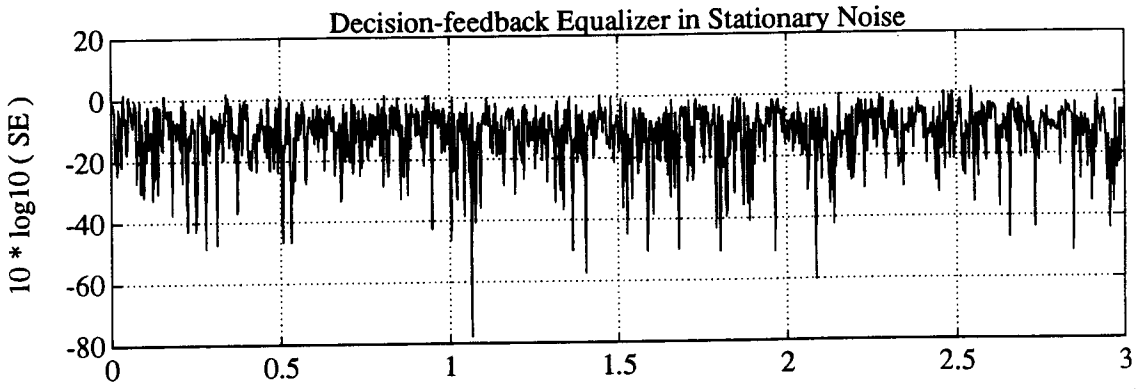

Do = 0.25 symbol periods
Bt = 1.00 symbol frequencies
No/2 = 3.20e-18 W/Hz
Rsr = 2 samples/symbol
It = 29971 symbol periods

M = 10 percent
L = 6 interferers
X = 1 cable cluster
Nfo = 25 taps
Nfe = 40 taps

S = 12 dB
1/T = 400000 Hz
De = 19 taps
Be = 5.00e-03
Ia = 1 run

[b]

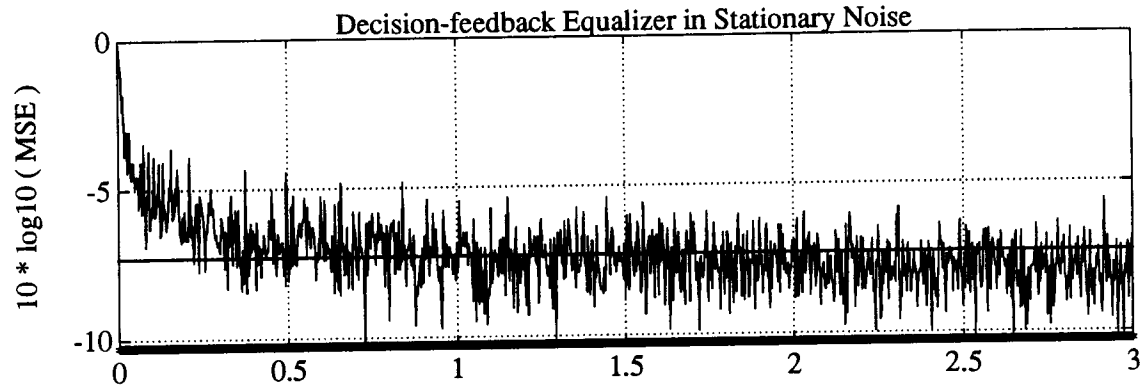

Do = 0.25 symbol periods
Bt = 1.00 symbol frequencies
No/2 = 3.20e-18 W/Hz
Rsr = 2 samples/symbol
It = 29971 symbol periods

M = 10 percent
L = 6 interferers
X = 1 cable cluster
Nfo = 25 taps
Nfe = 40 taps

S = 12 dB
1/T = 400000 Hz
De = 19 taps
Be = 5.00e-03
Ia = 50 runs

Figure 4.21 Square error and mean square error evolution versus time — narrow bandwidth — stationary noise

[a]

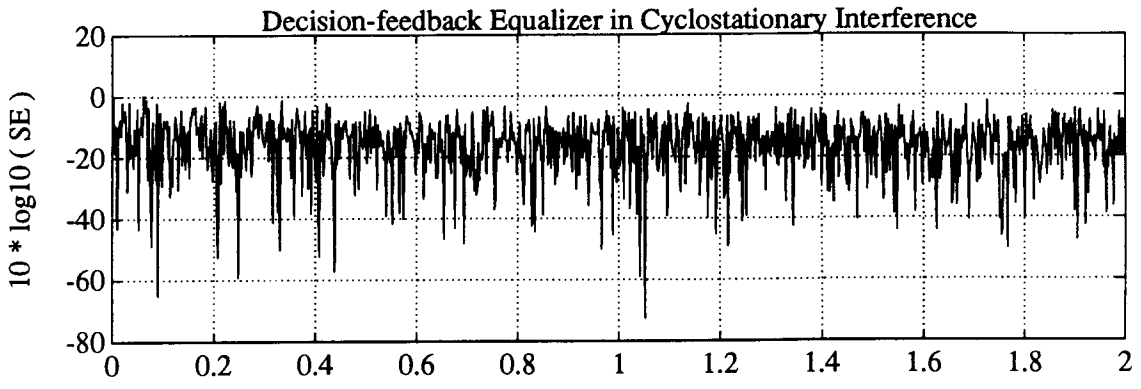

Do = 0.25 symbol periods	M = 10 percent	S = 12 dB
Bt = 1.00 symbol frequencies	L = 6 interferers	1/T = 400000 Hz
No/2 = 3.20e-18 W/Hz	X = 1 cable cluster	De = 29 taps
Rsr = 2 samples/symbol	Nfo = 25 taps	Be = 5.00e-03
It = 199981 symbol periods	Nfe = 40 taps	Ia = 1 run

[b]

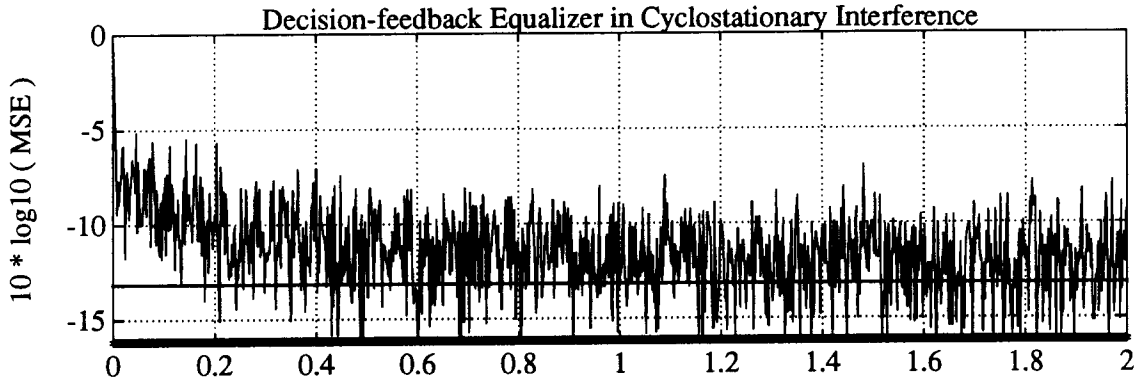

Do = 0.25 symbol periods	M = 10 percent	S = 12 dB
Bt = 1.00 symbol frequencies	L = 6 interferers	1/T = 400000 Hz
No/2 = 3.20e-18 W/Hz	X = 1 cable cluster	De = 29 taps
Rsr = 2 samples/symbol	Nfo = 25 taps	Be = 5.00e-03
It = 199981 symbol periods	Nfe = 40 taps	Ia = 10 runs

Figure 4.22 Square error and mean square error evolution versus time — narrow bandwidth — cyclostationary interference

questions will be answered by using something called a Gaussian plot. This type of plot is described here. After the equalizer reaches convergence, the error signal is a random process with zero mean, uncorrelated samples, and probability density functions which are symmetric about zero. Hence $|e[n]|$ is sufficient to convey information about the shape and variance of the distribution of $e[n]$, and the appropriate values of $|e[n]|$ are available from an SE versus time curve after equalizer convergence, such as in Fig. 4.22. The set of random variables $\{|e[n]|\}$ is obtained after equalizer convergence. The cumulative distribution function of random variables in the set $\{-|e[n]|, |e[n]|\}$ is plotted, but only that part of the distribution with positive values of $e[n]$ is meaningful. One common manner of plotting a cumulative distribution function is with the random variable on the abscissa and the probability on the ordinates. However, a different form will be used in order to convey the desired information.

In the form that was used, called a Gaussian plot, the roles of the abscissa and ordinates are reversed. The abscissa contains probabilities expressed in standard deviations about the mean of a Gaussian random variable, and the ordinates contain the values of the random variable. Mathematically this is stated as follows. The statistics of the equalizer error, $e[n]$, were examined. For $e[n]$, let μ be the estimate of the mean and σ be the unbiased estimate of the standard deviation. Form the following normalized random process which has a mean of zero and a variance of one: $(e[n] - \mu)/\sigma$; call this new random process $e_0[n]$. An estimate of the cumulative distribution function of $e_0[n]$ can be obtained and it is called $\widehat{F}_{E_0}(e_0)$. In a commonly used plot of the cumulative distribution function, $\sigma e_0[n] + \mu$ would appear on the abscissa and $\widehat{F}_{E_0}(e_0)$ would appear on the ordinates. However in the Gaussian plot, $Q^{-1}\left(1 - \widehat{F}_{E_0}(e_0)\right)$ appears on the abscissa and $\sigma e_0[n] + \mu$ appears on the ordinates, where $Q^{-1}(\bullet)$ is the inverse of the $Q(\bullet)$ function defined in (4.36). In other words, the cumulative distribution function of a Gaussian random variable is transformed into a line, and that line contains all the information to characterize the Gaussian random variable. The ordinate intercept of the line is the mean and the slope of the line is the standard deviation of the Gaussian random process.

The advantage of conveying information in a Gaussian plot is that a zero-mean wide-sense-stationary white Gaussian random process would appear as a line with a positive slope equal to the standard deviation of the Gaussian random variables. If the equalizer error, $e[n]$, were distributed as a Gaussian random variable, then the Gaussian plot would contain a line passing through the origin with a slope equal to the standard deviation of $e[n]$. Hence the Gaussian plot is a qualitative test to determine if $e[n]$ is Gaussian distributed. The BER at the output of the equalizer can be estimated or extrapolated from the Gaussian plot. If the plot contains a line with a large slope relative to the energy of the signal, then the standard deviation of $e[n]$ will be relatively large, and the BER will be large. If the plot contains a line with a small slope relative to the energy of the signal, then the standard deviation of $e[n]$ will be relatively small, and the BER will be small. For HDSL, the goal is to maintain a BER below 10^{-7}. Therefore the desired information from the Gaussian plot is whether or not the 10^{-7} BER specification is satisfied. Assuming a Gaussian distribution of the equalizer error, the method to determine this desired information is developed as follows.

Four-level pulse amplitude modulation (PAM) was used in the HDSL simulation. For four-level data, with variance one:

$$\left\{-\frac{3}{\sqrt{5}},\ -\frac{1}{\sqrt{5}},\ +\frac{1}{\sqrt{5}},\ +\frac{3}{\sqrt{5}}\right\} \tag{4.34}$$

and Grey code binary assignments to the four levels, the probability of bit error for additive white Gaussian noise is:

$$\text{BER} \ \cong\ \frac{3}{4}\,Q\left(\frac{d_{min}}{\sigma}\right) \tag{4.35}$$

where the Q function is:

$$Q(\bullet) \ =\ \frac{1}{\sqrt{2\pi}}\int_{\bullet}^{\infty} e^{-x^2/2}\ dx, \tag{4.36}$$

d_{min} is the minimum distance between a decision boundary and a transmitted signal level, and finally σ is the standard deviation of the additive white Gaussian noise. From

the four data levels shown above, d_{min} is given by:

$$\begin{aligned} d_{min} &= \frac{1}{\sqrt{5}} \\ &\approxeq 0.447 \quad . \end{aligned} \tag{4.37}$$

Therefore to maintain a BER of 10^{-7} the maximum permitted standard deviation of the Gaussian random variable is given by:

$$\begin{aligned} \sigma &= \frac{d_{min}}{Q^{-1}\left(\frac{4}{3}\,\mathrm{BER}\right)} \\ &= \frac{\frac{1}{\sqrt{5}}}{Q^{-1}\left(\frac{4}{3}\times 10^{-7}\right)} \\ &\approxeq 0.0869 \text{ standard deviations} \, . \end{aligned} \tag{4.38}$$

This means that if the Gaussian plot contains a straight line whose slope is less than about 0.0869, then the BER will be less than 10^{-7}. A line with such a slope will pass through the point:

$$\begin{aligned} &\left(\frac{\frac{1}{\sqrt{5}}}{0.0869}, \frac{1}{\sqrt{5}}\right) \\ &\approxeq (5.15, 0.447) \end{aligned} \tag{4.39}$$

on the Gaussian plot which means that the minimum distance to the decision boundary, 0.447 corresponds to 5.15 standard deviations of the additive white Gaussian noise. The Gaussian plot will be truncated to only those values of interest by having a lower left corner at $(0,0)$ and an upper right corner at $(5.15, 0.447)$. Finally, the BER will be less than the HDSL specification if the line on the Gaussian plot is of a sufficiently small slope than it intersects with the visible right vertical edge of the Gaussian plot. This will be the test to determine if the equalizer meets the BER specification.

Fig. 4.23 is a Gaussian plot of the equalizer error $e[n]$ after convergence for the case shown in Fig. 4.22. Since the curve is not a line, in this case the residual equalizer error does not closely approximate a Gaussian random variable. Therefore the BER cannot be determined in the same manner as with a Gaussian random variable. Since the curve in Fig. 4.23 does not intersect with the right edge of the plot, the BER appears to be greater than 10^{-7}.

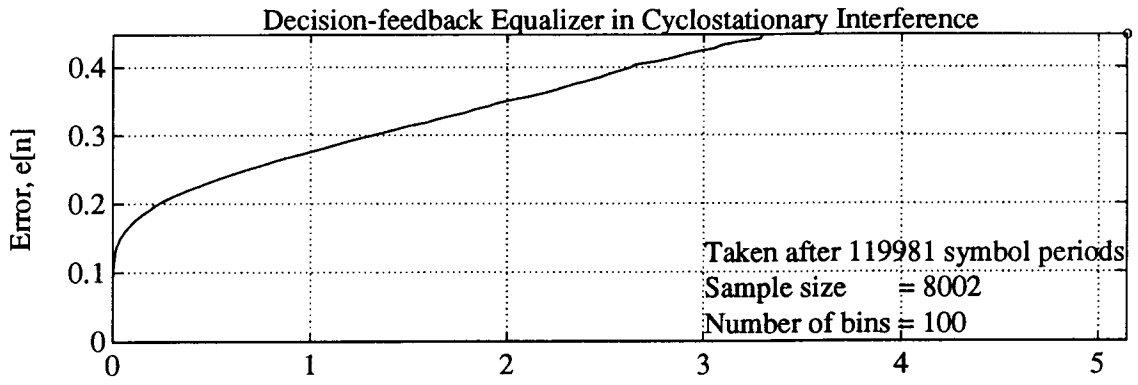

Figure 4.23 Gaussian plot of probability distribution function of equalizer error after convergence — narrow bandwidth

The second set of simulations was performed for a relatively wide bandwidth situation, B_t equal to 2.12 symbol frequencies. Just like the first set of simulations the number of taps in the forward filter, the number of taps in the feedback filter, the memory delay, and the adaptation constant were chosen appropriately to reach the desired level of convergence near the MMSE bounds of the performance evaluation section. Fig. 4.24 shows the SE and MSE for the stationary noise case. Fig. 4.25 shows the states of the forward and feedback taps at the end of the simulation whose SE is shown in Fig. 4.24a. For the cyclostationary interference case, Fig. 4.26 shows the SE and MSE; Fig. 4.27 shows the states of the forward and feedback taps at the end of the simulation whose SE is shown in Fig. 4.26a. After convergence in stationary noise, the forward filter suppresses precursor ISI by approximating the convolution of a matched filter, a sampler, and a (delayed) anti-causal T-spaced filter. Since the impulse response of the channel is very long, the shape in Fig. 4.25a is not unexpected. However, after convergence in cyclostationary interference, the forward filter approximates a bank of matched filters, samplers, and T-spaced filters; see Fig. 3.10. In cyclostationary interference the forward filter must suppress interference, in addition to precursor ISI. Compare the forward filter taps for both cases, Figs. 4.25a and 4.27a. In the simulation, the actual number of taps in the forward filter for the cyclostationary interference case is less than the stationary noise case, however the number of significant taps is about the same at 40. This is because the 20 forward filter taps are almost zero between 8 and 10 symbol periods. The differences in shape arise between the two cases because the forward filters try to achieve different goals. In stationary noise, the forward filter tries to minimize noise and precursor ISI, however in cyclostationary interference the forward filter tries to minimize noise, precursor ISI, and cyclostationary CCI (NEXT). Note that the equalizer in stationary noise has also converged closer to the MMSE bound; See Figs. 4.24 and 4.26. The smaller number of taps that were used in the cyclostationary interference case meant that a marginally larger adaptation constant could be used, 5×10^{-3} instead of 10^{-3} for stationary noise. Yet even with the slight difference in adaptation constant, the *rate of convergence* was approximately the same; note between

Figs. 4.24b and 4.26b that it took about 10 000 symbol periods to reach -7 dB. However the time to converge in cyclostationary interference was dramatically longer, 100 000 symbol periods versus 10 000 symbol periods for stationary noise. This was due to the MMSE in the cyclostationary interference case being 19 dB lower than in stationary noise. One miscellaneous final note is warranted. It was observed that during initial convergence in cyclostationary interference, the forward filter appears much like it would in the stationary noise case. This is probably due to the ISI being the initial dominant impairment. However as the convergence continues, the relative energy in the forward filter taps gets concentrated over a smaller time interval.

Fig. 4.28 shows plots of MSE versus fixed-point coefficient precision for stationary noise and cyclostationary interference. By visual inspection, for stationary noise the number of bits needed to reach an adequately low MSE is 11. As expected for cyclostationary interference, this value is higher. For the situation in this simulation, the value is 5 bits higher, at 16 bits. On the left side of both curves, the general trend indicates about 3 dB improvement in MSE for each added bit. Note that these results were obtained for a central office clock misalignment of $\mathrm{M} = 10$ percent which should impose near worst case precision requirements over stationary noise.

For the cyclostationary interference case with fixed-point coefficient precision, the SE and MSE evolution with time were simulated and the results are shown in Fig. 4.29. Fig 4.29 looks much like the floating point case in Fig. 4.26. Similar to the type of plot in Fig. 4.23, Fig. 4.30 contains Gaussian plot of the cumulative distribution function of the error $e[n]$. Since the curve in Fig. 4.30 is a line, the residual equalizer error closely approximates a Gaussian random variable over the 4 standard deviations shown in the figure. If this line were extrapolated, and assuming it maintained the same Gaussian properties, the it would intersect with the right edge of the plot. This means that the BER would be less than 10^{-7}. It is stressed that this case is for $\mathrm{L} = 6$ interferers, with correct decisions fed back, and a safety margin of $\mathrm{S} = 12$ dB. In general the residual error is white but not necessarily Gaussian. If it does exhibit Gaussian behavior, as in Fig. 4.30, then 3 dB of MMSE gain would correspond approximately to 3 dB of

[a]

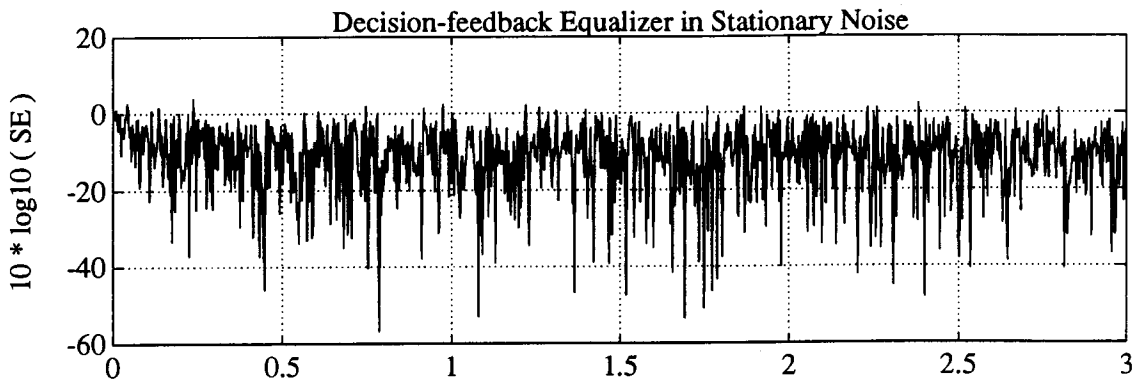

Do = 0.72 symbol periods	M = 10 percent	S = 12 dB
Bt = 2.12 symbol frequencies	L = 6 interferers	1/T = 400000 Hz
No/2 = 3.20e-18 W/Hz	X = 1 cable cluster	De = 45 taps
Rsr = 5 samples/symbol	Nfo = 60 taps	Be = 1.00e-03
It = 29971 symbol periods	Nfe = 20 taps	Ia = 1 run

[b]

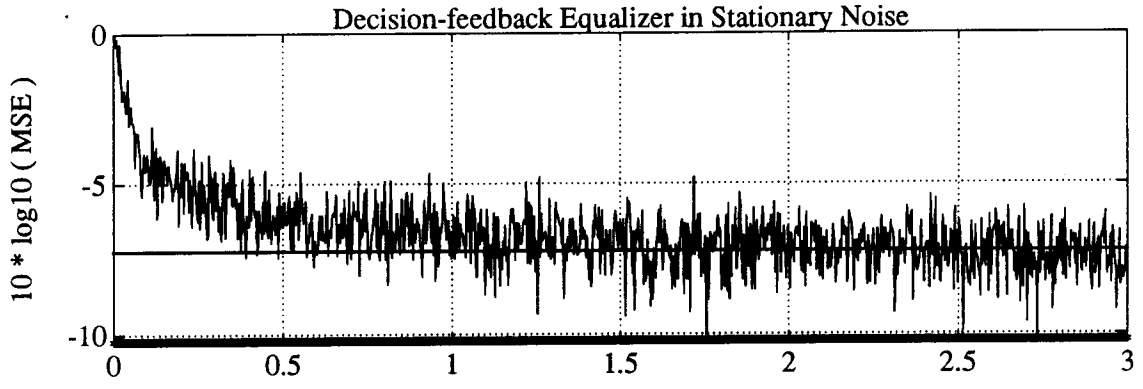

Do = 0.72 symbol periods	M = 10 percent	S = 12 dB
Bt = 2.12 symbol frequencies	L = 6 interferers	1/T = 400000 Hz
No/2 = 3.20e-18 W/Hz	X = 1 cable cluster	De = 45 taps
Rsr = 5 samples/symbol	Nfo = 60 taps	Be = 1.00e-03
It = 29971 symbol periods	Nfe = 20 taps	Ia = 50 runs

Figure 4.24 Square error and mean square error evolution versus time — wide bandwidth — stationary noise

[a]

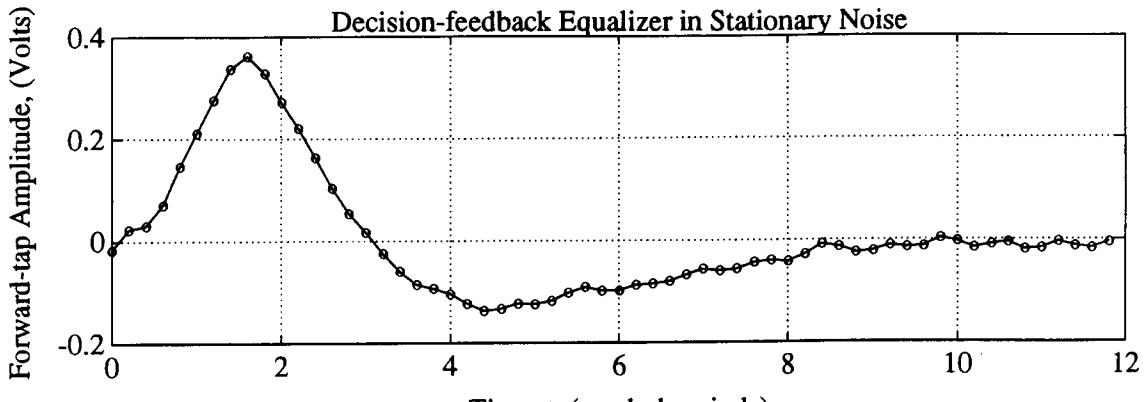

Do = 0.72 symbol periods	M = 10 percent	S = 12 dB
Bt = 2.12 symbol frequencies	L = 6 interferers	1/T = 400000 Hz
No/2 = 3.20e-18 W/Hz	X = 1 cable cluster	De = 45 taps
Rsr = 5 samples/symbol	Nfo = 60 taps	Be = 1.00e-03
It = 29971 symbol periods	Nfe = 20 taps	Ia = 1 run

[b]

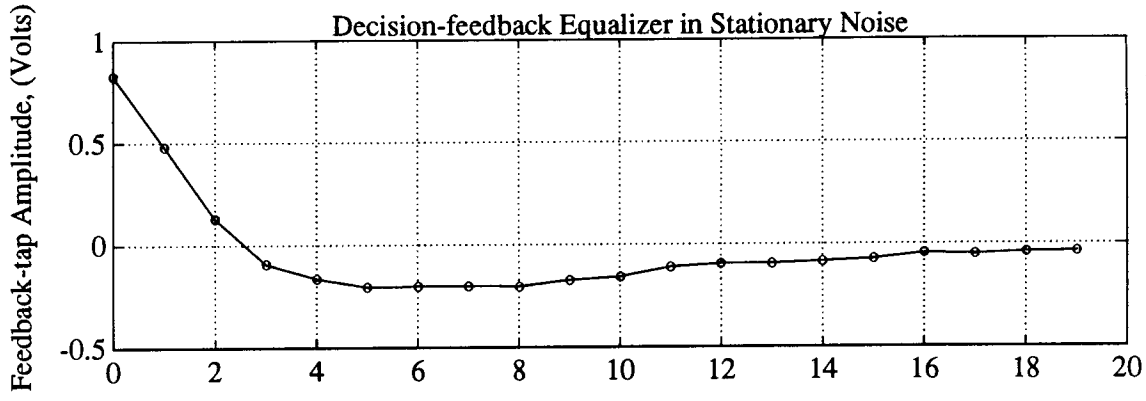

Do = 0.72 symbol periods	M = 10 percent	S = 12 dB
Bt = 2.12 symbol frequencies	L = 6 interferers	1/T = 400000 Hz
No/2 = 3.20e-18 W/Hz	X = 1 cable cluster	De = 45 taps
Rsr = 5 samples/symbol	Nfo = 60 taps	Be = 1.00e-03
It = 29971 symbol periods	Nfe = 20 taps	Ia = 1 run

Figure 4.25 Tap values after convergence — wide bandwidth — stationary noise

[a]

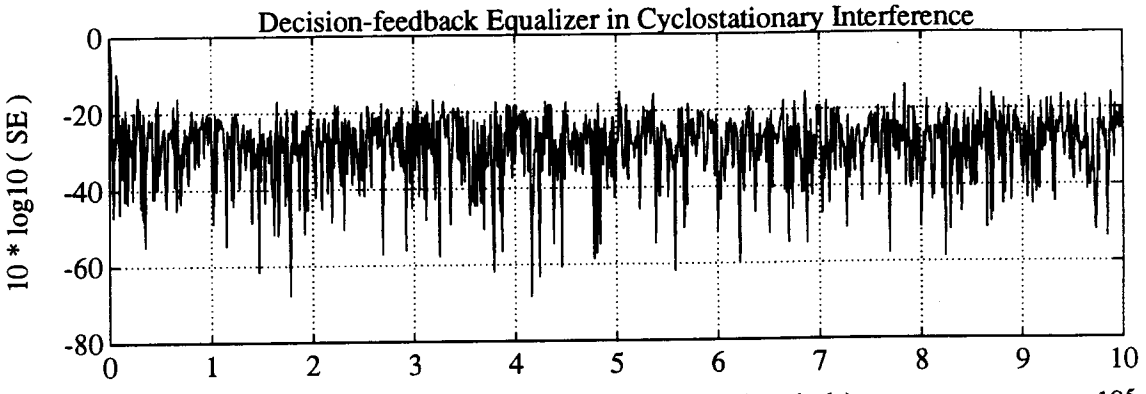

Do = 0.72 symbol periods
Bt = 2.12 symbol frequencies
No/2 = 3.20e-18 W/Hz
Rsr = 5 samples/symbol
It = 999981 symbol periods

M = 10 percent
L = 6 interferers
X = 1 cable cluster
Nfo = 40 taps
Nfe = 20 taps

S = 12 dB
1/T = 400000 Hz
De = 60 taps
Be = 5.00e-03
Ia = 1 run

[b]

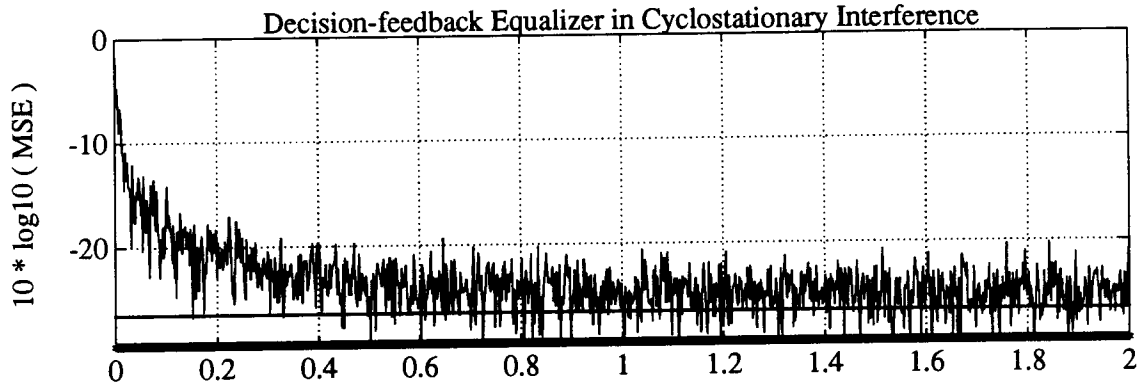

Do = 0.72 symbol periods
Bt = 2.12 symbol frequencies
No/2 = 3.20e-18 W/Hz
Rsr = 5 samples/symbol
It = 199801 symbol periods

M = 10 percent
L = 6 interferers
X = 1 cable cluster
Nfo = 40 taps
Nfe = 20 taps

S = 12 dB
1/T = 400000 Hz
De = 60 taps
Be = 5.00e-03
Ia = 10 runs

Figure 4.26 Square error and mean square error evolution versus time — wide bandwidth — cyclostationary interference

[a]

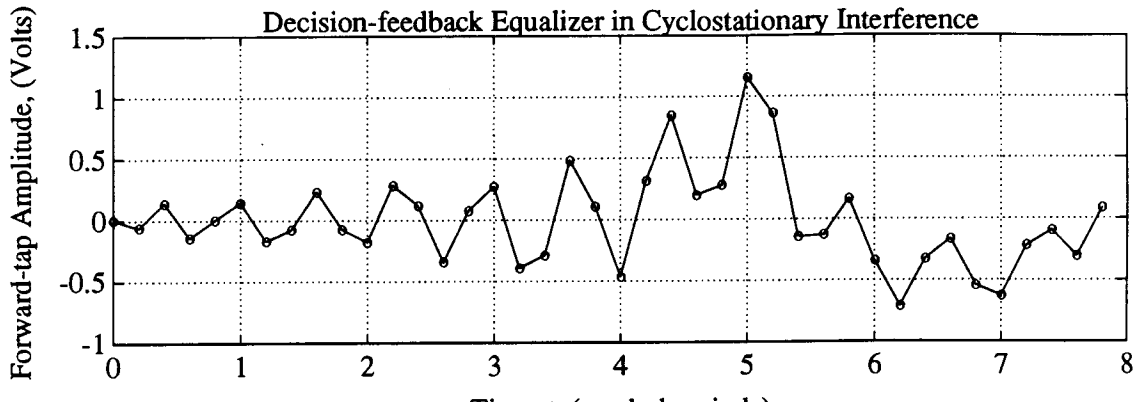

Do = 0.72 symbol periods
Bt = 2.12 symbol frequencies
No/2 = 3.20e-18 W/Hz
Rsr = 5 samples/symbol
It = 199801 symbol periods

M = 10 percent
L = 6 interferers
X = 1 cable cluster
Nfo = 40 taps
Nfe = 20 taps

S = 12 dB
1/T = 400000 Hz
De = 60 taps
Be = 5.00e-03
Ia = 1 run

[b]

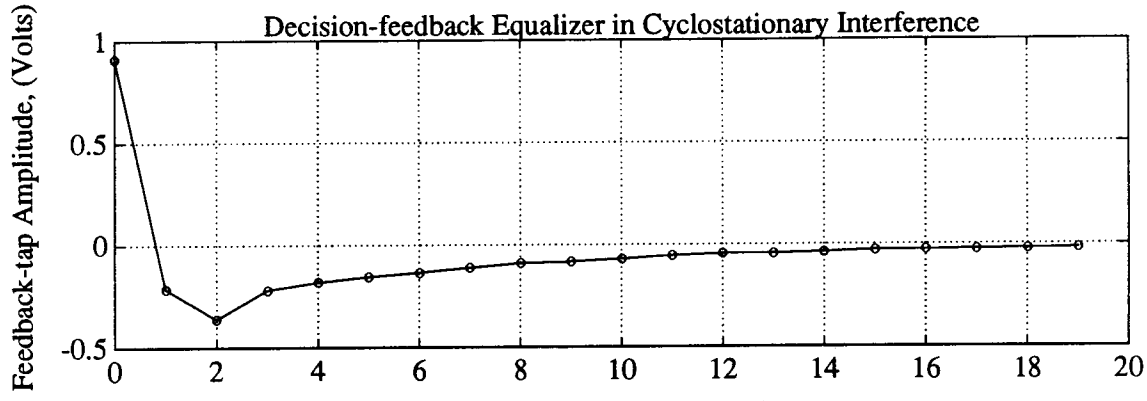

Do = 0.72 symbol periods
Bt = 2.12 symbol frequencies
No/2 = 3.20e-18 W/Hz
Rsr = 5 samples/symbol
It = 199801 symbol periods

M = 10 percent
L = 6 interferers
X = 1 cable cluster
Nfo = 40 taps
Nfe = 20 taps

S = 12 dB
1/T = 400000 Hz
De = 60 taps
Be = 5.00e-03
Ia = 1 run

Figure 4.27 Tap values after convergence — wide bandwidth — cyclostationary interference

[a]

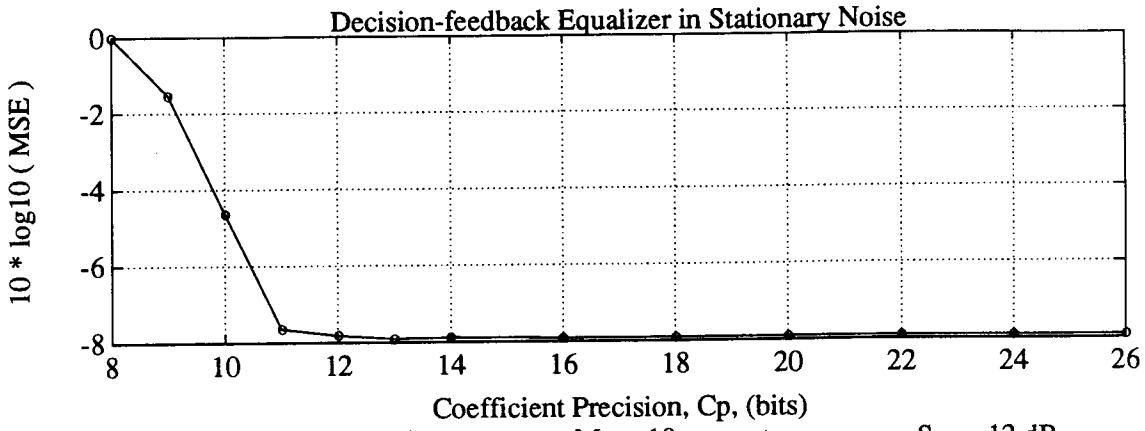

Do = 0.72 symbol periods
Bt = 2.12 symbol frequencies
No/2 = 3.20e-18 W/Hz
Rsr = 5 samples/symbol
It = 29971 symbol periods
Cm = 2 volts

M = 10 percent
L = 6 interferers
X = 1 cable cluster
Nfo = 60 taps
Nfe = 20 taps

S = 12 dB
1/T = 400000 Hz
De = 45 taps
Be = 1.00e-03
Ia = 1 run

[b]

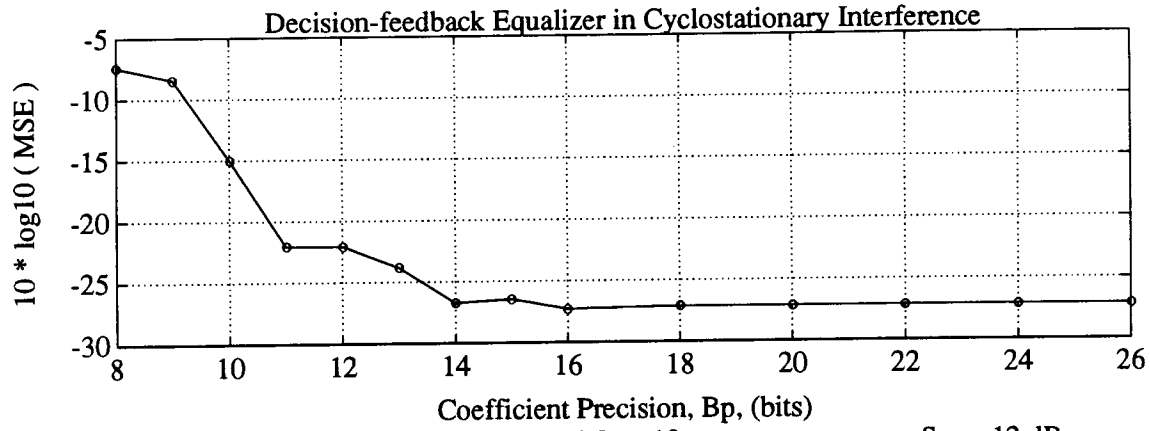

Do = 0.72 symbol periods
Bt = 2.12 symbol frequencies
No/2 = 3.20e-18 W/Hz
Rsr = 5 samples/symbol
It = 199801 symbol periods
Cm = 4 volts

M = 10 percent
L = 6 interferers
X = 1 cable cluster
Nfo = 40 taps
Nfe = 20 taps

S = 12 dB
1/T = 400000 Hz
De = 60 taps
Be = 5.00e-03
Ia = 1 run

Figure 4.28 Mean square error after convergence versus coefficient precision — stationary noise and cyclostationary interference

asymptotic SINR gain on a BER versus SINR curve. In any case, the MMSE provides an exponentially tight upper bound on the BER.

4.5 Discussion

This discussion on the ability of equalizers to exploit the cyclostationarity of subscriber-line NEXT is divided into two parts. The first deals with the gains and the second deals with the costs to achieve those gains.

The gains were evaluated using one worst case channel since accuracy is limited by that part of the model which introduces the most uncertainty, and it is believed to be the NEXT part. The channel considered was 9000 feet of 26 AWG wire and the NEXT model was obtained by processing measurements that were performed on a 50-pair subscriber-line cable bundle.

It was found that a joint combination of sufficiently wide transmitter bandwidth relative to the symbol rate with sufficiently aligned transmitter clock phase provided the opportunity for performance gains. These gains are a result of the equalizers being able to exploit the cyclostationary nature of the NEXT in order to achieve improved interference suppression. In the absence of any other known way to quantify the amount of alignment of the central office clock phases, a parameter was introduced called the interference misalignment. This parameter specifies the percentage of a symbol period over which the beginnings of the impulse responses of the interferers are uniformly distributed. For sufficiently small values of interference misalignment, 3 dB of MMSE gain is achievable over the case where the interference is perfectly misaligned and has the least amount of cyclostationarity. A summary of these points of 3 dB improvement are shown in Table 4.2 where the following parameters apply throughout the table:

$$\begin{aligned} D_0 &= 0.72 \text{ symbol frequencies} \\ S &= 12 \text{ dB} \\ No &= 3.2 \times 10^{-18} \frac{W}{Hz} \\ \frac{1}{T} &= 400 \text{ kHz}. \end{aligned} \tag{4.40}$$

[a]

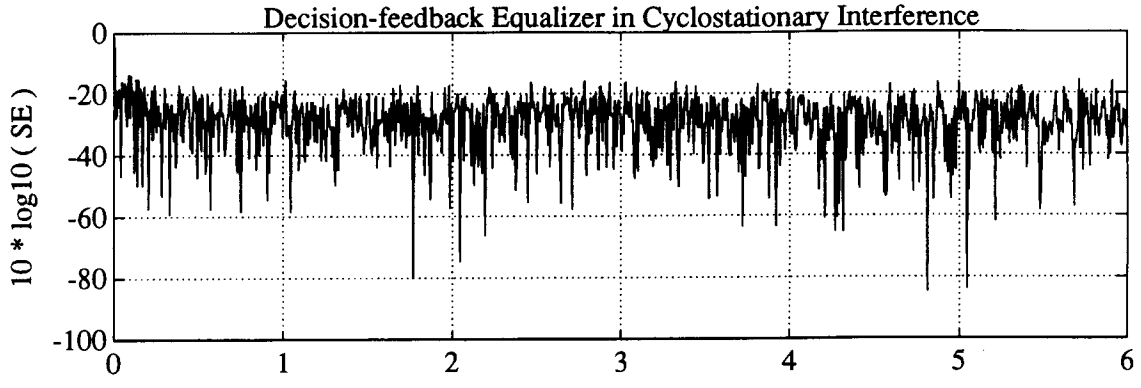

Do = 0.72 symbol periods	M = 10 percent	S = 12 dB
Bt = 2.12 symbol frequencies	L = 6 interferers	1/T = 400000 Hz
No/2 = 3.20e-18 W/Hz	X = 1 cable cluster	De = 60 taps
Rsr = 5 samples/symbol	Nfo = 40 taps	Be = 5.00e-03
It = 599991 symbol periods	Nfe = 20 taps	Ia = 1 run
Cm = 4 volts	Cp = 18 bits	

[b]

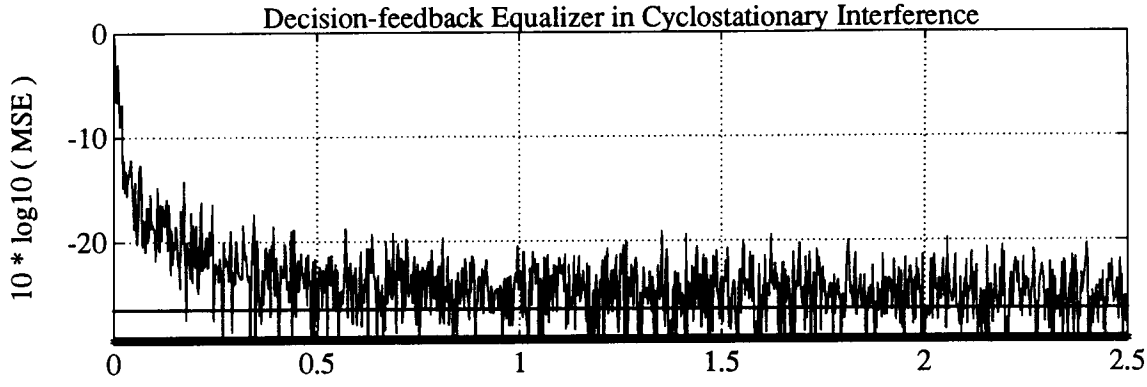

Do = 0.72 symbol periods	M = 10 percent	S = 12 dB
Bt = 2.12 symbol frequencies	L = 6 interferers	1/T = 400000 Hz
No/2 = 3.20e-18 W/Hz	X = 1 cable cluster	De = 60 taps
Rsr = 5 samples/symbol	Nfo = 40 taps	Be = 5.00e-03
It = 249991 symbol periods	Nfe = 20 taps	Ia = 6 runs
Cm = 4 volts	Cp = 18 bits	

Figure 4.29 Square error and mean square error evolution versus time — wide bandwidth — cyclostationary interference — fixed point

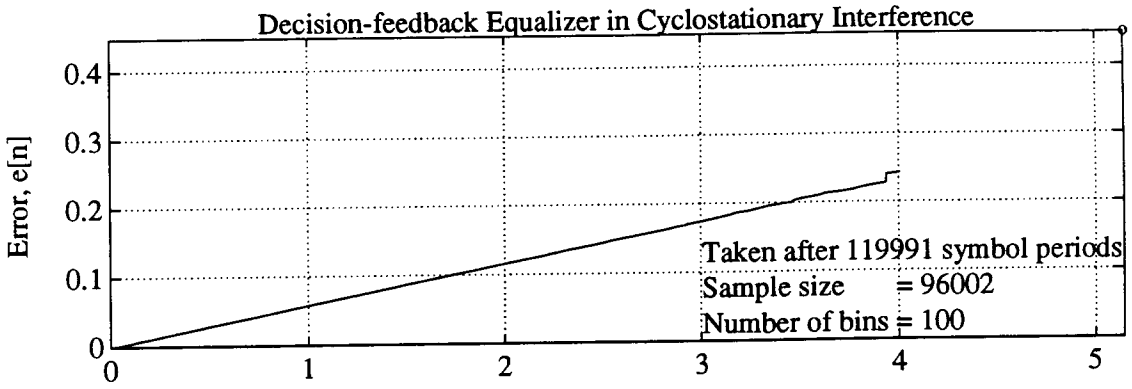

Do = 0.72 symbol periods
Bt = 2.12 symbol frequencies
No/2 = 3.20e-18 W/Hz
Rsr = 5 samples/symbol
It = 599991 symbol periods
Cm = 4 volts

M = 10 percent
L = 6 interferers
X = 1 cable cluster
Nfo = 40 taps
Nfe = 20 taps
Cp = 18 bits

S = 12 dB
1/T = 400000 Hz
De = 60 taps
Be = 5.00e-03
Ia = 1 run

Figure 4.30 Gaussian plot of probability distribution function of equalizer error after convergence — wide bandwidth — fixed point

Two important trends are evident from the table. The first trend is that an increase in relative transmitter bandwidth, with all other parameters being constant, results in a higher permitted interference misalignment. The second trend is that an increase in the number of cable clusters from 1 to 2 provides a significant degradation in that much narrower interference misalignments are required to maintain a 3 dB improvement, but note that 2 cable clusters do not completely eliminate the potential for gains. Two cable clusters corresponds to the situation where the 50-pair subscriber-line cable bundle is divided with each half going to a different rack of equipment in the central office.

With wider relative transmitter bandwidths, the power of NEXT interference increases relative to the power of the signal carrying the data of interest. Even with this relative power degradation, wider relative transmitter bandwidths permit performance improvements. Similar shapes of the NEXT impulse responses, as in these evaluations, facilitates improved interference suppression and note that the geometries of subscriber lines are more similar in the central office side, than in the customer side. As stated earlier, the gains come from exploiting not only the statistical properties[20], but also the deterministic properties of the interference[21].

Again note that the simulations were carried out using four-level PAM. Although different numbers of modulation levels were not investigated, it is expected that the number of levels would not significantly affect the results.

Some of the costs of achieving these gains will now be described. A system cost occurs with providing partial alignment of the phases of the transceiver clocks in the central office. Clock phase alignment in the central office would mean that a symbol rate (or some appropriate rate) clock should be fed to all the line cards. It is not suggested that the phases should be adjusted individually, but instead to provide whatever alignment is reasonable in order to improve the equalizer performance. Even if clock phase alignment is impractical, there may be enough cyclostationarity present to achieve

---

20 Interference power variations are one such statistical property.

21 The shapes of the interferer's impulse responses after equalization are one such algebraic property.

Table 4.2 Points of interference misalignment with 3 dB improvement of cyclostationary interference over stationary noise using a decision-feedback equalizer

Cable Clusters	Number of Interferers	Relative Transmitter Bandwidth	Interference Misalignment
X	L	B_t	M
(-)	(-)	(symbol frequencies)	(percent)
1	6	1.0	16.
1	6	1.5	46.
1	49	1.0	5.
1	49	1.5	46.
1	49	2.5	60.
1	49	4.0	75.
2	49	1.5	0.
2	49	2.5	15.
2	49	4.0	25.

some performance gains [13].

One increase in receiver complexity occurs with the use of fractionally spaced equalizers because higher sampling rates are required. As indicated earlier, the use of a fractionally spaced equalizer may require the use of a fractionally spaced echo canceller. With a fractionally spaced echo canceller, it must reduce the power of the echo signal sufficiently below the NEXT signal power levels otherwise the echo signal will appear as another cyclostationary interferer and the DFE will try to suppress it, in addition to the interference. Thus the DFE NEXT suppression capability would be reduced. Exploiting the cyclostationarity of the interference may put additional demands on the synchronizer. It is worth noting that echo canceller's already impose stringent low-jitter requirements on the synchronizer.

Simulations of equalizers in cyclostationary NEXT confirmed and quantified certain results. The simulations confirmed the expressions for the MMSE bounds of the performance evaluation section. The simulations also quantified two increases in implementation complexity. For a case where a T/5-spaced equalizer was simulated, the required coefficient precision increased from 11 to 16 bits when the interference misalignment was changed from 100 percent to 10 percent. The interference misalignment increase means that to the equalizer the interference properties change from being stationary noise to cyclostationary interference. Additionally the time for the equalizer to converge increased from 10 000 symbol periods to 100 000 symbol periods when the NEXT was changed from stationary noise to cyclostationary interference. The additional time was spent by the equalizer in converging from its MMSE value for stationary noise to its much lower MMSE value for cyclostationary interference. Finally it was found that in cyclostationarity interference, an increase in the relative transmitter bandwidth did not cause an increase in the required number of taps; it only reduced their spacing.

There are interesting trade-offs in adjustments of the LMS adaptation constant. As the equalizer adapts, there are decreasing amounts of interference. This may justify decreasing the adaptation constant as convergence is approached. Subscriber-line impulse responses can change slowly due to temperature variations. In this case

tracking of the changes by the equalizer is not difficult. However, in cyclostationary interference, the nature of the interference at the equalizer input may change abruptly with the appearance and disappearance of interferers when equipment gets turned on and off. Hence some form of tracking would be required.

The gains and costs of exploiting the cyclostationarity of the interference have been discussed. The extent to which the gains shown here apply to real subscriber lines could not be quantified much further. These are the most realistic results available in the absence of any other information on the practicality of aligning the phases of the clocks in the central office, and on a NEXT model which incorporates phase data of real subscriber lines. The techniques of exploiting cyclostationarity of the interference are not necessarily advocated alone, but in conjunction with other compatible techniques [13]. The design issues that have been discussed in the context of HDSL, may have relevance in other uses of twisted pairs where remote locations may have fewer twisted pairs and clock phase alignment becomes more practical.

Chapter 5
Application to Adjacent-channel Interference in Digital Radio

5.1 Background

The relevant background associated with using equalizers to suppress ACI has been briefly discussed in Section 1.2. The goal of this chapter is to show how the general analyses and systems design considerations in Chapter 3 can be used to analyze and improve the performance of equalizers which are impaired by cyclostationary ACI.

An important note about the calculations to follow is that they are based on a channel that does not fade. Thus, the calculations cannot be used to predict the exact performance in specific radio applications where fading exists [148]. However, the positive aspect to this approach is that it applies to unfaded conditions and it is not tied to any specific radio application.

The potential for equalizers to suppress cyclostationary ACI will be analyzed under conditions with no CCI, one receiver antenna, and various conditions of transmitter bandwidth, equalizer bandwidth, and carrier spacing. Based on the analyses in Sections 3.2 and 3.3, the performance criteria that are used are the existence of the generalized linear equalizer and the expressions for the MMSE of linear and decision-feedback equalizer in cyclostationary interference and stationary noise. The potential for performance improvements has implications on improved spectral efficiency and the choice of system operating conditions.

5.2 Models

As stated earlier the model of the system is described in Chapter 2. The symbol rate 1/T, the power at the input to the equalizer P_S, and the noise power spectral density No were fixed. Define the energy per symbol at the input to the receiver as:

$$E_S = P_S T. \tag{5.1}$$

Therefore the ratio of the energy per symbol at the input to the equalizer to the noise power spectral density is a constant, called E_S/No. The desired value of this constant was obtained from typical values found in digital microwave radio [44, 45]:

$$10 \log_{10}\left(\frac{E_S}{No}\right) = 64.2 \text{ dB}. \tag{5.2}$$

Although the specific values of the symbol rate, the transmitter output power, and the symbol rate are irrelevant, they are shown for completeness:

$$\begin{aligned} \frac{1}{T} &= 22.5 \text{ MHz} \\ P_S &= 0.5 \text{ mW} \\ No &= 8.4 \times 10^{-18} \frac{W}{Hz}. \end{aligned} \tag{5.3}$$

The conditions of no CCI and one receiver antenna are specified mathematically as:

$$\begin{aligned} N_c &= 0 \text{ CCI signals} \\ A_r &= 1 \text{ antenna} \quad . \end{aligned} \tag{5.4}$$

The transmitter filter is shown in Fig. 2.1, with its impulse response $p_{t,0}(t)$. A model for this impulse response will be developed here. The basis for this pulse is a commonly used pulse called a square-root raised cosine [86]:

$$P_{sr}(f\,;\,\alpha) = \begin{cases} \sqrt{T} & , 0 \le |f| < \frac{1-\alpha}{2T} \\ \sqrt{\frac{T}{2}\left(1 - \sin\left(\frac{\pi T}{\alpha}\left(|f| - \frac{1}{2T}\right)\right)\right)} & , \frac{1-\alpha}{2T} \le |f| < \frac{1+\alpha}{2T} \\ 0 & , \frac{1+\alpha}{2T} \le |f| \end{cases} \tag{5.5}$$

$$0 \le \alpha \le 1$$

where α is the excess bandwidth parameter. However $P_{sr}(f;\alpha)$ cannot have a bandwidth greater than $1/T$. To allow exploration of relatively wider bandwidths, the following pulse was defined:

$$P_{srw}(f\,;\,B_t) = \begin{cases} \sqrt{P_S T}\; P_{sr}(f\,;\,2B_t - 1) & , \frac{1}{2} \le B_t \le 1 \\ \sqrt{\frac{P_S T}{B_t}}\; P_{sr}\left(\frac{f}{B_t}\,;\,1\right) & , 1 < B_t \end{cases} \tag{5.6}$$

where the bandwidth of $P_{srw}(f;B_t)$ is B_t. When B_t is in the range $1/2 \le B_t \le 1$, $P_{srw}(f;B_t)$ behaves like a square-root raised cosine pulse. When B_t is in the range

$1 < B_t$, $P_{srw}(f; B_t)$ has the same shape as a square-root raised cosine pulse with 100 percent excess bandwidth, but it is stretched linearly in frequency in order that the maximum bandwidth be B_t/T and the amplitude is scaled to maintain a constant transmitter power. If the pulse $P_{srw}(f; B_t)$ were used for $P_{t,0}(f)$ in Fig. 2.1, then the power at the output of the transmitter filter in a 1 Ω resistor would be 0.5 mW, regardless of the choice for B_t:

$$\frac{1}{T}\int_{-\frac{B_t}{T}}^{\frac{B_t}{T}} |P_{srw}(f; B_t)|^2 \, df = 0.5\,\text{mW}. \tag{5.7}$$

The square of the magnitude response of $P_{srw}(f; B_t)$ is shown in Fig. 5.1 for various values of transmitter bandwidth. Notice that for the bandwidths where $B_t \in \{0.5, 0.75, 1.0\}$ $P_{srw}(f)$ behaves like a square-root raised cosine pulse. For the bandwidths where $B_t \in \{1.0, 1.25, 1.5\}$ $P_{srw}(f)$ behaves like a square-root raised cosine pulse with 100 percent excess bandwidth that has been stretched linearly in frequency with its amplitude scaled to maintain a constant transmitted power. However, $P_{srw}(f; B_t)$ does not have all the desirable properties of different baseband carrier frequencies for the evaluations in this chapter. Therefore for the transmitters shown or implied in Figs. 2.1, 2.2, and 2.4 define:

$$\begin{aligned} P_{t,i}(f) &= \mathcal{F}_{cc}[\, p_{t,i}(t)\,] \\ &= P_{srw}\left(f - m_A[i]\frac{C}{T}\,;\, B_t \right) \end{aligned} \tag{5.8}$$

where $m_A[i]$ is a mapping from the number of the interferer to its respective carrier frequency as shown in Table 5.1, and C is the carrier spacing relative to the symbol rate. Based on (3.21), (3.24) and (5.4), the number of ACI signals at the input to the equalizer is:

$$L = 2\,\text{int}\left(\frac{B_t + B_r}{C}\right). \tag{5.9}$$

Note also that L is even and greater than or equal to zero.

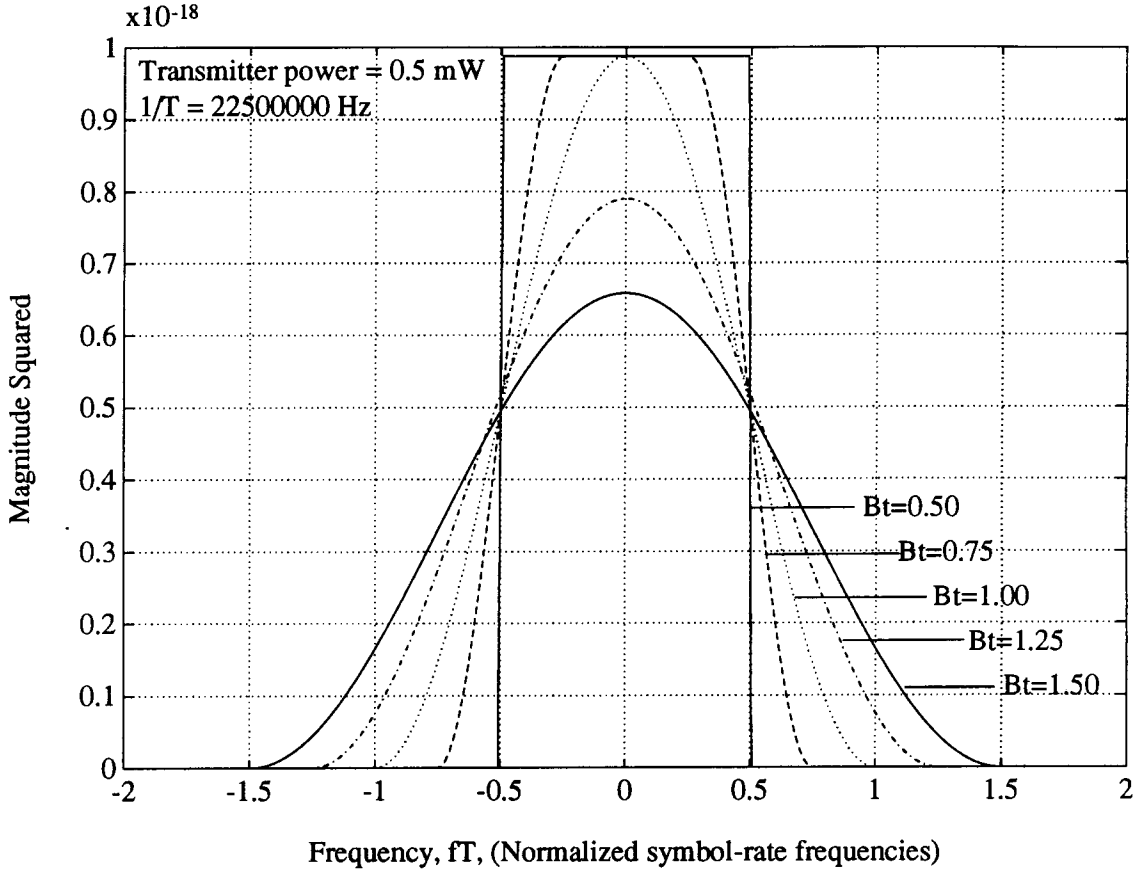

Figure 5.1 Magnitude response squared of the modified square-root raised cosine pulse, $|P_{srw}(f)|^2$, for various relative bandwidths.

Table 5.1 Mapping from the adjacent-channel interferer number to the carrier frequency number.

Interferer Number	Carrier Frequency Number
i	$m_A[i]$
L	$-\frac{L}{2}$
$\vdots$	$\vdots$
4	-2
2	-1
0	0
1	1
3	2
$\vdots$	$\vdots$
$L-1$	$\frac{L}{2}$

The channel and co-channels that have been used are ideal. There is no fading. The frequency responses of the channel and co-channels are:

$$C_i(f) \;=\; e^{-j2\pi(\mathrm{D}_i/\mathrm{T})(f-m_A[i])} \quad ; \quad i \in \mathsf{L}_0 \tag{5.10}$$

where the phase shifts (delays) of the interfering signals relative to the symbol period are denoted by $\{\mathrm{D}_i \mid i \in \mathsf{L}_1\}$ ($\{\mathrm{D}_i \in [0,1] \mid i \in \mathsf{L}_1\}$). Unless stated otherwise, for the evaluations to follow $\{\mathrm{D}_i \mid i \in \mathsf{L}_1\}$ were set to zero; this corresponds to one arbitrary choice for the values.

Fig. 3.3 introduces the concept of the receiver bandwidth. All signals are zero outside the frequencies $[-\mathrm{B_r/T}, \mathrm{B_r/T}]$. If the ACI were stationary noise, the optimal equalizer bandwidth would be the same as that of the signal carrying the data of interest. By contrast, in the presence of cyclostationary ACI, the optimal equalizer bandwidth could potentially be infinite. Therefore, a bandlimiting receiver filter is introduced, not only to limit the noise to the equalizer, but also to limit the complexity of the equalizer. By varying the bandwidth of the receiver filter, it permits analysis of the trade-off between performance and equalizer complexity. A difficulty is that the system model described in Chapter 2 does not have a fixed-bandwidth front-end receiver filter. To put in such a filter in the model, the receiver filter will actually be placed in the frequency responses of the combined channel and combined co-channels. That is, the receiver filter occurs before the white noise is added and this means that the equalizer is conceptually responsible for all the appropriate filtering. This *conceptual* placement of the receiver filter before the noise would result in more noise and pessimistic results when the receiver filter has magnitude less than one. If the magnitude response of the receiver filter is one and an ideal low-pass filter were used, then the placement of the receiver filter is irrelevant. However, if the magnitude response of the receiver filter is less than one then the conceptual placement of the receiver filter with the combined channel and combined co-channels means that the performance of a real system would be better than the conceptual system.

The frequency response of the receiver filter is:

$$P_r(f) = \begin{cases} \frac{1}{\sqrt{T}} P_{sr}(f\,;\,2B_r - 1) & , \frac{1}{2} \le B_r \le 1 \\ \frac{1}{\sqrt{T}} P_{sr}\left(\frac{f}{B_r}\,;\,1\right) & , 1 < B_r \end{cases} . \tag{5.11}$$

It is based on the same pulse that was used for the transmitter, except the magnitude of the receiver frequency response is always unity at zero frequency. The reason for not using an ideal low-pass filter is that it does not have very good time-domain properties [86].

Thus the frequency response of the combined channel is:

$$\Phi_0(f) = P_{t,0}(f)\, C_0(f)\, P_r(f) \tag{5.12}$$

and the frequency responses of the combined co-channels are:

$$\Phi_i(f) = P_{t,i}(f)\, C_i(f)\, P_r(f) \quad ; \quad i \in \mathsf{L}_1. \tag{5.13}$$

5.2.1 Properties

Fig. 5.2 shows the power spectral density of the signals at the input to the equalizer for two cases. The only difference between the two cases is that Fig. 5.2a is for the receiver bandwidth $B_r = 1.0$ symbol frequency and Fig. 5.2b is for the receiver bandwidth $B_r = 3.0$ symbol frequencies. Hence in Fig. 5.2b more of the spectrum is let into the equalizer. The effect of the previously mentioned issue of the placement of the receiver filter with the combined channel and combined co-channel can also be seen. This effect is the flat noise power spectral density at the input to the equalizer. If the receiver filter had been placed after the noise, then the noise level would approach zero near the edge of the receiver filter bandwidth. However, in more realistic receiver models such diminishing amounts of noise near the band edges are reasonable.

In, or implied in, Figs. 2.1, 2.2, 2.4, and 5.2, are the signal which carries the data of interest $s(t)$, the ACI without noise $\mu_{ci}(t)$, and the noise $n(t)$. Over the entire spectrum, the powers of three signals are denoted by P_S from (2.13), P_I from (2.27), and P_N from

[a]

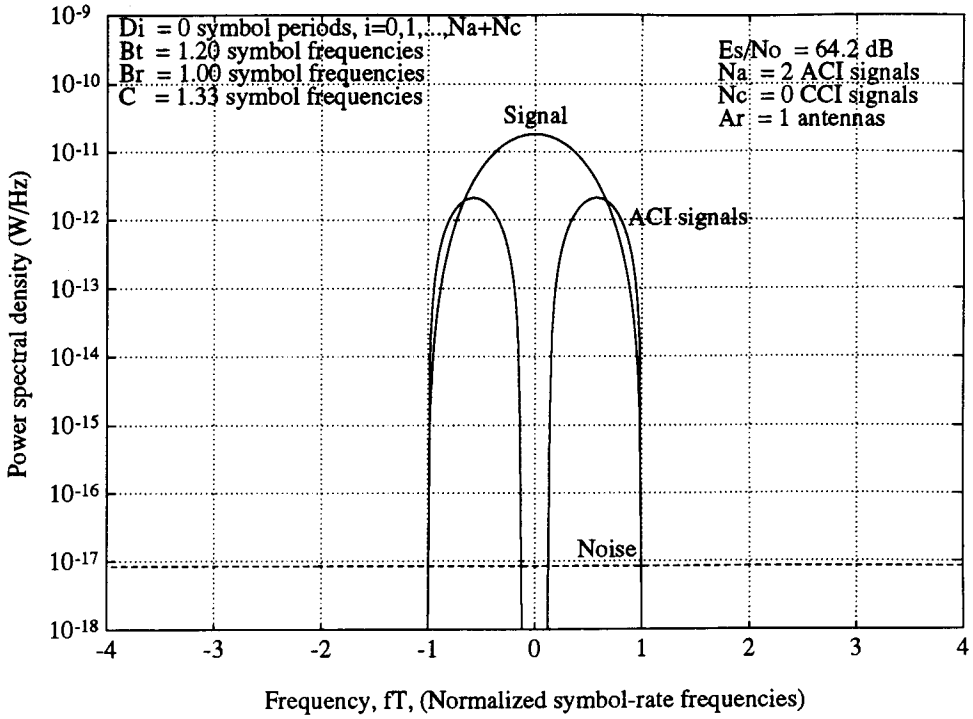

[b]

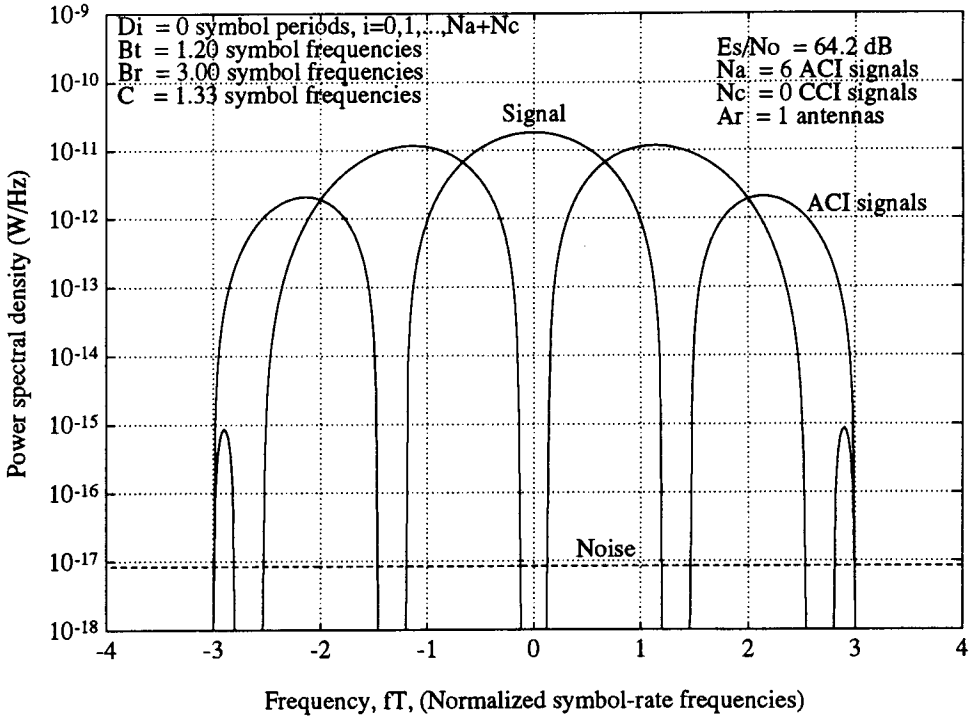

Figure 5.2 Power spectral densities at the input to the equalizer — two receiver bandwidth conditions

(2.25), respectively. However, the powers of interest were those obtained from the part of the spectrum which directly *overlaps* the frequencies of the signal carrying the data of interest. Therefore define the noise bandwidth, B_n, to be:

$$B_n = \min(B_t , B_r). \tag{5.14}$$

The power of the signal carrying the data of interest which overlaps with itself is:

$$P_{So} = \int_{-B_n}^{B_n} \frac{1}{T} |\Phi_0(f)|^2 \, df \tag{5.15}$$

and is the same as P_S from (2.13). The power of the ACI signals which overlap with the signal carrying the data of interest is:

$$P_{Io} = \int_{-B_n}^{B_n} \sum_{i=1}^{L} \frac{1}{T} |\Phi_i(f)|^2 \, df. \tag{5.16}$$

The power of the noise which overlaps with the signal carrying the data of interest is:

$$P_{No} = P_N. \tag{5.17}$$

P_N can be calculated from (2.25). The three powers P_{So}, P_{Io}, and P_{No}, were calculated for increasing transmitter bandwidth for the parameters shown in the two cases in Fig. 5.3. The only difference between the two cases is that Fig. 5.3a is for the receiver bandwidth $B_r = 1.0$ symbol frequency and Fig. 5.3b is for the receiver bandwidth $B_r = 3.0$ symbol frequencies. What is important to note is that the ratio of the powers of the signal carrying the data of interest to the ACI becomes much smaller as the transmitter bandwidth increases. An example of a point where the power ratio is small is when $B_t = 1.5$ symbol frequencies in Fig. 5.3b. The power ratio is -0.06 dB.

Fig. 5.4 is a two dimensional representation of a three dimensional surface. It is a contour plot of the power ratio:

$$10 \log_{10} \left(\frac{P_S}{P_I + P_N} \right) \tag{5.18}$$

[a]

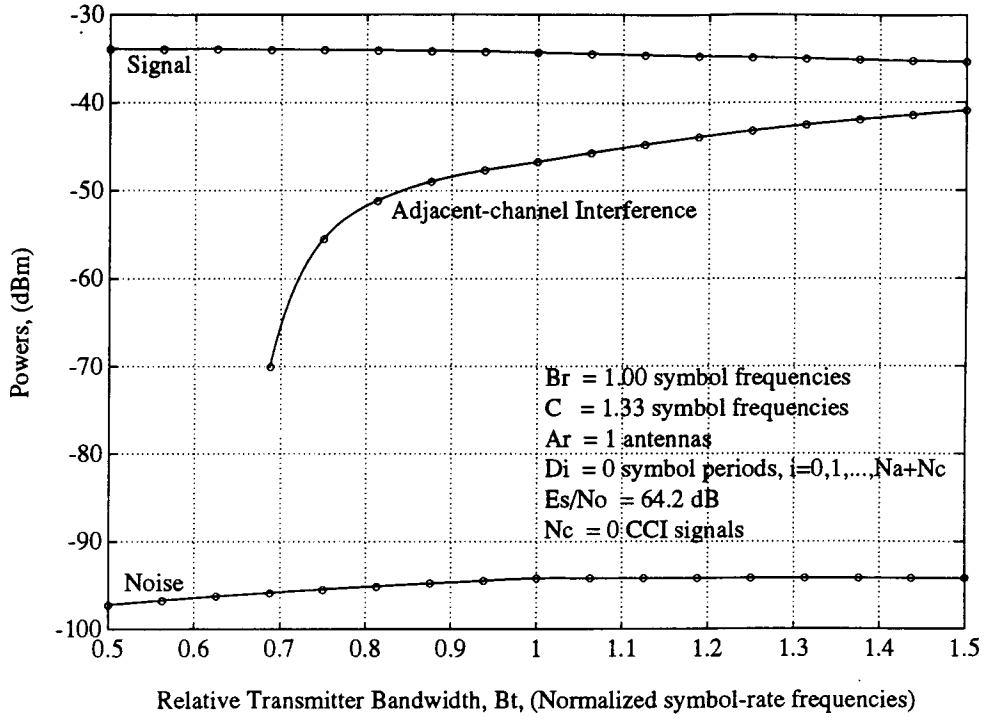

[b]

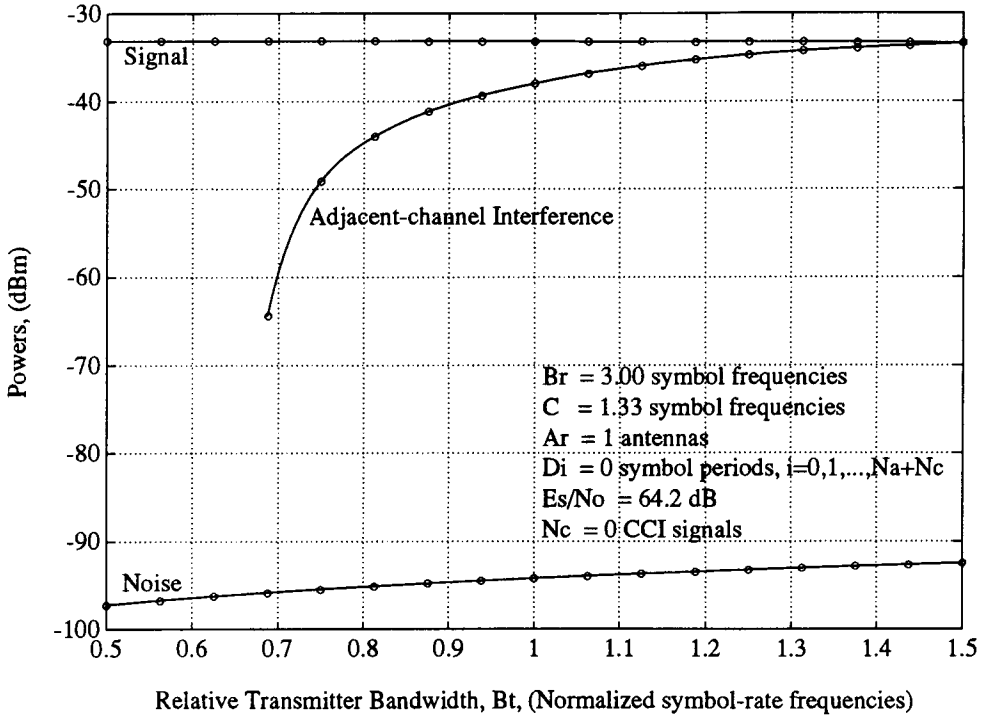

Figure 5.3 Powers of the signal, $s(t)$, the adjacent-channel interference, $\mu_{ci}(t)$, and the bandlimited noise — two receiver bandwidth conditions

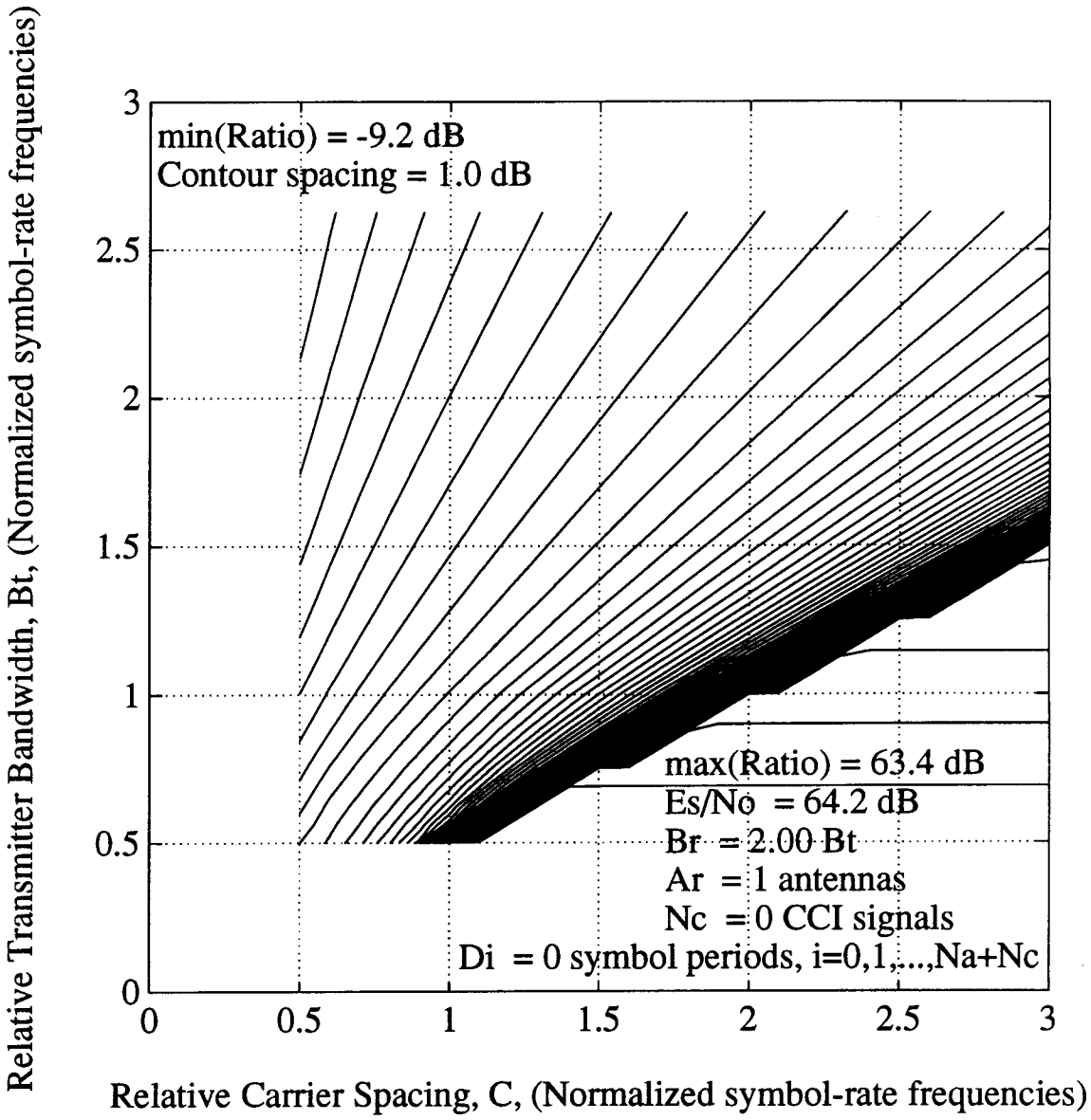

Figure 5.4 Power ratio of signal to interference-plus-noise at equalizer input versus transmitter bandwidth and carrier spacing

where the horizontal axis is carrier spacing, C, the vertical axis is transmitter bandwidth, B_t, and the noise bandwidth is equal to the receiver bandwidth. Interpret the figure as follows. The maximum value of the power ratio is 63.4 dB in lower right corner where $(C, B_t) = (3.0, 0.5)$. The minimum power ratio is -9.2 dB in the upper left where $(C, B_t) = (0.5, 2.625)$. Contour lines of constant power ratio are shown in the figure and the spacing between the lines is 1.0 dB. Thus a contour line where the power ratio is 62.4 dB occurs on the line from $(1.375, 0.7)$ to $(3.0, 0.7)$. Operating points in the lower right corner correspond to conditions where the ACI signals do not overlap with the signal carrying the data of interest. Note also that the lines between the transition from high to low power ratios should be smooth but instead they are jagged. This is due to the coarse granularity of the calculations. The number of points calculated were 910, 35 vertically by 26 horizontally.

5.3 Performance Evaluation

The goal of the performance evaluations of this section are to demonstrate the performance gains that are possible by having equalizers exploit the cyclostationarity of the ACI. Just as in Section 4.3, the performance gains that are of greater interest are the MMSE of linear and decision-feedback equalizers *relative* to the situation where the cyclostationary interference is treated as stationary noise. There is less emphasis in this section on the absolute system performance. The condition that has the largest effect on the gains is the equalizer's bandwidth relative to the symbol rate. It is shown in this section how sufficiently wide equalizer bandwidths provide opportunities for equalizers to exploit the cyclostationarity of the ACI. The results of MMSE calculations are compared to the predictions of the existence of a generalized zero-forcing linear equalizer from Section 3.2. It is also shown how equalizers are able to extract the signal carrying the data of interest and suppress the ACI even under conditions of complete spectral overlap. The four MMSE expressions that are calculated in this section are shown in Table 3.1. Both linear and decision-feedback equalizers are considered in the presence of cyclostationary interference and stationary noise. The frequency responses

of the combined channel and combined co-channels are given in (5.12) and (5.13), respectively. The relevant MMSE expressions in Table 3.1 have been evaluated by numerical integration to within a relative error of 10^{-3}. That which remains in this section are the results and interpretation of MMSE calculations under various conditions of the following parameters: the bandwidth of the transmitter pulses relative to the symbol rate B_t, the bandwidth of the equalizer relative to the symbol rate B_r, the carrier spacing relative to the symbol rate C, and the relative phase shift of the ACI signals $\{D_i \mid i \in L_1\}$. The number of interferers, L, is determined from the varied parameters. The following parameter is fixed:

$$D_0 = 0 \text{ symbol periods} \tag{5.19}$$

as well as the parameters indicated in (5.2), (5.3), and (5.4). Instead of showing the values of MMSE directly, the following expression is shown:

$$10 \log_{10} (\text{MMSE}). \tag{5.20}$$

Fig. 5.5 shows $10\log_{10}(\text{MMSE})$ for the four situations of two equalizers and two interference types versus the transmitter bandwidth B_t. Fig. 5.5a is for the receiver bandwidth $B_r = 1.0$ symbol frequency and Fig. 5.5b is for the receiver bandwidth $B_r = 3.0$ symbol frequencies. Note also that the parameters used in Fig. 5.5 are identical to those in Fig. 5.3. Compare Fig. 5.5a to Fig. 5.3a. As the transmitter bandwidth increases, there is an increasing amount of ACI overlapping the signal carrying the data of interest. The ACI power increases and the MMSE gradually increases. The cyclostationary interference and stationary noise situations give the same MMSE, but the decision-feedback equalizer has a lower MMSE than the linear equalizer. Compare Fig. 5.5b to Fig. 5.3b. Again the ACI power increases, but the MMSE for the cyclostationary interference cases are significantly lower than the stationary noise cases for transmitter bandwidths greater than 0.9 symbol frequencies. As stated earlier, when $B_t = 1.5$ symbol frequencies, the power ratio between the signal carrying the

[a]

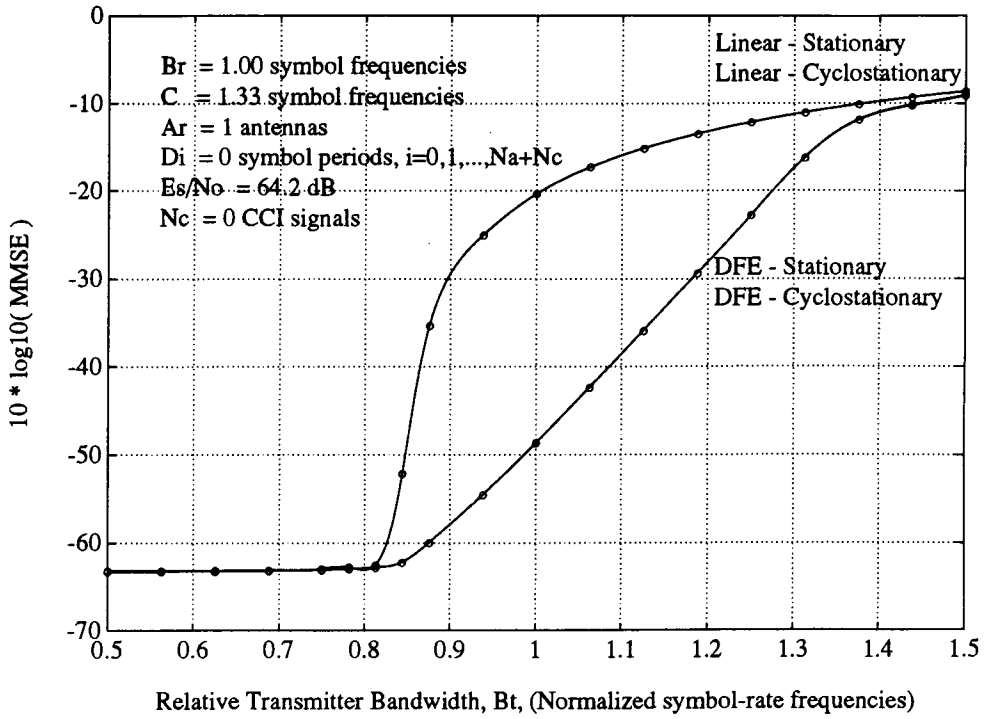

[b]

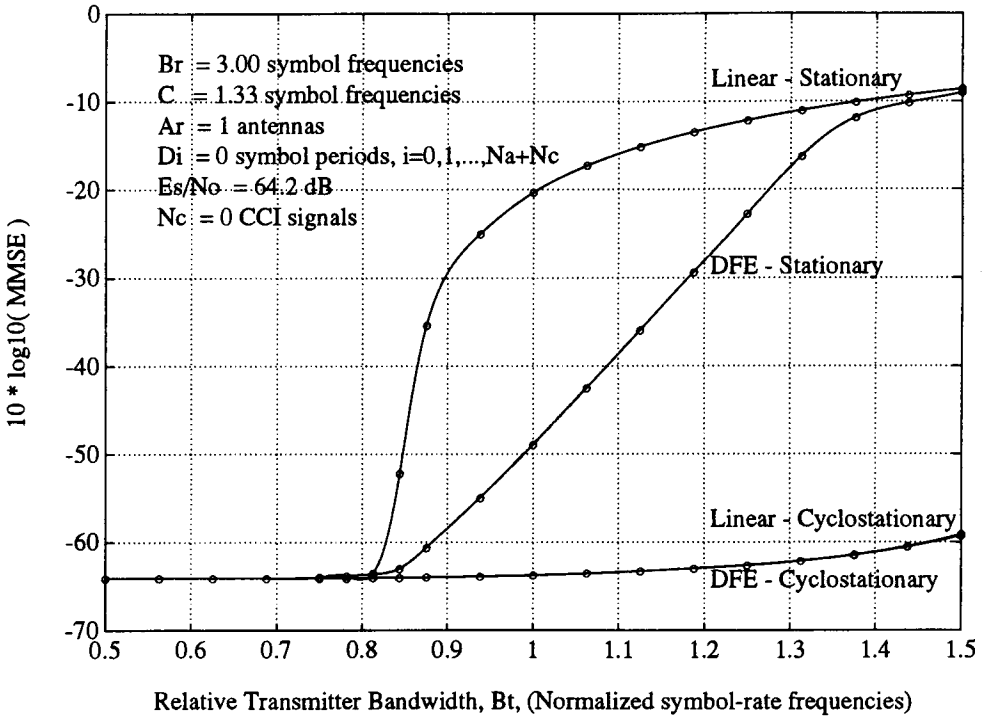

Figure 5.5 Linear and decision-feedback equalizer MMSE versus relative transmitter bandwidth — two receiver bandwidth conditions

data of interest and the ACI is -0.06 dB. But from Fig. 5.5b, the MMSE values for the cyclostationary interference are around -59 dB and for stationary noise they are around -9 dB. Therefore, for these idealistic situations the equalizers are able to suppress 50 dB of ACI by exploiting its cyclostationarity. This example was intended to demonstrate the extent to which equalizers are able to exploit the cyclostationarity of the interference. Whether or not there is any value in having systems operate at relatively wide transmitter bandwidths will be discussed in Section 5.4.

The same type of MMSE calculations of Fig. 5.5 were repeated in greater detail. The results of these calculations are shown in contour plots. For $B_r = B_t$ symbol frequencies, Figs. 5.6, 5.7, 5.8, and 5.9 show MMSE contours for a linear equalizer in stationary noise, a linear equalizer in cyclostationary interference, a decision-feedback equalizer in stationary noise, and a decision-feedback equalizer in cyclostationary interference, respectively. Note that the same granularity behavior exists that was present in Fig. 5.4. The number of points calculated were 1066, 41 vertically by 26 horizontally. The interpretation of the figures is the same as the previous contour plot in Fig. 5.4, except the maximum value of the MMSE occurs in the upper left corner and the minimum value of the MMSE occurs in the lower right corner. In Figs. 5.7 and 5.9 there are some peaks around $(C, B_t) = (1.75, 2.75)$; this effect will be described later. Comparing the stationary noise and cyclostationary interference curves, the equalizers are able to provide interference suppression for operating points in the upper right corners of the figures. Comparing the linear equalizer and decision-feedback equalizer curves, the interference suppression effects are similar but the decision-feedback equalizer performs better. The unusual shape of the linear equalizer curve in Fig. 5.7 was predicted in the $B_r = B_t$ curve in Fig. 3.5 and an explanation of the behavior can be found by the latter figure.

Figs. 5.10 and 5.11 are based on an equalizer bandwidth of $B_r = 2B_t$ symbol frequencies; they give the MMSE performance of linear and decision-feedback equalizers in cyclostationary interference, respectively. Curves for the stationary noise cases are not shown since they are not very much different than cases for $B_r = B_t$ that were

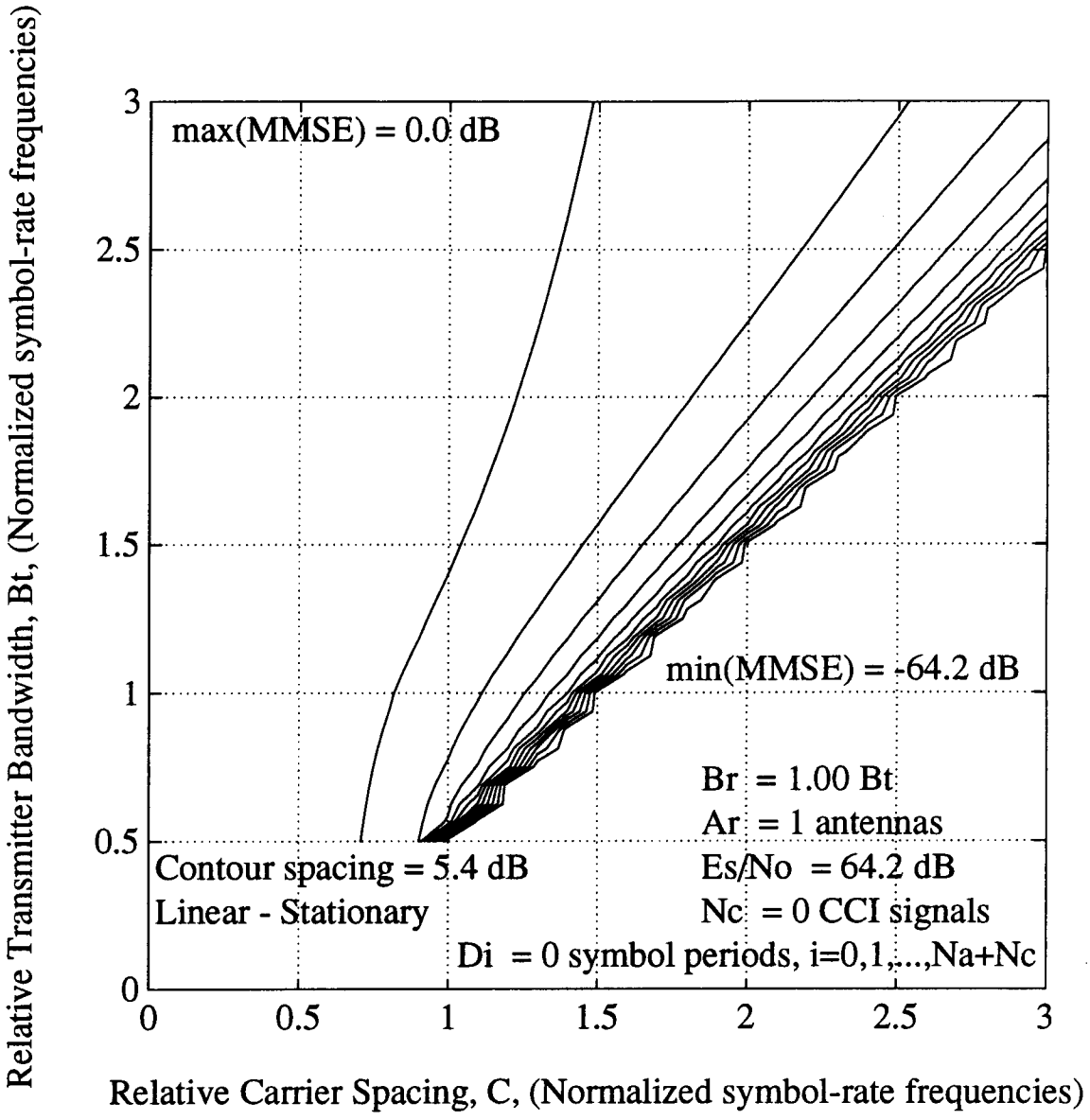

Figure 5.6 MMSE versus transmitter bandwidth and carrier spacing — linear equalizer — stationary noise — $B_r = B_t$

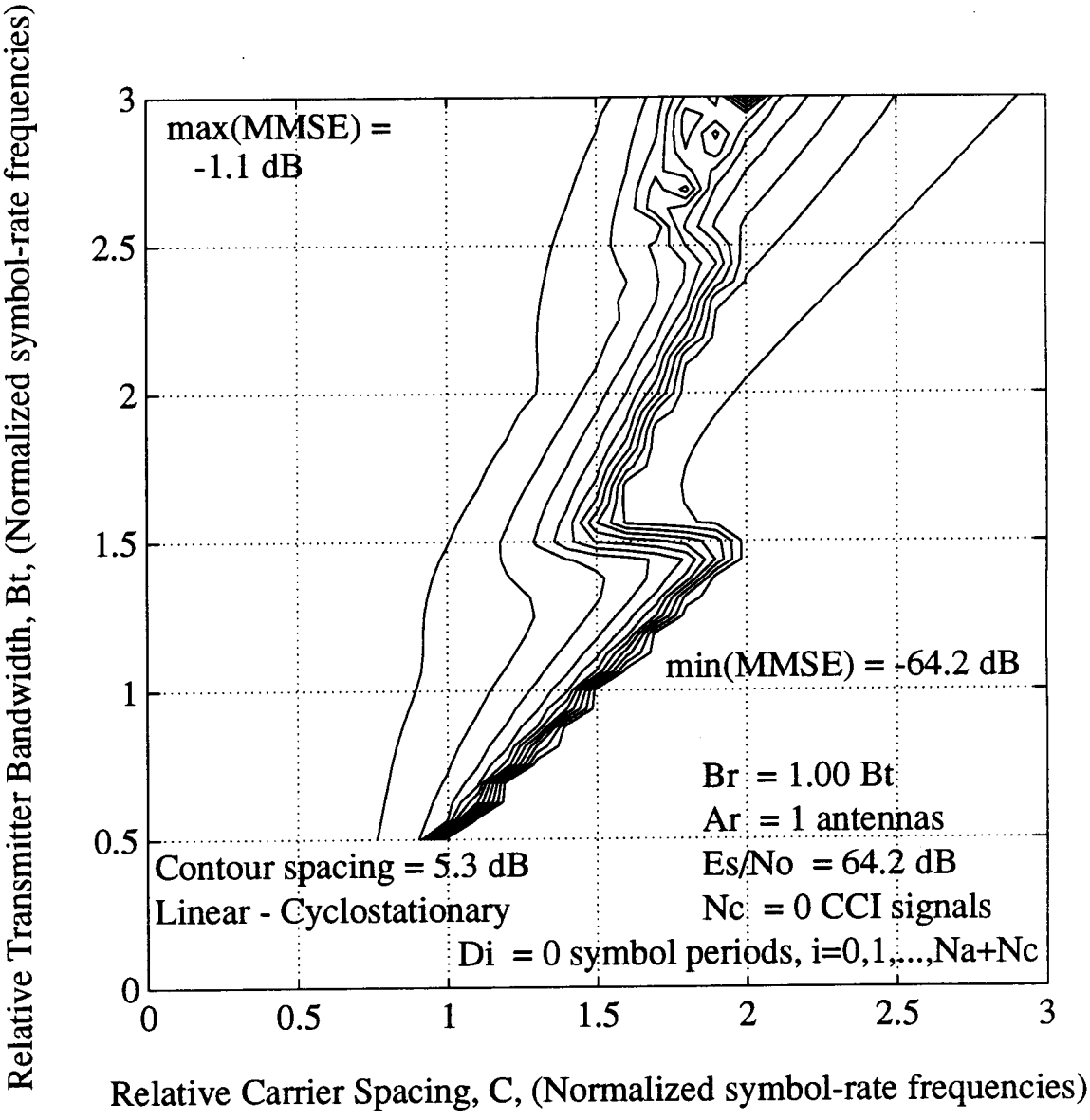

Figure 5.7 MMSE versus transmitter bandwidth and carrier spacing — linear equalizer — cyclostationary interference — $B_r = B_t$

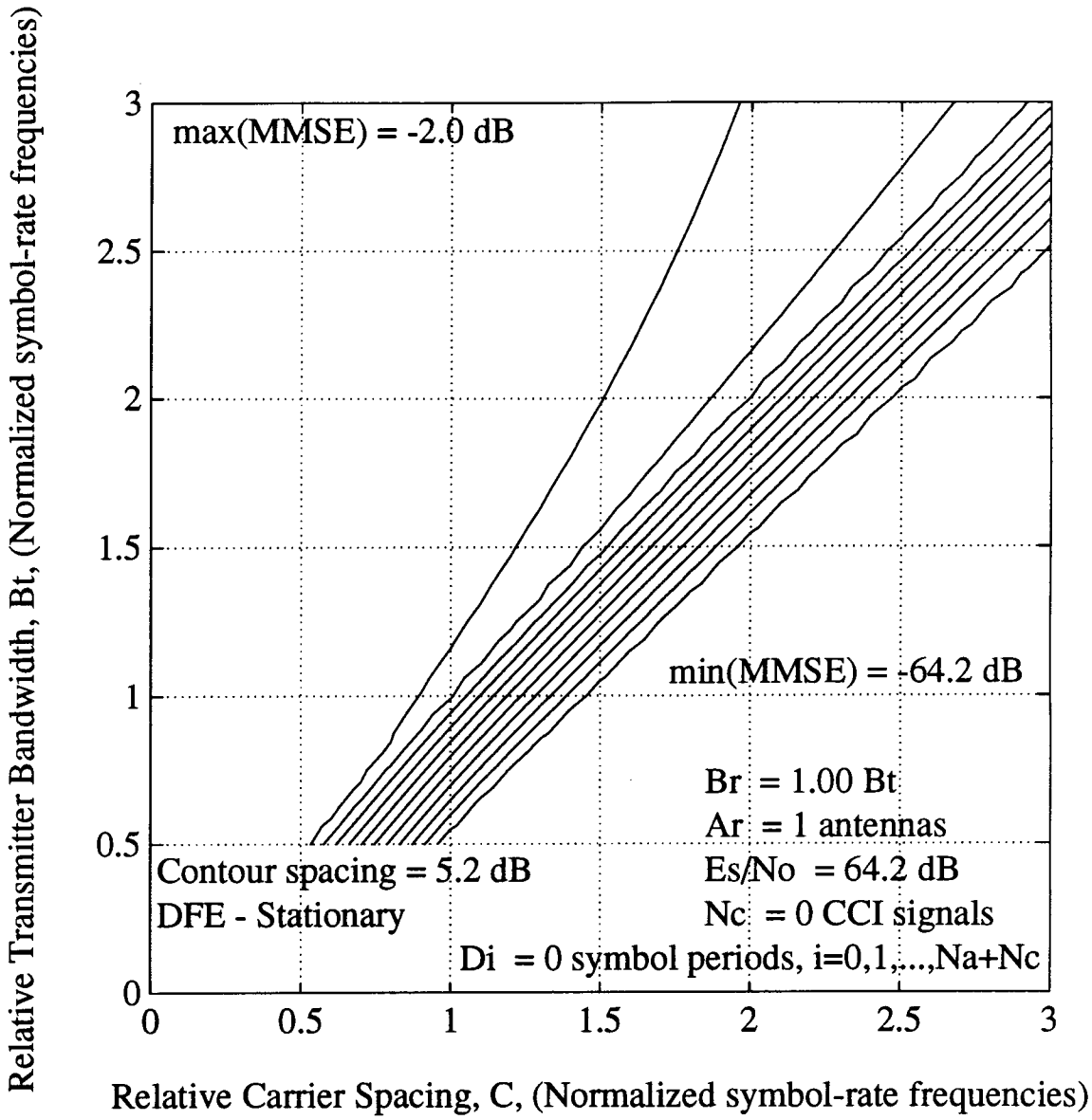

Figure 5.8 MMSE versus transmitter bandwidth and carrier spacing — decision-feedback equalizer — stationary noise — $B_r = B_t$

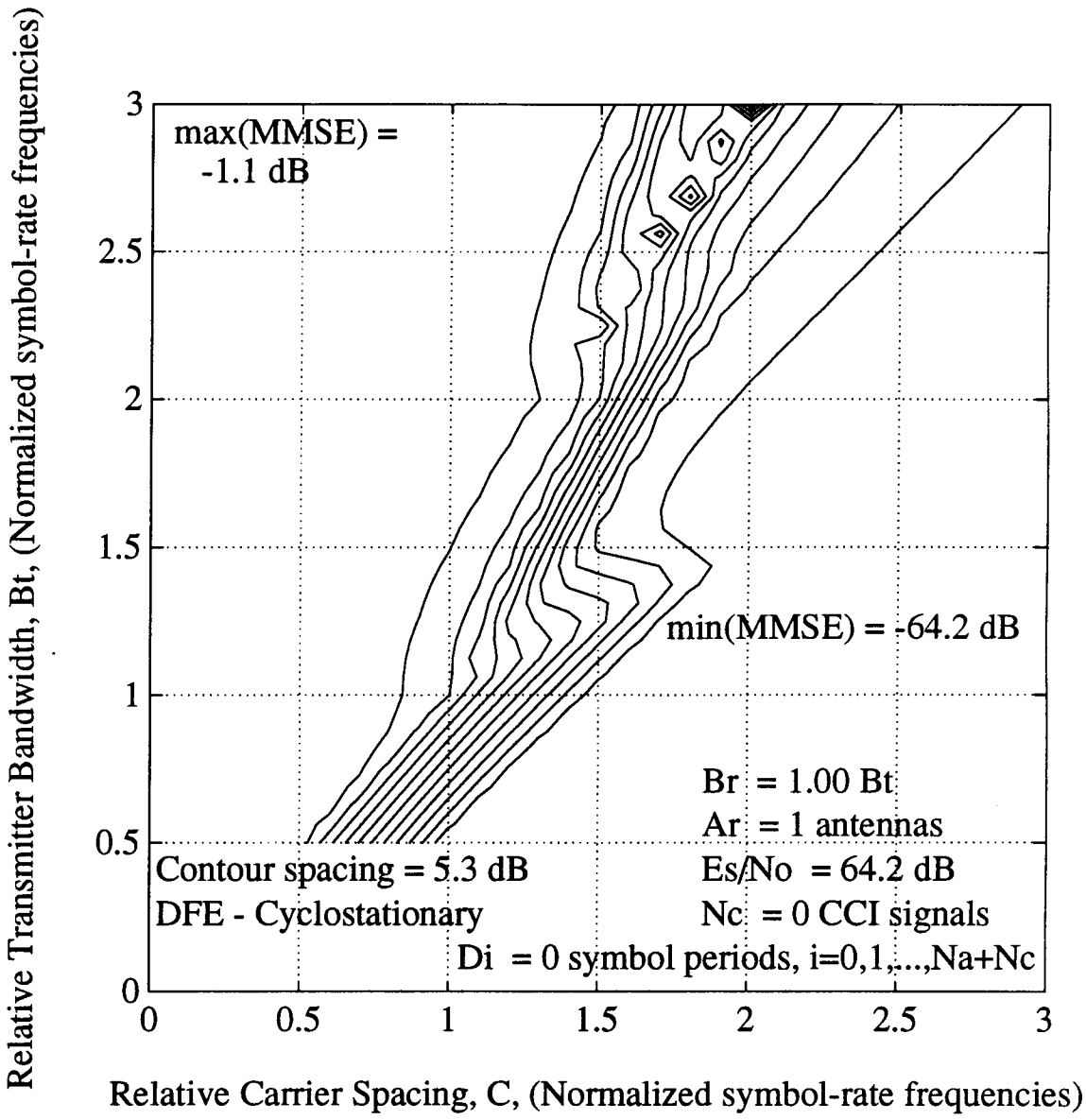

Figure 5.9 MMSE versus transmitter bandwidth and carrier spacing — decision-feedback equalizer — cyclostationary interference — $B_r = B_t$

shown in Figs. 5.6 and 5.8. Compare Fig. 5.7 to Fig. 5.10 as well as Fig. 5.9 to Fig. 5.11. The line of transitions from low-MMSE operating points to high-MMSE operating points has moved to the left.

Figs. 5.12 and 5.13 are based on an equalizer bandwidth of $B_r = 3B_t$ symbol frequencies; they give the MMSE performance of linear and decision-feedback equalizers in cyclostationary interference, respectively. Curves for the stationary noise cases are not shown since they are not very much different than cases for $B_r = B_t$ that were shown in Figs. 5.6 and 5.8. Compare Fig. 5.7 to Fig. 5.12 as well as Fig. 5.9 to Fig. 5.13. The line of transitions from low-MMSE operating points to high-MMSE operating points has moved to the left. But the changes are reaching diminishing returns with increasing equalizer bandwidths.

Fig. 5.14 contains perspective plots of Fig. 5.13 taken from four different angles. This is done to clarify the shape of the MMSE surface and to show the peaks. The reference corner denoted by O marks the point $(C, B_t) = (0.5, 0.5)$. Note that the peaks occur directly on the lines in Fig. 3.4 where there are transitions into operating regions with two additional interferers. These three dimensional peaks correspond to the two dimensional peaks of the high-speed digital subscriber-lines application in Fig. 4.13.

It was desirable to understand if these peaks could be made to appear at other locations in the (C, B_t) plane. Consider the point $(C, B_t) = (1.25, 0.84375)$ in Fig. 5.11 where there are $L = 2$ ACI interferers. Recall that the MMSE at this point has been calculated for the following relative phase shifts of the interferers:

$$\begin{aligned} D_1 &= 0 \text{ symbol periods} \\ D_2 &= 0 \text{ symbol periods.} \end{aligned} \tag{5.21}$$

These MMSE calculations were repeated for the situation where the two relative phase shifts of the ACI signals $\{D_i \mid i \in L_1\}$ were varied over the 676 points of the 26 by 26 ranges:

$$\begin{aligned} D_1 &\in \{\, 0.00,\ 0.04,\ 0.08,\ \ldots\ ,\ 1.00 \,\} \\ D_2 &\in \{\, 0.00,\ 0.04,\ 0.08,\ \ldots\ ,\ 1.00 \,\}. \end{aligned} \tag{5.22}$$

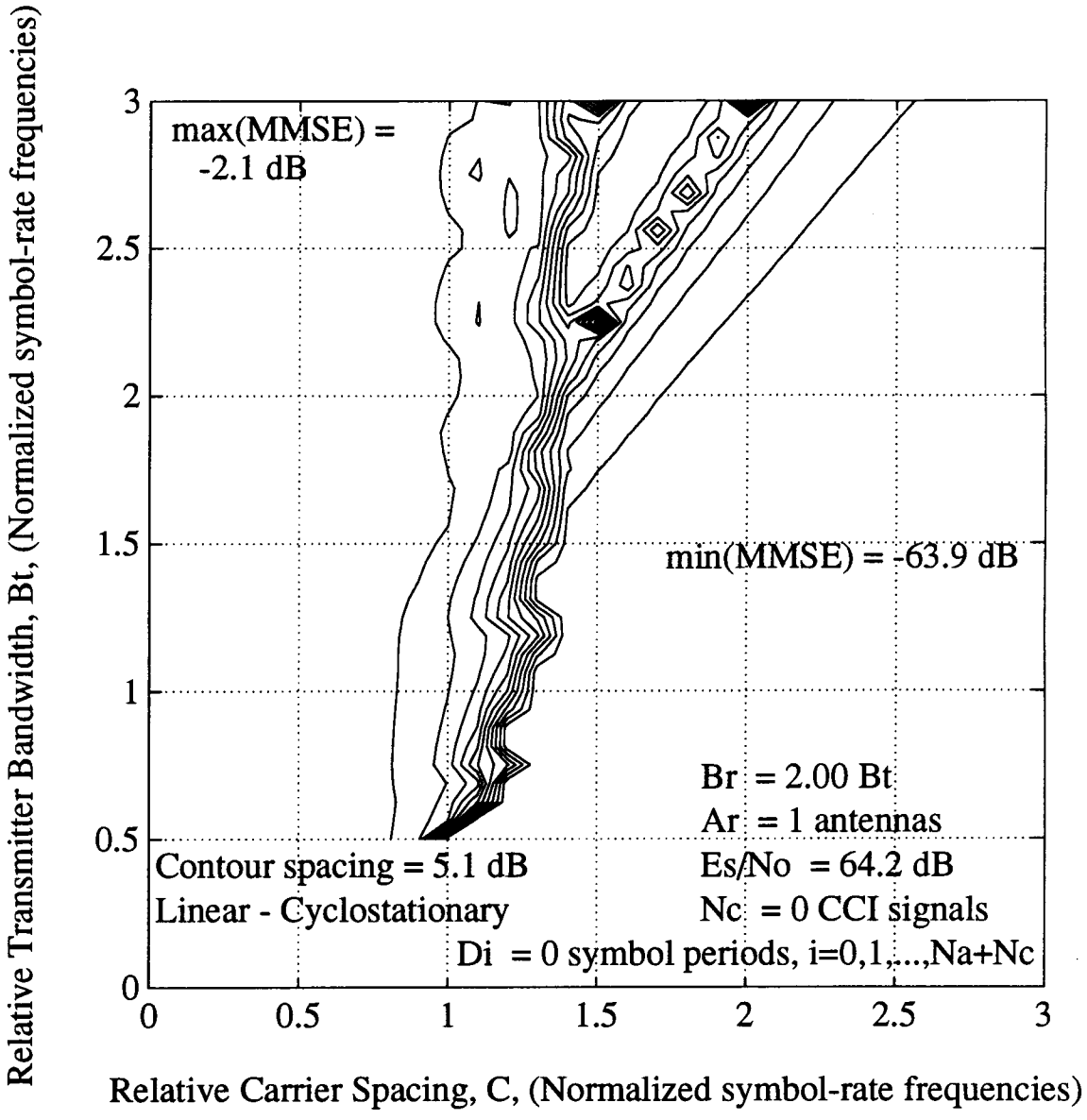

Figure 5.10 MMSE versus transmitter bandwidth and carrier spacing — linear equalizer — cyclostationary interference — $B_r = 2B_t$

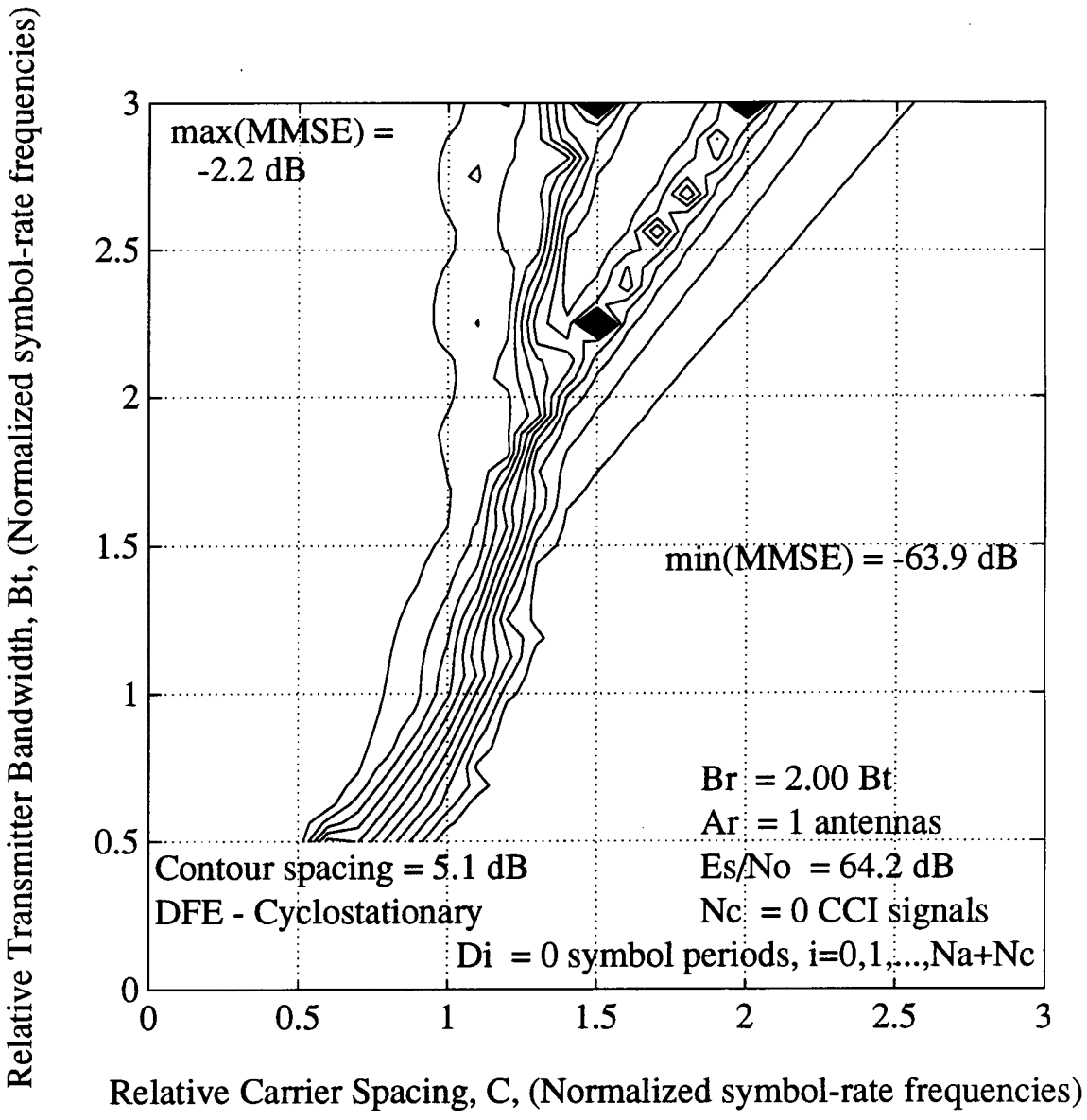

Figure 5.11 MMSE versus transmitter bandwidth and carrier spacing — decision-feedback equalizer — cyclostationary interference — $B_r = 2B_t$

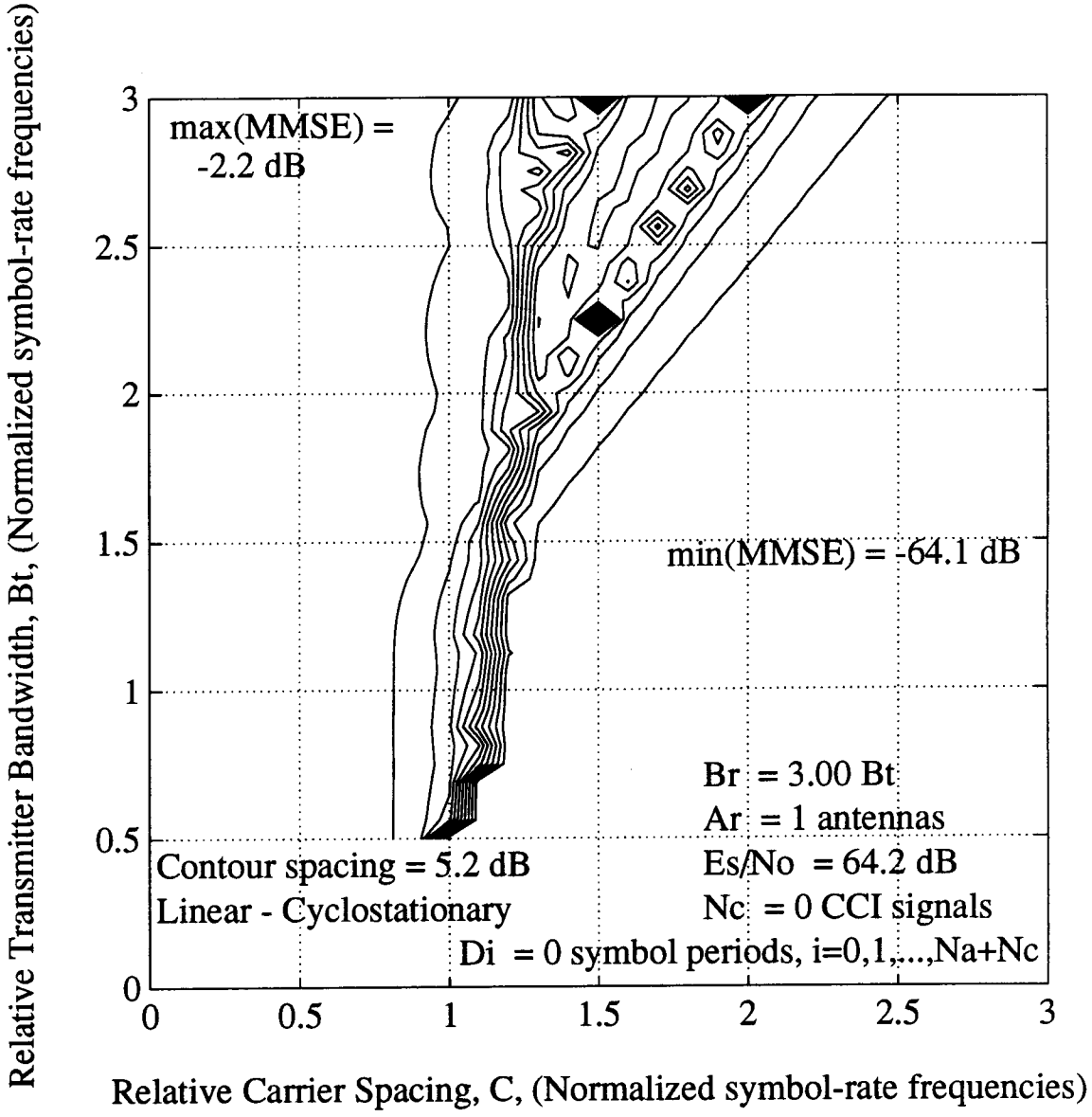

Figure 5.12 MMSE versus transmitter bandwidth and carrier spacing — linear equalizer — cyclostationary interference — $B_r = 3B_t$

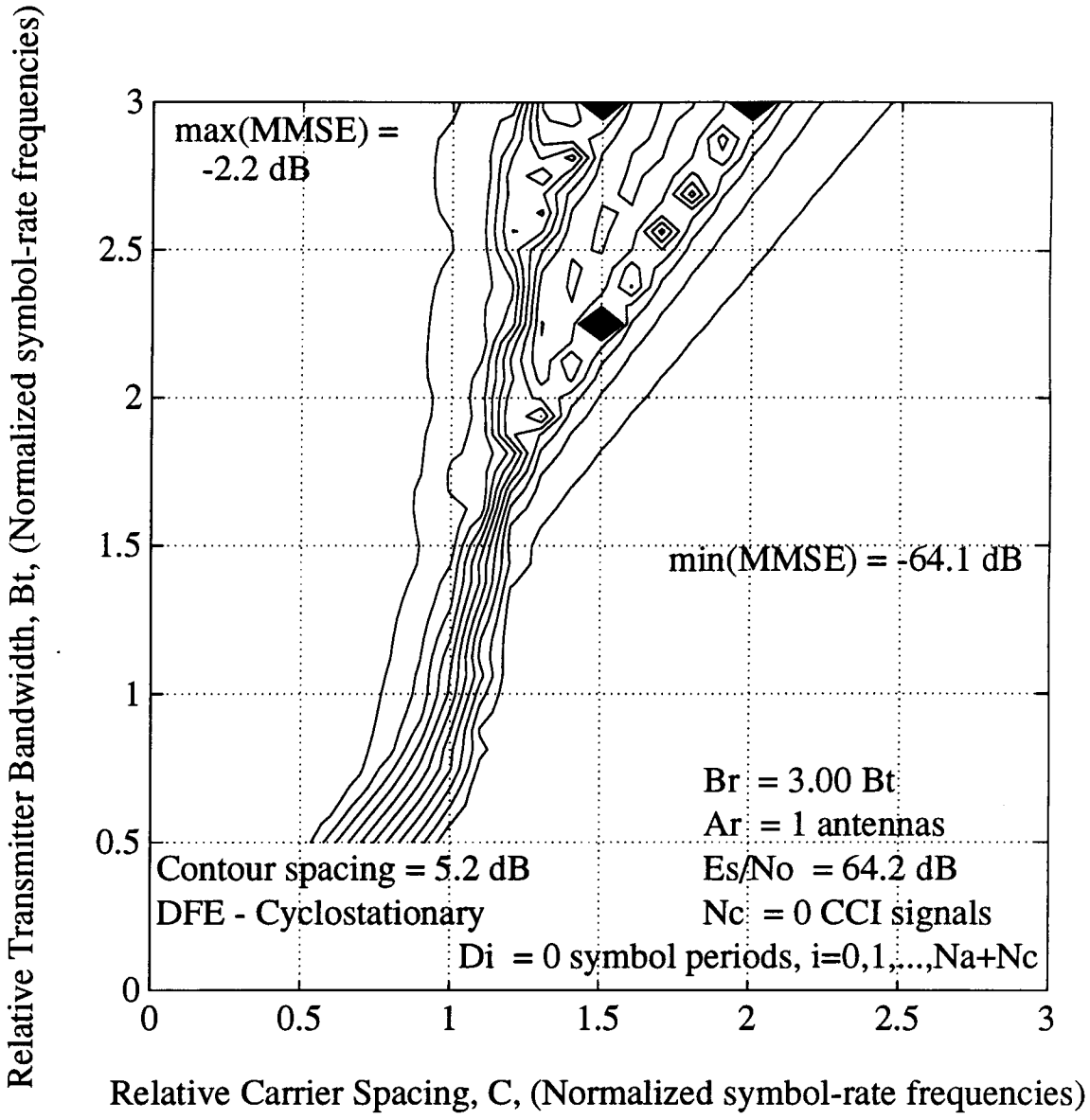

Figure 5.13 MMSE versus transmitter bandwidth and carrier spacing — decision-feedback equalizer — cyclostationary interference — $B_r = 3B_t$

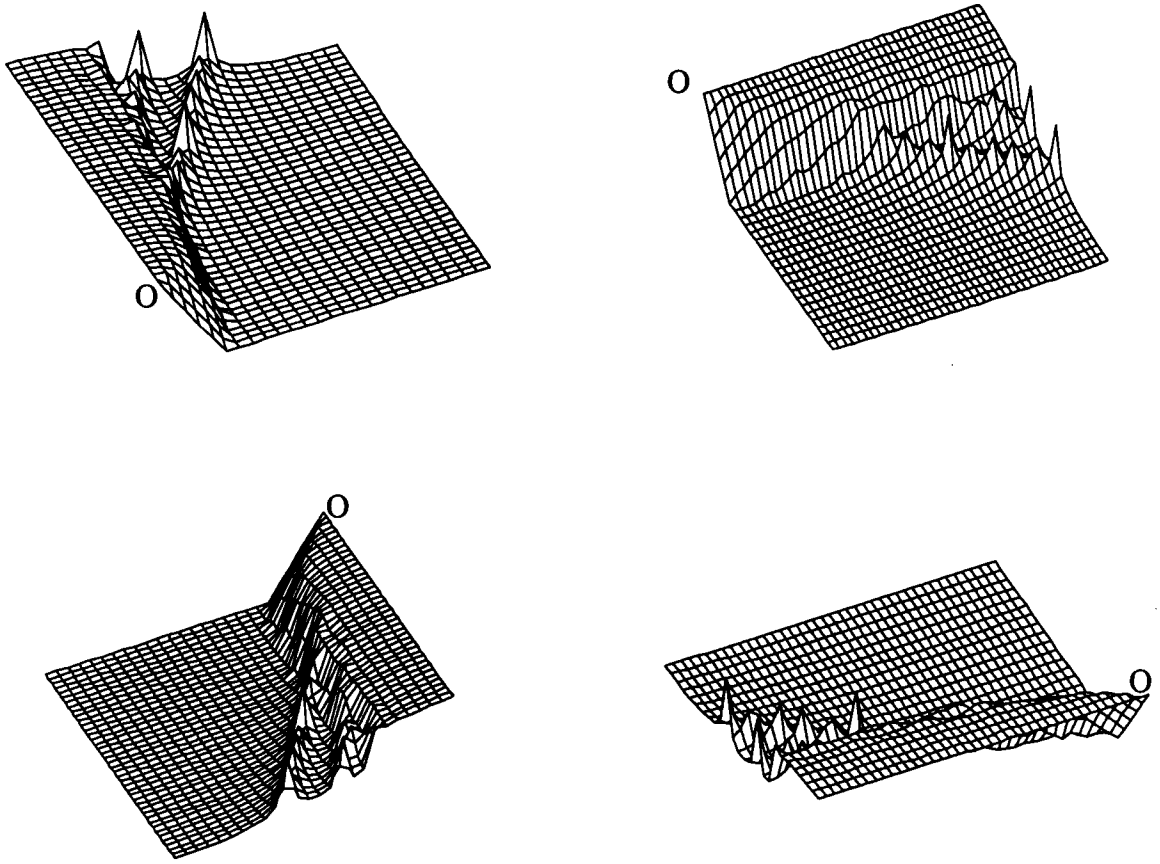

Figure 5.14 Four perspective plots for Fig. 5.13 — MMSE versus transmitter bandwidth and carrier spacing - decision-feedback equalizer - cyclostationary interference - $B_r = 3B_t$ {O denotes the point $(C, B_t) = (0.5, 0.5)$}

It was found that the MMSE of a decision-feedback equalizer in cyclostationary interference always remained around -63 dB. Although this is not enough to be conclusive about the effects of $\{D_i \mid i \in L_1\}$, these relative phase shifts do not appear to invalidate the gains available in exploiting the cyclostationarity of the ACI. In Chapter 4 it was also found that at the worst case relative phase shifts of the interference it was possible to exploit the cyclostationarity of the interference for performance improvement.

For a decision-feedback equalizer with a bandwidth $B_r = 3B_t$, the performance differences between the cyclostationary interference and stationary noise cases are plotted in Fig. 5.15. It is a plot of the gains available by exploiting the cyclostationarity of the interference. Conceptually, the surface is composed of two hills in the upper right corner, surrounded by a plain in the lower right, lower left, and upper left corners. The hills are divided by a valley which runs along a line from the point $(0, 0)$ to the point $(2, 3)$. The lowest points on the surface are at 0 dB on the plane around the hill. The highest point at 52 dB is on top of the lower right plateau. There are two points in the valley where the interference is of a nature where it is very difficult for a decision-feedback equalizer to exploit the interference cyclostationarity. At the points $(1.5, 2.25)$ and $(2, 3)$ the surface has the values 4.1 dB and 3.1 dB, respectively. The valley and the two hills do not end in the upper right corner of Fig. 5.15. This suggests that the gains continue beyond what is shown in the upper right corner of the figure.

Fig. 5.16 shows the operating points for two communication systems. The first system is Canadian digital microwave radio which has a (C, B_t) operating point at $(1.33, 0.75)$ [44, 45]. This point is denoted by the symbol o. The second system is North American digital mobile radio which has a (C, B_t) operating point at $(1.35, 0.675)$ [34, 41]. This point is denoted by the symbol $*$. These systems will be used as points of reference.

Figs. 5.17, 5.18, and 5.19 are overlays of previous figures and they represent the three equalizer bandwidth conditions $B_r = B_t$, $B_r = 2B_t$, and $B_r = 3B_t$, respectively.

Fig. 5.17 is an overlay of Figs. 3.5, 5.7, and 5.16. Fig. 5.18 is an overlay of Figs. 3.5, 5.10, and 5.16. Fig. 5.19 is an overlay of Figs. 3.5, 5.12, and 5.16.

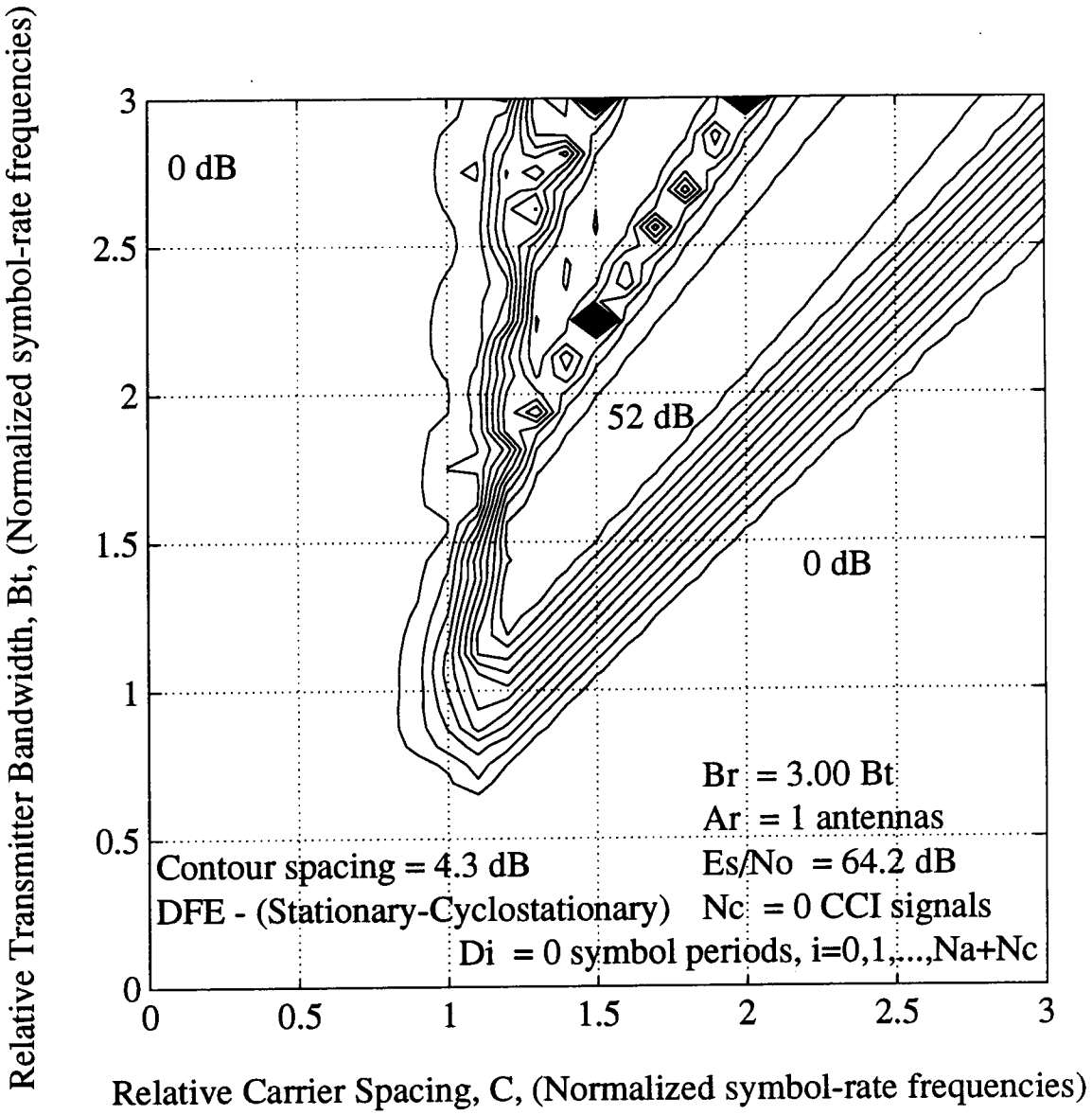

Figure 5.15 Stationary-noise MMSE less cyclostationary-interference MMSE, $10 \log_{10}(\varepsilon_{dso}) - 10 \log_{10}(\varepsilon_{dco})$**, versus transmitter bandwidth and carrier spacing — decision-feedback equalizer —** $B_r = 3B_t$

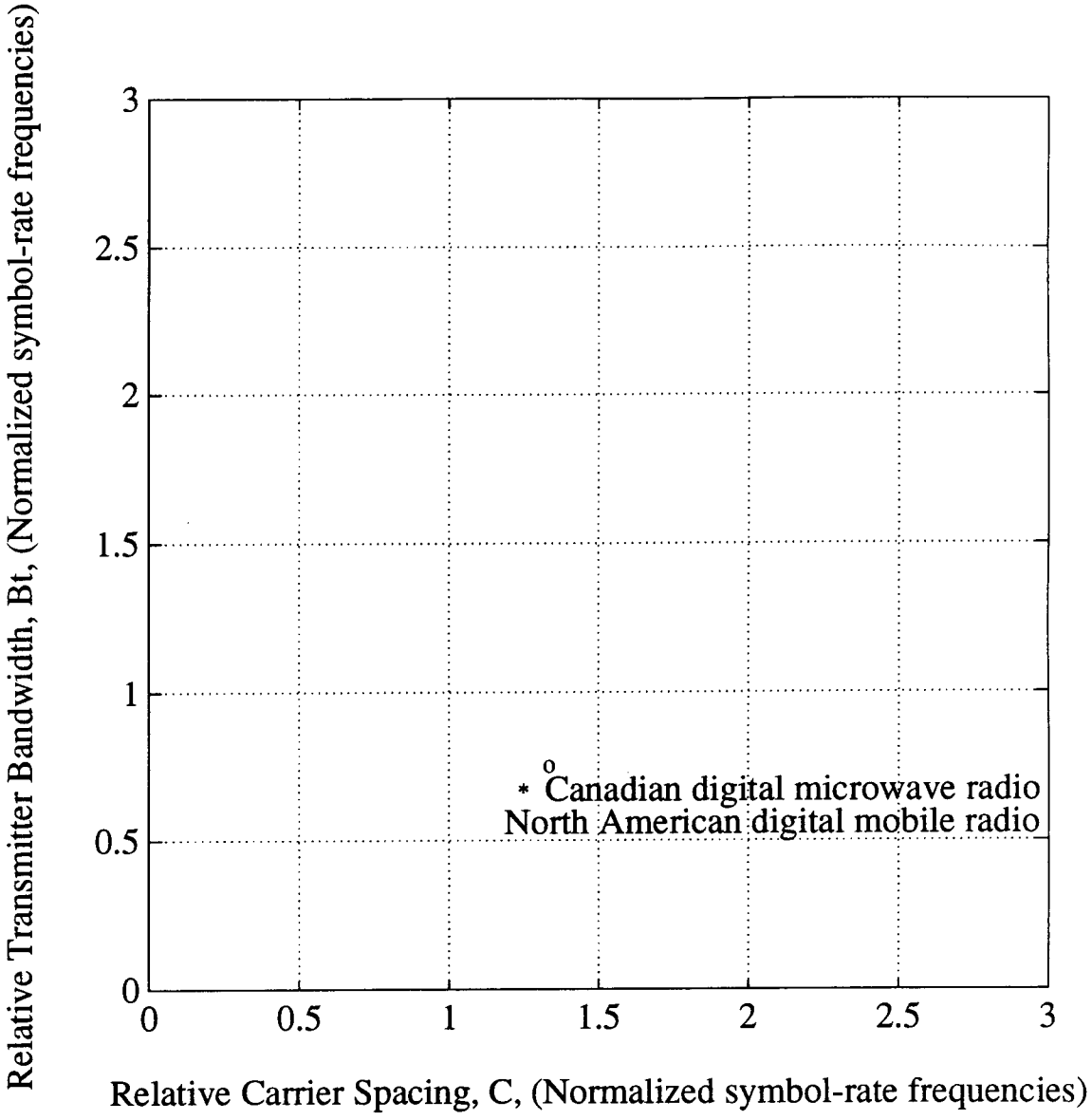

Figure 5.16 System operating points versus transmitter bandwidth and carrier spacing

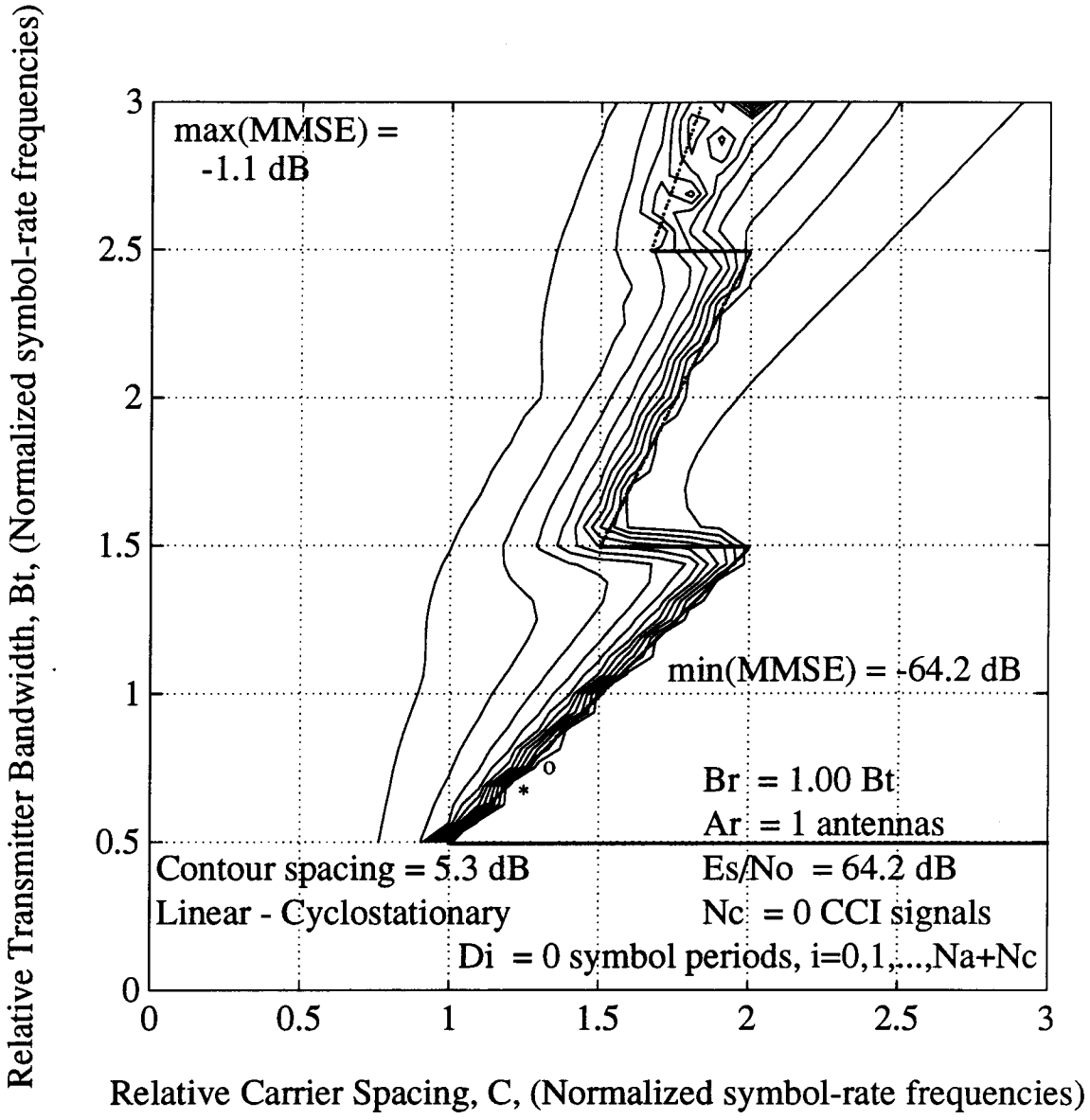

Figure 5.17 Overlay of Figs. 3.5, 5.7, and 5.16 — Existence of zero-forcing equalizer, MMSE, and system operating points versus transmitter bandwidth and carrier spacing — linear equalizer — cyclostationary interference — $B_r = B_t$

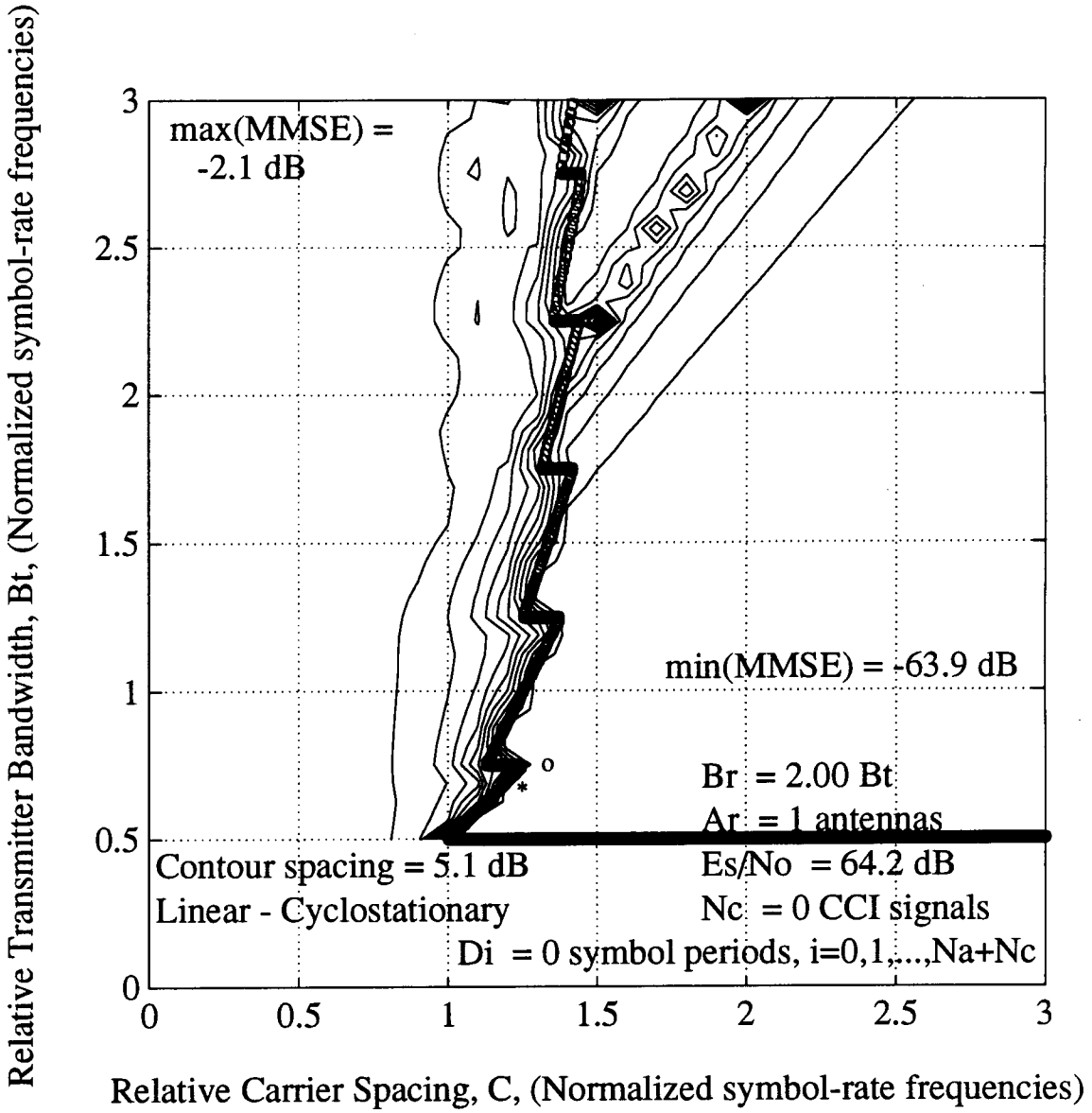

Figure 5.18 Overlay of Figs. 3.5, 5.10, and 5.16 — Existence of zero-forcing equalizer, MMSE, and system operating points versus transmitter bandwidth and carrier spacing — linear equalizer — cyclostationary interference — $B_r = 2B_t$

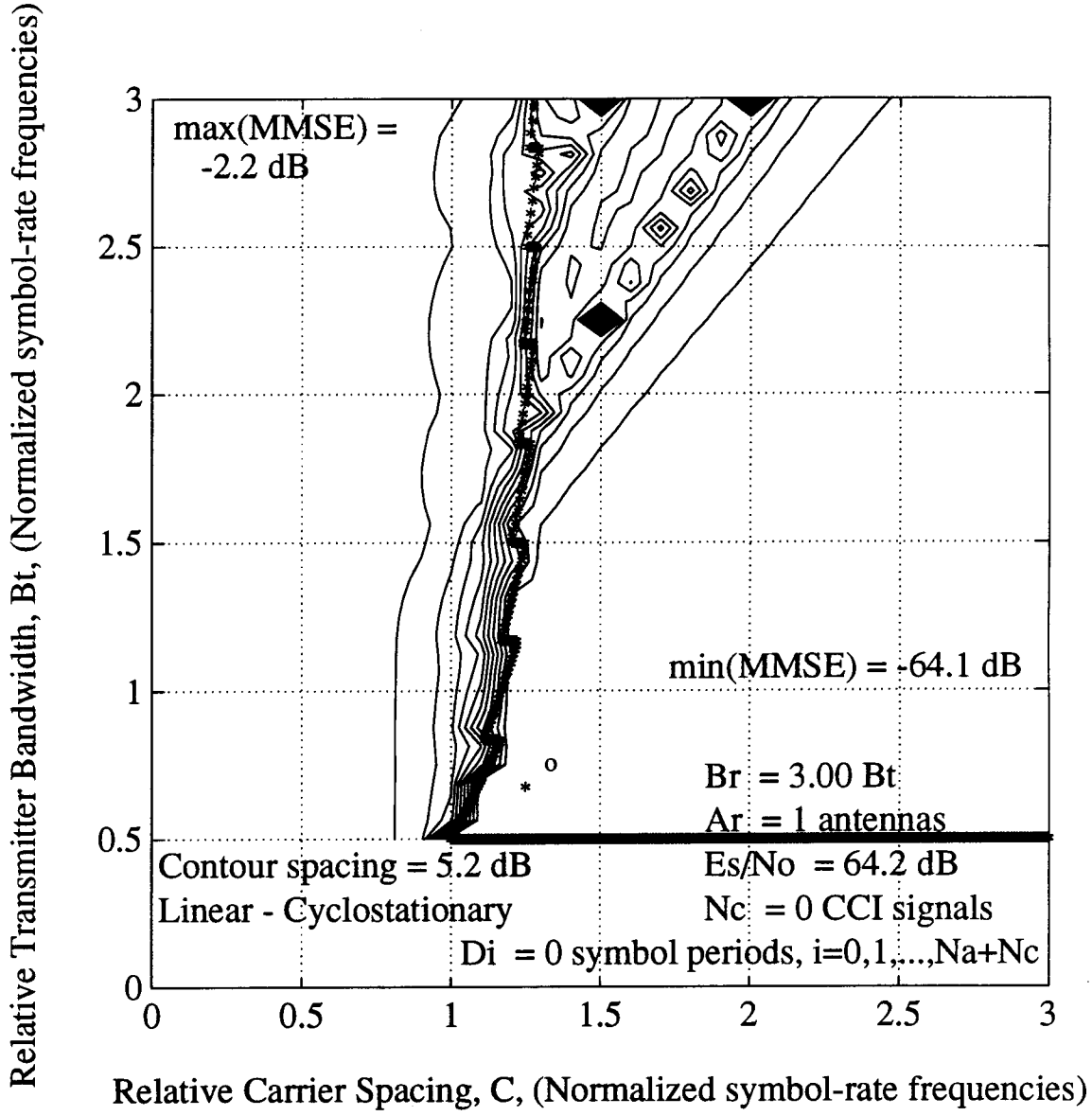

Figure 5.19 Overlay of Figs. 3.5, 5.12, and 5.16 — Existence of zero-forcing equalizer, MMSE, and system operating points versus transmitter bandwidth and carrier spacing — linear equalizer — cyclostationary interference — $B_r = 3B_t$

These figures have been overlaid for two reasons. The first is to make a comparison between two major types of analyses in Chapter 3, the existence of a generalized zero forcing linear equalizer and the minimum mean square error of an equalizer. The second is to demonstrate the improvements in spectral efficiency that may be achieved by exploiting the cyclostationary nature of the ACI. Inspection of Figs. 5.17, 5.18, and 5.19 shows a very close agreement between the region where a generalized zero-forcing linear equalizer exists and where low MMSE values occur. The agreement is closer at the lower bandwidths in the figures. A change from an equalizer bandwidth of $B_r = B_t$ to $B_r = 2B_t$ does not offer much improvement in spectral efficiency at the lower bandwidths near the two system operating points o and $*$. However, a change from $B_r = 2B_t$ to $B_r = 3B_t$ offers a larger potential improvement in spectral efficiency. This can be seen in Fig. 5.19 because the two system operating points could be moved farther to the left before encountering the rising MMSE values. Such a move would correspond to lower carrier spacings. Figs. 5.17, 5.18, and 5.19 also suggest that for a linear equalizer with one receiver antenna, the equalizer cannot maintain complete ACI suppression when the carrier spacing goes below $1/T$. In such a situation, the interference sets a limit on the spectral efficiency.

5.4 Discussion

In Chapter 3 it was emphasized that the ability of equalizers to extract the data of interest while simultaneously suppressing the interference requires inherent differences in the frequency responses of the combined channel and combined co-channels. In the system model used here the baseband transmitter pulses are identical. The differences among the interferers are a result of the different carrier shifts associated with each transmitter pulse. These differences allow equalizers to exploit the cyclostationarity of the interference for improved performance over the case where the interference is treated as stationary noise.

Using the model of the system described in Chapter 2 for linear and decision-feedback equalizers with one receiver antenna in ACI, the operating points which

provide the highest spectral efficiency are those with relative transmitter bandwidths equal to $1/(2T)$ where the symbol rate is $1/T$. Improvements in spectral efficiency for transmitter bandwidths in excess of $1/(2T)$ are possible by using wider equalizer bandwidths relative to the symbol rate. However, the spectral efficiency is fundamentally limited in that the carrier spacings cannot go below $1/T$ while maintaining complete ACI suppression. Note again that these results are only for a linear and decision-feedback equalizer with one receiver antenna.

Conditions have been given among the transmitter bandwidth, the receiver bandwidth, and the carrier spacing which provide the opportunity to linear and decision-feedback equalizers for intersymbol and adjacent-channel interference suppression. These conditions have been given through two types of evaluations. The first was the analysis of the existence of a generalized zero-forcing linear equalizer. The second was calculations of MMSE values. The MMSE calculations in this chapter confirmed the predictions of the existence of a generalized zero-forcing linear equalizer from Section 3.2. This confirmation is also intended to provide an increase in the confidence about the other presently unconfirmed predictions that have been obtained in Section 3.2.

The MMSE calculations have been carried out using a ratio of received signal energy to power spectral density fixed at 64.2 dB. This high value provides a sharp distinction between regions where adjacent-channel interference can be suppressed and cannot be suppressed. Such high values exist in some radio environments. Although the effect of white noise levels was not closely examined in this thesis, the white noise will influence the behavior of the equalizers. In other environments with lower relative levels of signal compared to the noise, the interference suppression capability of the equalizers might be reduced. This occurs because possible equalizer impulse responses which suppress interference may have large amplitudes and accentuate the noise. Thus with interference present and relatively high levels of noise, it is not possible here to be conclusive about whether or not the MMSE values could still be reduced to levels of those around the noise floor.

Regions of highest spectral efficiency lie around the smallest transmitter bandwidth,

zero-percent excess bandwidth. It has been shown that by exploiting the cyclostationarity of the adjacent-channel interference, there are conditions where it is theoretically possible to operate at an infinite transmitter bandwidth and completely suppress all adjacent-channel interference. More realistically, MMSE calculations incorporating the effects of noise showed that under conditions of severe spectral overlap, linear and decision-feedback equalizers were able to provide significant interference suppression. Interestingly large transmitter bandwidths relative to the symbol rate occur in spread spectrum systems. This work suggests that there may be benefits to exploiting the cyclostationarity of the interference in a spread spectrum system; such potential benefits are being explored in [190]. Such benefits may exist because in a spread spectrum system the differences between the combined channel and combined co-channels are designed by using different spreading sequences.

In the model for adjacent-channel interference used in this work, under certain conditions of transmitter bandwidth and carrier spacing equalizers were not able to achieve significant gains by exploiting the cyclostationary nature of the interference. These conditions occurred where the number of ACI signals made a transition from 4 to 6, as well as 6 to 8; see Figs. 3.4, 5.13, and 5.14.

Relevant issues that have not been addressed are synchronization, fading, and tracking. The requirement of using equalizers with wider bandwidths increases the complexity of the tracking problem. This is because larger equalizer bandwidths mean more parameters to track and to maintain interference suppression it is necessary for the equalizers to track the variations of the combined co-channels as well as the combined channel.

Chapter 6
Conclusions

A linear equalizer which suppresses all ISI, ACI, and CCI has been called a generalized zero-forcing linear equalizer [106]. This equalizer has been analyzed with particular attention given to the effect of bandwidths relative to the symbol rate. These analyses are based upon the idea that such an equalizer is likely to exist when the number of degrees of freedom is less than or equal to the number of constraints. Larger bandwidths relative to the symbol rate provide more degrees of freedom, however larger numbers of interferers provide more constraints. Although these analyses are based on a generalized zero-forcing linear equalizer, they also provide insight regarding the interference suppression capability of MMSE linear and decision-feedback equalizers. System operating points which provide opportunities to equalizers for interference suppression are suggested by these analyses and these suggestions can be used in evaluations based on more realistic performance criteria, such as the MMSE. It turns out that the ability of an equalizer to extract the data of interest while simultaneously suppressing the interference is based on the difference between the combined channel response and combined co-channel responses. Often increases in relative bandwidth enhance the differences. Based on the presence of CCI, the following results were obtained:

1. *Every increase in transmitter total bandwidth of size equal to the symbol rate may provide the flexibility to completely suppress an additional cyclostationary interferer by means of linear equalization.*
2. *The number of interferers that may be suppressible by a linear equalizer increases with the product of the total bandwidth relative to the symbol rate and the number of antennas.*

Based on the presence of ACI and CCI, the following results were obtained:

1. *With one antenna and a linear equalizer, arbitrarily large receiver bandwidths allow for marginal improvements in spectral efficiency through decreased carrier spacing,*

but the improvements cannot go below the fundamental carrier spacing value equal to the symbol rate.

2. *Large receiver bandwidths assist multiple antennas in improving the spectral efficiency in that the carrier spacing value can be less than the symbol rate, even in the presence of co-channel interference.*

Also included is a terse demonstration of how these analyses can be applied to systems which use different symbol rates that have a ratio equal to a rational number.

The results of the aforementioned analyses positively demand evaluation using more appropriate and realistic performance criteria. One such new result has been derived. It is an expression for the MMSE of a continuous-time infinite-length decision-feedback equalizer in the presence of intersymbol interference, additive white noise, and cyclostationary interference from neighboring systems which use identical symbol rates. This equalizer was shown to be time invariant, which has the implication that conventional adaptive equalizers can be used for implementation. The new expression for the MMSE has been theoretically compared with other expressions for the linear equalizer and for the cases where the co-channels contain stationary noise with the same power spectrum as cyclostationary interference. A result of these comparisons is that equalizer performance in cyclostationary interference can be better or worse than that in stationary noise. But in the applications considered in this thesis, situations were rare in which the equalizer performance in cyclostationary interference was worse than in stationary noise, and when the cyclostationary interference cases were worse the differences were very small.

The first application studied was high-speed digital subscriber lines. For the model of the system that was considered, equalizers are able to achieve improved interference suppression under certain joint conditions of wide enough transmitter pulse bandwidths and sufficiently aligned phases of the transceiver clocks in the central office. Costs to achieve these gains include the use of wide transmitter bandwidths relative to the symbol rate, increases in equalizer complexity through decreased tap spacings relative to the symbol period, increases in coefficient precision, increases in adaptive equalizer

convergence times, and other potential receiver complexity increases such as in the echo canceller. Another required cost is the hardware and provisioning for sufficient, but not perfect, alignment of the phases of the clocks in the central office transmitters. Further exploration of the gains and the practicality of exploiting the cyclostationary nature of the interference should be tempered by practical considerations. This work included contacts with representatives of telephone operating companies to gain as much insight as possible into practical difficulties [68, 74, 139, 172, 184–186, 198, 199]. However, the companies would make the final determination of the value of the gains versus the cost of the implementation. Such a determination would require evaluations similar to those in this thesis, but incorporating wideband NEXT measurements of subscriber lines with more realistic geometries. In any case, a result of this work is a demonstration of the potential for gains and a presentation of it to the telephone operating companies. Even if these results are not incorporated in the proposed HDSL system, such design considerations may be more relevant in future uses of twisted-pair copper loops [3, 7, 15].

In the application to adjacent-channel interference in digital radio, the analyses and calculations demonstrated how equalizers are able to exploit the cyclostationarity of the interference in order to extract the data of interest and suppress the interference. This ability is maintained under conditions of complete spectral overlap by the interference of the signal carrying the data of interest. The MMSE calculations of equalizer performance confirmed the predictions offered by the analyses of the generalized zero-forcing linear equalizer. This confirmation increases the confidence in the analyses of the generalized zero-forcing linear equalizer and the other predictions associated with them. The MMSE calculations also found that certain combinations of carrier spacing and transmitter bandwidth were particularly bad because the equalizers were unable to achieve good performance. These combinations occurred at the transitions where the number of ACI signals, overlapping the signal carrying the data of interest, jumped from 4 to 6 as well as 6 to 8.

As previously stated, the premise of this thesis is that the channel is presently, or will be, a critical resource whose efficient use requires the use of interference analysis

and suppression techniques. The contributions of this thesis are interference analysis and suppression techniques for linear and decision-feedback equalizers operating in the presence of intersymbol interference, additive white noise, and cyclostationary interference arising from neighboring systems. It was not possible to address all the related communication system design issues that could reduce the optimistic gains reported here. One important topic for future work is exploration of other applications to address further the potential improvements of equalization in cyclostationary interference.

6.1 Open Issues

Both disjoint and interrelated issues regarding potential future work are discussed here. Since the following discussion stems from introductory observations, it should be remembered that the ideas are not completely evaluated.

In an HDSL system, there is a need for synchronization circuits to maintain low amounts of timing jitter due to its effect on echo canceller accuracy. It is possible that no additional requirements would be placed on the synchronizer if an equalizer were designed to exploit the cyclostationarity of the NEXT. However, it was pointed out that the use of a fractionally spaced equalizer may require the use of a fractionally spaced echo canceller. In such a case, the synchronization problem may have to be reconsidered. Another area that may be impacted is efficient implementation techniques for reducing the complexity of the DFE and echo canceller. Such techniques exploit the properties of the tails of the impulse responses. If the forward filter of a DFE synthesizes an unusual impulse response in order to suppress the NEXT, the shape of the tail may be affected. It has been mentioned that more cyclostationary interference suppression is achieved by using fractionally spaced equalizers with smaller tap spacings. Hence, some form of implementation complexity reduction would be required.

Fading is a major impairment to maintaining reliable radio communication. Problems caused by fading include difficulty in maintaining synchronization and in tracking the variations of the channels. It is not certain how difficult it would be to exploit the cyclostationarity of the interference in a rapidly changing environment. For cellular

radio, a previously mentioned idea which has not been explored is re-using different pulse shapes much like re-using carrier frequencies. This re-use would enhance the differences between the signal and interferers. In a sense the idea of pulse shape re-use has been explored in spread spectrum systems. This work suggests that spread spectrum systems may achieve performance improvements by exploiting the cyclostationarity of the interference [190].

Specific applications would show the extent of the interference suppression capability which is offered by the combined use of antenna diversity and relative transmitter and receiver bandwidth. Analytical transmitter pulse shape optimization may provide valuable choices of transmitter pulse shapes. The optimal number bits transmitted per symbol may be different in cyclostationary interference than stationary noise. This work has been based on coherent detection using linear modulation schemes. There may be similar approaches that can be tried for non-linear modulation schemes.

Non-linear receiver implementations may also be effective structures to suppress interference. Non-linearities cause a relative bandwidth expansion and it has been demonstrated how large relative bandwidths provide opportunities for interference suppression. However, non-linearities also introduce inter-modulation products and these may reduce the effectiveness of such receiver implementations.

This thesis demonstrated the ability of equalizers to improve the MSE by exploiting the cyclostationarity of the interference. Since the MSE is not as direct a measure as the BER of communication system performance, further research into the effects on the BER may be valuable. It is difficult to predict the results since there is not a clear relationship between the MSE and the BER.

In the applications in this thesis the use of wide relative bandwidths has been shown to offer improved interference suppression capability. This arises because of enhanced differences between the combined channel response and combined co-channel responses. In a sense these enhanced differences might also be called distances, and this suggests application to coded systems. Thus, in systems which are impaired by interference, wide relative bandwidths may enhance the performance of coded systems. Non-linear

receivers, such as maximum likelihood sequence estimators, may also find interference suppression benefits in relatively wide bandwidths.

Appendix A Time-Variant Decision-feedback Equalizer Analysis

A.1 Systems with Identical Symbol Rates

This section describes in more detail why the *time-invariant* continuous-time infinite-length decision-feedback equalizer in Section 3.3 achieves the minimum mean square error in the presence of intersymbol interference, additive white noise, and co-channel interference. Note again that the transmitters of the data of interest and the interferers use identical symbol rates.

The development in this section parallels the one in Section 3.3 except the following assumptions are changed to allow analysis of a time-variant decision-feedback equalizer. In Fig. 3.9 the impulse responses of the forward and feedback filters become $r_d(t,\tau)$ and $b_d[n,m]$ instead of $r_d(t)$ and $b_d[n]$, respectively. The notation means that $r_d(t,\tau)$ is the impulse response in time t due to an impulse arriving at time τ, $\delta(t-\tau)$. Similarly, the notation means that $b_d[n,m]$ is the impulse response in time n due to an impulse arriving at time m, $\delta[n-m]$. Equation (2.43) becomes:

$$b_d[n,m] = 0 \quad ; \quad n-m \leq 0. \tag{A.1}$$

For continuous-time signals, convolution with a time-variant impulse response takes the following form:

$$x_a(t) = \int_{-\infty}^{\infty} x_b(t,\tau)\, x_c(\tau)\, d\tau \tag{A.2}$$

where $x_a(t)$ is the linear-filter output signal, $x_b(t,\tau)$ is the time-variant linear-filter impulse response, and $x_c(t)$ is the linear-filter input signal. For discrete-time signals, convolution with a time-variant impulse response takes the following form:

$$x_a[n] = \sum_{m=-\infty}^{\infty} x_b[n,m]\, x_c[m] \tag{A.3}$$

where $x_a[n]$ is the linear-filter output signal, $x_b[n,m]$ is the time-variant linear-filter impulse response, and $x_c[n]$ is the linear-filter input signal.

The MSE given in (3.37) is unchanged:

$$\varepsilon_{dc}(b_d, r_d) \;=\; E\left[\left|\widehat{d}_0[n] - d_0[n]\right|^2\right]. \tag{A.4}$$

Using the changes described above, the analysis was repeated and $\varepsilon_{dc}(b_d, r_d)$ from (A.4) becomes:

$$\begin{aligned}
\varepsilon_{dc}(b_d, r_d) \;=\; & \int_{-\infty}^{\infty} r_d^*(n\mathrm{T}, t) \left(\int_{-\infty}^{\infty} k_l(t,\tau)\, r_d(n\mathrm{T}, \tau)\, d\tau \right) dt \\
& - \int_{-\infty}^{\infty} r_d^*(n\mathrm{T}, t)\, \phi_0^*(t - n\mathrm{T})\, dt \\
& - \int_{-\infty}^{\infty} r_d(n\mathrm{T}, t)\, \phi_0(t - n\mathrm{T})\, dt \\
& + 1 \\
& - \sum_{m=-\infty}^{\infty} \left(\int_{-\infty}^{\infty} \phi_0^*(t - n\mathrm{T})\, r_d^*(n\mathrm{T}, t)\, dt \right) b_d[n,m] \\
& - \sum_{m=-\infty}^{\infty} \left(\int_{-\infty}^{\infty} \phi_0(t - n\mathrm{T})\, r_d(n\mathrm{T}, t)\, dt \right) b_d^*[n,m] \\
& + \sum_{m=-\infty}^{\infty} |b_d[n,m]|^2
\end{aligned} \tag{A.5}$$

where now the expression $n\mathrm{T}$ appears frequently since the MSE is minimized at time $n\mathrm{T}$ and since the channel is wide-sense stationary when sampled at a rate $1/\mathrm{T}$. Equation (A.5) is the time-variant equivalent of (3.41).

Instead of (3.51), the optimal value for $b_d[n,m]$, called $b_{dco}[n,m]$, is now given by:

$$b_{dco}[n,m] \;=\; \begin{cases} 0 & , \; n - m \leq 0 \\ \int_{-\infty}^{\infty} r_d(n\mathrm{T}, t)\, \phi_0(t - m\mathrm{T})\, dt & , \; n - m > 0. \end{cases} \tag{A.6}$$

Substitute $b_{dco}[n,m]$ from (A.6), into (A.5) to get the MSE which is only a function of $r_d(t,\tau)$:

$$\begin{aligned}\varepsilon_{dc}(b_d, r_d) \;=\; & \int_{-\infty}^{\infty} r_d^*(n\mathrm{T},t)\left(\int_{-\infty}^{\infty} k_d(t,\tau)\, r_d(n\mathrm{T},\tau)\, d\tau\right) dt \\ & - \int_{-\infty}^{\infty} r_d^*(n\mathrm{T},t)\, \phi_0^*(t-n\mathrm{T})\, dt \\ & - \int_{-\infty}^{\infty} r_d(n\mathrm{T},t)\, \phi_0(t-n\mathrm{T})\, dt \\ & + 1\end{aligned} \tag{A.7}$$

$$\begin{aligned}\therefore\; \varepsilon_{dc}(b_d, r_d) \;=\; & \int_{-\infty}^{\infty} r_d^*(n\mathrm{T}, n\mathrm{T}+t)\left(\int_{-\infty}^{\infty} k_d(t,\tau)\, r_d(n\mathrm{T}, n\mathrm{T}+\tau)\, d\tau\right) dt \\ & - \int_{-\infty}^{\infty} r_d^*(n\mathrm{T}, n\mathrm{T}+t)\, \phi_0^*(t)\, dt \\ & - \int_{-\infty}^{\infty} r_d(n\mathrm{T}, n\mathrm{T}+t)\, \phi_0(t)\, dt \\ & + 1.\end{aligned} \tag{A.8}$$

For clarity define:

$$r_{dn}(t) \;=\; r_d(n\mathrm{T}, n\mathrm{T}+t). \tag{A.9}$$

Therefore $\varepsilon_{dc}(b_d, r_d)$ from (A.8) becomes:

$$\therefore \varepsilon_{dc}(r_{dn}) \;=\; < r_{dn}\,,\, K_d r_{dn} >_c \;-\; < r_{dn}\,,\, \phi_0^* >_c \;-\; < r_{dn}^*\,,\, \phi_0 >_c \;+ 1. \tag{A.10}$$

By use of the calculus of variations similar to that in Appendix B.2, the value of $r_{dn}(t)$ which minimizes $\varepsilon_{dc}(r_{dn})$ in (A.10), called $r_{dno}(t)$, satisfies the following

equation:

$$K_d r_{dno}(t) \;=\; \phi_0^*(t) \tag{A.11}$$

where

$$r_{dno}(t) \;=\; r_{dco}(n\mathrm{T}, n\mathrm{T}-t) \tag{A.12}$$

which can be expanded to get the following integral equation for the unknown $r_{dno}(t)$:

$$\int_{-\infty}^{\infty} k_d(t,\tau)\, r_{dno}(\tau)\, d\tau \;=\; \phi_0^*(t)\,. \tag{A.13}$$

Equation (A.13) is similar to the time-invariant integral equation in (3.59). In (A.13), the parameter n only appears in $r_{dno}(t)$. Therefore $r_{dno}(t)$ is not a function of n.

Equations (A.9) and (A.12) mean that not all values of $r_d(t,\tau)$ are constrained. Only those values of $r_d(t,\tau)$ which lie on the lines:

$$t \;=\; n\mathrm{T} \tag{A.14}$$

are constrained to certain values. Furthermore, since $r_{dno}(t)$ is not a function of n, and since $r_{dno}(t)$ is equal to $r_{dco}(n\mathrm{T}, n\mathrm{T}+t)$, therefore $r_{dco}(n\mathrm{T}, n\mathrm{T}+t)$ is only a function of the difference between $n\mathrm{T}$ and $n\mathrm{T}+t$. Therefore $r_{dco}(n\mathrm{T}, n\mathrm{T}+t)$ is periodically time invariant.

The values of $r_d(t,\tau)$ not on the lines

$$t \;=\; n\mathrm{T} \tag{A.15}$$

are not constrained. Therefore, they may be chosen to advantage. They can be chosen in order that $r_d(t,\tau)$ is time invariant over all the plane (t,τ).

Therefore the impulse response of the feedback filter in (A.6) is can also be time invariant since:

$$\begin{aligned} b_{dco}[n,m] \;&=\; \begin{cases} 0 & ,\; n-m \le 0 \\ \int_{-\infty}^{\infty} r_{dco}(n\mathrm{T}, t)\, \phi_0(t-m\mathrm{T})\, dt & ,\; n-m > 0 \end{cases} \\ &=\; \begin{cases} 0 & ,\; n-m \le 0 \\ \int_{-\infty}^{\infty} r_{dco}(n\mathrm{T}-t)\, \phi_0(t-m\mathrm{T})\, dt & ,\; n-m > 0 \end{cases} \\ &=\; \begin{cases} 0 & ,\; n-m \le 0 \\ \int_{-\infty}^{\infty} r_{dco}(t)\, \phi_0((n-m)\mathrm{T}-\mathrm{t})\, dt & ,\; n-m > 0. \end{cases} \end{aligned} \tag{A.16}$$

Thus, the time-invariant decision-feedback equalizer used in the development in Section 3.3 can achieve the minimum mean square error in the presence of cyclostationary interference from neighboring systems operating at the same symbol rate as transmitter for the data of interest.

A.2 Systems with Mixed Symbol Rates

By an example of particular systems, this appendix justifies how equalizers can be used to suppress cyclostationary interference between systems which use *mixed* symbol rates. The concept of interference between systems with mixed symbol rates has been dealt with in [64, 73, 77, 79, 80, 107], but in this appendix, which describes a specific equalizer application, this concept is expanded to include the effect of bandwidth relative to the symbol rate from Section 3.2. It will be demonstrated that the cyclostationary interference from sources with different symbol rates can be suppressed under certain conditions of bandwidth and increased equalizer complexity.

Fig. A.1 shows two transmitters and two linear equalizers which are linked by a cross-coupled channel. This system uses similar notation to that of Chapter 2. The major difference over Chapter 2 is the use of different symbol rates. The output of transmitter 0 is the signal:

$$\sum_{n=-\infty}^{\infty} d_0[n]\ p_{t,0}(t - n\mathrm{T}_0) \tag{A.17}$$

where $1/\mathrm{T}_0$ is the symbol rate. The output of transmitter 1 is the signal:

$$\sum_{n=-\infty}^{\infty} d_0[n]\ p_{t,1}(t - n\mathrm{T}_1) \tag{A.18}$$

where $1/\mathrm{T}_1$ is the symbol rate. For purposes of explanation, the following specific case has been considered where the symbol rate of transmitter 1 is twice that of transmitter 0:

$$\begin{aligned} \frac{1}{\mathrm{T}_1} &= 2\,\frac{1}{\mathrm{T}_0} \\ \therefore\ \mathrm{T}_1 &= \frac{1}{2}\,\mathrm{T}_0. \end{aligned} \tag{A.19}$$

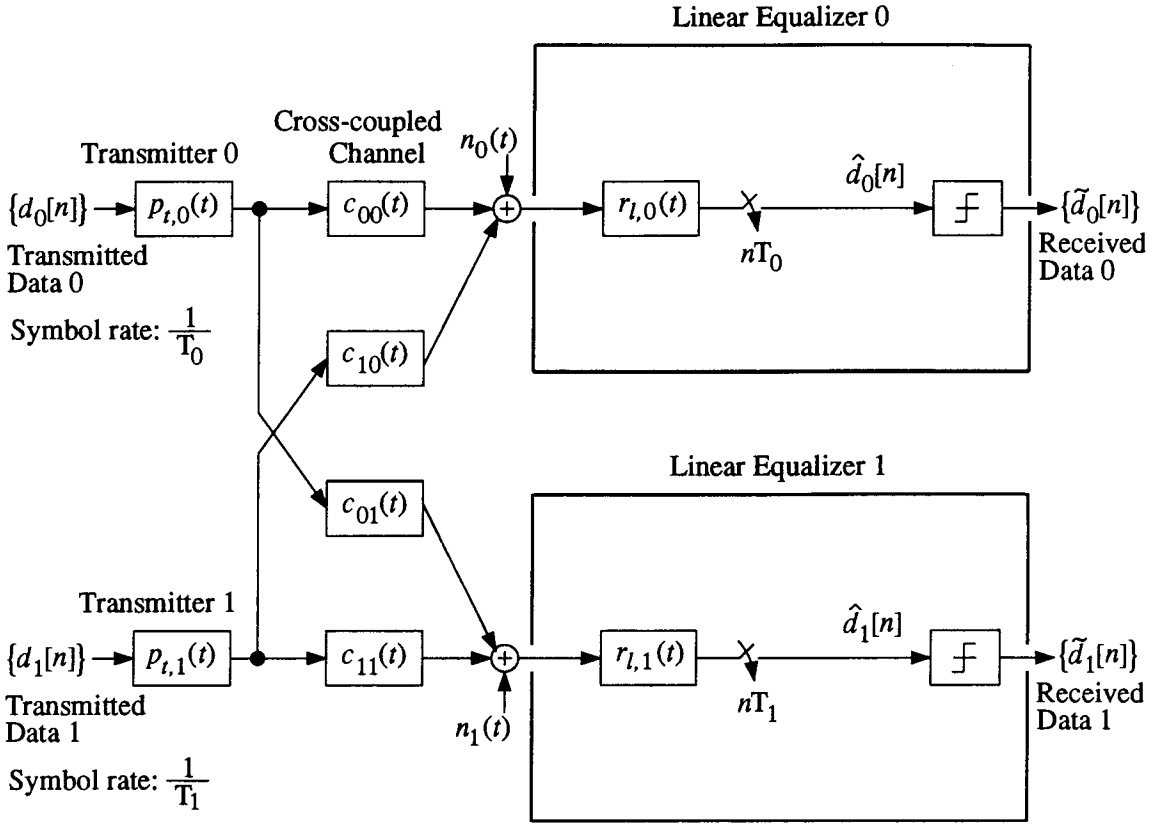

Figure A.1 Mixed symbol rates — time-invariant linear equalizers

The explanation would be fundamentally similar for any case where T_0/T_1 is a rational number. Cases where T_0/T_1 is not necessarily a rational number will not developed, but their development would include the fundamental principles of the separability of cyclostationary interference described in [64, 79, 80]. Also transmitter 0 will be strictly bandlimited to $1/T_0$ and transmitter 1 will be strictly bandlimited to $1/T_1$. Thus, each system would be transmitting a signal which has the same bandwidth relative to its symbol rate as a 100-percent excess bandwidth raised-cosine pulse. These parameters are summarized in Table A.1.

First, consider the case where the systems are not cross-coupled. Therefore $c_{10}(t)$ and $c_{01}(t)$ are zero. Both systems are required to suppress only intersymbol interference. The system parameters that are required to achieve complete intersymbol interference suppression, based solely on the bandwidth analysis in Section 3.2, are shown in Table A.2. Clearly, a linear equalizer bandwidth of $1/(2T_0)$ would not be practical in an implementation; a higher bandwidth would be required. What is assumed in this analysis is that the bandwidth required by an implementation would be approximately proportional to the absolute minimum bandwidths shown in this analysis. By this assumption, it will be suggested that increasing absolute minimum bandwidths lead to increasingly complex equalizer implementations.

Second, consider the case where the channel is cross-coupled. Both systems are required to suppress intersymbol interference and co-channel interference. Let the equalized combined channels and equalized combined co-channels be defined as follows:

$$\begin{aligned} h_{00}(t) &= p_{t,0}(t) \star c_{00}(t) \star r_{l,0}(t) \\ h_{01}(t) &= p_{t,0}(t) \star c_{01}(t) \star r_{l,1}(t) \\ h_{10}(t) &= p_{t,1}(t) \star c_{10}(t) \star r_{l,0}(t) \\ h_{11}(t) &= p_{t,1}(t) \star c_{11}(t) \star r_{l,1}(t). \end{aligned} \tag{A.34}$$

Table A.1 System parameters

System Parameters		Parameter Values	
		Transmitter and Linear Equalizer 0	**Transmitter and Linear Equalizer 1**
Symbol rate		$\frac{1}{T_0}$	$\frac{1}{T_1}$
Symbol-rate relationship	Identical	$\frac{1}{T_0} = \frac{1}{T_1}$	
	Mixed	$\frac{1}{T_0} = \frac{1}{2}\frac{1}{T_1}$	
Transmitter Bandwidth		$\frac{1}{T_0}$	$\frac{1}{T_1}$

Table A.2 Equalizer parameters — mixed symbol rates — uncoupled channel — time-invariant implementation

Parameters of an Equalizer Implementation	Parameter Values	
	Transmitter and Linear Equalizer 0	Transmitter and Linear Equalizer 1
Receiver Bandwidth	$\frac{1}{2T_0}$	$\frac{1}{2T_1}$
Sampling Rate	$\frac{1}{T_0}$	$\frac{1}{T_1}$
Tap Spacing	$\frac{T_0}{1}$	$\frac{T_1}{1}$
Number of time-invariant impulse responses	1	1

In the time domain, the condition for complete ISI and CCI suppression is:

$$\begin{aligned} h_{00}(n\mathrm{T}_0) &= \delta[n] \\ h_{01}(n\mathrm{T}_1) &= 0 \\ h_{10}(n\mathrm{T}_1) &= 0 \\ h_{11}(n\mathrm{T}_1) &= \delta[n]. \end{aligned} \tag{A.35}$$

In the frequency domain, the condition for ISI and CCI suppression is:

$$\begin{aligned} \frac{1}{\mathrm{T}_0}\sum_{k=-\infty}^{\infty} H_{00}\left(f+\frac{k}{\mathrm{T}_0}\right) &= 1 \\ \frac{1}{\mathrm{T}_1}\sum_{k=-\infty}^{\infty} H_{01}\left(f+\frac{k}{\mathrm{T}_1}\right) &= 0 \\ \frac{1}{\mathrm{T}_1}\sum_{k=-\infty}^{\infty} H_{10}\left(f+\frac{k}{\mathrm{T}_1}\right) &= 0 \\ \frac{1}{\mathrm{T}_1}\sum_{k=-\infty}^{\infty} H_{11}\left(f+\frac{k}{\mathrm{T}_1}\right) &= 1 \end{aligned} \tag{A.36}$$

where

$$H_{nm}(f) = \mathcal{F}_{cc}[h_{nm}(t)] \quad ; \quad n,m \in \{0,1\}. \tag{A.37}$$

The situation corresponding to (A.35) is shown in Fig. A.2. Based on the bandwidth analysis in Section 3.2, both equalizer 0 and equalizer 1 are able to achieve complete ISI and CCI suppression. However, linear equalizer 1 is not able to achieve the MMSE since it is a time invariant implementation. The system parameters that would allow the equalizers in Fig. A.1 to achieve their best performance are shown in Table A.3.

Based upon the analysis in [20, 73], and that in Appendix A.1, the time-variant structure shown for linear equalizer 1 in Fig. A.3 is the linear equalizer capable of achieving the minimum mean square estimates of the data. Linear equalizer 1 now has two impulse responses, $r_{l,1e}(t)$ and $r_{l,1o}(t)$, corresponding to the data at even and odd sample numbers. In addition to (A.34), define the following equalized combined

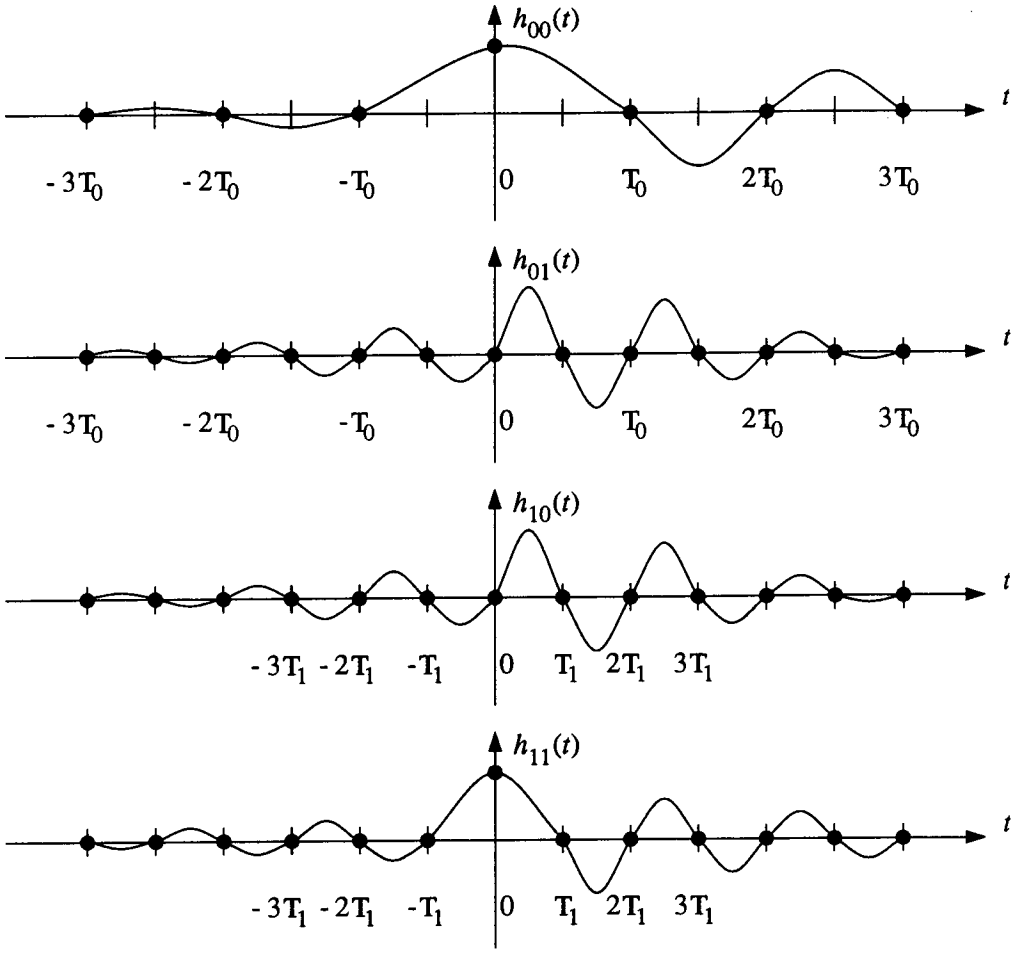

Figure A.2 Mixed symbol rates — time-invariant linear equalizers — generalized zero-forcing condition

Table A.3 Equalizer parameters — mixed symbol rates — coupled channel — time-invariant implementation

Parameters of an Equalizer Implementation	Parameter Values	
	Transmitter and Linear Equalizer 0	Transmitter and Linear Equalizer 1
Receiver Bandwidth	$\frac{2}{T_0}$	$\frac{1}{T_1}$
Sampling Rate	$\frac{4}{T_0}$	$\frac{2}{T_1}$
Tap Spacing	$\frac{T_0}{4}$	$\frac{T_1}{2}$
Number of time-invariant impulse responses	1	1

Note the MMSE is not achievable for linear equalizer 1.

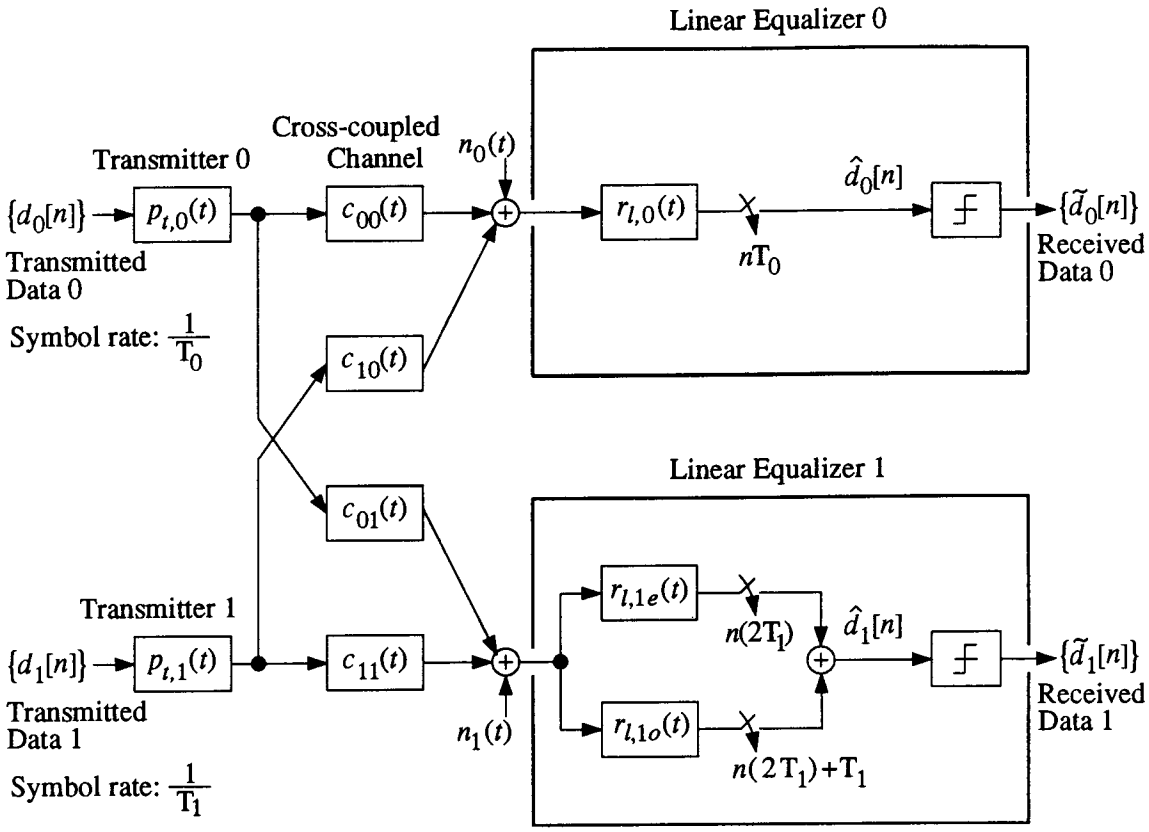

Figure A.3 Mixed symbol rates — time-variant linear equalizers

channels and equalized combined co-channels:

$$\begin{aligned} h_{01e}(t) &= p_{t,0}(t) \star c_{01}(t) \star r_{l,1e}(t) \\ h_{01o}(t) &= p_{t,0}(t) \star c_{01}(t) \star r_{l,1o}(t) \\ h_{11e}(t) &= p_{t,1}(t) \star c_{11}(t) \star r_{l,1e}(t) \\ h_{11o}(t) &= p_{t,1}(t) \star c_{11}(t) \star r_{l,1o}(t). \end{aligned} \tag{A.46}$$

In the time domain, the condition for complete ISI and CCI suppression is:

$$\begin{aligned} h_{00}(n\mathrm{T}_0) &= \delta[n] \\ h_{01e}(n\mathrm{T}_0) &= 0 \\ h_{01o}(n\mathrm{T}_0) &= 0 \\ h_{10}(n\mathrm{T}_1) &= 0 \\ h_{11e}(n\mathrm{T}_1) &= \delta[n] \\ h_{11o}(n\mathrm{T}_1) &= \delta[n]. \end{aligned} \tag{A.47}$$

In the frequency domain, the condition for complete ISI and CCI suppression is:

$$\begin{aligned} \frac{1}{\mathrm{T}_0}\sum_{k=-\infty}^{\infty} H_{00}\left(f+\frac{k}{\mathrm{T}_0}\right) &= 1 \\ \frac{1}{\mathrm{T}_0}\sum_{k=-\infty}^{\infty} H_{01e}\left(f+\frac{k}{\mathrm{T}_0}\right) &= 0 \\ \frac{1}{\mathrm{T}_0}\sum_{k=-\infty}^{\infty} H_{01o}\left(f+\frac{k}{\mathrm{T}_0}\right) &= 0 \\ \frac{1}{\mathrm{T}_1}\sum_{k=-\infty}^{\infty} H_{10}\left(f+\frac{k}{\mathrm{T}_1}\right) &= 0 \\ \frac{1}{\mathrm{T}_1}\sum_{k=-\infty}^{\infty} H_{11e}\left(f+\frac{k}{\mathrm{T}_1}\right) &= 1 \\ \frac{1}{\mathrm{T}_1}\sum_{k=-\infty}^{\infty} H_{11o}\left(f+\frac{k}{\mathrm{T}_1}\right) &= 1 \end{aligned} \tag{A.48}$$

where

$$H_{n1e}(f) = \mathcal{F}_{cc}[h_{n1e}(t)] \quad ; \quad n \in \{0,1\} \tag{A.49}$$

and

$$H_{n1o}(f) \;=\; \mathcal{F}_{cc}[h_{n1o}(t)] \quad ; \quad n \in \{0,1\}. \tag{A.50}$$

The situation corresponding to (A.47) is shown in Fig. A.4. The system parameters that are required to achieve complete ISI and CCI suppression, based solely on the bandwidth analysis in Section 3.2, are shown in Table A.4.

The results in this appendix can also be compared to the case where the two systems use identical symbol rates. If the symbol rate for linear equalizer 1 had been the same as for linear equalizer 0, and an uncoupled channel were used, then results would be those in Table A.5. If instead, a coupled channel were used, then results would be obtained from the CCI analysis, see (3.20), would be those in Table A.6.

The results in the tables of this appendix will now be compared. To facilitate discussion the topics dealt with in Tables A.2, A.3, A.4, A.5, and A.6 are grouped in Table A.7.

With mixed symbol rates and a coupled channel, a comparison of Tables A.3 and A.4 shows similar structures, except for the number of time-variant impulse responses. In all cases the linear equalizers are able to achieve complete ISI and CCI suppression, but the time-variant equalizer may have a MMSE which is less than the time-invariant equalizer.

For identical symbol rates, the addition of coupling in the channel means that for the linear equalizers to maintain complete ISI and CCI suppression, the tap spacing for both equalizers must be decreased by a factor of two; this is obtained by a comparison of Tables A.5 and A.6.

For an uncoupled channel, an increase of the symbol rate of transmitter 1 from the identical case to the mixed case shows, between Tables A.5 and A.2, that no change to the tap spacing occurs *relative* to the symbol rates. But there is an increase in complexity in absolute terms.

For a coupled channel, a change from identical to mixed symbol rates means that for the MMSE linear equalizers to maintain complete ISI and CCI suppression, the tap spacing for linear equalizer 0 must be decreased by a factor of two, and the number

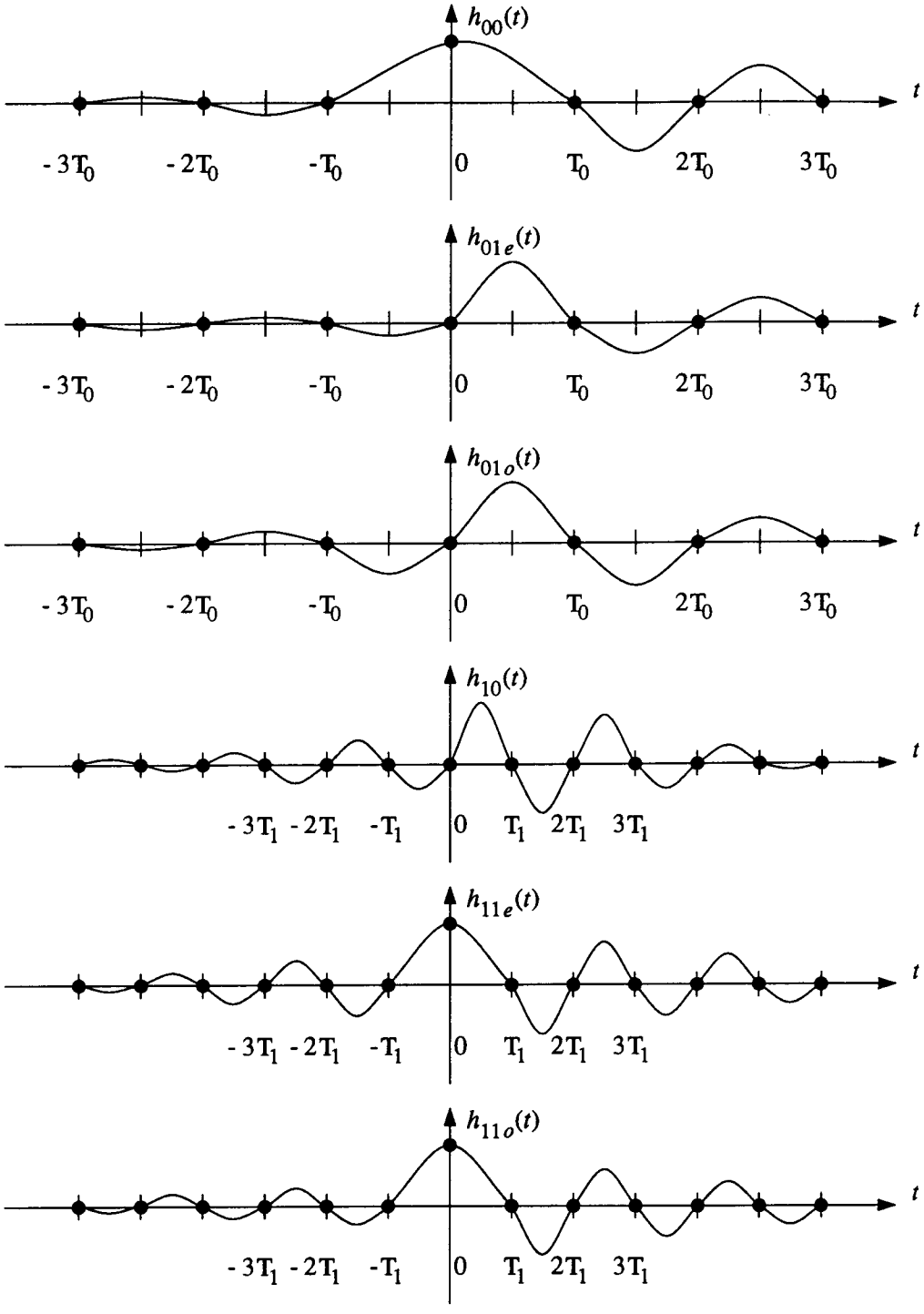

Figure A.4 Mixed symbol rates — time-variant linear equalizers — generalized zero-forcing condition

Table A.4 Equalizer parameters — mixed symbol rates — coupled channel — time-variant implementation

Parameters of an Equalizer Implementation	Parameter Values	
	Transmitter and Receiver 0	Transmitter and Receiver 1
Receiver Bandwidth	$\frac{2}{T_0}$	$\frac{1}{T_1}$
Sampling Rate	$\frac{4}{T_0}$	$\frac{2}{T_1}$
Tap Spacing	$\frac{T_0}{4}$	$\frac{T_1}{2}$
Number of time-invariant impulse responses	1	2

Note the MMSE is achievable.

Table A.5 Equalizer parameters — identical symbol rates — uncoupled channel — time-invariant implementation

Parameters of an Equalizer Implementation	Parameter Values	
	Transmitter and Linear Equalizer 0	**Transmitter and Linear Equalizer 1**
Receiver Bandwidth	$\frac{1}{2T_0}$	$\frac{1}{2T_1}$
Sampling Rate	$\frac{1}{T_0}$	$\frac{1}{T_1}$
Tap Spacing	$\frac{T_0}{1}$	$\frac{T_1}{1}$
Number of time-invariant impulse responses	1	1

Table A.6 Equalizer parameters — identical symbol rates — coupled channel — time-invariant implementation

Parameters of an Equalizer Implementation	Parameter Values	
	Transmitter and Linear Equalizer 0	Transmitter and Linear Equalizer 1
Receiver Bandwidth	$\frac{1}{T_0}$	$\frac{1}{T_1}$
Sampling Rate	$\frac{2}{T_0}$	$\frac{2}{T_1}$
Tap Spacing	$\frac{T_0}{2}$	$\frac{T_1}{2}$
Number of time-invariant impulse responses	1	1

Table A.7 Equalizer parameters — identical symbol rates — coupled channel — time-invariant implementation

		Channel Type	
		Uncoupled	Coupled
Symbol Rates	Identical	Table A.5	Table A.6
	Mixed	Table A.2	Table A.4 (Table A.3, time invariant, non-MMSE implementation)

impulse responses in linear equalizer 1 must be increased by a factor of two; this is seen by a comparison of Tables A.6 and A.4.

This analysis suggests that it is possible to use an equalizer to suppress cyclostationary interference arising from systems which use symbol rates that are different by a factor equal to a rational number. The suppression of the intersymbol interference and co-channel interference depends on conditions of bandwidth relative to the symbol rate, the ratio of the symbol rates, and the number of interferers. The results of this appendix also *suggest* that to achieve complete interference suppression capability, it requires complexity (tap spacing and number of time-invariant impulse responses) increases proportional to the integer ratio of the symbol rates of the systems.

Appendix B Mean Square Error Minimization for Decision-feedback Equalizer

B.1 Differential Calculus Solution of Feedback Filter

Given the following from equation (3.43):

$$\begin{aligned}\varepsilon_{dc}(b_d, r_d) = \quad & < r_d \, , \, K_l r_d >_c \; - \; < r_d \, , \, m_0 >_c \; - \; < r_d^* \, , \, m_0^* >_c \; + 1 \\ & - \; < K_0 r_d \, , \, b_d >_d \\ & - \; < K_0 r_d^* \, , \, b_d^* >_d \\ & + \; < b_d \, , \, b_d >_d \end{aligned} \tag{B.1}$$

where the inner product $< \bullet, \blacklozenge >_c$ was defined in (3.44), the inner product $< \bullet, \blacklozenge >_d$ was defined in (3.45), the Fredholm integral operator K_l was defined in (3.46) with its kernel defined in (3.42), the linear transformation K_0 was defined in (3.48), and the function $m_0(t)$ was defined in (3.49). All scalars and functions are known, except for the coefficients $b_d[n]$ and the function $r_d(t)$. The problem is to find the optimal coefficients of the feedback filter, called $b_{dco}[n]$, which make $\varepsilon_{dc}(b_d, r_d)$ in (B.1) the smallest. One would expect that $b_{dco}[n]$ may depend on the other unknown function $r_d(t)$.

Equation (2.43) implies that $\{b_{dco}[n] \mid n \leq 0\}$ are zero. Therefore, only $\{b_{dco}[n] \mid n > 0\}$ need to be determined; these optimal coefficients will be determined by the calculus of derivatives.

The optimal coefficients may be obtained from the following two partial derivative equations for the real and imaginary components:

$$\frac{\partial \varepsilon_{dc}(r_d, b_d)}{\partial \Re[b_d[n]]}\Big|_{\Re[b_d[n]]=\Re[b_{dco}[n]]} = 0 \quad ; \quad n > 0 \tag{B.2}$$

$$\frac{\partial \varepsilon_{dc}(r_d, b_d)}{\partial \Im[b_d[n]]}\Big|_{\Im[b_d[n]]=\Im[b_{dco}[n]]} = 0 \quad ; \quad n > 0 \tag{B.3}$$

where the function $\Re[\bullet]$ denotes the real part of $\bullet$, and the function $\Im[\bullet]$ denotes the imaginary part of $\bullet$.

Evaluating (B.2) gives:

$$-K_0 r_d^*[n] - K_0 r_d[n] + 2\Re[b_{dco}[n]] = 0 \quad ; \quad n > 0 \tag{B.4}$$

$$\therefore \Re[b_{dco}[n]] = \Re[K_0 r_d[n]] \quad ; \quad n > 0. \tag{B.5}$$

Evaluating (B.3) gives:

$$-jK_0 r_d^*[n] + jK_0 r_d[n] + 2\Im[b_{dco}[n]] = 0 \quad ; \quad n > 0 \tag{B.6}$$

$$\Im[b_{dco}[n]] = \Im[K_0 r_d[n]] \quad ; \quad n > 0. \tag{B.7}$$

Combining (B.5) and (B.7) gives:

$$b_{dco}[n] = K_0 r_d[n] \quad ; \quad n > 0. \tag{B.8}$$

Therefore the optimal values for $b_d[n]$ are:

$$b_{dco}[n] = u[n-1]\, K_0 r_d[n] \tag{B.9}$$

where the discrete-time unit step function is defined to be:

$$u[n] = \begin{cases} 0 & , n < 0 \\ 1 & , n \geq 0. \end{cases} \tag{B.10}$$

B.2 Calculus of Variations Solution of Forward Filter

Given the following functional[22] from equation (3.55):

$$\varepsilon_{dc}(r_d) \;=\; < r_d \;,\; K_d r_d >_c \;-\; < r_d \;,\; m_0 >_c \;-\; < r_d^* \;,\; m_0^* >_c \;+ 1 \qquad \text{(B.11)}$$

where the inner product $< \bullet, \blacklozenge >_c$ was defined in (3.44), the linear transformation K_d was defined in (3.56), the kernel, $k_d(t,\tau)$, of the Fredholm integral operator was defined in (3.57), and the function $m_0(t)$ was defined in (3.49). All scalars and functions are known, except for the function $r_d(t)$. The problem is to find the optimal function for $r_d(t)$ which makes the output of the functional $\varepsilon_{dc}(r_d)$ the smallest. This optimal function is denoted by $r_{dco}(t)$.

The optimal function will be determined by the calculus of variations. Define:

$$r_d(t) \;=\; r_{dco}(t) \;+\; \xi\, \Xi(t) \qquad \text{(B.12)}$$

where ξ is a complex scalar and $\Xi(t)$ is an arbitrary complex function[23]. Substitute $r_d(t)$ from (B.12) into (B.11) and express $\varepsilon_{dc}(r_d)$ as:

$$\begin{aligned} \varepsilon_{dc}(r_d, \Re[\xi], \Im[\xi]) \;=\; & < r_d + \xi\Xi \;,\; K_d(r_d + \xi\Xi) >_c \\ & - \; < r_d + \xi\Xi \;,\; m_0 >_c \\ & - \; < (r_d + \xi\Xi)^* \;,\; m_0^* >_c \\ & + \; 1 \end{aligned} \qquad \text{(B.13)}$$

where the following notation is introduced for scalar multiplication:

$$(\xi\bullet)(t) \;=\; \xi \;(\; \bullet(t) \;) \qquad \text{(B.14)}$$

and for addition of functions:

$$(\bullet + \blacklozenge)(t) \;=\; \bullet(t) \;+\; \blacklozenge(t). \qquad \text{(B.15)}$$

---

22 A functional accepts a function as input and produces a scalar as output.

23 The function $\Xi(t)$ is chosen to be sufficiently well behaved to allow analysis; its real and imaginary parts have up to, and including, second order derivatives with respect to t [177].

Since $\varepsilon_{dc}(r_d, \Re[\xi], \Im[\xi])$ has a minimum at the point $(\Re[\xi], \Im[\xi]) = (0,0)$, the following two partial derivative properties are true:

$$\frac{\partial \varepsilon_{dc}(r_d, \Re[\xi], \Im[\xi])}{\partial \Re[\xi]}|_{\Re[\xi]=0} = 0 \tag{B.16}$$

$$\frac{\partial \varepsilon_{dc}(r_d, \Re[\xi], \Im[\xi])}{\partial \Im[\xi]}|_{\Im[\xi]=0} = 0. \tag{B.17}$$

Evaluating (B.16) gives:

$$\begin{aligned} < \Xi , K_d r_{dco} >_c + < r_{dco} , K_d \Xi >_c + 2\Re[\xi] < \Xi , K_d \Xi >_c \\ - < \Xi , m_0 >_c \\ - < \Xi^* , m_0^* >_c \quad |_{\Re[\xi]=0} = 0 \end{aligned} \tag{B.18}$$

$$\begin{aligned} \therefore < \Xi , K_d r_{dco} >_c + < r_{dco} , K_d \Xi >_c \\ - < \Xi , m_0 >_c - < \Xi^* , m_0^* >_c = 0. \end{aligned} \tag{B.19}$$

But since K_d has a Hermitian kernel

$$\begin{aligned} \therefore < \Xi , K_d r_{dco} >_c + < \Xi^* , K_d r_{dco}^* >_c \\ - < \Xi , m_0 >_c - < \Xi^* , m_0^* >_c = 0 \end{aligned} \tag{B.20}$$

$$\therefore \Re\left[< \Xi , K_d r_{dco} - m_0 >_c\right] = 0. \tag{B.21}$$

Evaluating (B.17) by a similar approach gives:

$$\Im\left[< \Xi , K_d r_{dco} - m_0 >_c\right] = 0. \tag{B.22}$$

Combining (B.21) and (B.22) gives:

$$< \Xi , K_d r_{dco} - m_0 >_c = 0. \tag{B.23}$$

But since $\Xi(t)$ is arbitrary it means that:

$$(K_d r_{dco} - m_0)(t) = 0. \tag{B.24}$$

Therefore, the optimal function for $r_d(t)$ satisfies the following equation [177]:

$$\therefore \; K_d r_{dco}(t) \; = \; m_0(t). \tag{B.25}$$

Thus the function $r_{dco}(t)$ which satisfies (B.25) minimizes $\varepsilon_{dc}(r_d)$ in (B.11).

Appendix C Anti-causal Operator

The discrete-time continuous-frequency Fourier transform pair is defined to be:

$$\begin{aligned} X_a^{\mathrm{T}}(f) &= \mathcal{F}_{dc}[x_a[n]] \\ &= \sum_{n=-\infty}^{\infty} x_a[n]\, e^{-j2\pi n\mathrm{T}f} \end{aligned}$$

$$\begin{aligned} x_a[n] &= \mathcal{F}_{dc}^{-1}\left[X_a^{\mathrm{T}}(f)\right] \\ &= \mathrm{T}\int_{-\frac{1}{2\mathrm{T}}}^{\frac{1}{2\mathrm{T}}} X_a^{\mathrm{T}}(f)\, e^{j2\pi f\mathrm{T}n}\, df \end{aligned} \tag{C.1}$$

where $x_a[n]$ and $X_a^{\mathrm{T}}(f)$ represent time-domain and frequency-domain functions, respectively. Note that the superscript T with $X_a^{\mathrm{T}}(f)$ denotes that $X_a^{\mathrm{T}}(f)$ is periodic in frequency, with period equal to 1/T.

Then the anti-causal operator, $[\bullet]_-$, operating on $X_a^{\mathrm{T}}(f)$ is defined as:

$$\begin{aligned} \left[X_a^{\mathrm{T}}(f)\right]_- &= \sum_{n=-\infty}^{0} x_a[n]\, e^{-j2\pi n\mathrm{T}f} \\ &= \mathcal{F}_{dc}\left[\, u[-n]\;\mathcal{F}_{dc}^{-1}\left[X_a^{\mathrm{T}}(f)\right]\,\right] \end{aligned} \tag{C.2}$$

where the discrete-time unit step function is defined in (B.10).

The following three associated operators are also defined:

$$\begin{aligned} \left[X_a^{\mathrm{T}}(f)\right]_{--} &= \sum_{n=-\infty}^{-1} x_a[n]\, e^{-j2\pi n\mathrm{T}f} \\ \left[X_a^{\mathrm{T}}(f)\right]_{+} &= \sum_{n=0}^{\infty} x_a[n]\, e^{-j2\pi n\mathrm{T}f} \\ \left[X_a^{\mathrm{T}}(f)\right]_{++} &= \sum_{n=1}^{\infty} x_a[n]\, e^{-j2\pi n\mathrm{T}f}. \end{aligned} \tag{C.3}$$

Let the same notation used with $x_a[n]$ apply to the sequences $x_b[n]$ and $x_c[n]$. The following is a list of relevant properties of the anti-causal operator:

Table C.1 Properties of the anti-causal operator

Properties	
$\left[\zeta \, X_a^{\mathrm{T}}(f) \right]_- = \zeta \left[X_a^{\mathrm{T}}(f) \right]_- \quad ; \quad \zeta \in \mathbb{C}$	(C.4)
$\left[X_a^{\mathrm{T}}(f) \, X_b^{\mathrm{T}}(f) \right]_- = \left[X_b^{\mathrm{T}}(f) \, X_a^{\mathrm{T}}(f) \right]_-$	(C.5)
$\left[X_a^{\mathrm{T}}(f) \, X_b^{\mathrm{T}}(f) \right]_- + \left[X_a^{\mathrm{T}}(f) \, X_c^{\mathrm{T}}(f) \right]_- = \left[X_a^{\mathrm{T}}(f) \left(X_b^{\mathrm{T}}(f) + X_c^{\mathrm{T}}(f) \right) \right]_-$	(C.6)
$X_a^{\mathrm{T}}(f) = \left[X_a^{\mathrm{T}}(f) \right]_- + \left[X_a^{\mathrm{T}}(f) \right]_{++}$	(C.7)
$X_a^{\mathrm{T}}(f) = \left[X_a^{\mathrm{T}}(f) \right]_{--} + \left[X_a^{\mathrm{T}}(f) \right]_+$	(C.8)
$\left[\left[X_a^{\mathrm{T}}(f) \right]_+ \right]_- = x_a[0]$	(C.9)
$\left[\left[X_a^{\mathrm{T}}(f) \right]_{++} \right]_- = 0$	(C.10)
$\left[\left[X_a^{\mathrm{T}}(f) \right]_+ \left[X_b^{\mathrm{T}}(f) \right]_{++} \right]_- = 0$	(C.11)

Appendix D Equalizer Minimum Mean Square Error Expressions

This appendix describes the sources of the MMSE expressions for *six* cases; As indicated in Section 3.4 they are obtained from *two* equalizer types in the presence of *three* interference types. The two equalizer types are linear and decision-feedback. The three interference types are white noise, stationary noise of Chapter 2, and cyclostationary interference of Chapter 2. This summary and notation was based on similar results for a linear equalizer [68, 184]. The results for the linear equalizer are included.

Note the following assumptions for all six cases. The combined channel and combined co-channels are strictly bandlimited to $K_t/(2\mathrm{T})$; see (3.71). Correct equalizer decisions are assumed. The equalizers are continuous in time and infinite in length. The MMSE expressions for the six cases are presented in Tables 3.1 and 3.2 where related quantities are defined as follows: $\langle\bullet\rangle$ from (3.90), $\mathbf{I}_{2K_t-1}$ is an identity matrix of order $2K_t-1$, and diag[•] denotes the square diagonal matrix obtained from square matrix •. Note the following properties about the quantities in Table 3.2. Since $\mathbf{W}_\bullet(f)$ is positive definite, then $\mathbf{W}_\bullet^{-1}(f)$ is positive definite. Therefore $M_\bullet^{\mathrm{T}}(f)$ is greater than or equal to zero.

D.1 Linear Equalizer — Stationary Noise

Consider the system shown in Fig. D.1 which contains a linear channel with additive white noise. This is based on the system model in Chapter 2 except that for the development of this case the impulse response of the combined channel is denoted by $\psi_0(t)$. Define:

$$\Psi_0(f) \;=\; \mathcal{F}_{cc}[\psi_0(t)]. \tag{D.1}$$

Assuming correct decisions, the MMSE performance, called ε_{lwo}, of the linear equalizer in Fig. D.1 is given by the following expression [105]:

$$\varepsilon_{lwo} \;=\; \left\langle \frac{1}{1+M_w^{\mathrm{T}}(f)} \right\rangle \tag{D.2}$$

$$M_w^{\mathrm{T}}(f) \;=\; \frac{1}{\mathrm{No}}\frac{1}{\mathrm{T}}\sum_{k=-\infty}^{\infty}\left|\Psi_0\left(f+\frac{k}{\mathrm{T}}\right)\right|^2. \tag{D.3}$$

Since the combined channels and combined co-channels are strictly bandlimited to $K_t/(2\mathrm{T})$, then $M_w^{\mathrm{T}}(f)$ may be rewritten as:

$$M_w^{\mathrm{T}}(f) \;=\; \frac{1}{\mathrm{T}}\,\mathbf{\Phi}_0^*(f)\,\mathbf{W}_w^{-1}(f)\,\mathbf{\Phi}_0(f) \tag{D.4}$$

where $\mathbf{W}_n(f)$ is the $(2K_t-1)\times(2K_t-1)$ matrix:

$$\mathbf{W}_n(f) \;=\; \mathrm{No}\mathbf{I}_{2K_t-1} \tag{D.5}$$

and $\mathbf{\Phi}_0(f)$ was defined in (3.74).

The case of interest is the linear-equalizer MMSE performance in the stationary noise model of Chapter 2. This case occurs when $\nu(t)$ in Fig. 2.1 is equal to $\nu_{sn}(t)$ in Fig. 2.4, and when the receiver shown in Fig. 2.1 is expanded using the linear equalizer shown in Fig. 2.5. By moving the filter in Fig. 2.4 with the frequency response $\Phi_{sn}(f)$, to a new place between the adder and receiver in Fig. 2.1 and putting another filter with frequency response $1/\Phi_{sn}(f)$ between the channel and adder, then a situation equivalent to that in Fig. D.1 is obtained [200]; due to the presence of white noise, the magnitude of $\Phi_{sn}(f)$, see (2.35) , is always positive and therefore $1/\Phi_{sn}(f)$ always exists. The frequency response of the combined channel in Fig. D.1 is:

$$\Psi_0(f) \;=\; \frac{\Phi_0(f)}{\Phi_{sn}(f)} \tag{D.6}$$

$$\therefore\;\Psi_0(f) \;=\; \frac{\Phi_0(f)}{\sqrt{\frac{1}{\mathrm{No}}\left(\mathrm{No}+\frac{1}{\mathrm{T}}\sum_{i=1}^{\mathrm{L}}|\Phi_i(f)|^2\right)}}. \tag{D.7}$$

Therefore, the expression for MMSE of a linear equalizer in stationary noise is:

$$\varepsilon_{lso} \;=\; \left\langle\frac{1}{1+M_{sn}^{\mathrm{T}}(f)}\right\rangle \tag{D.8}$$

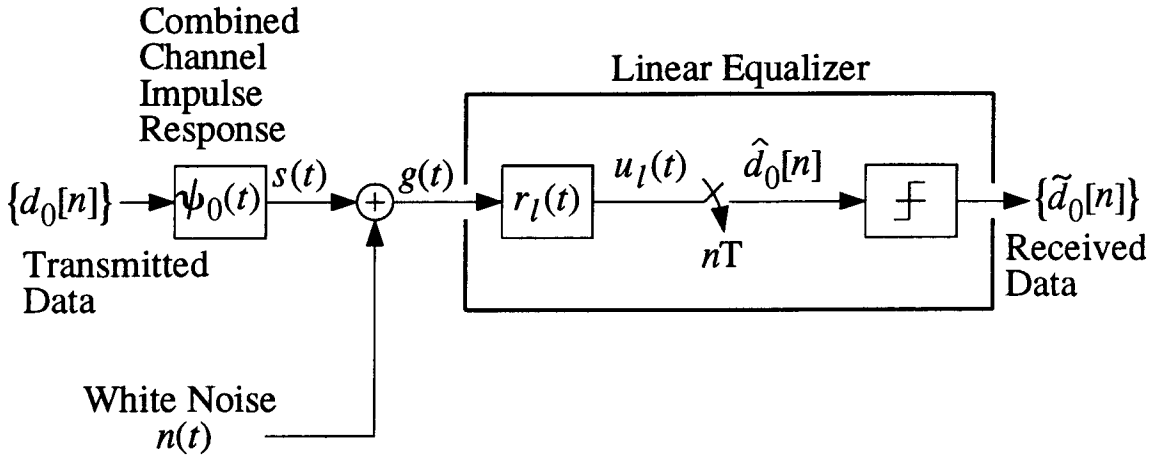

Figure D.1 Linear equalizer in white noise

where

$$M_{sn}^{\mathrm{T}}(f) \;=\; \frac{1}{\mathrm{No}}\frac{1}{\mathrm{T}}\sum_{k=-\infty}^{\infty}\left|\Psi_0\left(f+\frac{k}{\mathrm{T}}\right)\right|^2. \tag{D.9}$$

Since the combined channels and combined co-channels are strictly bandlimited to $K_t/(2\mathrm{T})$, then $M_{sn}^{\mathrm{T}}(f)$ may be rewritten as:

$$M_{sn}^{\mathrm{T}}(f) \;=\; \frac{1}{\mathrm{T}}\,\mathbf{\Phi}_0^*(f)\,\mathbf{W}_{sn}^{-1}(f)\,\mathbf{\Phi}_0(f) \tag{D.10}$$

where $\mathbf{W}_{sn}(f)$ is the $(2K_t-1)\times(2K_t-1)$ matrix:

$$\mathbf{W}_{sn}(f) \;=\; \mathrm{No}\mathbf{I}_{2K_t-1} \;+\; \frac{1}{\mathrm{T}}\sum_{i=1}^{\mathrm{L}}\mathrm{diag}[\mathbf{\Phi_i}(f)\,\mathbf{\Phi_i^*}(f)] \tag{D.11}$$

and $\mathbf{\Phi}_i(f)$ was defined in (3.74).

D.2 Linear Equalizer — Cyclostationary Interference

The expression for the MMSE of a linear equalizer in cyclostationary interference is well known [54, 67, 68, 74, 107, 115, 120, 124, 125, 127, 184] and will be only be stated.

$$\varepsilon_{lco} \;=\; \left\langle \frac{1}{1+M_{ci}^{\mathrm{T}}(f)} \right\rangle \tag{D.12}$$

where $M_{ci}^{\mathrm{T}}(f)$ is defined in the same manner as for the decision-feedback equalizer in cyclostationary interference based on (3.81), (3.77), (3.74), (3.71), and (3.36) .

D.3 Decision-feedback Equalizer — Stationary Noise

Consider the system shown in Fig. D.2 which contains a linear channel with additive white noise. This is based on the system model in Chapter 2 except that for the development of this case the impulse response of the combined channel is denoted by $\psi_0(t)$. Assuming correct decisions, the MMSE performance, called ε_{dwo}, of the

decision-feedback equalizer in Fig. D.2 is given by the following expression [108, 109]:

$$\varepsilon_{lwo} = e^{-\left\langle ln\left(1+M_w^{\mathrm{T}}(f)\right)\right\rangle} \tag{D.13}$$

where $M_w^{\mathrm{T}}(f)$ was defined in (D.4).

The case of interest is the decision-feedback-equalizer MMSE performance in the stationary noise model of Chapter 2. This case occurs when $\nu(t)$ in Fig. 2.1 is equal to $\nu_{sn}(t)$ in Fig. 2.4, and when the receiver shown in Fig. 2.1 is expanded using the decision-feedback equalizer shown in Fig. 2.6. By using the same innovations approach [200] of Appendix D.1, the expression for the MMSE of a decision-feedback equalizer in stationary noise is:

$$\varepsilon_{dso} = e^{-\left\langle \ln\left(1+M_{sn}^{\mathrm{T}}(f)\right)\right\rangle} \tag{D.14}$$

where $M_{sn}^{\mathrm{T}}(f)$ was defined in (D.10).

D.4 Decision-feedback Equalizer — Cyclostationary Interference

The expression for the MMSE of a decision-feedback equalizer in cyclostationary interference was derived in Section 3.3 and is stated in (3.93).

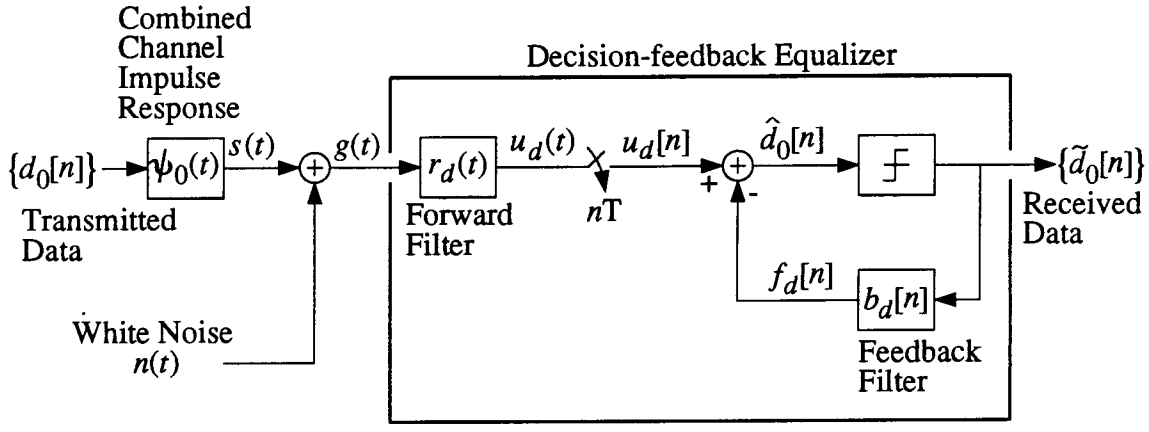

Figure D.2 Decision-feedback equalizer in white noise

References

[1] D. C. Cox, "Universal digital portable radio communications," *Proc. IEEE*, vol. 75, no. 4, pp. 436–477, Apr. 1987.

[2] American National Standards Institute, *Integrated services digital network (ISDN) basic access interface for use on metallic loops for application on the network side of the NT (layer 1 specification)*, ANSI T1-601-1988, Sept. 1988.

[3] P. Cochrane and M. Brain, "Future optical fiber transmission technology and networks," *IEEE Communications Magazine*, vol. 26, no. 11, pp. 45–60, Nov. 1988.

[4] IEEE, "High-speed digital subscriber-lines workshop." (Parsippany, NJ), sponsored by Bell Communications Research, Inc., 445 South Street, Morristown, NJ 07960, no proceedings, Mar. 28-29, 1990.

[5] R. A. Mosbacher and J. Obuchowski, "U.S. Spectrum Management Policy: Agenda for the Future," Tech. Rep. NTIA special pub. 91-23, U.S. Dept. of Commerce, National Telecommunications and Information Administration, through U.S. Government Printing Office, Washington, DC, 20402, Feb. 1991.

[6] D. C. Cox, W. S. Gifford, and H. Sherry, "Low-power digital radio as a ubiquitous subscriber loop," *IEEE Communications Magazine*, vol. 29, no. 3, pp. 92–95, Mar. 1991.

[7] D. L. Waring, J. W. Lechleider, and T. R. Hsing, "Digital subscriber line technology facilitates a graceful transition from copper to fiber," *IEEE Communications Magazine*, vol. 29, no. 3, pp. 96–104, Mar. 1991.

[8] G. Kaplan, "A special guide to data comunications," *IEEE Spectrum*, vol. 28, no. 8, p. 21, Aug. 1991.

[9] S. Sampei, "Development of the Japanese adaptive equalizing technology toward high bit rate data transmission in land mobile communications," *Trans. IEICE*, vol. E 74, no. 6, pp. 1512–1521, June 1991.

[10] D. G. Messerschmitt, "Design issues in the ISDN U-interface transceiver," *IEEE J. Select. Areas Commun.*, vol. SAC-4, no. 8, pp. 1281–1293, Nov. 1986.

[11] J. W. Lechleider, "Loop transmission aspects of ISDN basic access," *IEEE J. Select. Areas Commun.*, vol. SAC-4, no. 8, pp. 1294–1301, Nov. 1986.

[12] G. Stix, "Telephone wiring: a conduit for networking standards," *IEEE Spectrum*, vol. 25, no. 6, pp. 38–41, June 1988.

[13] J. W. Lechleider, "High bit rate digital subscriber lines: A review of HDSL progress," *IEEE J. Select. Areas Commun.*, vol. 9, no. 6, pp. 769–784, Aug. 1991.

[14] Ad Hoc Group on Draft Standard, *Draft standard for ISDN basic access interface for application at the network side of NT1, layer 1 specification*, T1D1.3/86-145R2, Jan. 5 1987.

[15] P. D. Lattner, R. L. Fike, and G. A. Nelson, "Business and residential services for the evolving subscriber loop," *IEEE Communications Magazine*, vol. 29, no. 3,

pp. 109–114, Mar. 1991.

[16] C. L. Jackson, "The allocation of the radio spectrum," *Scientific American*, vol. 242, no. 2, pp. 34–39, Feb. 1980.

[17] D. C. Cox, "Cochannel interference considerations in frequency reuse small-coverage-area radio systems," *IEEE Trans. on Commun.*, vol. COM-30, no. 1, pp. 135–142, Jan. 1982.

[18] S. Wang and S. S. Rappaport, "Signal-to-interference calculations for balanced channel assignment patterns in cellular communications," *IEEE Trans. on Commun.*, vol. COM-37, no. 10, pp. 1077–1087, Oct. 1989.

[19] L. E. Franks, *Signal Theory*. Englewood Cliffs, NJ: Prentice-Hall, Inc., 1969.

[20] W. A. Gardner and L. E. Franks, "Characterization of cyclostationary random processes," *IEEE Trans. on Inform. Theory*, vol. IT-21, no. 1, pp. 4–14, Jan. 1975.

[21] S. U. H. Qureshi, "Adaptive equalization," *Proc. IEEE*, vol. 73, no. 9, pp. 1349–1387, Sept. 1985.

[22] S. A. Cox and P. F. Adams, "An analysis of digital transmission techniques for the local network," *Br. Telecom Technol. J.*, vol. 3, no. 3, pp. 73–85, July 1985.

[23] R. J. C. Bultitude, S. A. Mahmoud, and W. A. Sullivan, "A comparison of indoor radio propagation characteristics at 910 MHz and 1.75 GHz," *IEEE J. Select. Areas Commun.*, vol. 7, no. 1, pp. 20–30, Jan. 1989.

[24] R. J. C. Bultitude, "Measurement, characterization and modeling of indoor 800/900 MHz radio channels for digital communications," *IEEE Communications Magazine*, vol. 25, no. 6, pp. 5–12, June 1987.

[25] J. C. Tu, J. S. Chow, G. P. Dudevoir, and J. M. Cioffi, "Crosstalk-limited performance of a computationally efficient multichannel transceiver for high rate digital subscriber lines," in *Conf. Rec. IEEE Globecom 89*, vol. 3, (Dallas, TX), pp. 1940–1944, Nov. 27-30, 1989.

[26] C. L. Despins, D. D. Falconer, and S. A. Mahmoud, "Coding and optimum baseband combining for wideband TDMA indoor wireless channels," in *Conf. Rec. IEEE Globecom 90*, vol. 3, (San Diego, CA), pp. 1832–1837, Dec. 2-5, 1990.

[27] C. L. Despins, D. D. Falconer, and S. A. Mahmoud, "Coding and optimum baseband combining for wideband TDMA indoor wireless channels," *Can. J. Elect. & Comp. Eng.*, vol. 16, no. 2, pp. 53–62, Apr. 1991.

[28] C. L. Despins, D. D. Falconer, and S. A. Mahmoud, "Compound strategies of coding, equalization, and space diversity for wideband TDMA indoor wireless channels," in *Proceedings of the IEEE International Symposium on Personal, Indoor and Mobile Radio Communications*, vol. 1, (London, England), pp. 69–74, Sept. 23-25, 1991.

[29] W. C. Jakes, ed., *Microwave Mobile Communications*. New York, NY: John Wiley & Sons Inc., 1973.

[30] J. H. Winters, "Optimum combining in digital mobile radio with cochannel interference," *IEEE J. Select. Areas Commun.*, vol. SAC-2, no. 4, pp. 528–539, July 1984.

[31] J. H. Winters, "Upper bounds for the bit error rate of optimum combining in digital mobile radio," in *Conf. Rec. IEEE Globecom 84*, vol. 1, pp. 173–178, Nov. 26-29, 1984.

[32] S. C. Gupta, R. Visawanathan, and R. Muammar, "Land mobile radio systems - A tutorial exposition," *IEEE Communications Magazine*, vol. 23, no. 6, pp. 34–45, June 1985.

[33] S. Sampei and M. Yokoyama, "Rejection method of adjacent-channel interference for digital land mobile communications," *Trans. IECE Japan*, vol. E69, no. 5, pp. 578–580, May 1986.

[34] N. W. K. Lo, "Adaptive equalization and diversity combining for a mobile radio channel," Master's thesis, Dept. of Systems and Computer Engineering, Carleton University, Ottawa, Ont., Canada, SCE-90-09, May 1990.

[35] N. Kinoshita and S. Sampei, "Method of rejecting adjacent channel interference using an adaptive equalizer," *Electronics and Communications in Japan, Part I: Communications*, vol. 72, no. 11, pp. 1–10, Oct. 1989.

[36] M. Nakajima and S. Sampei, "Performance of a decision-feedback equalizer under frequency selective fading in land mobile communications," *Electronics and Communications in Japan, Part I: Communications*, vol. 73, no. 9, pp. 86–96, Nov. 1990.

[37] M. Uesugi, K. Honma, and K. Tsubaki, "Adaptive equalization in TDMA digital mobile radio," in *Conf. Rec. IEEE Globecom 89*, vol. 1, (Dallas, TX), pp. 95–101, Nov. 27-30, 1989.

[38] R. A. Ziegler and J. M. Cioffi, "A comparison of least squares and gradient equalization for multipath fading in wideband digital mobile radio," in *Conf. Rec. IEEE Globecom 89*, vol. 1, (Dallas, TX), pp. 102–105, Nov. 27-30, 1989.

[39] S. Sampei and T. Sunaga, "Performance of multi-level QAM with maximal ratio combining space diversity for land mobile communications," in *Conf. Rec. IEEE VTC 90*, (Orlando, FL), pp. 459–464, May. 6-9, 1990.

[40] S. N. Crozier, *Short-block Data Detection Techniques Employing Channel Estimation for Fading Time-Dispersive Channels*. PhD thesis, Dept. of Systems and Computer Engineering, Carleton University, Ottawa, Ont., Canada, SCE-90-11, May 1990.

[41] N. W. K. Lo, D. D. Falconer, and A. U. H. Sheikh, "Adaptive equalization and diversity combining for a mobile radio channel," in *Conf. Rec. IEEE Globecom 90*, vol. 2, (San Diego, CA), pp. 923–927, Dec. 2-5, 1990.

[42] S. Sampei, "Performance of trellis coded 16QAM/TDMA system for land mobile communications," in *Conf. Rec. IEEE Globecom 90*, vol. 3, (San Diego, CA), pp. 1953–1957, Dec. 2-5, 1990.

[43] B. R. Petersen and D. D. Falconer, "Interference cancellation techniques for digital

mobile and portable radio systems," in *Proceedings, Wireless 91, The Third National Seminar & Workshop on Wireless Personal Communications*, vol. 1, (Calgary, Alberta), July 8-10, 1991.

[44] D. P. Taylor and P. R. Hartmann, "Telecommunications by microwave digital radio," *IEEE Communications Magazine*, vol. 24, no. 8, pp. 11–16, Aug. 1986.

[45] M. Despinic and D. P. Taylor, "A simulation study of ACI and TCM in M-QAM digital microwave radio," Tech. Rep. CRL 196, Communications Research Laboratory, Faculty of Engineering, McMaster University, Hamilton, Ont., Canada, L8S 4K1, Oct., 1988.

[46] E. D. Horton, "An adaptive co-channel interference suppression system to suppress high level interference in satellite communication earth terminals," in *National Telecommunications Conference*, vol. 1, (Dallas, TX), pp. 13.4–1 – 13.4–5, Nov. 29-Dec. 1, 1976.

[47] J. J. Spilker, Jr., *Digital Communications by Satellite*. Englewood Cliffs, NJ: Prentice-Hall, Inc., 1977.

[48] S. Murakami, Y. Furuya, Y. Matsuo, and M. Sugiyama, "Optimum modulation and channel filters for nonlinear satellite channels," *IEEE Trans. on Commun.*, vol. COM-27, no. 12, pp. 1810–1819, Dec. 1979.

[49] I. Oka, K. Ishida, and I. Endo, "Co-channel interference in an on-board processing satellite," in *6th Symposium and Technical Exhibition on Electromagnetic Compatibility*, vol. 1, (Zurich, Switzerland), pp. 605–609, Mar. 5-7, 1985.

[50] A. Sakurai, N. Koda, I. Oka, and I. Endo, "Interference canceling techniques in on-board processing satellites," in *7th International Zurich Symposium of Technical Exhibition on Electromagnetic Compatibility*, vol. 1, (Zurich, Switzerland), pp. 399–403, Mar. 3-5, 1987.

[51] D. G. Messerschmitt, L. C. Barbosa, and T. D. Howell, "A study of sampling detectors for magnetic recording," Tech. Rep. RJ 4081 (45459) (declassified July 7, 1987), IBM Almaden Research Center, San Jose, CA 95120, July 16, 1984.

[52] J. W. M. Bergmans and A. J. E. M. Janssen, "Robust data equalization, fractional tap spacing and the Zak transform," *Philips J. Res.*, vol. 42, no. 4, pp. 351–398, Nov. 23, 1987.

[53] J. M. Cioffi, W. L. Abbott, H. K. Thapar, C. M. Melas, and K. D. Fisher, "Adaptive equalization in magnetic-disk storage channels," *IEEE Communications Magazine*, vol. 28, no. 2, pp. 14–29, Feb. 1990.

[54] W. van Etten, "An optimum linear receiver for multiple channel digital transmission systems," *IEEE Trans. on Commun.*, vol. COM-23, no. 8, pp. 828–834, Aug. 1975.

[55] W. van Etten, "Maximum likelihood receiver for multiple channel transmission systems," *IEEE Trans. on Commun.*, vol. COM-24, no. 2, pp. 276–283, Feb. 1976.

[56] W. A. Gardner, "The structure of least-mean square linear estimators for synchronous M-ary signals," *IEEE Trans. on Inform. Theory*, vol. IT-19, no. 2, pp. 240–243, Mar. 1973.

[57] P. Stavroulakis, *Interference Analysis of Communication Systems*. New York, NY: IEEE Press, 1980.

[58] J. C. Campbell, A. J. Gibbs, and B. M. Smith, "The cyclostationary nature of crosstalk interference from digital signals in multipair cable-Part I: Fundamentals and Part II: Applications and further results," *IEEE Trans. on Commun.*, vol. COM-31, no. 5, pp. 629–649, May 1983.

[59] B. M. Smith and P. G. Potter, "Design criteria for crosstalk interference between digital signals in multipair cable," *IEEE Trans. on Commun.*, vol. COM-34, no. 6, pp. 593–599, June 1986.

[60] W. A. Gardner, "The role of spectral correlation in the design and performance analysis of synchronizers," *IEEE Trans. on Commun.*, vol. COM-34, no. 11, pp. 1089–1095, Nov. 1986.

[61] D. Bukofzer, "Optimum and suboptimum detector performance for signals in cyclostationary noise," *IEEE J. Oceanic Eng.*, vol. OE-12, no. 1, pp. 97–115, Jan. 1987.

[62] W. A. Gardner, "Spectral correlation of modulated signals-Part I: Analog modulation," *IEEE Trans. on Commun.*, vol. COM-35, no. 6, pp. 584–594, June 1987.

[63] W. A. Gardner, W. A. Brown, III, and C. Chen, "Spectral correlation of modulated signals-Part II: Digital modulation," *IEEE Trans. on Commun.*, vol. COM-35, no. 6, pp. 595–601, June 1987.

[64] W. A. Gardner, *Statistical Spectral Analysis: A Nonprobabilistic Theory*. Englewood Cliffs, NJ: Prentice-Hall, Inc., 1987.

[65] M. Abdulrahman, "Decision-feedback equalization with cyclostationary interference for DSL," Master's thesis, Dept. of Systems and Computer Engineering, Carleton University, Ottawa, Ont., Canada, SCE-89-16, June 1989.

[66] M. Abdulrahman and D. D. Falconer, "Cyclostationary crosstalk suppression by decision feedback equalization on digital subscriber loops." Carleton University, Ottawa, Ont., Canada, K1S 5B6, to appear in *IEEE J. Select. Areas Commun.*, 1992.

[67] B. R. Petersen and D. D. Falconer, "Equalization in Cyclostationary Interference," Tech. Rep. SCE 90-01, Department of Systems and Computer Engineering, Carleton University, Ottawa, Ont., Canada, K1S 5B6, Jan. 1990.

[68] G. D. Golden, consultant AT&T Bell Labs., "Cancellation of synchronous cyclostationary interference (SCI) using fractionally spaced equalizers." invited seminar, Dept. of Systems and Computer Engineering, Carleton University, Ottawa, Ont., K1S 5B6, Mar. 7, 1990.

[69] B. R. Petersen and D. D. Falconer, "Equalization bounds in cyclostationary subscriber-loop interference." IEEE High-speed digital subscriber-lines workshop, no proceedings, (Parsippany, NJ), Mar. 28-29, 1990.

[70] B. R. Petersen, "Equalization for cyclostationary interference," in *ISDN Technologies to Applications: An OCRI/TRIO presentation*, (Ottawa, ON), Mar. 7, 1990.

[71] B. R. Petersen and D. D. Falconer, "Equalization bounds in cyclostationary interference," in *Proc. of the 15th Biennial Symposium on Communications*, vol. 1, (Kingston, ON), pp. 268–271, June 3-6, 1990.

[72] G. Xu and T. Kailath, "Direction-of-arrival estimation via exploitation of cyclostationarity - A combination of temporal and spatial processing." Information Systems Laboratory, Stanford University, Stanford, CA, 94305, submitted to *IEEE Trans. on ASSP*, private communication received July 30, 1990.

[73] J. H. Reed and T. C. Hsia, "The performance of time-dependent adaptive filters for interference rejection," *IEEE Trans. on Acoust., Speech, Signal Processing*, vol. 38, no. 8, pp. 1373–1385, Aug. 1990.

[74] P. M. Crespo, M. L. Honig, and K. Steiglitz, "Suppression of near- and far-end crosstalk by linear pre- and post-filtering." Bell Communications Research, Inc., 445 South Street, Morristown, NJ 07960-1910, to appear in *IEEE Trans. on Commun.*, private communication received Aug. 1, 1990.

[75] V. Joshi and D. D. Falconer, "Sequence estimation techniques for digital subscriber loop transmission with crosstalk interference," *IEEE Trans. on Commun.*, vol. 38, no. 9, pp. 1367–1374, Sept. 1990.

[76] A. Duel-Hallen, "Equalizers for multiple input/multiple output channels and PAM systems with cyclostationary input sequences." School of Electrical Engineering, Cornell University, Ithaca, NY 14853, to appear in *IEEE Trans. on Commun.*, private communication received Oct. 26, 1990.

[77] W. A. Gardner and S. Venkataraman, "Performance of optimum and adaptive frequency-shift filters for cochannel interference and fading," in *Proc. Twenty-fourth Asilomar Conference on Signals, Systems, and Computers*, vol. 1, (Pacific Grove, CA), pp. 242–245, Nov. 5-7, 1990.

[78] B. R. Petersen and D. D. Falconer, "Exploiting cyclostationary subscriber-loop interference by equalization," in *Conf. Rec. IEEE Globecom 90*, vol. 2, (San Diego, CA), pp. 1156–1160, Dec. 2-5, 1990.

[79] W. A. Gardner, *Introduction to Random Processes with Applications to Signals and Systems*. New York, NY: McGraw-Hill Publishing Company, 2nd ed., 1990.

[80] W. A. Gardner, "Exploitation of spectral redundancy in cyclostationary signals," *IEEE Signal Processing Magazine*, vol. 8, no. 2, pp. 14–36, Apr. 1991.

[81] B. R. Petersen and D. D. Falconer, "Equalization in cyclostationary subscriber-line interference." in *Proceedings TRIO Researcher Retreat*, Trent University, (Peterborough, Ont.), May 8-10, 1991.

[82] B. R. Petersen and D. D. Falconer, "Adjacent-channel interference in digital radio." poster presentation at the *First Virginia Tech Symposium on Wireless Personal Communications*, (Blacksburg, Virginia), June 3-5, 1991.

[83] B. R. Petersen and D. D. Falconer, "Minimum mean-square equalization in cyclostationary and stationary interference - analysis and subscriber-line calculations," *IEEE J. Select. Areas Commun.*, vol. 9, no. 6, pp. 931–941, Aug. 1991.

[84] J. M. Wozencraft and I. M. Jacobs, *Principles of Communication Engineering*.

New York, NY: John Wiley & Sons Inc., 1965.

[85] R. W. Lucky, J. Salz, and E. J. Weldon, *Principles of Data Communication.* New York, NY: McGraw-Hill Inc., 1968.

[86] J. G. Proakis, *Digital Communications.* New York, NY: McGraw-Hill Inc., 1983.

[87] E. A. Lee and D. G. Messerschmitt, *Digital Communication.* Boston, MA: Kluwer Academic Publishers, 1988.

[88] C. E. Shannon, "Communications in the Presence of Noise," *Proc. of the IRE*, vol. 37, pp. 10–21, Jan. 1949.

[89] R. G. Gallager, *Information Theory and Reliable Communication.* New York, NY: John Wiley & Sons Inc., 1968.

[90] B. Widrow, P. E. Mantey, L. J. Griffiths, and B. B. Goode, "Adaptive antenna systems," *Proc. IEEE*, vol. 55, no. 12, pp. 2143–2159, Dec. 1967.

[91] D. D. Falconer, K. H. Mueller, and S. B. Weinstein, "Echo cancellation techniques for full-duplex data transmission on two-wire lines," in *National Telecommunications Conference*, vol. 1, (Dallas, TX), pp. 8.3–1 – 8.3–6, Nov. 29-Dec. 1, 1976.

[92] D. D. Falconer and K. H. Mueller, "Adaptive echo cancellation/AGC structures for two-wire, full-duplex data transmission," *Bell Syst. Tech. J.*, vol. 58, no. 7, pp. 1593–1615, Sept. 1979.

[93] H. Date, K. Fukudome, and S. Konda, "Automatic cancellation method of multipath echo distortion in FM broadcasting receivers," *IEEE Trans. Broadcast.*, vol. BC-28, no. 2, pp. 73–81, June 1982.

[94] D. D. Falconer, "Adaptive reference echo cancellation," *IEEE Trans. on Commun.*, vol. COM-30, no. 9, pp. 2083–2094, Sept. 1982.

[95] D. D. Falconer, "Timing jitter effects on digital subscriber loop echo cancellers: Part I-Analysis of the effect and Part II-Considerations for squaring loop timing recovery," *IEEE Trans. on Commun.*, vol. COM-33, no. 8, pp. 826–838, Aug. 1985.

[96] D. G. Messerschmitt, "Asynchronous and timing jitter insensitive data echo cancellation," *IEEE Trans. on Commun.*, vol. COM-34, no. 12, pp. 1209–1217, Dec. 1986.

[97] P. M. Crespo and M. L. Honig, "A simulation study of near- and far-end crosstalk cancellation for multi-channel data transmission," in *Advances in Communications and Control Systems (ComCon88)* (W. A. Porter and S. C. Kak, eds.), vol. 129, pp. 219–230, Berlin, Germany: Springer-Verlag, 1989.

[98] G. W. Davidson and D. D. Falconer, "Reduced complexity echo cancellation using orthonormal functions," Tech. Rep. SCE 89-12, Department of Systems and Computer Engineering, Carleton University, Ottawa, Ont., Canada, K1S 5B6, Mar. 13, 1989.

[99] D. W. Lin, "Minimum mean-squared error echo cancellation and equalization for digital subscriber line transmission-Part I: Theory and computation and Part II: A

simulation study," *IEEE Trans. on Commun.*, vol. 38, no. 1, pp. 31–45, Jan. 1990.

[100] P. Monsen, "MMSE equalization of interference on fading diversity channels," *IEEE Trans. on Commun.*, vol. COM-32, no. 1, pp. 5–12, Jan. 1984.

[101] S. K. Wilson and J. M. Cioffi, "Multi-dimensional equalization for adjacent-channel interference," in *Conf. Rec. IEEE ICC 91*, vol. 3, (Denver, CO), pp. 1398–1402, June 23-26, 1991.

[102] M. Kavehrad, "Baseband cross-polarization interference cancellation for M-quadrature amplitude-modulated signals over multipath fading radio channels," *AT&T Tech. J.*, vol. 64, no. 8, pp. 1913–1926, Oct. 1985.

[103] S. Verdú, "Optimum multiuser asymptotic efficiency," *IEEE Trans. on Commun.*, vol. COM-34, no. 9, pp. 890–897, Sept. 1986.

[104] H. Nyquist, "Certain Topics in Telegraph Transmission Theory," *Trans. AIEE*, vol. 47, pp. 617–664, Feb. 1928.

[105] T. Berger and D. W. Tufts, "Optimum pulse amplitude modulation-Part I: Transmitter-receiver design and bounds from information theory and Part II: Inclusion of timing jitter," *IEEE Trans. on Inform. Theory*, vol. IT-13, no. 2, pp. 196–216, Apr. 1967.

[106] D. A. Shnidman, "A generalized Nyquist criterion and an optimum linear receiver for a pulse modulation system," *Bell Syst. Tech. J.*, vol. 46, no. 9, pp. 2163–2177, Nov. 1967.

[107] W. A. Gardner and W. A. Brown, "Frequency-shift filtering theory for adaptive co-channel interference removal," in *Proc. Twenty-third Asilomar Conference on Signals, Systems, and Computers*, vol. 2, (Pacific Grove, CA), pp. 562–567, Oct. 30 - Nov. 1, 1989.

[108] J. Salz, "Optimum mean-square decision feedback equalization," *Bell Syst. Tech. J.*, vol. 52, no. 8, pp. 1341–1373, Oct. 1973.

[109] J. Salz, "On mean-square decision feedback equalization and timing phase," *IEEE Trans. on Commun.*, vol. COM-25, no. 12, pp. 1471–1476, Dec. 1977.

[110] M. Kavehrad and J. Salz, "Cross-polarization cancellation and equalization in digital transmission over dually polarized multipath fading channels," *AT&T Tech. J.*, vol. 64, no. 10, pp. 2211–2245, Dec. 1985.

[111] M. Abdulrahman and D. D. Falconer, "Crosstalk suppression by DFE on digital subscriber loops," in *Proc. Canadian Conf. on Electrical and Computer Eng.*, vol. 2, (Ottawa, ON), pp. 78.2.1–78.2.4, Sept. 4-6, 1990.

[112] H. V. Poor and S. Verdú, "Single-user detectors for multiuser channels," *IEEE Trans. on Commun.*, vol. COM-36, no. 1, pp. 50–60, Jan. 1988.

[113] V. Joshi, *Sequence estimation techniques for enhanced digital subscriber loop transmission capability*. PhD thesis, Dept. of Systems and Computer Engineering, Carleton University, Ottawa, Ont., Canada, OCIEE-88-04, June 1988.

[114] E. Biglieri, M. Elia, and L. LoPresti, "Optimal linear receiving filter for digital transmission over nonlinear channels," in *Conf. Rec. IEEE Globecom 84*, vol. 2,

(Atlanta, GA), pp. 1063–1067, Nov. 26-29, 1984.

[115] E. Biglieri, M. Elia, and L. LoPresti, "The optimal linear receiving filter for digital transmission over nonlinear channels," *IEEE Trans. on Inform. Theory*, vol. 35, no. 3, pp. 620–625, May 1989.

[116] P. Niger and P. Vandamme, "Performance of equalization techniques in a radio environment," in *Conf. Rec. IEEE ICC 90*, vol. 2, (Atlanta, GA), pp. 473–477, Apr. 16-19, 1990.

[117] P. Niger and P. Vandamme, "Performance of equalization techniques in a radio environment," *IEEE Trans. on Commun.*, vol. 39, no. 3, pp. 452–457, Mar. 1991.

[118] M. L. Dukić, Z. D. Stojanović, and I. S. Stojanović, "Performance of direct-sequence spread-spectrum receiver using decision feedback and transversal filters for combatting narrowband interference," *IEEE J. Select. Areas Commun.*, vol. 8, no. 5, pp. 907–914, June 1990.

[119] R. A. Iltis, J. A. Ritcey, and L. B. Milstein, "Interference rejection in FFH systems using least-squares estimation techniques," *IEEE Trans. on Commun.*, vol. 38, no. 12, pp. 2174–2183, Dec. 1990.

[120] A. R. Kaye and D. A. George, "Transmission of multiplexed PAM signals over multiple channel and diversity systems," *IEEE Trans. on Commun.*, vol. COM-18, no. 5, pp. 520–526, Oct. 1970.

[121] P. Balaban and J. Salz, "Dual diversity combining and equalization in digital cellular radio," *IEEE Trans. on Vehicular Technology*, vol. 40, no. 2, pp. 342–354, May 1991.

[122] D. J. Harrison, "Adaptive equalization for channels with crosstalk," Master's thesis, Faculty of Engineering, Carleton University, Ottawa, Ont., Canada, Sept. 1969.

[123] L. H. Brandenburg and A. D. Wyner, "Capacity of the Gaussian channel with memory: the multivariate case," *Bell Syst. Tech. J.*, vol. 53, no. 5, pp. 745–778, May-June 1974.

[124] N. Amitay and J. Salz, "Linear equalization theory in digital data transmission over dually polarized fading radio channels," *AT&T Tech. J.*, vol. 63, no. 10, pp. 2215–2259, Dec. 1984.

[125] J. Salz, "Digital transmission over cross-coupled linear channels," *AT&T Tech. J.*, vol. 64, no. 6, pp. 1147–1159, July-Aug. 1985.

[126] J. W. Lechleider, "The feasibility of using adaptive tranmitters to suppress crosstalk," in *Conf. Rec. IEEE ICC 89*, vol. 1, (Boston, MA), pp. 548–551, June 11-14, 1989.

[127] P. M. Crespo, M. L. Honig, and K. Steiglitz, "Optimization of pre- and post-filters in the presence of near- and far- end crosstalk," in *Conf. Rec. IEEE ICC 89*, vol. 1, (Boston, MA), pp. 541–547, June 11-14, 1989.

[128] P. M. Crespo, M. L. Honig, and K. Steiglitz, "Optimization of pre- and post-filters in the presence of near- and far-end crosstalk (superceded by [74])." Bell

Communications Research, Inc., 445 South Street, Morristown, NJ 07960-1910, submitted to *IEEE Trans. on Commun.*, private communication received Sept. 26, 1989.

[129] V. A. Barker, ed., *Sparse Matrix Techniques*. New York, NY: Springer-Verlag, 1977.

[130] AT&T, *Telecommunications Transmission Engineering : Volume 1 — Principles*. Winston-Salen, NC: Western Electric Co. Inc. Technical Publications, AT&T Co., 1977.

[131] AT&T, *Telecommunications Transmission Engineering : Volume 2 — Facilities*. Winston-Salen, NC: Western Electric Co. Inc. Technical Publications, AT&T Co., 1977.

[132] AT&T, *Telecommunications Transmission Engineering : Volume 3 — Networks and Services*. Winston-Salen, NC: Western Electric Co. Inc. Technical Publications, AT&T Co., 1977.

[133] D. W. Lin, "High bit rate digital subscriber line transmission with noise-predicative decision feedback equalization and block coded modulation," in *Conf. Rec. IEEE ICC 89*, vol. 1, (Boston, MA), pp. 531–535, June 11-14, 1989.

[134] G. P. Dudevoir, J. S. Chow, J. M. Cioffi, and S. Kasturia, "Combined equalization and coding for T1 data rates on carrier serving areas subscriber loops," in *Conf. Rec. IEEE ICC 89*, vol. 1, (Boston, MA), pp. 536–540, June 11-14, 1989.

[135] R. G. Hunt, J. W. Cook, K. H. Kirkby, and N. G. Cole, "The potential for high-rate digital subscriber loops," in *Conf. Rec. IEEE ICC 89*, vol. 1, (Boston, MA), pp. 520–524, June 11-14, 1989.

[136] P. Mohanraj, V. Joshi, D. D. Falconer, and T. A. Kwasniewski, "Reduced-complexity trellis coding/decoding for high bit rate digital subscriber loop transmission," in *Conf. Rec. IEEE ICC 89*, vol. 1, (Boston, MA), pp. 525–530, June 11-14, 1989.

[137] H. Cravis and T. V. Crater, "Engineering of T1 carrier system repeated lines," *Bell Syst. Tech. J.*, vol. 42, no. 2, pp. 431–486, Mar. 1963.

[138] E. Arnon and E. Ehrlich, "Measurement results of an HDSL transmission system." in T1E1.4/90-153, (Itaska, IL), June, 1990.

[139] E. Arnon, "private communication." Bell Northern Research, P. O. Box 3511, Station H, Ottawa, Ont., K1Y 4H7, received July 26, 1991.

[140] A. Fung, L. S. Lee, and D. D. Falconer, "A facility for near end crosstalk measurements on ISDN subscriber loops," in *Conf. Rec. IEEE Globecom 89*, vol. 3, (Dallas, TX), pp. 1592–1596, Nov. 27-30, 1989.

[141] M. L. Honig, K. Steiglitz, and B. Gopinath, "Multichannel signal processing for data communications in the presence of crosstalk," *IEEE Trans. on Commun.*, vol. 38, no. 4, pp. 551–558, Apr. 1990.

[142] A. V. Oppenheim and R. W. Schafer, *Digital Signal Processing*. Englewood Cliffs, NJ: Prentice-Hall, Inc., 1975.

[143] R. D. Gitlin and S. B. Weinstein, "On the required tap-weight precision of digitally implemented, adaptive, mean-squared equalizers," *Bell Syst. Tech. J.*, vol. 58, no. 2, pp. 301–321, Feb. 1979.

[144] M. L. Honig and D. G. Messerschmitt, *Adaptive Filters: Structures, Algorithms and Applications*. Boston, MA: Kluwer Academic Publishers, 1984.

[145] S. S. Haykin, *Adaptive Filter Theory*. Englewood Cliffs, NJ: Prentice-Hall, Inc., 1986.

[146] V. K. Prabhu, "Interference analysis and performance of linear digital communication systems," in *Advanced Digital Communications: Systems and Signal Processing Techniques* (K. Feher, ed.), pp. 459–487, Englewood Cliffs, NJ: Prentice-Hall, Inc., 1987.

[147] K. S. Brunner and C. F. Weaver, "A comparison of synchronous and fractional-spaced DFE's in a multipath fading environment," in *Conf. Rec. IEEE Globecom 88*, vol. 3, (Hollywood, FL), pp. 1452–1456, Nov. 28 - Dec. 1, 1988.

[148] S. Stein, "Fading channel issues in system engineering," *IEEE J. Select. Areas Commun.*, vol. SAC-5, no. 2, pp. 68–89, Feb. 1987.

[149] J. H. Winters, "On the capacity of radio communication systems with diversity in a Rayleigh fading environment," *IEEE J. Select. Areas Commun.*, vol. SAC-5, no. 5, pp. 871–878, June 1987.

[150] E. Eleftheriou and D. D. Falconer, "Tracking properties and steady state performance of RLS adaptive filter algorithms," *IEEE Trans. on Acoust., Speech, Signal Processing*, vol. ASSP-34, no. 5, pp. 1097–1110, Oct. 1986.

[151] S. Chennakeshu, A. Narasimhan, and J. B. Anderson, "Decision feedback equalization for digital cellular radio," in *Conf. Rec. IEEE ICC 90*, vol. 4, (Atlanta, GA), pp. 1492–1496, Apr. 16-19, 1990.

[152] H. M. Hafez, "private communication." Dept. of Systems and Computer Engineering, Carleton University, Ottawa, Ont., Canada, K1S 5B6, received June 28, 1989.

[153] R. Kohno, H. Imai, and M. Hatori, "Cancellation techniques of co-channel interference in asynchronous spread spectrum multiple access systems," *Trans. IECE Japan*, vol. J66-A, no. 5, pp. 416–423, May 1983.

[154] M. K. Simon, J. K. Omura, R. A. Scholtz, and B. K. Levitt, *Spread Spectrum Communications, Vol. I, II, III*. Rockville, MD: Computer Science Press, 1985.

[155] S. Verdú, "Minimum probability of error for asynchronous Gaussian multiple-access channels," *IEEE Trans. on Inform. Theory*, vol. IT-32, no. 1, pp. 85–96, Jan. 1986.

[156] R. Vijayan and H. V. Poor, "Nonlinear techniques for interference suppression in spread spectrum systems," *IEEE Trans. on Commun.*, vol. 38, no. 7, pp. 1060–1065, July 1990.

[157] G. Ungerboeck, "Fractional tap-spacing equalizer and consequences for clock recovery in data modems," *IEEE Trans. on Commun.*, vol. COM-24, no. 8,

pp. 856–864, Aug. 1976.

[158] L. E. Franks, "Carrier and bit synchronization in data communication - a tutorial review," *IEEE Trans. on Commun.*, vol. COM-28, no. 8, pp. 1107–1121, Aug. 1980.

[159] M. Moeneclaey, "Linear phase-locked loop theory for cyclostationary input disturbances," *IEEE Trans. on Commun.*, vol. COM-30, no. 10, pp. 2253–2259, Oct. 1982.

[160] J. B. Carruthers, D. D. Falconer, H. M. Sandler, and L. Strawczynski, "Bit synchronization in the presence of co-channel interference," in *Proc. Canadian Conf. on Electrical and Computer Eng.*, vol. 1, (Ottawa, ON), pp. 4.1.1–4.1.7, Sept. 4-6, 1990.

[161] R. Price, "Nonlinearly feedback-equalized PAM versus capacity for noisy filter channels," in *Conf. Rec. IEEE ICC 72*, vol. 1, (Philadelphia, PA), pp. 22.12–22.16, June 19-21, 1972.

[162] W. F. McGee, "Coding, equalization and feedback of digital cable pair signals," *Can. Elec. Eng. J.*, vol. 7, no. 1, pp. 3–8, Jan. 1982.

[163] G. J. Pottie, "Comparison of baseband versus passband systems for HDSL." in T1E1.4/90-164, (Portland, OR), Sept. 24, 1990.

[164] J. C. Madden, "private communication." STC Enterprises, 3290 Cypress St., Vancouver, BC, Canada, V6J 3N6, received May 9, 1991.

[165] A. J. Viterbi and J. K. Omura, *Principles of Digital Communication and Coding*. New York, NY: McGraw-Hill Publishing Company, 1979.

[166] S. Lin and D. J. Costello, Jr., *Error Control Coding: Fundamentals and Applications*. Englewood Cliffs, NJ: Prentice-Hall, Inc., 1980.

[167] G. C. Clark and J. B. Cain, *Error-Correction Coding for Digital Communications*. New York, NY: Plenum Press, 1981.

[168] G. Ungerboeck, "Channel coding with multilevel/phase signals," *IEEE Trans. on Inform. Theory*, vol. IT-28, no. 1, pp. 55–67, Jan. 1982.

[169] H. S. Malvar and D. H. Staelin, "Optimal pre- and postfilters for multichannel signal processing," *IEEE Trans. on Acoust., Speech, Signal Processing*, vol. 36, no. 2, pp. 287–289, Feb. 1988.

[170] J. M. Cioffi, G. P. Dudevoir, M. V. Eyuboğlu, and G. D. Forney, Jr., "MMSE decision-feedback equalizers and coding - Part I: General results." Information Systems Laboratory, Stanford, CA 94395 and Codex Corporation, Mansfield, MA 02048, to appear in *IEEE Trans. on Commun.*, private communication received Aug. 8, 1990.

[171] A. Papoulis, *Random Variables and Stochastic Processes*. New York, NY: McGraw-Hill Book Company, 2nd ed., 1984.

[172] G. D. Golden, "private communication." AT&T Bell Laboratories, Crawfords Corner Rd., Holmdel, NJ, 07733, received Dec. 13, 1990.

[173] L. Brown, "private communication." Motorola Information Systems, 9445 Airport

Road, Brampton, Ont:, L6S 4J3, Canada, received Mar. 29, 1990.

[174] N. A. Zervos, "private communication." AT&T Bell Laboratories, 200 Laurel Ave., Middletown, NJ 07748, U.S.A., received Nov. 16, 1990.

[175] R. D. Gitlin and S. B. Weinstein, "Fractionally-spaced equalization: an improved digital transversal filter," *Bell Syst. Tech. J.*, vol. 60, no. 2, pp. 275–296, Jan. 1981.

[176] G. E. Shilov, *An Introduction to the Theory of Linear Spaces*. Englewood Cliffs, NJ: Prentice-Hall, Inc., 1961.

[177] A. E. Danese, *Advanced Calculus : An Introduction to Applied Mathematics*. Boston, MA: Allyn and Bacon, Inc., 1965.

[178] G. M. Fikhtengol'ts, *The Fundamentals of Mathematical Analysis*, vol. II. Oxford, England: Pergamon Press Ltd., 1965.

[179] M. L. Honig, "private communication." Bell Communications Research, Inc., 445 South Street, Morristown, NJ 07960-1910, received Jan. 12, 1991.

[180] R. D. Strum and D. E. Kirk, *First Principles of Discrete Systems and Digital Signal Processing*. Reading, MA: Addison-Wesley Publishing Co. Inc., 1988.

[181] G. Strang, *Linear Algebra and Its Applications*. New York, NY: Academic Press, Inc., 1980.

[182] H. L. Van Trees, *Detection, Estimation and Modulation Theory, Part I*. New York, NY: John Wiley & Sons Inc., 1968.

[183] H. V. Poor, *An Introduction to Detection and Estimation*. New York, NY: Dowden & Culver Inc., 1988.

[184] G. D. Golden, "private communication." AT&T Bell Laboratories, Crawfords Corner Rd., Holmdel, NJ, 07733, received Jan. 16, 1991.

[185] G. D. Golden, "private communication." AT&T Bell Laboratories, Crawfords Corner Rd., Holmdel, NJ, 07733, received Apr. 10, 1991.

[186] G. D. Golden, "private communication." AT&T Bell Laboratories, Crawfords Corner Rd., Holmdel, NJ, 07733, received Apr. 22, 1991.

[187] C. G. Broyden, *Basic Matrices*. London, England: The Macmillan Press Ltd., 1975.

[188] M. R. Spiegel, *Complex Variables*. New York, NY: McGraw-Hill Publishing Company, 1972.

[189] H. Anton, *Elementary Linear Algebra*. New York, NY: John Wiley & Sons Inc., 4th ed., 1984.

[190] M. Abdulrahman, "Fractionally-Spaced DFE for Spread Spectrum Multiple Access System." Ph.D. Proposal (in progress), Dept. of Systems and Computer Engineering, Carleton University, Ottawa, Ont., Canada, 1991.

[191] D. Sibbald, H. W. Silcock, and E. S. Usher, "Digital transmission over existing subscriber cable," *IEEE Trans. on Commun.*, vol. COM-27, no. 6, pp. 918–924, June 1979.

[192] S. H. Lin, "Statistical behaviour of multipair crosstalk," *Bell Syst. Tech. J.*, vol. 59,

no. 6, pp. 995–974, July-Aug. 1980.

[193] K. Széchényi, "On the NEXT and impulse noise properties of subscriber loops," in *Conf. Rec. IEEE Globecom 89*, vol. 3, (Dallas, TX), pp. 1569–1573, Nov. 27-30, 1989.

[194] R. J. S. Bates, "private communication." IBM Corporation, P. O. Box 218, Route 134, Yorktown Heights, NY, 10598, received Mar. 18, 1991.

[195] J. J. Werner, "private communication." AT&T Bell Laboratories, 200 Laurel Ave., Middletown, NJ, 07748, received Jan. 26, 1990.

[196] W. A. Gardner, *Introduction to Random Processes with Applications to Signals and Systems*. London, England: Collier Macmillan Publishers, 1986.

[197] Z. Kopal, *Numerical Analysis*. London, England: Chapman & Hall Ltd., 2nd ed., 1961.

[198] W. Chomik, M. Elder, and E. Arnon, "private communication." Bell Northern Research, P. O. Box 3511, Station H, Ottawa, Ont., K1Y 4H7, received Oct. 11, 1989.

[199] G. D. Golden, "private communication." AT&T Bell Laboratories, Crawfords Corner Rd., Holmdel, NJ, 07733, received Apr. 17, 1991.

[200] T. Kailath, "The innovations approach to detection and estimation theory," *Proc. IEEE*, vol. 58, no. 5, pp. 680–695, May 1970.

Equalization in Cyclostationary Interference

Brent Robert Petersen, B.Eng., M.A.Sc.

Department of Systems and Computer Engineering
Carleton University
Ottawa, Ontario, Canada, K1S 5B6

January 6, 1992

OCIEE-92-01